UNIVERSITY OF CALGARY

Viscosity and Stability of Visbroken Fractionated Oils

by

Amirabbas Abbaspourmehdiabadi

A THESIS
SUBMITTED TO THE FACULTY OF GRADUATE STUDIES
IN PARTIAL FULFILMENT OF THE REQUIREMENTS FOR THE
DEGREE OF MASTER OF SCIENCE

GRADUATE PROGRAM IN CHEMICAL AND PETROLEUM ENGINEERING

CALGARY, ALBERTA

MARCH, 2021

Abstract

One challenge facing Western Canada is the limited capacity to transport bitumen through pipelines. Bitumen has a high density and viscosity that both exceed pipeline specifications. It must be diluted for transport, but the diluent occupies a capacity that would otherwise be available for the bitumen. One possible solution is to reduce the amount of diluent by decreasing the density and viscosity of the bitumen through a combination of deasphalting and visbreaking processes. Visbreaking reduces the viscosity of the oil, however, if carried too far, this process can destabilize the oil (cause asphaltene precipitation and coke formation). Deasphalting decreases the oil density and can allow more intensive visbreaking without destabilizing the oil. These processes can be applied to both bitumen and vacuum bottom feeds. In all cases, it is necessary to predict the product properties and stability to optimize the process design.

This thesis aims to measure and model the effect of visbreaking on the density, viscosity, and stability of a bitumen, a vacuum bottom, and a deasphalted oil. Each oil was visbroken at two different severities (combinations of temperature and residence time) in an in-house continuous visbreaker. The feeds and their products were separated into distillates, saturates, aromatics, resins, and asphaltenes, and the properties (molecular weight, density, viscosity, and solubility) of each fraction were measured. Previously developed correlations for molecular weight, density model parameters, viscosity model parameters, and solubility parameters were updated. The density of the oils was determined with a volumetric mixing rule and their viscosity with the Expanded Fluid viscosity model. Their stability versus asphaltene precipitation was determined with the Modified Regular Solution phase equilibrium model. The average deviation of the modeled densities and viscosities were 2 kg/m^3 and 19%, respectively. The average deviation in the modeled onset of asphaltene precipitation (solvent content at which precipitation first occurred) was 4.4 wt% *n*-heptane. The average deviation of the modeled asphaltene yield (mass of precipitated asphaltenes divided by the mass of feed oil) was 2.3 wt%.

Acknowledgments

This project has granted me the experience of a lifetime to meet, work, and gain valuable skills among outstanding professionals. I would like to express my sincere and profound gratitude to my supervisor, Dr. Harvey Yarranton, for his unstinting support, guidance, and encouragement throughout the course of my study. I would not have achieved my goals and deadlines but for his helpful inputs and invaluable assistance during the most crucial stages of my work. It was a privilege and honor to be a part of his research group and work under his guidance towards my Master's degree.

My gratitude also extends to Florian Schoeggl, our PVT lab manager, for his constructive advice and lessons that can be applied not only inside the lab but also to real-life circumstances. I learned valuable insights from our philosophical discussions that changed my point of view. I will not forget the joy and excitement of playing chess during the fifteen-hour pilot plant runs. Thank you for your dedication and patience. It was truly an honor to have you as a friend and mentor.

I would also like to thank Elaine Baydak for her unconditional support and assistance with the experimental work and editing process of my thesis. She was always available to help, especially with continuing my experiments during my breaks. Elaine has made me feel welcomed and supported throughout my time in the lab.

Finally, I want to thank my friend, Hanna Nguyen, for her encouragement and moral support during the final stages of my thesis. Her assistance has made this journey more enjoyable and productive for me.

To my dedicated parents and beautiful sister.

تقدیم به پدر و مادرم

که همواره مدیون زحماتشان هستم

و خواهر عزیزم.

Table of Content

List of Tables

List of Figures

List of Symbols, Abbreviations and Nomenclature

Symbol

b	Temperature dependency for density
C5-Asph	Extracted asphaltenes
c_2	Viscosity response to expansion (EF fluid specific parameter)
c_3	Viscosity response to pressure (EF fluid specific parameter)
H/C	Hydrogen to carbon ration
K	Partition Coefficient
l_{jk}	MRS: Binary interaction parameter
MW	Molecular weight
n	Gamma function: Shape factor exponent
n-alkane	Normal alkane
P_0	Atmospheric Pressure
R	Universal gas constant
SG	Specific Gravity
T	Temperature
T_b	Boiling point
w	Weight fraction
wt	Weight fraction
X	Conversion

Abbreviations

A	Athabasca
AAD	Average absolute deviation
AARD	Average absolute relative deviation

AET	Atmospheric equivalent temperature
ASTM	American Society for Testing Materials
API	American Petroleum Institute
B	Bitumen
BIP	Binary interaction parameter
BPR	Back pressure regulator
CI	Confidence Interval
CCR	Conradson carbon residue
CSS	Cyclic steam stimulation
Cum.	Cumulative
DAO	Deasphalted oil
EF	Expanded fluid model
EOS	Equation of State
FBP	Final boiling point
GC	Gas chromatography
IBP	Initial boiling point
MAD	Maximum absolute deviation
MARD	Maximum absolute relative deviation
MCR	Micro carbon residue
MRS	Modified Regular Solution
SBD	Spinning band distillation
SAFT	Statistical associating fluid theory
SAGD	Steam-assisted gravity drainage
SAR	Saturates, aromatics, and resins fractions
SARA	Saturates, aromatics, resins, and asphaltenes fractions
SDA	Solvent deasphalting process
SimDist	Simulated distillation
Std. Dev.	Standard deviation
TBP	True boiling point
Temp.	Temperature
TI	Toluene insoluble particles

VB	Vacuum bottom
VIS	Visbreaking
VR	Vacuum residue
VPO	Vapour pressure osmometer
WC	Western Canada

Greek letter

α	Gamma shape factor
α_{ij}	EF model: Binary Interaction Parameter
β	EF model term: Captures the effect of density on viscosity
Γ	Gamma probability function
γ	Activity coefficient
ρ	Density
ρ_s^*	EF model term: Compressed state density in a vacuum
ρ_s^o	EF model parameter: Compressed state density
v	Molar volume
ϕ	Volume fraction
Δ	Difference (Delta)
δ	Solubility parameter
ξ	Tuning parameter
μ	Viscosity

Subscripts

0	Feedstock property
37.7	Property at 37.7°C
273	Property at 273K

a	Aromatic fraction
Asph	Asphaltenes
avg	Average
D	Distillate fraction
dist	Distillate fraction
f	Feedstock property
m	Mixture
max	Maximum
Me	Measured property
min	Minimum
mix	Mixture
mono	Monomer
pr	Predicted property
s	Saturate fraction
r	Resin Fraction
Ref	Property at reference condition (273K)

Superscripts

α	Phase α
L	Liquid phase
H	Heavy phase

Chapter 1: Introduction

Alberta Energy Regulator estimated Alberta's oil sand proven reserves about 165.4 billion barrels of heavy oil and bitumen, the third largest oil sand reserves (Government of Alberta 2020). In Alberta, bitumen production is restricted by the limited pipeline capacity to external markets. The capacity is further limited because the bitumen must be diluted with a solvent to meet the pipelines' viscosity and density specifications (Luhning *et. al.*, 2002).

One way to increase the capacity for bitumen is to use a combination of partial deasphalting and visbreaking (Gray 2015; Zachariah and De Klerk 2017) to reduce the density and viscosity of the bitumen so that less diluent is required. Partial deasphalting uses a poor solvent to precipitate and remove some of the asphaltenes from the bitumen. The asphaltenes are the densest fraction of the bitumen; hence deasphalting reduces the product density but only moderately reduces its viscosity. Vibreaking is a mild liquid-phase thermal cracking method that only moderately changes the density of the bitumen but significantly reduces its viscosity (Joshi *et. al.*, 2008; Marquez *et. al.*, 2020). The viscosity reduction that can be achieved in a visbreaking process depends on the severity (residence time and temperature) of the process. There is an optimum severity below which there is less viscosity reduction and above which coke forms. Coke formation is undesirable because it leads to fouling. The visbroken product must also be stable versus asphaltene precipitation when blended with a diluent. Therefore, to optimize a visbreaking process it is necessary to predict the viscosity and stability (versus asphaltene precipitation) of the product.

Combining visbreaking and deasphalting processes may allow higher conversions to be attained in the visbreaking step by removing asphaltenes from the feed so that coking is delayed or removed from the product to increase its stability. Potential applications include treating the produced bitumen from an in-situ recovery surface prior to pipeline transport or treating a distilled product

such as a vacuum bottom from an oil sands extraction/froth treatment process. Hence it is necessary to predict the visbroken product properties from feeds including deasphalted oils, bitumen, and vacuum bottoms.

In previous studies, Rodriguez *et. al.,* (2019) visbroke a Western Canadian bitumen at five different combinations of temperature and residence time and measured the product stability in terms of asphaltene precipitation from the product diluted in *n*-heptane. They characterized the oils into distillate, saturate, aromatic, resins, and asphaltene fractions. They developed molecular weight, density, and solubility parameter correlations for each fraction for use in the Modified Regular Solution (MRS) model. The MRS model is a liquid-liquid phase equilibrium model developed to predict asphaltene precipitation from heavy oils diluted with solvents (Alboudwarej *et. al.,* 2003). Similarly, Marquez *et al.,* (2020) examined the same feed and products and updated the density correlations for the same fractions to predict the product density using a volumetric mixing rule. They also developed correlations for these fractions for use in the Expanded Fluid (EF) model to predict the product viscosity. The EF model correlates viscosity to density and was developed for heavy oils (Yarranton and Satyro 2009). The inputs for MRS and EF models are:

- The distillate, saturate, aromatic, resin, and asphaltene contents of the feed and product (from a distillation assay and residue SARA assay – see Section 2.2 for a description of the assays),
- The properties (density, molecular weight, solubility parameter, and viscosity model parameters) of the distillates and the SARA fractions of the feed.

Recommended property values were provided but these studies only considered a Western Canadian bitumen.

The objective of this project is to extend the models developed by Rodriguez *et. al.,* (2019) and Marquez *et al.,* (2020) to fractionated oils. A feed oil, its vacuum bottoms, and a partially deasphalted oil are evaluated. The oils are characterized into pseudo-components based on their distillation and SARA assays. The model parameters (molecular weight, density, viscosity, and solubility parameter) for each pseudo-component are measured or determined from existing correlations. The property correlations and models are tested on solubility and viscosity data collected for maltenes, vacuum residues, and whole oils and are updated as required.

1.1 Objectives

The goal of this study is to test and update and enhance the Expanded Fluid viscosity and the Modified Regular Solution stability model correlations to predict the viscosity and stability of visbroken oils. The method to predict their density is also updated. The methodology previously proposed by Rodriguez *et. al.*, (2019) and Marquez *et. al.*, (2020) was followed and included the following specific tasks:

1. Visbreak each oil at 2 different severity conditions.
2. Measure the density, viscosity, and solubility of the feed and product oils.
3. Perform a Simulated Distillation assay on each feed and product oil to determine the conversion. Conversion is a measure of the extent of reaction and will be discussed in Chapter 2.
4. Perform a spinning band distillation (SBD) on each feed and product oil to separate the oil into distillate and SBD residue fractions.
5. Measure the distillate density. Determine its molecular weight and viscosity from the distillation assay using an established methodology.
6. Measure the density, viscosity, and solubility of the SBD residues.
7. Perform a SARA fractionation on the SBD residues.
8. Measure the density and viscosity of the maltenes (all of the oil except the asphaltenes and distillates).
9. Measure or otherwise determine the density, viscosity, molecular weight, and solubility parameter of the SARA fractions.
10. Compare the fraction properties with the previously developed molecular weight, density, viscosity model parameter, and solubility parameter correlations and modify as required.
11. Test the density and viscosity predictions for the maltenes, residue and whole oil from the EF model and update the density and EF model mixing rules as required.
12. Test the solubility predictions for the residue and whole oil from the MRS model and update the model as required.

The solubility tests involve measuring the amount of asphaltene precipitation from mixtures of the oil and *n*-heptane or from a mixture of an oil fraction (saturates or aromatics) with asphaltenes and either toluene or *n*-heptane. The precipitation data for the oil fractions are fit with the MRS model

to determine the solubility parameter of that fraction. The precipitation data from the oils and residues are used to determine the distillate and asphaltene solubility parameters. The methodology is described in more detail in Chapter 4.

1.2 Thesis Structure

This thesis is organized in eight chapters and the remaining chapters are as follows:

- Chapter 2 provides the background information relevant to measuring and modeling the viscosity and stability of deasphalted and visbroken heavy oil. Asphaltene related phase behavior and the Modified Regular Solution are discussed. Heavy oil viscosity behavior and models include the EF model are presented. Finally, deasphalting and visbreaking processes are explained, their effects on oil composition and properties are described, and a review on combination of the processes is provided.
- Chapter 3 explains the experimental methods used in this thesis including: the procedures to separate the feed and product samples into distillates, residues, and SARA fractions; the apparatus and procedure used to visbreak the feed oils; the procedures to measure the molecular weight, density, viscosity of the oils and their fractions; and the measurements required to determine the fraction solubility parameters.
- Chapter 4 describes the methodology used to apply the Expanded Fluid viscosity model and the Modified Regular Solution stability model for visbroken oils. The oil characterization methodology is discussed and the Expanded Fluid and Modified Regular Solution models are presented. The methodology used to measure and determine the properties required for the models is also discussed.
- Chapter 5 presents the data measured in this study and describes the effect of visbreaking on oil composition and the molecular weight, density parameters, viscosity parameters, and solubility parameter of the fractions.
- Chapter 6 presents the modeling of the density and viscosity of the visbroken oils from the thesis dataset. Updated density and viscosity model parameter correlations and recommended values are proposed. The accuracy of the density mixing rule and EF model with the previous and updated correlations is compared. A tuning method is also proposed.
- Chapter 7 presents the modeling of the stability of the visbroken oils from the thesis dataset. Updated molecular weight and solubility parameter correlations and recommended values are

proposed. The accuracy of the MRS model with the previous and updated correlations is compared. A tuning method is also proposed.

- Chapter 8 summarizes the major outcomes of the project and provides recommendations for future work.

Chapter 2: Literature Review

The background information relevant to measuring and modeling the viscosity and stability of deasphalted and visbroken heavy oil is reviewed. Petroleum chemistry and petroleum characterization methods are discussed. Asphaltene related phase behavior data and models are presented. Similarly, heavy oil viscosity behavior and models are presented. Finally, the upgrading methods of deasphalting and visbreaking are explained and a review on the combination of the processes is provided.

2.1 Petroleum Chemistry

Petroleum materials can be categorized into three categories: native, derived, and manufactured (Speight 2006) as shown in Table 2.1. Native petroleum fluids are further classified based on their density and viscosity as shown in Table 2.2. This thesis is concerned with heavy oil, extra heavy oil, and bitumen.

Table 2-1. Classification of petroleum fluids (Gray 2015).

Native Materials	Derived Materials	Manufactured Materials
Natural gas	Saturates	Synthetic crude oil
Petroleum	Aromatics	Distillates
Heavy Oil	Resins	Lubricating Oils
Bitumen	Asphaltenes	Wax
Asphaltite	Carbenes	Residuum
Asphaltoid	Carboids	Asphalt
Ozocerite (Natural wax)		Coke
Kerogen		Tar
Coal		Pitch

Table 2-2 Definitions of petroleum fluids. The properties are at the standard condition of 15 °C. (Gray 2015)

Material	Gravity °API[1]	Density, kg/m³	Viscosity, mPa·s
Bitumen	<10	>1000	$>10^5$
Extra heavy oil	<10	>1000	$<10^5$
Heavy oil	10 – 19	900 – 1000	$10^2 – 10^5$
Medium crude oil	19 – 34	855 – 900	—
Light crude oil	34 – 42	815 – 855	—

[1] American Petroleum Institute gravity index

Crude oil is a mixture of an extensive range of hydrocarbons and other compounds that contain non-hydrocarbon elements such as sulfur, nitrogen, oxygen, and metals (Speight 2006). The content of carbon is usually in the range of 80 to 85 wt% while the hydrogen varies from 5 wt% in heavy residues to up to 14 wt% in light distillates. The sulfur, nitrogen, and oxygen contents are typically less than 4, 0.1, and 2 wt%, respectively (Fahim *et. al.*, 2010). The metals in crude oil are predominantly vanadium and nickel, typically in the range of 200 to 180 ppm and 80 to 50 ppm, respectively, for Albertian bitumens (Gray 2015). Metal contents are typically lower for lighter oils. The composition of some Alberta bitumens is given in Tables 2-3 and 2-4.

Table 2-3. Alberta bitumen composition in wt.% (Gray 2015)

Bitumen	Origin	C	H	N	O	S
Athabasca	Syncrude	83.1	10.6	0.4	1.1	4.8
Athabasca	Suncor	83.9	10.5	0.4	1.0	4.2
Cold Lake	-	83.7	10.4	0.4	1.1	4.4
Lloydminster	-	—	—	—	—	4.3

Table 2-4. Metal content of vacuum residues (+524 °C) (Gray 2015)

Origin	Metals, ppm	
	Nickel	Vanadium
Athabasca	150	290
Cold Lake	200	490
Lloydminster	140	190
Peace River	130	410

The molecules within petroleum fluids can be categorized into two broad categories, hydrocarbons and heterocompounds (Stenby and Yan 2005). Organic molecules that consist of only hydrogen (H) and carbon (C) are identified as hydrocarbons (Riazi 2005). Hetero compounds also contain one or more sulfur (S), nitrogen (N), oxygen (O), vanadium (V), nickel (Ni), or iron (Fe) atoms (Stenby and Yan 2005).

The general formula of a hydrocarbon is C_xH_y. Hydrocarbons can be categorized as paraffins, olefins, naphthenes, and aromatics. The three first groups are also known as aliphatic compounds. Each category is described below.

- Paraffins are also known as alkanes and their general formula is $C_nH_{2n+2,}$ where *n* is a natural number. They can make up to 20% of the crude oil volume. There are two types of paraffins, normal and isoparaffins. Normal paraffins (*n*-paraffins or *n*-alkanes) are saturated straight-chain hydrocarbons. Isoparaffins have branched structures.
- Olefins have at least one double bond in their chain structure. The double bond(s) makes the structure unsaturated and more reactive. Therefore, they do not usually occur naturally in petroleum fluids; however, they can be generated through cracking processes in refineries.
- Naphthenes or cycloalkanes have a cyclic structure. The general formula of these hydrocarbons is C_nH_{2n} (n>3) where five and six carbon naphthenic rings are the more stable configuration (Riazi 2005). Cycloalkanes can make up to 60% of the crude oil volume.
- Aromatics are found in almost all types of petroleum fluid and contain at least one aromatic ring (Speight 2017). An aromatic ring is an unsaturated planar compound of six carbons with the general formula of C_6R_6, where R can be any functional group. A widespread aromatic group in petroleum is alkylbenzene. Alkylbenzenes are composed of an aromatic with an alkyl group with the general formula of C_nH_{2n-6}. The species in heavy fractions or the residues of crude oil contain multiple benzene and naphthene rings and are solid under standard conditions. These molecules are termed polyaromatics or polynuclear aromatics.

There is a large variety of heterocompounds in crude oil. High-resolution mass spectroscopy has identified hundreds of thousands of species found in a large number of overlapping homologous

series (Marshall and Rodgers 2008, 2004; Hughey *et. al.*, 2001). A large number of chemical families have been identified including (Fahim *et. al.*, 2010b):

- Sulphur compounds such as mercaptans or thiols, sulphides, thiophenes, and polycyclic sulphides.
- Oxygen compounds such as alcohols, ethers, carboxylic acids, phenolic compounds, ketones, esters, and anhydrides.
- Nitrogen compounds in basic forms such as pyridines and non-basic compounds such as pyrroles.
- Metals such as zinc, titanium, calcium, and magnesium can be present as oil-soluble organometallic compounds in the form of organometallic soaps. Metals such as vanadium, nickel, copper, and iron can be present in complexes with pyrrole compounds.

Overall, petroleum is a complex mixture of many hydrocarbon compounds and it is impossible to determine its exact composition. However, the crude oil species generally follow consistent trends in properties such as boiling point and molecular weight as shown in Figure 2-1. These trends make it possible to characterize the property distributions of crude oils into a set of representative fractions.

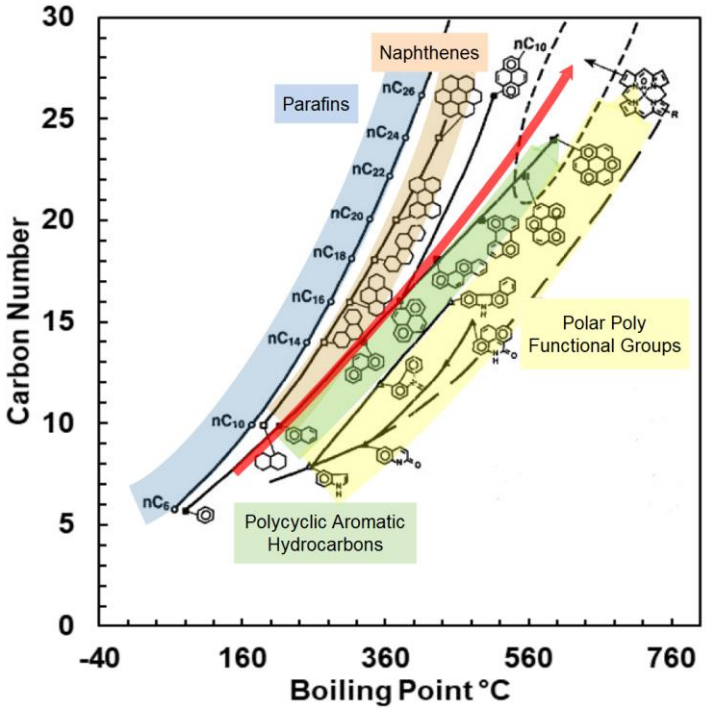

Figure 2-1. Effect of chemical structure on boiling temperature. The red line shows how the average carbon number and boiling point follow a monotonic trend (Adapted from Altgelt and Boduszynski, 1994).

2.2 Petroleum Characterization

Petroleum characterization is the division of petroleum into components and pseudo-components that represent the distribution of properties within the petroleum. Since petroleum contains a broad mixture of ill-defined molecular species, it is impossible or practical to characterize it by its molecular composition. Instead, petroleum is characterized based on other types of compositional analysis (Riazi 2005). The main types of analysis used in the oil industry are distillation, gas chromatography, and SARA fractionation, and each is described below.

2.2.1 Distillation

Refineries commonly fractionate petroleum by distillation (Speight 2014). In distillation, the oil is slowly and evenly heated, using vacuum or not, and the temperature and volume of the distillates are measured. The recorded temperatures at the operating pressure are converted to a standard of atmospheric distillation and the data is reported as true boiling point (TBP) or atmospheric equivalent temperature (AET) versus the volume distilled (Riazi 2005), as shown in Figure 2-2.

The first recorded number is the boiling point of the lightest component and it is known as the initial boiling point (IBP) and the last recorded number is called the final boiling point (FBP). The FBP of crude oils cannot be measured accurately since the heavy fractions may never vaporize. Also, heating the oil to temperatures higher than 350°C may alter the chemistry of the compounds instead of vaporizing. Therefore, FBP is the maximum temperature of the test. The remaining oil that has not vaporized after reaching FBP is called residue (Riazi 2005).

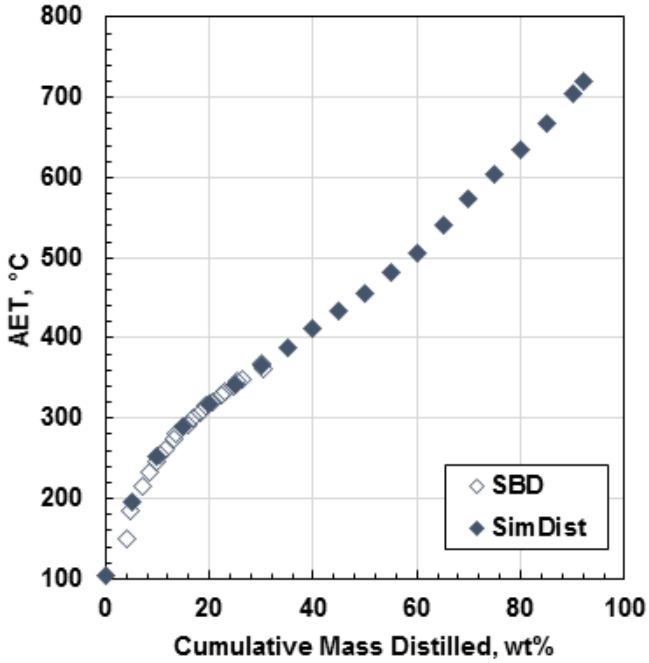

Figure 2-2. A boiling curve for the WC-B-A4 bitumen obtained from spinning band distillation (SBD) compared with simulated distillation (SimDist) data.

The standard distillation techniques developed for crude oil are summarized below.

- ASTM D86: The test is conducted with 100 mL of sample at atmospheric pressure. The results report the directly measured boiling point temperature versus cumulative vaporized volume. Usually, the final boiling point is not accurate and is lower than the TBP. Although cracking reactions are only significant at temperatures above 350°C, the reported temperatures above 250°C should be used with caution (Riazi 2005; ASTM 2015).
- ASTM D1160: This procedure was developed for heavy oils where atmospheric distillation temperatures might alter their chemistry with cracking reactions. Here the pressure is reduced from atmospheric and typically for heavy oils is conducted at 1, 2, 10, or 50 mm Hg. The

distillation is finished when the vapour temperature reaches 400°C. The vapor temperatures are converted to AET using Maxwell and Bonnell (1957) correlations (Riazi 2005; Drews 2008).

- ASTM D2892: The procedure is for distillation of crude oils to a final boiling temperature of 400°C AET. The test is conducted with a column consisting of 14 to 18 theoretical plates and operates at the reflux ratio of 5:1. The pressure can be set to atmospheric or lower to 2 mm Hg and when vacuum is used, the vapour temperatures should be converted to AET using Maxwell and Bonnell (1957) correlations (ASTM Standard D2892 2009).
- ASTM D5236: This test is an extension of ASTM D2892 and is typically for heavy petroleum mixtures with initial boiling points greater than 150ºC. Therefore, if the oil has light fractions, ASTM D2892 should be conducted before performing ASTM D5236. The operating pressure is kept between 0.1 to 50 mm Hg and the FBP is no more than 565ºC AET. A downside of this method is that it does not have the separation capability of ASTM D2892, and consequently, the recorded boiling points are lower than TBP (Drews 2008).
- Spinning Band Distillation (SBD): This technique uses a rotating helical band to create a high number of theoretical plates. The rotating band creates intimate contact between the two phases by forcing the rising vapours into close contact with the descending condensate. This technique typically creates 50 theoretical plates and TBP are determined with a reflux ratio of 5:1. The pressure of the column can be reduced to 1 mm Hg and AET up to 450ºC can be achieved. Maxwell and Bonnell (1957) correlations are used to convert the recorded vapour temperatures to AET. This method was used in this thesis and is described in more detail in Chapter 3. An example of an SBD distillation curve is provided in Figure 2-2.

2.2.2 Gas Chromatography

Chromatography is a separation method where the separated components are distributed over two phases, the stationary and mobile phases. The mobile phase is defined as a fluid or gas that percolates through or along the stationary bed. The stationary phase may be a solid, gel or liquid (Ardrey 2004). In the petroleum industry, many chromatographic methods have been developed. The method relevant to this thesis is simulated distillation.

In this method, the oil sample is injected into a stream of carrier gas which sweeps the sample into a lengthy column in an oven. The column is packed with a specified adsorbent which preferentially adsorbs the heavier components of the oil. As the oven temperature is ramped up, the lighter adsorbed components are the first to be volatilized and swept to a thermal conductivity detector; hence, they have lower retention times. The normal boiling points of compounds are calibrated to their retention time. The amount of each compound is proportional to the signal intensity. Hence, this technique yields the boiling point curve (Adlard 1995; Riazi 2005). Depending on the fluid to be analyzed, there are several simulated distillation methods such as ASTM D2887, D5307, D6352, and D7169. ASTM D7169 was used in this thesis since the final boiling point of this test is 720°C which is suitable for bitumen analysis. A typical boiling curve by simulated distillation is shown in Figure 2-2.

2.2.3 SARA Fractionation

Jewell *et al.* (1972) developed a technique for oil characterization that led to standard SARA fractionation methodologies (Kharrat et al. 2007). SARA fractions are often used to characterize bitumens since bitumens have a small distillable fraction and the information provided by distillation is limited. SARA represents saturates, aromatics, resins, and asphaltenes. The asphaltenes are separated from the oil by precipitation with an *n*-alkane (usually *n*-pentane or *n*-heptane) and hence are a solubility class. The deasphalted oil (maltenes) is then separated into saturates, aromatics, and resins by liquid chromatography (Riazi 2005). Hence, the saturates, aromatics, and resins are adsorption classes. SARA fractionation is used in this thesis and is described in more detail in Chapter 3.

The saturates consist of paraffinic and naphthenic species with an average carbon number in the range of C38-50. The aromatics, resins, and asphaltenes are a continuum of aromatic species with increasing molecular weight, density, aromaticity, polarity, and heteroatom content (Riazi 2005). Aromatics are slightly aliphatic with lightly condensed aromatic rings and an average carbon number of C41-53. Resins have fused aromatic rings with 40 to 53% of aromatic carbon content. Asphaltenes have a more complex aromatic structure than resins due to their multiple fused aromatic rings (Shukla 2018; Sawarkar et al. 2007). The asphaltenes are a key component of this thesis and are discussed in more detail in the next section.

2.3 Asphaltenes and Oil Stability

2.3.1 Asphaltene Chemistry

Asphaltenes are defined as the crude oil components that are insoluble in *n*-alkanes such as *n*-pentane or *n*-heptane, but soluble in aromatic solvents such as toluene (Speight 2006). They are the heaviest and the most polar constituents of petroleum (Mohammed *et. al.,* 2021). Their molecular structures consist of polyaromatics cores with attached heteroatoms and aliphatic chains (Tavakkoli et al. 2015). Their atomic composition typically falls within the following ranges: carbon 82±3 wt%, hydrogen 8.1±0.7 wt%, oxygen 0.3-4.9 wt%, sulfur 0.3-10 wt%, and nitrogen 0.6-3.3 wt% giving an average atomic formula of approximately $C_{61}H_{72}O_{1.4}S_{1.4}N$ assuming a molecular weight of 1000 g/mol. They typically contain the majority of the metals (vanadium, nickel, and iron) within the crude oil (Chacón-Patiño *et. al.,* 2v017; Alimohammadi *et. al.,* 2019; Mohammed *et al.,* 2021). Their molecular weights range from 6z00-1000 g/mol (Chacon-Patino *et al.,* 2018).

Asphaltenes have a variety of chemical structures. The two main structure models are the island and archipelago models. The island model states that a monomeric asphaltene structure consists of 6-7 aromatic rings condensed with several aliphatic groups. The archipelago model states that monomeric asphaltenes have dispersed polynuclear aromatic groups connected by alkyl or other types of bridges (Chacón-PatinÌo *et. al.*, 2018). The bridging chains in this structure create many molecular conformations that are different from the island model and form a more complex set of aggregates (Murgich 2003). Several studies have shown that both of these two structures may co-exist within asphaltenes (Gray *et. al.,* 2011; Mullins *et. al.*, 2012; Chacón-PatinÌo *et. al.*, 2018).

Asphaltene can self-associate through various mechanisms (such as π–π bonding, acid-base interactions, and hydrogen bonding) to form larger structures termed nano-aggregates (Yarranton, 2005; Afra *et. al.*, 2017). Asphaltene self-association has been observed with various techniques such as small-angle neutron and x-ray scattering (Xu *et. al.,* 1995; Barré *et al.,* 2009), size exclusion chromatography (Juyal *et. al.,* 2005), and vapour pressure osmometry (Yarranton *et. al.*, 2000). Vapour pressure osmometry is the only method that provides molecular weight rather than size and has shown that the nano-aggregates molecular weights can reach 50,000 g/mol or higher. The average molecular weights are in the order of 5000 g/mol, indicating an aggregation number

of 5-10 molecules per aggregate (Yarranton 2005). The extent of aggregation decreases at lower asphaltene content, higher temperature, in better solvents, and in the presence of resins (Yarranton *et. al.*, 2000; Yarranton 2005; Yarranton *et. al.,* 2007; Yarranton *et al.,* 2013).

2.3.2 Asphaltene Precipitation

Asphaltenes can precipitate and deposit upon a change of temperature, pressure, or composition, leading to flow assurance challenges during oil production, recovery, and refining operations (Zheng *et al.,* 2020; Riazi 2005). The application of interest in this thesis is the precipitation of asphaltenes from heavy oils and visbroken products with the addition of a solvent. Asphaltene precipitation from unmodified heavy oils is discussed in this section. The effects of visbreaking are discussed later.

Mixtures of heavy oil and paraffinic solvents can exhibit vapor-liquid, liquid-liquid, and vapor-liquid-liquid equilibrium depending on the temperature, pressure, composition, and the carbon number of *n*-alkane (Johnston *et al.,* 2017). For example, Figure 2-3a illustrates the phase behavior of a mixture of a bitumen with pentane at 180°C. At conditions below the saturation pressure, the solvent is mostly in the vapor phase with a finite solubility in the liquid phase. When the pressure is raised above the saturation pressure at a low fixed solvent content, the mixture forms a single liquid phase. When the pressure is raised above the saturation pressure, at a high enough fixed solvent contents, two liquid phases form: a light solvent-rich phase and a heavy asphaltene-rich phase. Similarly, when the solvent is added to a mixture at a fixed pressure above the saturation pressure, the initial liquid phase will separate into two liquid phases. The condition at which the second phase forms is termed the “onset”. Usually, the onset of precipitation is defined as the temperature, pressure, or composition at which the precipitated asphaltenes first form. In this thesis, the onset is defined as the solvent content at which precipitation occurs.

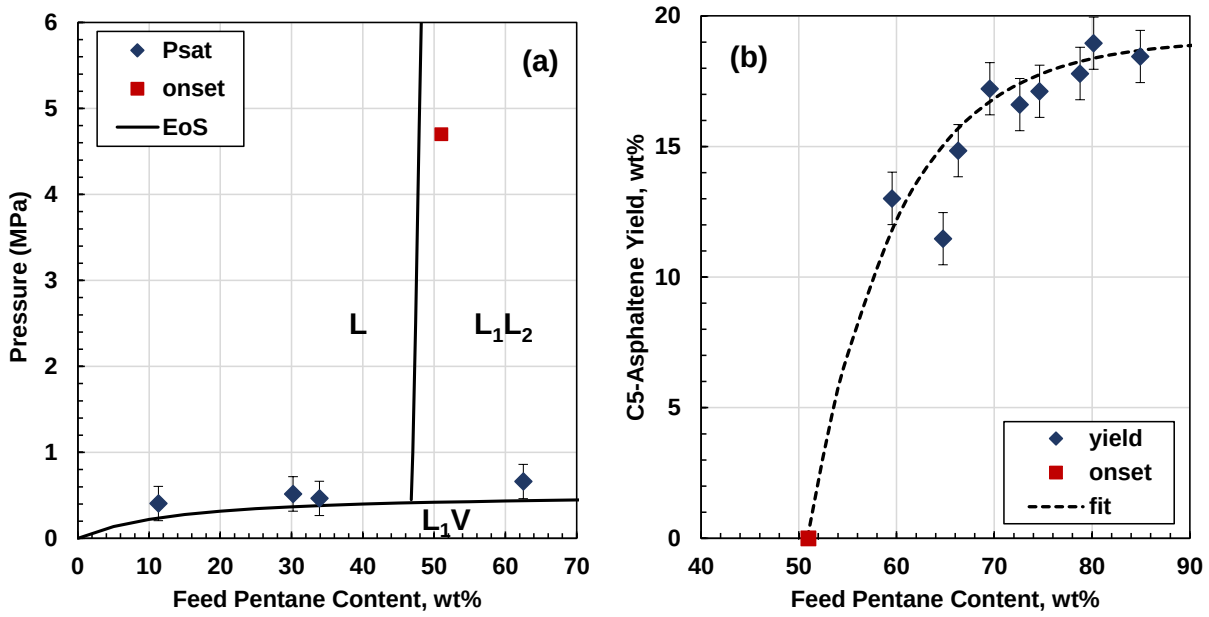

Figure 2-3. Phase diagrams for mixtures of Western Canadian bitumen with *n*-pentane at 90°C: a) vapor-liquid and liquid-liquid boundaries; b) asphaltene yield in the liquid-liquid region at 4.8 MPa (Adapted from Johnston *et. al.*, 2017).

This thesis is concerned only with the liquid-liquid region. In this region, the amount of heavy phase (and therefore the amount of asphaltene precipitation) increases as the solvent content increases as shown in Figure 2-3a. The amount of asphaltene precipitation is commonly presented as a yield where yield is defined as the mass of asphaltenes in the precipitate (or heavy liquid phase) divided by the mass of crude oil in the feed.

The main factors determining the onset and yield of asphaltene precipitation in solvent and heavy mixtures are the solvent type and content (Johnston *et al.*, 2017). Most of the available phase behavior data are for mixtures of heavy oil and *n*-alkanes. Asphaltene solubility in these mixtures increases as the carbon number of the *n*-alkane increases from 3 to 7 and then slightly decreases for carbon numbers above 10 (Ali and Al-Ghannam 1981; Andersen and Birdl 1990; Hu and Guo 2001; Mannistu *et. al.*, 1997; Wiehe *et al.* 2005; Johnston *et al.*, 2017). The more soluble the asphaltenes, the more poor *n*-alkane is needed to reach the onset and the amount of precipitants are less at a given *n*-alkane content above the onset (Johnston et al. 2017). Figure 2-3b shows how yield increases with increasing solvent content.

Temperature and pressure have less effect on asphaltene precipitation from heavy oils. Some researchers have stated that the solubility increases with temperatures up to 100°C (Akbarzadeh *et al.*, 2005; Ali and Al-Ghannam 1981; Hu and Guo 2001) and then possibly decreases (Andersen and Birdi, 1990). Johnston *et. al.,* (2017) found a maximum in asphaltene solubility in mixtures of *n*-pentane and heavy oil at approximately 90°C. However, the temperature had little or no effect on asphaltene precipitation, consisting of heavy oil and *n*-butane (Perez Claro *et. al.,* 2019) and propane (Mancilla-Polanco *et. al.,* 2017). An increase in pressure was found to increase asphaltene solubility slightly in all cases (Johnston *et. al.,* 2017; Perez Claro *et. al.,* 2019; Mancilla-Polanco *et. al.,* 2017).

In addition to the solubility, temperature affects the physical appearance of the asphaltenes. In mixtures of asphaltenes and *n*-pentane or higher carbon number *n*-alkanes and at temperatures below 100°C, the asphaltene-rich phase appears as glass-like micron-scale particles rapidly flocculate (Luo *et.al.*, 2010; Rastegari *et. al.*, 2004). At temperatures above 100°C, the asphaltene-rich phase appears as a liquid (Agrawal *et al*., 2012; Zou *et. al.*, 2005). The transition from glass to liquid states depends on temperature, *n*-alkane content, and the carbon number of the *n*-alkane. The transition temperature is lower for propane and *n*-butane than for *n*-pentane (Johnston *et. al.,* 2017; Perez Claro *et. al.,* 2019; Mancilla-Polanco *et. al.,* 2017). This thesis is concerned only with the low-temperature region where asphaltenes appear as particles.

2.3.3 Asphaltene Precipitation Modeling

There are two approaches to describe asphaltene phase behaviour: colloidal theory-based and thermodynamic solubility models (Alimohammadi *et. al.,* 2019). The colloidal approach assumes that asphaltenes are dispersed in the oil as colloids consisting of stacked asphaltene molecules. The colloids are stabilized by resins adsorbed on or surrounding the colloids and preventing their flocculation. When a sufficient amount of resins is desorbed, asphaltenes flocculate and physically separate from the oil. However, this model is not predictive and does not explain why asphaltenes remain dispersed after dilution with aromatic solvents (Powers *et al.,* 2016; Mohammed *et al.,* 2021).

Solubility approaches are more commonly used. The asphaltene nano-aggregates are considered to be soluble in the oil and asphaltene precipitation is simply a reversible chemical thermodynamic phase transition. Changes in temperature, pressure, and composition can cause the crude oil to split into two liquid phases. The two main approaches in this category are equations-of-state and regular solution models.

Equation of State (EOS) approaches, such as Peng-Robinson and Soave-Redlich-Kwong, describe the full phase equilibria and are well-performed for predicting phase envelopes in vapour-liquid phases (Soave 1972; Peng and Robinson 1976). However, their ability to predict asphaltene yields is poor (Díaz *et al.*, 2011; Johnston *et al.*, 2017). Better predictions have been obtained with the cubic plus association EOS (Li and Firoozabadi 2010b, 2010a; Arya *et al.*, 2016, 2017) and the statistical associating fluid theory (SAFT) EOS (Ting *et. al.*,2003; Gonzalez *et al.*, 2005). However, these models are complicated and not yet widely used in commercial simulators.

The Regular Solution Model is an activity coefficient-based phase equilibrium model based on two thermodynamic contributions of enthalpy and entropy of mixing. The entropy of mixing is based on Flory and Huggins lattice theory that developed a thermodynamic model for mixtures of polymers and solvents (Flory 1941; Huggins 1941). The enthalpy of mixing is based on Scatchard-Hildenbrand theory built on the Van Laar activity model (Scatchard 1949; Hildebrand 1949). The model has been modified and successfully applied to predict asphaltene precipitation in asphaltene solvents and bitumen-solvent systems (Hussein Alboudwarej et al. 2003; Akbarzadeh et al. 2005, 2004). The modified model was extended to samples that undergo thermal cracking (Powers *et al.* 2016) and visbreaking Rodriguez *et al.*, (2019) reactions. This thesis uses the Modified Regular Solution approach and the model is presented in more detail in Chapter 4.

2.4 Oil Viscosity

Viscosity is arguably the most important transportation property of heavy oil and is a function of temperature and pressure. The temperature has a strong effect as shown in Figure 2-4a where the viscosity changes four orders of magnitude from 20 to 180°C. The addition of solvents can have an equally significant effect as shown in Figure 2-4b (Ramos-Pallares *et al.*, 2016). Heavy oils have high amounts of asphaltenes and can exhibit non-Newtonian behavior (Abivin *et. al.*, 2012;

Soto-Castruita *et al.*, 2015). However, in most practical applications, the temperature is high enough (above approximately 30°C) or solvent is added, and the heavy oil is Newtonian. Therefore, only Newtonian viscosity is considered here.

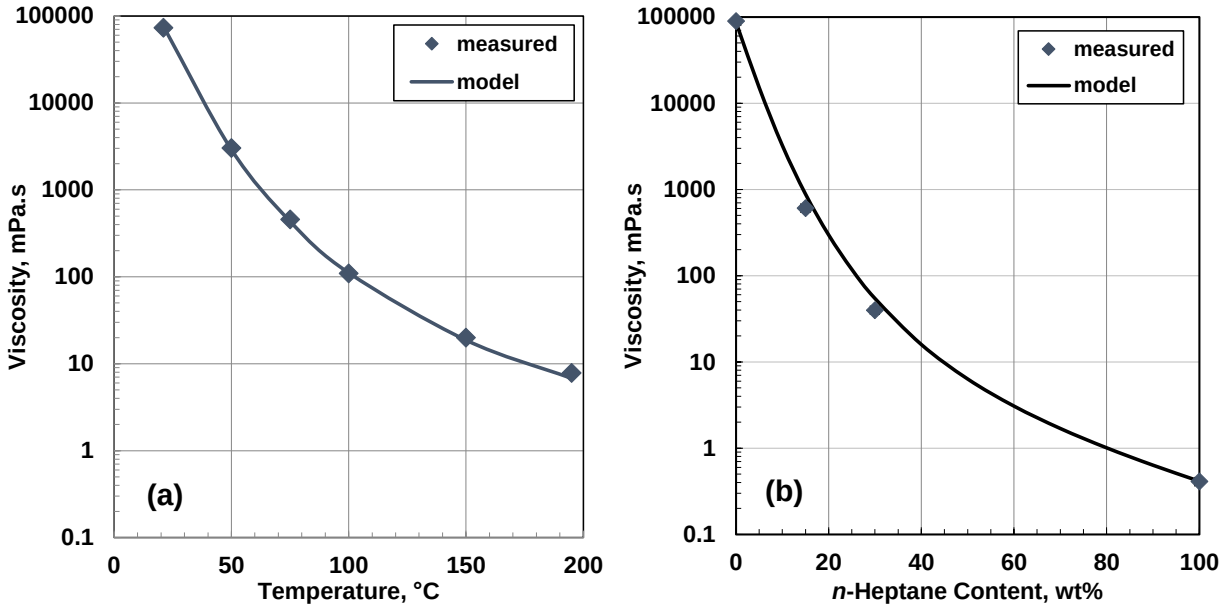

Figure 2-4. Measured and modeled (EF model) viscosity of a Western Canadian bitumen at atmospheric pressure: a) effect of temperature on undiluted bitumen; b) effect of *n*-heptane content on diluted bitumen (adapted from Ramos-Pallares *et al.*, 2016).

Since petroleum is a mixture of undefined fluids that must be characterized to obtained relevant parameters, it has proven challenging to develop a theoretical or even a semi-theoretical method for viscosity calculation (Collett and. Robson, 2010). Many correlations and models have been proposed. The main models applicable to the complete gas-liquid phase diagram (and therefore for process simulation) are outlined below.

2.4.1 Corresponding States Models

The corresponding state principle concept is that the reduced or dimensionless property of one fluid is equal to another reference substance at the same reduced conditions. In viscosity modeling, the reduced properties are temperature and pressure (Baled *et al.* 2018). Ely and Hanley (1981a,b) proposed the Transport Properties Prediction (TRAPP) model with methane as the reference fluid. The model requires two empirical shape factors for which correlations were provided. The inputs

of the model are the viscosity and density of methane (reference fluid), and the critical properties of the fluid to be modeled. This model was tested on various crude oils and fractions and the average and maximum deviations were 6.5% and 32.7, respectively (Baltatu 1982). While 33% may seem like a high deviation, it is challenging to model viscosity because it changes exponentially with changes in temperature and composition. Deviations below 30% are usually considered to be acceptable for modeling the viscosity of crude oils and their fractions. However, the model errors for high boiling hydrocarbons and polar liquids may be significantly higher (Das and Singh, 1999).

Tham and Gubbins (1970), Christensen and Fredenslund (1980), and Pedersen *et. al.,* (1984, 1987) developed a corresponding states approach for light oils. The model also uses methane as the reference fluid and requires one empirical parameter, and the rotational coupling coefficient captures the molecular size and density effects. The accuracy of the model compared to measured data was reported to be within 10 to 15%. Lindeloff *et al.* (2004) found that the accuracy decreased for fluids with viscosities higher than 10 mPa·s.

Teja and Rice (1981) extended the corresponding states principle to use two non-spherical reference fluids for the liquid mixtures. However, this method requires that the reference fluids be chosen that are similar to the fluid of interest, and such reference fluids are not available for heavy oils (Baled *et. al.,* 2018). Aasberg-Petersen *et. al.,* (1991) adapted this approach using methane and *n*-decane as the two reference fluids. The model predicts the viscosity of hydrocarbons using molecular mass instead of the acentric factor used in the Teja-Rice model. The model is only applicable to the reduced temperatures above 0.47 and predicts the viscosity of light petroleum fractions accurately. Moharam and Fahim, (1995) extended the model to bitumens and fractions using *n*-decane and *n*-eicosane as reference fluids. Their model applies to reduced temperatures between 0.47 and 0.4 and was tested on heavy petroleum fractions with 5% overall deviation.

2.4.2 Friction Theory

In this approach, viscosity is expressed as a residual property or departure function from the diluted gas viscosity. The diluted gas viscosity is only relevant to calculate gas viscosities and for liquids near the critical point. The term is often neglected for liquid viscosities. Quiñones-Cisneros *et. al.,*

(2000) developed the friction theory from the classical friction concept to predict the viscosity of dense fluids. The residual viscosity term is linked to the repulsive and attractive terms of pressure (P_r and P_a) of an equation-of-state (Soave 1972; Stryjek and Vera 1986). The model requires three fitted friction coefficients and was successfully tested on *n*-alkanes up to *n*-decane. Baylaucq *et. al.,* (2002) modified the model for elevated pressures.

Quiñones-Cisneros *et. al.,* (2001a) later proposed a generalized version of their model where the model parameters were only dependant on the reduced temperature and were correlated to 16 universal EOS specific constants (Quiñones-Cisneros, Zéberg-Mikkelsen, and Stenby 2001a). The authors extended their model to well-categorized oils and live reservoir oils (Quiñones-Cisneros *et. al.*, 2001b, 2003). The accuracy of the friction model for live oils was reported to be within the uncertainty of the measurements; that is, up to 20% (Quiñones-Cisneros *et. al.*, 2003). The extended model was tested on several oils and an average absolute deviation (AAD) of 15% was reported (Quiñones-Cisneros *et. al.*, 2001b). The friction theory application to heavy oils has been reported to have large uncertainties because of the difficulty in acquiring their critical properties (Kumar *et. al.*, 2011).

2.4.3 Free Volume Theory

This model assumes that viscosity is exponentially related to the free volume inverse where free volume is the space between molecules (Cohen and Turnbull, 1959; Doolittle, 1951). The free volume is expressed as the ratio of the volume of the fluid at a given state divided by the fully compressed dense state volume. The free volume fraction was later related to temperature and a diffusion energy barrier using fluctuation-dissipation theory (Allal *et. al.,* 2001a, 2001b). The dense state viscosity was related to the size of the molecules in the fluid. The model requires three parameters for each fluid that must be obtained from fitting experimental data (Baled et al. 2018). Optimized values of the parameters have been determined for some common fluids (Tan *et al.*, 2005; Burgess *et al.*, 2012; Llovell *et. al.,* 2013). Free volume theory has been coupled with the soft-SAFT EOS and the parameters were correlated to the molecular weight of *n*-alkanes (Blas and Vega 1997; Llovell *et. al.*, 2004; Llovell and Vega 2006).

The free volume theory was evaluated on different fluids over wide ranges of temperature and pressure. The average absolute deviation reported for the model was reported as less than 10% for in the gas, liquid, and dense states (Boned *et al.*, 2004; Llovell *et. al.*, 2013; Burgess *et al.*, 2013; Yoshimura *et al.*, 2010; Meng and Wu 2013; Oliveira *et al.*, 2014; Polishuk and Yitzhak 2014; Shen *et al.*, 2014; Abolala *et. al.*, 2015). Porte and Kossack (2014) applied the free volume theory to long chain *n*-alkanes up to C_{64} and reported an AAD of 6% with a maximum deviation of 31%. Porte *et. al.*, (2014) extended the work to model viscosity of heavy oils in thermal recovery methods such as CSS, SLD, and SAGD. The error for the viscosity modeling was reported explicitly.

2.4.4 Expanded Fluid Viscosity Model

The Expanded Fluid (EF) model developed by Yarranton and Satyro, (2009) is specifically for heavy oils but applies to all hydrocarbon liquids. They observed that the inverse of viscosity and fluidity increases as the fluid expands and proposes a double exponential relationship to density. The model has three empirical fluid specific parameters. Tables of parameters were provided for common hydrocarbons. Motahhari *et al.*, (2013) and Ramos-Pallares *et al.*, (2016) extended the model to characterized crude oils. Correlations were provided for the fluid specific parameters of the boiling cut fractions characterized based on a distillation assay. The error of the model for the heavy hydrocarbons, heavy oils, and bitumens was reported as 2.7, 9, and 2% of ARD, respectively (Yarranton and Satyro 2009). This model is used in this thesis and is presented in more detail in Chapter 4.

2.5 Deasphalting and Visbreaking Heavy Oil

2.5.1 Deasphalting Processes

Solvent deasphalting (SDA) processes use light paraffin solvents such as propane, butane, pentane, or hexane to precipitate the least soluble fractions of petroleum. The precipitants can be used in the range of one to 50% of the original feed depending on the solvent and the desired solvent-to-bitumen ratio (Gray 2019). The solvent can be in the liquid or supercritical phase (Castañeda *et. al.*, 2012).

SDA processes have been adopted in some refineries prior to catalytic cracking (Maples 2000; Speight 2011). The deasphalted oil has a lower density, sulfur, nitrogen, and metals and a lower Conradson carbon residue or micro carbon residue (MCR) number (Gray, 2019). Hence, there is less potential for coke formation and catalyst activation in the reactor. The DAO can be used as the feed for finished lubricant preparation, catalytic cracking, hydrocracking plants, or to produce a low-cost feed for gasification process (Castañeda *et. al.*, 2012). DAO have a lower density than the feed and therefore SDA processes can also be used to lower the amount of required diluent for bitumen to meet pipeline specifications (Gray 2019).

Two disadvantages of SDA processes are a lack of residue conversion and the high viscosity of the produced asphalt (Castañeda *et. al.*, 2012). The asphalt residue cannot be processed in visbreaking due to the high amount of coke produced (Carrillo and Corredor 2013). The residues can be used for low-grade fuel, material for packing roads, or can be utilized in gasification to produce heat and hydrogen (Lee et al. 2014); otherwise, they must be sold or disposed of (Gray 2019). However, in Western Canada, the asphalt market is already filled and the produced asphalt cannot be sold (Gray, 2015).

2.5.2 Effect of Deasphalting on Oil Properties

Several studies have shown that the first precipitated fraction of asphaltenes in solvent processes have the highest molecular weights, metal contents, and aromaticity and lowest hydrogen-to-carbon ratio and solubility of all the oil fractions (Tojima *et. al.*, 1998; Okhotnikova *et. al.*, 2011; Trejo *et. al.*, 2004, 2007; Fossen *et. al.*, 2007). Deasphalting removes the least soluble asphaltenes, and therefore, the product oil is expected to have higher hydrocarbon content, lower, density, lower viscosity, and greater stability. The effect on stability is predictable. By its nature, deasphalting will shift the onset of precipitation to approximately the solvent content at which the deasphalting was performed. Fractionation studies have shown that selectivity is low in solvent-based fractionations (Rogel *et. al.*, 2015) even though data are scarce and likely specific to the asphaltenes in the study. Hence, the composition of the remaining and many properties of the asphaltenes may not differ to a great extent from the separated asphaltenes. Viscosity is an exception because it can be sensitive to small changes in the material.

Few published studies quantified the effect of deasphalting on density and viscosity. Gray (2015) found that deasphalting processes did not dramatically decrease the density of the oil. The effect on viscosity was more significant than the viscosity. For example, deasphalting 28 wt% of a Cold Lake bitumen decreased the respective density and viscosity from 1000 kg/m³ and 54500 mPa·s at 25°C to 960 kg/m³ and 1200 mPa·s (Brons and Yu 1995). If 40 wt.% of the bitumen was separated, the specific gravity would be 940 kg/m³ and the viscosity would be near pipeline specifications (Gray 2015; Brons and Yu 1995). Ramos-Pallares *et. al.*, (2016) found that deasphalting a bitumen with 16 wt% asphaltenes reduced the density by 20 kg/m³ and the viscosity by an order of magnitude.

2.5.3 Visbreaking Processes

Thermal processes such as visbreaking decompose, rearrange, or combine molecules of hydrocarbons by application of heat. Visbreaking, or viscosity breaking, is a relatively low-cost and low severity thermal cracking process that was initially introduced to lower the viscosity and upgrade the residues into saleable fuel oil. Currently, the process is the most popular choice of processing heavy feeds and residues (Gray 2015). Low conversion thermal cracking processes can partially remove entangled sidechains that are thought to create high viscosities in oil. This makes the process attractive in meeting specification for transportation pipelines (Speight 2014; Gray 2015). In Canada, visbreaking has emerged as an important technology to partially upgrade bitumens and reduce their viscosity (Yan *et al*., 2020).

Two versions of visbreaking are generally practiced in the industry as the furnace (coil) and soaker processes. The coil processes operate at high temperatures of 470-500°C and short residence time from less than a second to a few minutes. Soaker technology uses a soaker drum combined with the furnace to reach the same conversion level at lower temperatures of 430-450°C with higher residence times in the range of 10 to 30 minutes. The pressure, in either case, is kept at 0.3 to 5 MPa to maintain the fluid in the liquid phase so that the residence time is uniform and there is no fluid bypass (Speight 2014; Joshi et al. 2008; Gray 2015). The extent of the reaction, or conversion, is defined based on the change in the fraction of vacuum residue with boiling points above 524°C, denoted as +524°C (Powers *et al.*, 2016).

$$X = \frac{(+524℃\ Feed) - (+524℃\ Product)}{+524℃\ Feed} \quad (2.1)$$

where *X* is the conversion.

Visbreaking depends on the process residence time and temperature. Thermal cracking initially decreases the viscosity of the oil. However, as the intensity (temperature and residence time) of the process increases, the reacted asphaltenes lose their alkyl side chains and become less soluble in the reacted fluid. In addition, the chemical changes in the rest of fluid make it a poorer solvent for asphaltenes. Consequently, at high enough conversions, the asphaltenes precipitate (Speight 1998; Rodriguez *et al.*, 2019). The reacted asphaltene can also polymerize. At high conversions, condensation reactions predominate and lead to the formation of coke which is a solid phase, carbon-rich, and hydrogen-lean substance that fouls reactors (Joshi et al. 2008; Speight 1998). Coke formation is related to asphaltene content and severity of thermal cracking (Yan 1989; Del Bianco *et. al.*, 1993). Therefore, the operating condition of the visbreaking process is limited by the stability of the products and coke formation.

2.5.4 Effect of Visbreaking on Oil Composition

It is challenging to predict the distribution of products in thermal cracking since the involved reactions are a network of cracking and condensation reactions in parallel (Marquez 2019). The changes in oil composition have mainly been examined in terms of distillates and SARA fractions. Wiehe (1992) thermal cracked various residues and reacted SARA fractions independently to investigate the change in their properties. He proposed reaction pathways for each fraction as shown in Figure 2-5. The product contains an additional fraction, the volatiles. This fraction consists of light saturates and aromatics which cannot be easily separated into saturates and aromatics fractions due to their low boiling point. Note that the new generated SARA fractions may chemically differ from the same fraction class in the native oil. In addition, the proposed reaction pathways for the resins and asphaltenes may be an oversimplification. It has been reported in the literature that asphaltenes can produce resins and that resins can also contribute to coke formation (Fernando Trejo *et. al.*, 2010).

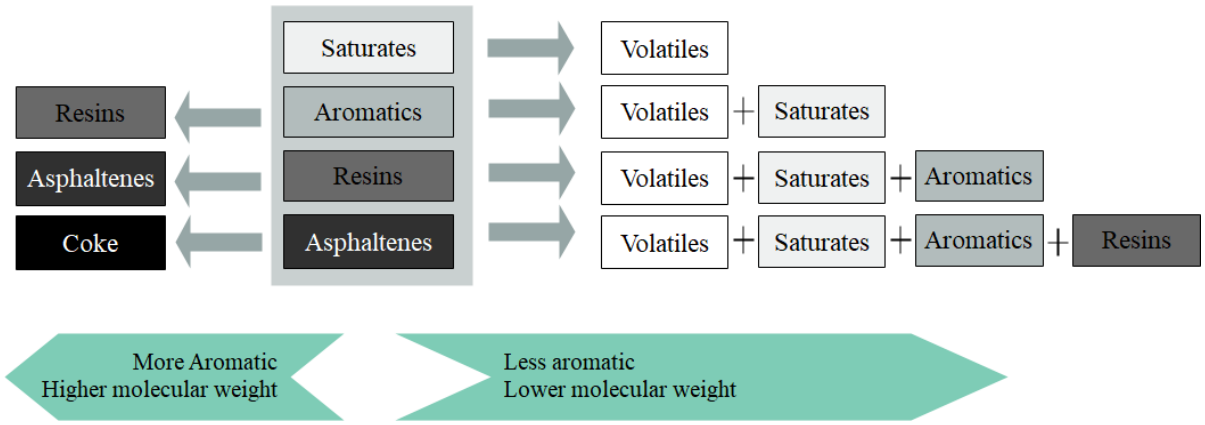

Figure 2-5. Simplified reaction paths for SARA fractions (Adapted from Wiehe, 1992).

In general, increasing the severity of thermal cracking leads to the formation of more volatile components, that is, distillable components (Al-Soufi *et al.*, 1988; Henderson and Weber 1965; Krishna *et al.*, 1988; Shu and Venkatesan 1983). The type of generated light ends depends on the composition of the feed. Dealkylation reaction dominated in oils with higher polar fractions while splitting reactions dominate in oils rich with saturates. Therefore, oils with more asphaltenes, resins, and polar tend to produce more gas. Oils that are rich in saturates have a higher tendency to produce gas-oil (Di Carlo and Janis 1992).

The saturate fraction mostly converts to shorter paraffinic chains and olefins through free radical mechanisms. The produced olefins can undergo thermal cracking to produce smaller olefins or diolefins that are highly reactive and can cause stability problems (Gray 2019). Aromatic compounds can produce smaller compounds such as saturates through de-alkylation reactions. However, aromatic polymerization (usually at high conversion) generates more aromatic and bigger size compounds and may form coke (Dawson *et al*., 1989).

Wiehe (1993) visbroke a Cold Lake vacuum residue and concluded that, at low conversions, asphaltenes would react to produce only compounds with lower molecular weights, consistent with a loss of side chains. He found that coke formation is infrequent as long as asphaltenes remain soluble since maltenes terminate the free generated radicals. However, at high conversions, a second phase, asphaltene-rich, forms and recombination of radical asphaltenes leads to coke formation.

At high conversion, non-asphaltene fractions can also react to form asphaltenes. Tannous and De Klerk (2019) thermally cracked a deasphalted oil at 400°C and employed indene to exacerbate asphaltene formation. They concluded that indene reacted with itself and the deasphalted oil, leading to the formation a new *n*-pentane insoluble phase. Indene diluted in indane and indene diluted in naphthalene were also added to the deasphalted oil prior to the thermal cracking. The addition of indene increased asphaltene formation. The addition of indene diluted with naphthalene reduced that amount while dilution of indene with indane had the lowest asphaltene formation. The result confirmed hydrogen transfer reaction chemistry based on molecule-induced homolysis, free radical addition, and propagation/termination.

Rodriguez *et al.*, (2019) visbroke a Western Canadian bitumen at conversions up to 38%. They confirmed that the main change in composition with conversion was an increase in the distillates content. The relative proportion of asphaltenes in the residue decreased as conversion increased up to approximately 10% conversion and then increased, possibly indicating a change in the reaction mechanism. The relative proportion of saturate, aromatics, and resins changed little with the conversion. At conversions above 10%, the toluene insoluble content increased notably indicating a loss of solubility in the former asphaltene fraction.

2.5.5 Effect of Visbreaking on Oil Density and Viscosity

Many studies have reported that visbreaking significantly reduces the viscosity of the oil but does not affect the density much (Gray 2019, 2015; Gray 1994; Speight 2011; El-Gendy and Speight 2015; Speight 2019). However, only a few publications quantify the effect of visbreaking on both density and viscosity. Shen *et al.*, (2008) studied the effect of residence time and reacting temperature on the density and viscosity of visbroken products. They visbroke an inner Mongolia oil sand bitumen mixed with an anti-coke agent (0.3 wt%) in a batch reactor at temperatures from 360 to 425°C and residence times from 20 to 100 minutes. They found that viscosity decrease almost exponentially both with increasing reaction temperature and with increasing residence time. They achieved up to 90% viscosity reduction. They also found that the product density increased almost linearly with increasing reaction temperature, by up to 20 kg/m^3 at 425°C.

Castillo and De Klerk, (2019) studied relatively low temperature visbreaking of Athabasca deasphalted vacuum residue. The visbreaking was performed in a microbatch reactor at a pressure of 5 MPa, temperatures of 280, 320, 360, and 400°C, and residence times of 10 to 360 minutes. The reaction had little effect at 280°C, but some viscosity reduction was observed at 320°C. The viscosity reduction increases at higher reaction temperatures, reaching four orders of magnitude at 400°C and 90 min residence time. The viscosity decreased exponentially with residence time and there was no viscosity reversal at high residence times. Viscosity reversal has been reported elsewhere and coincides with product instability (Meyers 2016). The product density increased with residence time by as much as 50 kg/m³ up to intermediate residence times but began to increase at higher residence times.

Marquez *et. al.*, (2020) thermally cracked a Western Canadian bitumen at five different conversions. They also observed an exponential decrease in viscosity with increasing conversion and achieved a 97% reduction in viscosity at the highest conversion (38%). Unlike Shen *et al.*, (2008), they found that the product density decreased up to 20% conversion and then increased at higher conversions. The maximum change in density was 14 kg/m³. They also characterized the oils into distillates and SARA fractions and measured the density and viscosity of the fractions. They observed that with increasing conversion, the viscosity of all of the fractions decreased. The density of the asphaltenes, resins, and aromatics increased with increasing conversion, but the distillate and saturate density decreased.

Dente *et. al.*, (1997) developed a viscosity correlation based on the Eyring viscosity model (Eyring 1936) for visbroken tars as a function of molecular weight, composition, temperature, and boiling point. However, they did not mention the effect of visbreaking on density. Rueda-Velásquez and Gray (2017) modeled cracked heavy oil viscosity using a lumped-kinetic model based on the pseudo-component boiling points and correlated physical properties. The input of their model was viscosity, density, and the distillation curve (SimDist result) of the feed oil and the process condition. The oil was characterized into pseudo-components based on the distillation curve. The kinetic model calculated the product yields of each pseudo-component and the properties of the pseudo-components were estimated with correlations tuned to the experimental data. It was

assumed that the reactions changed to the amount of each pseudo-component but not the properties of that pseudo-component fraction. The viscosity of the products was estimated by recombining the properties of the pseudo-components using mixing rules. No attempt to study the density of the oil was made.

Marquez *et al.*, (2020) characterized a heavy oil into distillates and SARA fractions. Densities and viscosities of the fractions were measured and input into the Expanded Fluid viscosity model developed by Yarranton and Satyro, (2009). The fluid specific parameters for each fraction were obtained. They correlated the specific parameters of the EF model and the fluid density to the conversion of visbreaking reaction and matched both the fraction and whole oil properties of the products.

2.5.6 Effect of Visbreaking on Oil Stability

Stability in the context of visbreaking refers to the ability of the oil to keep asphaltenes in solution. Visbreaking impacts stability in two ways: 1) the reacted asphaltenes are less soluble than the original asphaltenes; 2) the reacted maltenes are a poorer solvent than the original maltenes. Both factors decrease the stability of the oil.

Thermal cracking reactions split off aliphatic side chains from asphaltene molecules, and therefore, reduce their molecular hydrogen to carbon ratio. The product asphaltenes have lower molecular weight, are more aromatic, have higher solubility parameters, and are less soluble in the surrounding fluid medium (Speight 2014). The higher the conversion, the less soluble the asphaltenes (Casalini *et. al.*, 1990; Rogel, 1997; Carbognani *et. al.*, (2007); Rogel *et. al.*, 2010; Lababidi *et. al.*, (2014); Powers *et. al.*, (2016); Rodriguez *et al.*, 2019). Powers *et. al.*, (2016) quantified the effect of thermo- and hydro-cracking on asphaltene properties and proposed correlations for the molecular weight, density, and solubility parameters of the reacted asphaltenes as a function of the feed properties and conversion.

Visbreaking also affects the surrounding environment for the reacted asphaltenes. Visbreaking produces distillates that have low solubility parameters relative to the asphaltenes. The saturates, aromatics, and resins are slightly altered by the reactions and impact the oil's ability to solubilize

asphaltenes (Powers *et al.*, 2016; Rodriguez *et al.*, 2019). Rodriquez *et al.* (2019) proposed correlations for the molecular weight, density, and solubility parameters of the reacted distillates, saturates, aromatics, and resins as a function of the feed properties and conversion.

Rodriguez *et al.*, (2019) also extended the modified regular solution approach to predict the stability of visbreaking products using the aforementioned property correlations. The correlations are discussed in more detail in Chapter 4. Their model was evaluated on a Western Canadian bitumen and its products with absolute deviations of 1.2 wt.% and 0.4 wt.% for residue and whole visbroken oils, respectively.

2.5.7 Combined Visbreaking and Deasphalting

Combined thermal cracking and deasphalting processes have been used in refineries to optimize the feed for downstream processes. An example is the HSC-ROSE process developed by Toyo Engineering, Mitsu Coke Company, and Kerr-McGee Corporation. The process combined high conversion soaker cracker (HSC) of Toyo/Mitsui with the ROSE supercritical fluid technology of Kerr-McGee. The ROSE process is based on a liquid-liquid extraction of an asphaltene rich phase using supercritical propane (Gray 2015). The products of this process had a lower metal content and MCR, lower capital cost, and higher yields than a delayed coker (Chen *et. al.*, 1994; Hwang 1993).

Chen *et al.*, (1994) investigated solvent deasphalting and mild thermal cracking in a process referred to as mild cracking solvent deasphalting (MCSD). In this process, a solvent stream and feed were preheated and then mixed. The mixture was fed to a thermal cracking reactor and the thermal-cracked residue was mixed with a second stream of cold solvent to instantly reach the extraction equilibrium condition. This mixture was then separated into an alight phase and an asphalt stream. Then the solvent and thermally cracked deasphalted oil in the light phase were separated. The process was reported to produce more deasphalted oil with lower MCR and metal content than a solvent deasphalting process. The density and viscosity of the product were not discussed.

In this thesis, the main target is to lower both the density and viscosity of a bitumen feed in order to minimize the amount of solvent (also termed diluent) addition required to meet pipeline density and viscosity specifications. As noted previously, visbreaking is limited by the formation of coke at higher conversions. It may be possible to obtain greater viscosity reduction and some density reduction by deasphalting prior to visbreaking. Alternatively, the viscosity and density of a visbroken oil can be further reduced by deasphalting after visbreaking. In either case, a combination of deasphalting, visbreaking can minimize the required amount of solvent addition (Gray 2019). The operating space for a possible combination of deasphalting, visbreaking, and solvent addition is illustrated in Figure 2-6.

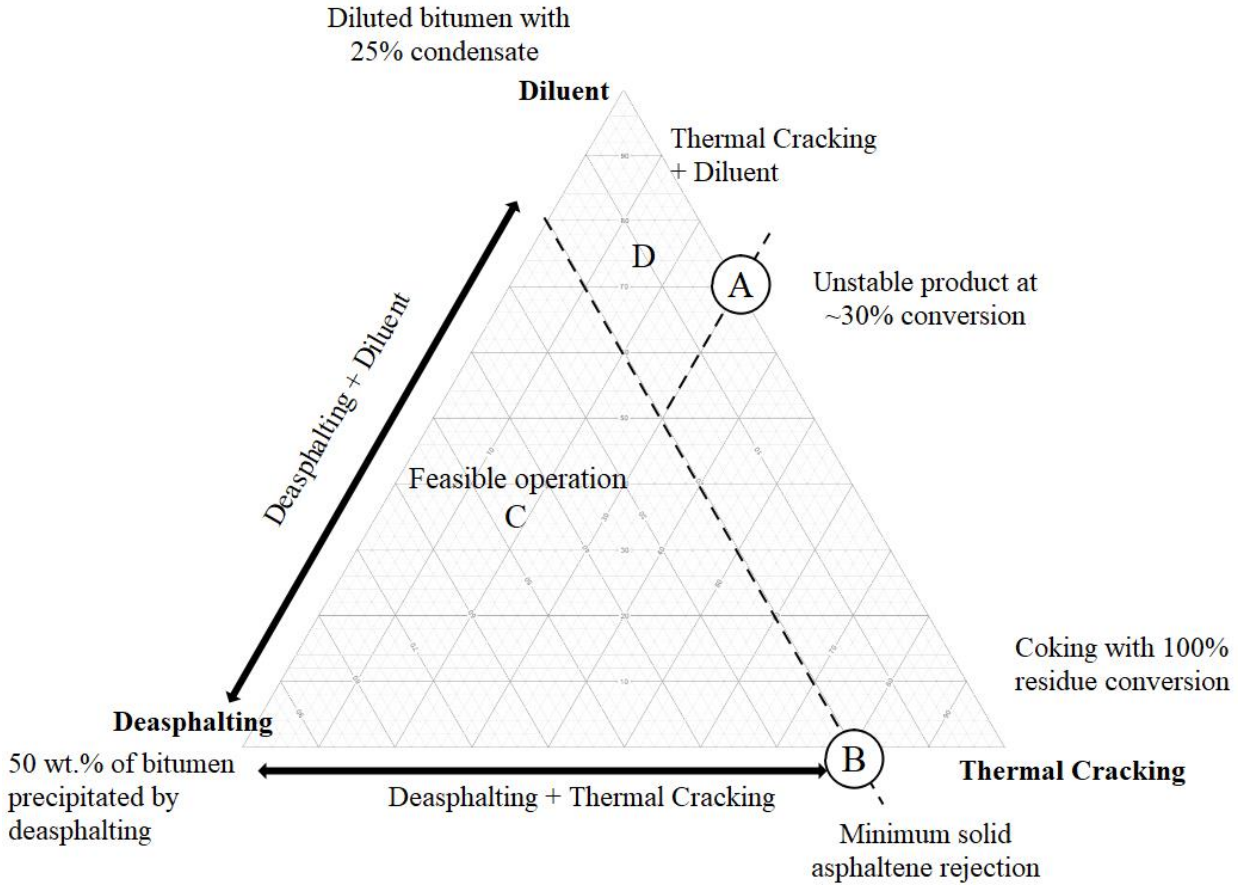

Figure 2-6. Feasible operating space for combining deasphalting, thermal cracking, and diluent addition for Athabasca bitumen (Adapted from Gray 2019).

Zachariah and De Klerk, (2017) investigated combinations of visbreaking (VIS) and deasphalting (SDA) of bitumen. The visbreaking process was conducted at 380°C, 85 minutes of residence time,

and 4 MPa pressure in a micro-batch reactor. The deasphalting process used bitumen to *n*-pentane ratio of 1:40 g oil to mL solvent at room temperature to obtain a solvent diluted DAO. The solvents were removed from the DAO by vacuum filtration and rotary evaporation. They found that the SDA-VIS combination achieved 2% higher liquid yield with a lower hydrogen to carbon ratio compared to the VIS-SDA combination. The SDA-VIS and VIS-SDA combinations reduced the viscosity of the feed oil at 60°C from 955 mPa·s to 13 mPa·s and 25 mPa·s, respectively. The processes reduced the density of the feed oil at 30°C from 1013 kg/m³ to 981 kg/m³ and 977 kg/m³, respectively (at 30°C). They used a diluent with density and viscosity of 656 kg/m³ and 0.46 mPa·s at 7.5°C to meet a pipeline specification of 940 kg/m³ and 350 mPa·s. They reported that the original bitumen required 23.6 wt% diluent while the required diluent for SDA-VIS and VIS-SDA reduced to 14.7 wt% and 13.8 wt%, respectively. Therefore, they concluded that with either combination of processes, the required diluent amount was reduced to almost 40% of its original value.

As noted previously, Castillo and De Klerk, (2019) studied relatively low-temperature visbreaking of Athabasca deasphalted vacuum residues (VR DAO). They compared their results to those of Sivaramakrishnan *et. al.,* (2019), who studied thermal cracking of Athabasca bitumen in similar micro-batch reactors without any deasphalting. Castillo and Klerk, (2019) reported that with SDA before visbreaking, higher conversions could be achieved without coke formation than with visbreaking alone and visbreaking deasphalted vacuum residue can meet higher conversions than bitumen at the same conditions. Table 2-5 summarizes the density and viscosity data of thermal cracking at 400°C for both studies. The two studies used different feeds: an Athabasca bitumen for Sivaramakrishnan *et. al.* versus an Athabasca vacuum residue for Castillo and De Klerk. Also, the sources of oils were from different locations in the same region. Therefore, some caution is advised in making a direct comparison. Nonetheless, the relative reduction in viscosity was greater for the deasphalted vacuum residue feed.

Table 2-5. Summary of density and viscosity data of an Athabasca bitumen after thermal cracking and an Athabasca vacuum residue after deasphalting followed by thermal cracking.

Study	**Residence Time Minute**	**Viscosity Pa·s (40°C)**	**Density kg/m^3 (40°C)**
Sivaramakrishnan *et. al.*, (2019) (Athabasca bitumen)	0	36.2	998.23
	15	0.87	989.02
	30	0.34	976.55
	45	0.078	952.98
	60	0.052	942.44
	75	0.042	925.05
	90	0.0314	931.87
Castillo and De Klerk, (2019) (Athabasca deasphalted vacuum residue)	0	3720	1049.8
	10	44	1020.2
	30	4.7	1006.6
	45	1.7	1003.3
	60	2.0	1014.4
	90	1.1	1023.8

Chapter 3: Experimental Methods

This chapter presents the experimental methods used in this thesis. The apparatus and procedure used to visbreak the oil samples are described. The procedures to separate the feed and product samples into distillates, residues, and SARA fractions are provided. The procedures to measure the molecular weight, density, viscosity of the oils and their fractions are also provided. Finally, the measurements required to determine the fraction solubility parameters are explained.

3.1 Materials

The three feed oils used in this thesis project were a Western Canadian bitumen (WC-B-A4), a vacuum bottom residue (WC-VB-A1), and a deasphalted oil (WC-DAO-A1). Suncor Energy Ltd provided all three samples. The WC-B-A4 bitumen is the product from an oil sand extraction/naphthenic froth treatment process. The vacuum bottom is a fraction from the same process. The deasphalted oil is the product from an oil sand/paraffinic froth treatment process feed. The source bitumens are similar but not identical to each other.

Various solvents were used in the preparation and assaying of the feed and products. Toluene, acetone (both ACS of purity >99.5%), *n*-pentane (>98% purity), and *n*-heptane (Technical grade), were purchased from Fisher Scientific and were used for asphaltene precipitation, solubility tests, SAR fractionation and toluene insolubles removal. OmniSolve high purity toluene (99.99%) purchased from VWR International LLC was used for molecular weight measurements. Sucrose octaacetate (98%) and octacosane (99%), from Sigma-Aldrich Chemical Company (now MilliporeSigma), were used for vapour pressure osmometer calibrations.

3.2 Visbreaking Unit

The visbreaker unit is used to visbreak heavy oil under continuous flow. It was originally designed by Schlumberger, built by Zeton Inc., and was previously reconfigured for visbreaking research at the University of Calgary (Rodriguez *et al.*, 2019). The unmodified University of Calgary

configuration is described below, and any modifications made for this thesis are discussed afterwards.

3.2.1 Apparatus

The continuous flow visbreaking unit consists of three main sections: the feed, reaction, and recovery sections. The purpose of the feed section is to pump the feed oil and filter out any solid particles from that sample. Since the solid contents for all the oils in the study were negligible (below 1 wt%), filtering was not required for this thesis. The visbreaking reaction occurs in the reaction section. The products are passed into the recovery section, where the pressure is reduced to atmospheric pressure, the gas phase separates, and the liquid phase is collected. A simplified schematic of the unit is provided in Figure 3-1.

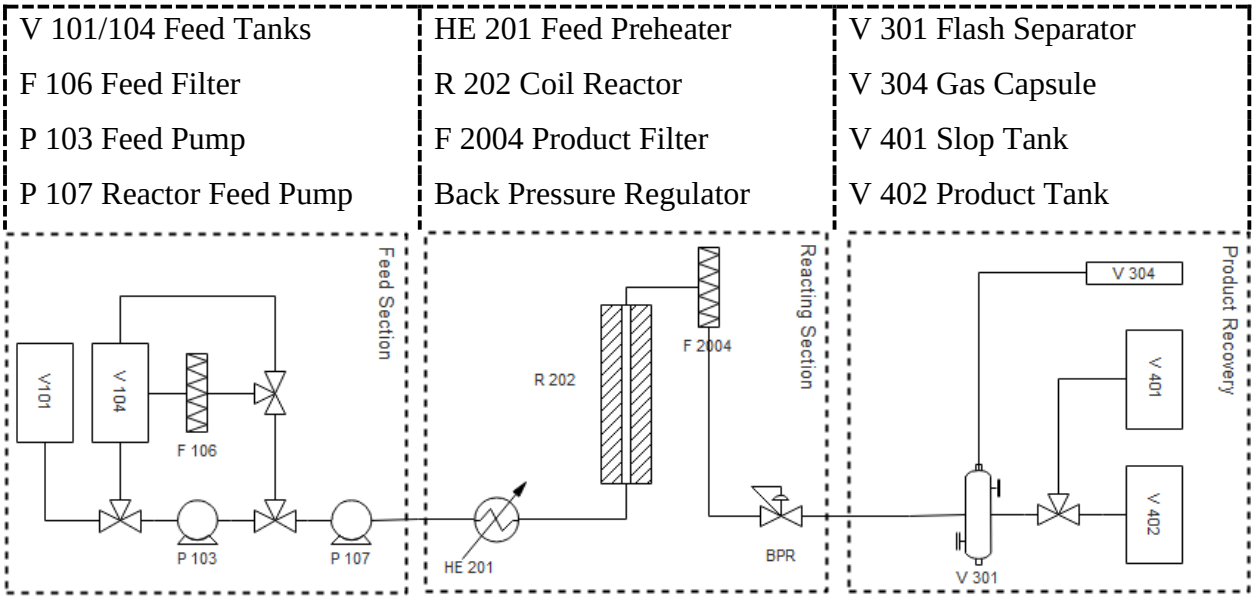

Figure 3-1. Schematic of the visbreaker unit.

Feed Section

The feed section consists of two tanks, two positive displacement pumps, and two filters, as shown in Figure 3-2. The specifications for each major component are outlined below.

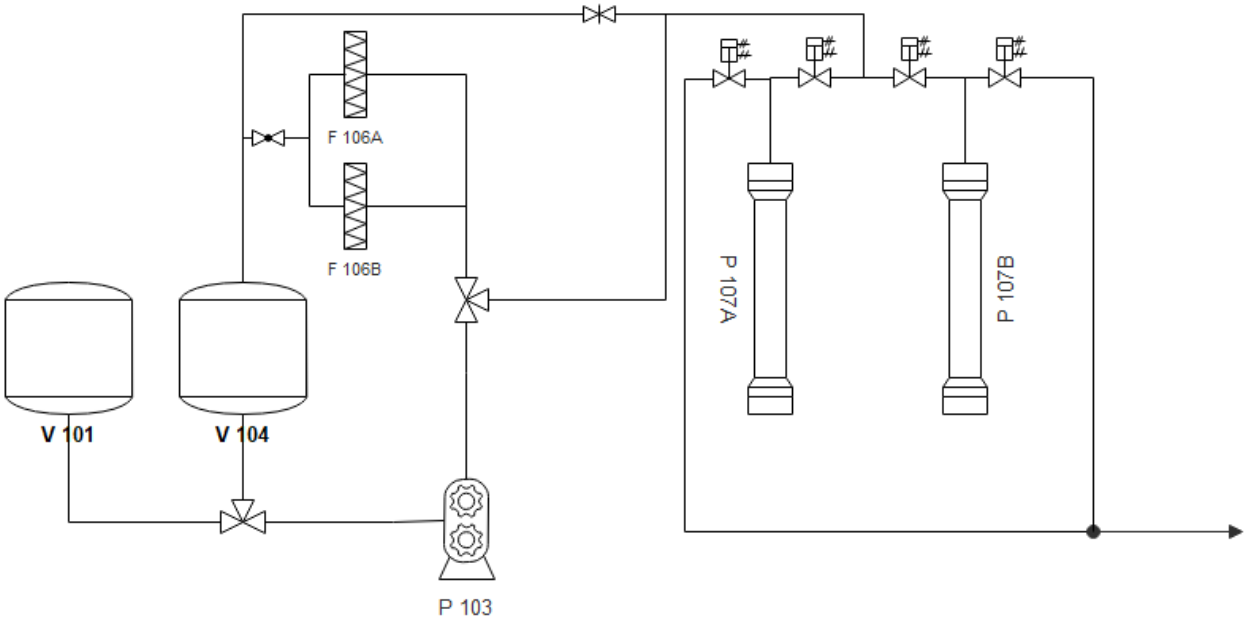

Figure 3-2. Feed section of the visbreaker unit.

Feed Tanks (V 101 and V 104): The two feed tanks in the feed section are identical. The purpose of V 101 is to contain the oil sample with solid particles and V 104 is to store filtered oil. Each tank is 11 L made from stainless steel and is equipped with electrical heaters and insulation. The vessels are isolated from atmosphere with seals and have a nitrogen line to sweep the trapped air. This also provides positive pressure to prevent any vacuum from entering the gear pump section. Electronic controllers control the temperature of the vessels and a low liquid level controller alerts the operator in case of depletion.

Gear Pump (P 103): The filtered feed pump is a Liquiflo Model H3FL3333500000US 3-Series Magnetic Drive gear positive displacement pump equipped with a 1 MPag relief. The operating conditions are limited to a maximum pressure of 1.38 MPa, temperatures up to 190ºC, and fluids with viscosities less than 100 Pa·s.

Feed Filter (F 106): Two Porvair Filtration Group Model 6008 filters are placed in parallel to separate the solid particles from the feed. The filters are equipped with a filter cartridge with a maximum operating pressure of 2.03 MPa monitored with a pressure differential transmitter. As noted above, this component was not used for this thesis.

Piston Pumps (P 107 A and B): Two coupled Teledyne Isco 500HV high-pressure positive displacement pumps are the reactor feed pumps. Each cylinder has capacity of 507.38 cm^3 with a dead volume of 4 cm^3, is limited to pressures up to 25.86 MPa and has flow rate range of 1 µL/min to 204 mL/min. The cylinders were modified to handle fluids with temperatures up to 100ºC. The two-cylinder pumps can operate together in a constant flow or constant pressure regime, or independently of each other.

Reaction Section

The major components of this section are the preheater, reactor, quench zone, filters, and back-pressure regulator. The pressure is set and kept high enough to keep the fluid at the liquid phase by the back-pressure regulator. The oil is heated in the preheater section to a temperature below the starting point of the reaction (300°C). The oil is further heated to, and held at, the target reaction temperature in the reaction section. After the oil exits the reactor, it is passed through an uninsulated line where it is cooled to quench the reaction. The oil is then flowed through filters to separate any solid particles that might have been produced during the reaction. A schematic of the reaction section is provided in Figure 3-3.

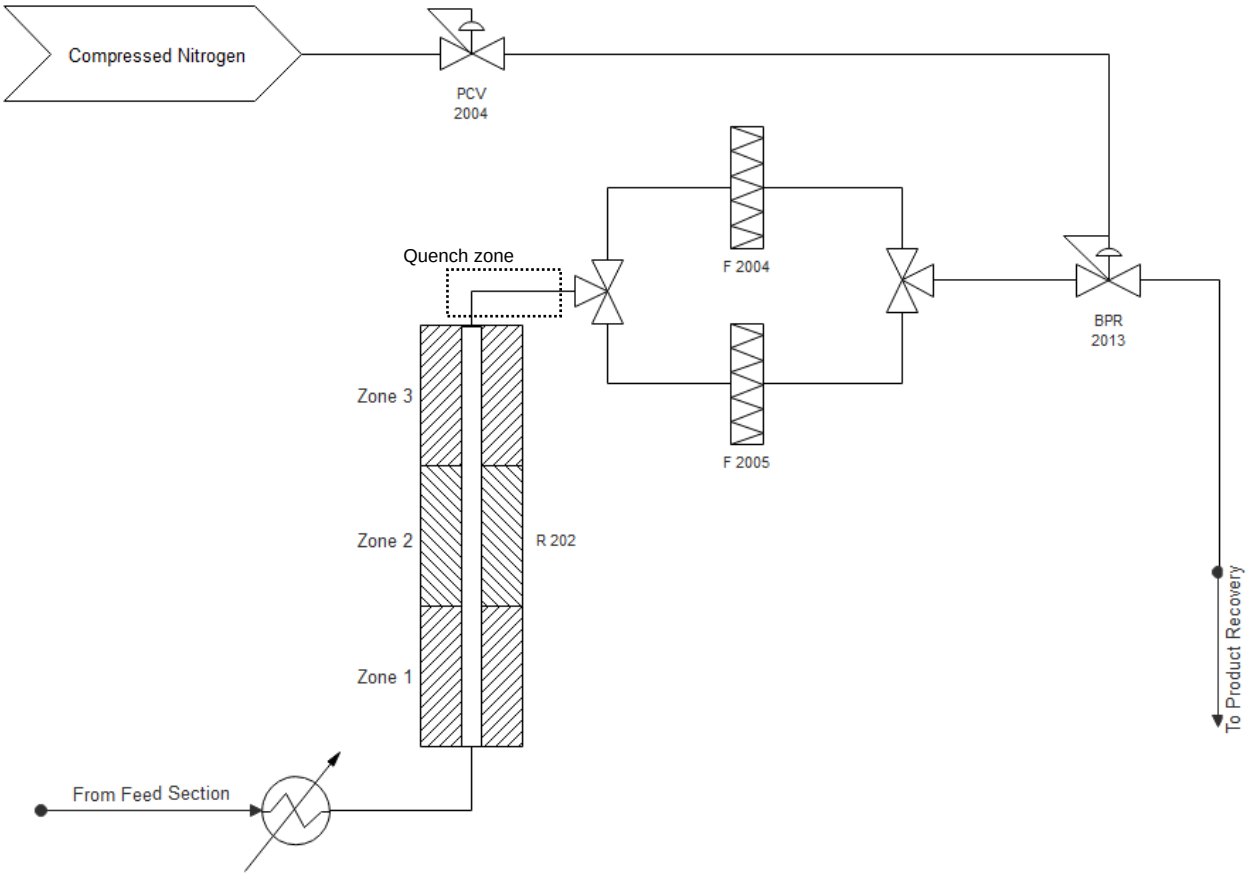

Figure 3-3. Schematic of the reaction section of the visbreaker unit.

Preheater (HE 201): The preheater is a 40 cm coiled tube equipped with a Watlow electric heater inside an insulated aluminum casing. Two thermocouples are placed to measure the temperature inside the apparatus and the temperature of the outlet fluid.

Reactor (R 202): The reactor is a 68.5 cm length stainless steel tube with an inner diameter of 1.27 cm equipped with three electrical heaters placed inside an insulated cover. The heater can raise the temperature to 550ºC. The three heaters create three independent and equal-length heating zones to keep the fluid inside at a constant temperature. The first heating zone brings the fluid to the reacting temperature and the other two zones maintain the temperature.

Quench Zone: The quench zone is an uninsulated 0.6 m long 1.27 cm I.D. stainless steel pipe.

Back Pressure Regulator (BPR): A BPR is a valve that only allows flow to pass through when the passing fluid pressure is higher than the regulating pressure. It maintains constant pressure in the system. The piston pumps in the feed section operate at a constant flow; therefore, the pressure is slightly higher than the regulating pressure in order for the flow to pass through the BPR. The BPR in the visbreaker uses pressurized nitrogen to set the regulating pressure.

Product Filters (F 2004 and F 2005): The two filters are mini Norman 4100 Tee-Type Series filters. They separate solids from 0.5 µm to 300 µm and operate at pressures up to 103.42 MPa.

Product Recovery

The product from the reaction section is depressurized and fed to the separator. The gas phase from the separator flows to a condenser and then a coalescer. The coalescer condenses a portion of the gas and returns it to the separator. The remaining gas is vented. The volume of vented gas is measured with a flow meter and, if desired, can be sampled. The liquid phase that exits the separator is discarded into a slop tank unless the apparatus has reached the stationary mode. In this case, the liquid is collected in the sampling vessel. A nitrogen line is connected to the slop tank and sampling vessels to sweep any produced gas into the vent. The components used for this thesis were the separator, gas meter, slop tank, and sampling vessel. A schematic of this section, as originally configured, is provided in Figure 3-4. The original configuration was used for the WC-DAO-A1 feed. The configuration was modified for the WC-B-A4 and WC-VB-A1 feeds, as will be discussed later.

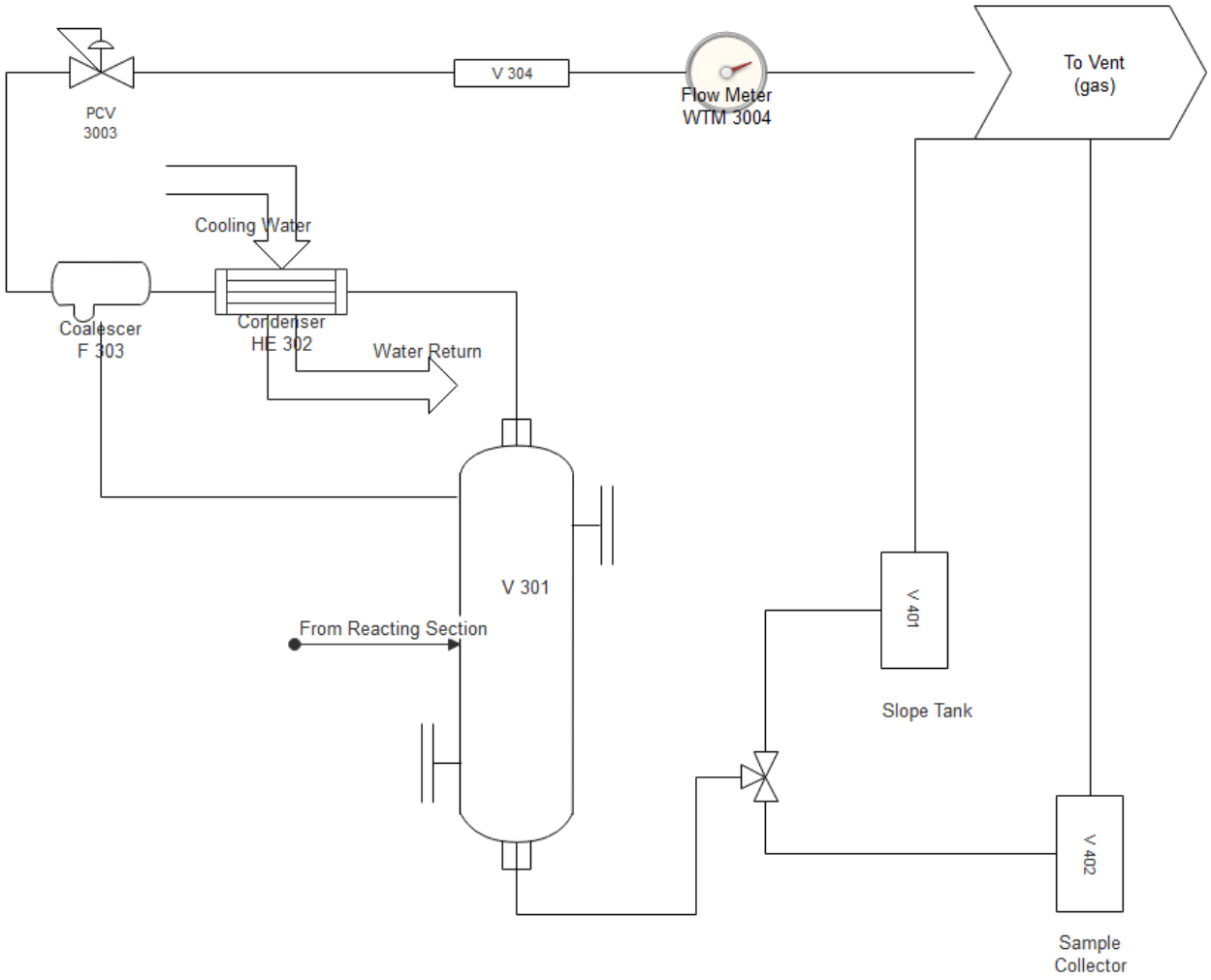

Figure 3-4. Schematic of the product recovery section of the visbreaker unit, as originally configured.

Flash Separator (V 301): The vertical separator in the recovery section is a 0.9 L stainless steel vessel with a 5.2 cm I.D. and a 40 cm length. The vessel operates at pressures up to 1.2 MPag and the pressure of the vessel is controlled by a pressure control valve on the vapour outlet line. A liquid level controller controls the height of the liquid inside the separator. The vessel also has a glass section where the liquid level can be observed.

Condenser (HE 302): The condenser is a counter-current double pipe heat exchanger with a ¼ in inner pipe carrying the separator output and a ½ in outer pipe carrying cold water with tube lengths of 1.778 m.

Coalescer (F303): The coalescer is a Bulletin T.I.-167AM compressed air and gas in-line filter. The operating conditions of the apparatus are limited to 1.72 MPa and 54ºC.

Gas Meter (WTM 3004): The gas meter is a drum-type Wet Test Meter TG1-PVC-PVC (polyvinylchloride Casing, polyvinylchloride Drum). The measuring range of the apparatus is 2 – 120 L/hr at a maximum of 5 kPa pressure.

Gas Sampling Cylinder (V 304): The cylinder is a 316 L stainless steel double-ended DOT-compliant sample cylinder. The vessel has a capacity of 300 cm^3 and a maximum operating pressure of 12.41 MPa.

Slop Tank (V 401): The slop tank is an 11.4 L stainless steel vessel equipped with heating elements to warm up the fluid to reduce the liquid viscosity and ease drainage. The slop tank is equipped with a nitrogen line and a venting line to sweep any produced gases.

Sampling Chamber (V 402): The sampling chamber is a 1.25 L stainless steel cylinder containing a 0.9 L glass jar to collect the product. The chamber is sealed to avoid emitting potentially produced hazardous gases. Similar to the slop tank, a nitrogen line sweeps the gases in the chamber to the gas vent.

Visbreaker Modifications

Produced gases were not evaluated in this project, and therefore, no gas was collected, and the condenser was bypassed. The separator was set to atmospheric pressure and the liquid level was set to zero. These changes avoided the need to run three separator volumes of product through the separator to purge it and therefore reduced the run times. The lack of gas analysis limits the ability to assess the reaction pathways during the visbreaking process, but reaction analysis was not part of this study. In addition, very little gas was produced in these reactions. The gas rate was not measured for most runs but the produced gas was passed through a wet gas meter for the DAO runs and approximately 2 L/h of gas was detected. Based on the feed rate of 7.8 mL/min (lowest rate) and assuming a gas molecular weight of 72 g/mol (high end of the range from literature (Shadbahr *et. al*, 2011), the maximum estimate for the amount of produced gas is 1.5% of the feed.

For the VB and A4 oils, the quench zone was modified to prevent the formation of a viscous plug. The last 0.4 m of the tube was insulated, and the first 0.2 m was left exposed. Heat tapes were added under the insulated section and the temperature was set to 60°C. The sections after the reactor outlet, including the filters and separator, were bypassed. The back-pressure regulator was replaced with a manual pressure control valve so that samples could be collected directly from the quench zone into the collecting jars. These modifications were made because the WC-VB-A1 oil was too viscous to pass through the lines and filters. In addition, it was not practical to heat the oil in the separators to a sufficient temperature to ensure flow. The modifications were kept for the visbreaking run for the WC-B-A4 oil because, with no gas collection, the modified apparatus performed the same functions as the original apparatus but with less complexity.

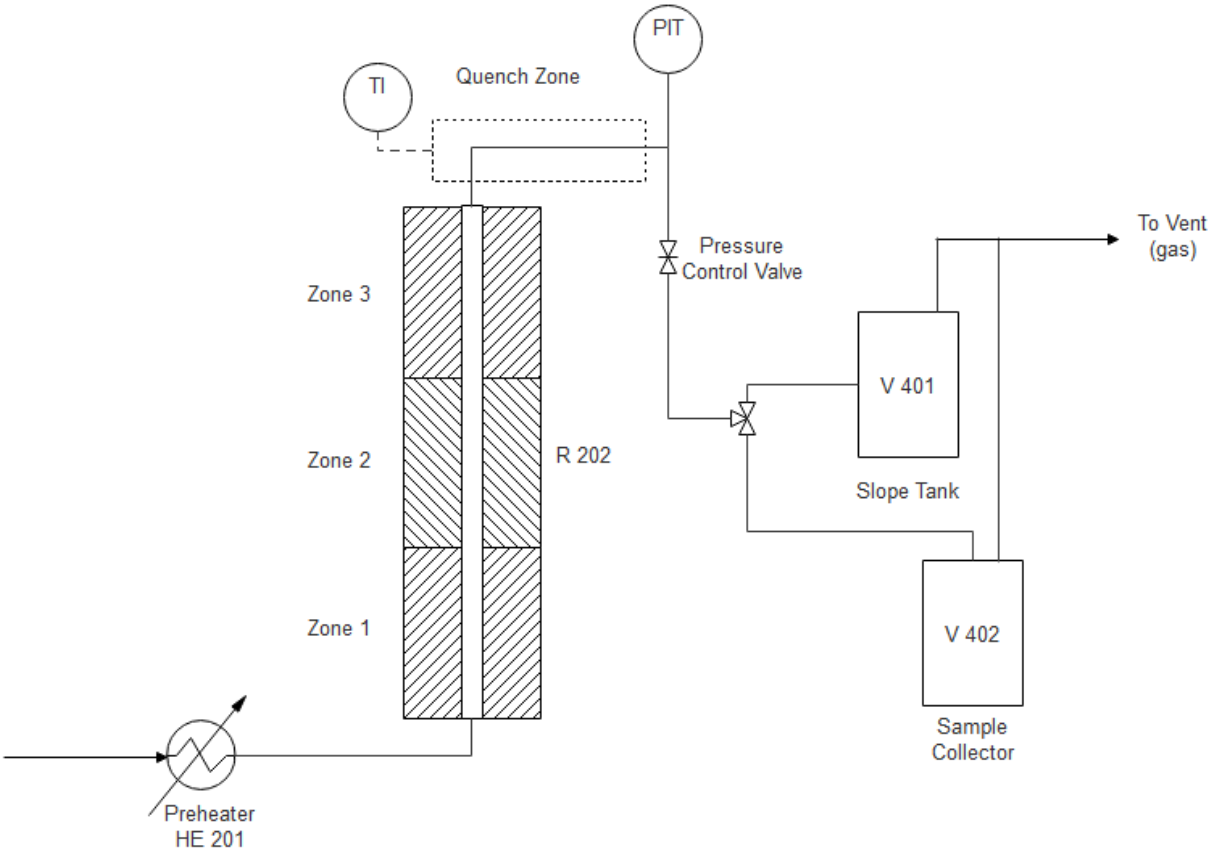

Figure 3-5. Schematic of the reaction and product section after the modifications. The product recovery section (Figure 3-4) was bypassed in this case.

3.3 Visbreaking Procedure

The feed filter section was not used because the samples had solid contents of lower than 1 wt%. Therefore, for all the three samples, the filtered tank was used directly. After pouring a sample into the filtered tank, the lid was left slightly open, the tank was purged with nitrogen for approximately 10 minutes, and then immediately sealed. The sealed tank was pressurized by the nitrogen line to 70 kPag and heated up to the temperatures given in Table 3-1 to reduce the viscosity of the feed and facilitate flow.

Table 3-1. Temperature set-point of each component in the visbreaker

Component	WC-B-A4 /WC-DAO-A	WC-VB-A1
Filtered feed tank	60ºC	130ºC
Gear pump	60ºC	110ºC
Feed section lines	60ºC	100ºC
Piston pumps	60ºC	80ºC
Preheater	300ºC	300ºC
Reactor	450ºC	430ºC
Quench zone	20ºC	60ºC
Product recovery lines	40ºC	60ºC

The heated feed was pumped from the gear pump (P 103) to the piston pumps (P 107 A and B). The inlet pressure at the piston pumps was set to approximately 0.69 MPag to make the refilling of the piston pumps possible. The piston pumps were set to operate at constant flow and the flow rate was calculated based on the residence time of the sample in the reactor (from 5.8 to 10.88 mL/min). The outlet pressure was set using the back-pressure regulator (BPR 2013) placed after the reactor. The pressure was monitored with two pressure transreducers located at the inlet and outlet of the reactor.

The feed oil was pumped through the preheater (H 201) where it was heated to 300°C and then fed into the reactor (R 202). The temperature of the reactor was monitored with the three thermocouples located in each zone of the reactor. Once the three thermocouples were within ±5°C of the temperature setpoint for 30 minutes, it was assumed that the apparatus had reached its steady

state. The sampling started when the apparatus purged at least three volumes of the lines after the reactor with the stabilized visbroken fluid.

The product from the reactor was flowed through the quench zone to stop the thermal cracking reactions. In the original design used for the WC-DAO-A1 runs, the quenched product was passed through the filters (F 2004 and 2005) to remove any produced coke. Then, the flow passed through the flash separator (V 301), where it was flashed to atmospheric pressure. The separated gasses were vented since they were not part of the study of this research. The liquid was sent to the slope tank (V 401) until the stabilized visbroken flow purged the lines after the reactor. Then, the stabilized flow was redirected to the product chamber (V 402), in which a 0.9 L glass jar is placed to collect the samples. After finishing the collection, nitrogen was purged into the collection chamber to sweep any produced hazardous gases.

In the modified configuration used for the WC-B-A4 and WC-VB-A1 runs, the filters in the reacting section and all the components in the recovery section were bypassed. The cooled visbroken sample after the quench zone was directly passed to the slop tank. In this case, the slope tank was equipped with a vent line to remove any hazardous gases. After reaching steady state and purging the lines with three times of their volume, the product was manually directed to the collection jars also equipped with a vent line.

3.4 Bitumen Characterization

The bitumen samples were separated into distillate, saturate, aromatic, resin, and asphaltene fractions. The first step of the characterization procedure was to separate distillates using the spinning band distillation (SBD). The SBD residues were then divided into SARA fractions. The SBD and SARA procedures are presented below.

3.4.1 Spinning Band Distillation

The first step in bitumen characterization was spinning band distillation (SBD) to separate distillate components, *i.e.*, components with boiling points less than 370°C. The apparatus is a B/R Instrument Corporation B.R. 36-100 mini distillation system, and the schematic is shown in Figure 3-6. The spinning monel band is equivalent to 50 theoretical trays in an ordinary distillation tower.

The column is connected to a vacuum pump and the system pressure is set to 0.4 kPa. The bitumen is poured into a boiling pot with a stirrer and a thermocouple records the temperature. At the top of the column before the condenser, a second thermocouple measures the vapour temperature. The reflux valve adjusts the reflux ratio by keeping the collection line open at corresponding time portions.

To perform a distillation, approximately 120 g of bitumen was poured into the boiling pot. Initially, the pressure was set to 6.67 kPa to avoid foam that could rise into the column. After reaching 80°C, the pressure was gently decreased to 0.4 kPa. When the first droplet of condensate was observed at the top of the column, the sample initial boiling point was recorded. The heating rate was then adjusted to equilibrate the column; that is, until the condensation rate reached one droplet per second. Then, the second boiling point was recorded. After equilibration, sample collection was started at a reflux ratio of 5:1. The heating rate was adjusted to keep the temperatures difference between the vapour and pot temperature constant over time. The vapour temperature was recorded after every 2 mL of distillate collection. The distillation was stopped when the pot reached 300°C to avoid thermal cracking reactions that could alter the oil residue. The average sample loss was 2%. The losses were considered to be escaped vapors and were added to the front end of the distillation curve. The repeatability of distillable fraction and the measured boiling points were ±3 wt% and ±4°C, respectively; details are provided in Appendix G.

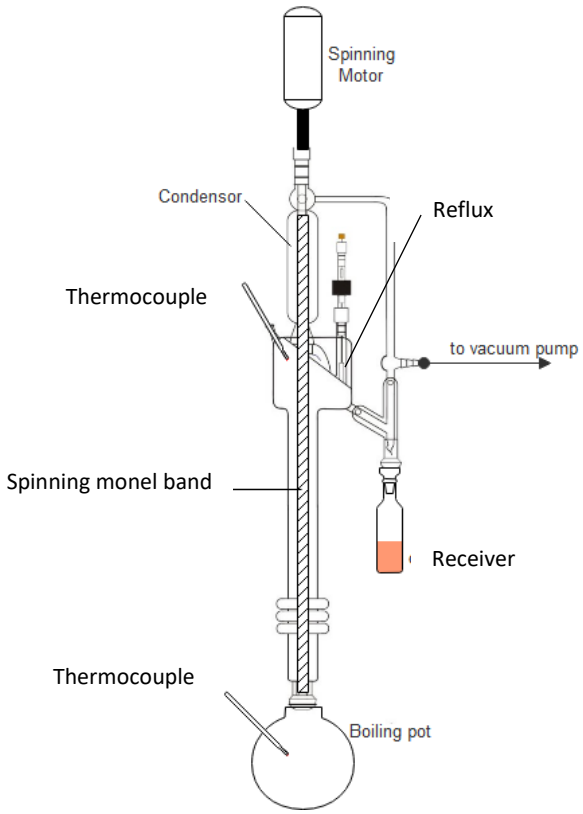

Figure 3-6. Schematic of the spinning band distillation apparatus.

3.4.2 Simulated Distillation

Simulated distillation, or SimDist, is a gas chromatographic method where boiling points are calculated based on the retention time distribution for the sample. The distillation curve is expressed as boiling points versus weight fractions of oil. Detailed procedures are provided in ASTM D2887 or ASTM D7160 (ASTM 2008). The ASTM D7160 SimDist method was performed for all three feed oils, WC-B-A4, WC-VB-A1, WC-DAO-A1, and their reacted products at Core Laboratories Canada Ltd. The repeatability of the ASTM test is ±7°C.

3.4.3 SARA Separation

The SARA procedure was a modified ASTM D4124 procedure (Alboudwarej *et al.*, 2002). This process consists of three main steps: 1) separation of asphaltenes and maltenes from the oil; 2) separation of toluene insoluble material from the asphaltenes; and 3) separation of the maltenes into saturates, aromatics, and resins by liquid chromatography.

Asphaltene and Maltene Separation

Approximately 40 g of spinning band residue was poured into a 2 L beaker and *n*-pentane was added at a ratio of 40:1 *n*-pentane volume to oil mass (mL/g) in order to precipitate asphaltenes from the oil. The covered beaker was sonicated for 2 h and settled for a contact time of 24 h. Then, 80% of the supernatant was passed through VWR GR413 25 cm diameter filter paper of known mass and the filtrate was collected in a 2 L Erlenmeyer flask. *n*-Pentane was added to the beaker a second time at a ratio of 4:1 *n*-pentane volume to initial oil. The covered beaker was sonicated for 60 minutes and left to settle for 16 hours. All of the beaker contents were then poured through the same filter.

The asphaltene filter cakes were washed with at least 25 mL of *n*-pentane three times per day for five days to remove entrained maltenes. The washings were added to the previously collected filtrate and the *n*-pentane was evaporated from the filtrate in a rotary evaporator to recover the maltenes. The asphaltenes from the filter paper and the collected maltenes were left in a fume hood for one day and then placed in separate vacuum ovens at 60°C and -21 kPa for five weeks to dry.The final dry mass of the maltenes and asphaltenes were recorded. The insoluble material recovered by this procedure includes the *n*-pentane insoluble asphaltenes or "C5-asphaltenes" plus any other *n*-pentane insoluble material in the oil such as sand, clay, and heavy organic material.

Removal of Toluene Insolubles

To remove the toluene insoluble material, the impure asphaltenes were dissolved in toluene. Approximately 2 g of asphaltenes were added and weighed in a 250 mL Erlenmeyer flask. 200 mL of toluene was added, and the mixture was sonicated for 60 minutes and settled for 1 hour. Approximately 20 mL of the mixture was transferred to a weighed Nalgene HDPE centrifuge tube, capped, and centrifuged at 4000 rpm for 6 minutes in a Heraeus Megafuge. The supernatant was removed with a pipette and collected in a tared 500 mL beaker. The remaining toluene-asphaltene mixture was centrifuged the same way while accumulating the toluene-insolubles in a single centrifuge tube. The tube and beaker were placed in a fume hood until the toluene evaporated and then placed in a vacuum oven at 60°C and -21 kPag until a constant mass was observed. The mass of toluene-insolubles (TI) was determined from the mass difference of the centrifuge tube. Then the toluene content of the asphaltenes and the oil were determined.

Chromatographic Separation of Maltenes: Saturates, Aromatics, and Resins

The process of separating saturate, aromatic and resin (SAR) fractions uses two adsorbents and three solvents. The adsorbents used were silica gel (Sigma Aldrich, Grade 12, 28-200 mesh) and attapulgus clay (Georgia Clay Co.). The adsorbents are activated by heating at 150°C in a vacuum oven overnight.

Column Preparation: Three columns were prepared: two top columns and one bottom column. The bottom column was packed with 200 g of silica gel at the bottom and 50 g of Attapulgus clay at the top. The top columns were packed with 100 g of Attapulgus clay. The column packing was consolidated by tapping the column with a rubber mallet for at least two minutes. A wad of glass wool was placed at the top of each column to disperse the eluting solvents.

Elutions: 5 g of maltenes were weighed into each of two 125 mL Erlenmeyer flasks. 25 mL of *n*-pentane was added to each flask and the mixtures were sonicated for 20 minutes or until dissolved. The first upper column was connected to the lower column. The top column was prewet with 25 mL of *n*-pentane and the maltene solution was quickly poured into the top of the column. An additional amount of 20 mL of *n*-pentane was used to wash out the remaining maltenes from the flask into the column. 480 mL of *n*-pentane was used to elute saturates into a receiving beaker. Then, the upper column was replaced with the second upper column and the same elution procedure was repeated. The eluted mixtures of *n*-pentane and saturates were collected in a beaker and set aside.

The aromatics were eluted in two steps. First, the upper and lower columns were left connected and eluted with 1.6 L of 50 vol% toluene/*n*-pentane. The upper columns were switched, and the procedure was repeated. The eluted aromatic mixtures were collected in a beaker and set aside. Second, the columns were disconnected, and the remaining aromatics were eluted from the lower column by Soxhlet reflux with toluene for at least two hours. The recovered eluted aromatics were recovered at the end of Soxhlet reflux and were added to the aromatics in the beaker. Finally, to recover the resins, both upper columns were connected and eluted with 900 mL of 50 vol% toluene/acetone. The eluted resins were collected in a beaker and set aside.

Solvent Removal: The solvents were evaporated from the saturate, aromatic, and resin samples using a rotary evaporator, followed by 24 h of drying in a fume hood drying in a vacuum oven at 60°C and -21 kPag until a constant mass was achieved.

The SARA and TI content of the bitumen was determined from the fraction masses. The repeatability of the SARA and TI contents are ±1.9, 3.0, 2.8, 0.15, and 0.04 wt% for the saturates, aromatics, resins, asphaltenes, and toluene insolubles (TI), respectively (Yarranton *et. al.*, 2018). The repeatability of the component separations in this thesis is provided in Appendix G.

3.5 Physical Property Measurements

The properties required for this thesis are the density, viscosity, and solubility parameters of the whole oil, distillates, residue, maltenes, and SARA fractions. The molecular weights of the distillates and SARA fractions are also required. Molecular weight, density, and viscosity are discussed in this section. Solubility parameters will be discussed in the next section.

Not all of the properties could be measured directly for every fraction. Figure 3-7 summarizes the properties that were measured directly. Of the remaining properties, the viscosity and molecular weight of distillates were calculated from their boiling point distribution using correlations (Ramos-Pallares *et al.*, 2016). The resin density was calculated from the measured maltene density using a volumetric mixing rule (assuming zero excess volume of mixing). Similarly, the asphaltene density was determined from the whole oil density. The asphaltene viscosity was calculated using the Expanded Fluid viscosity model fitted to the residue viscosity.

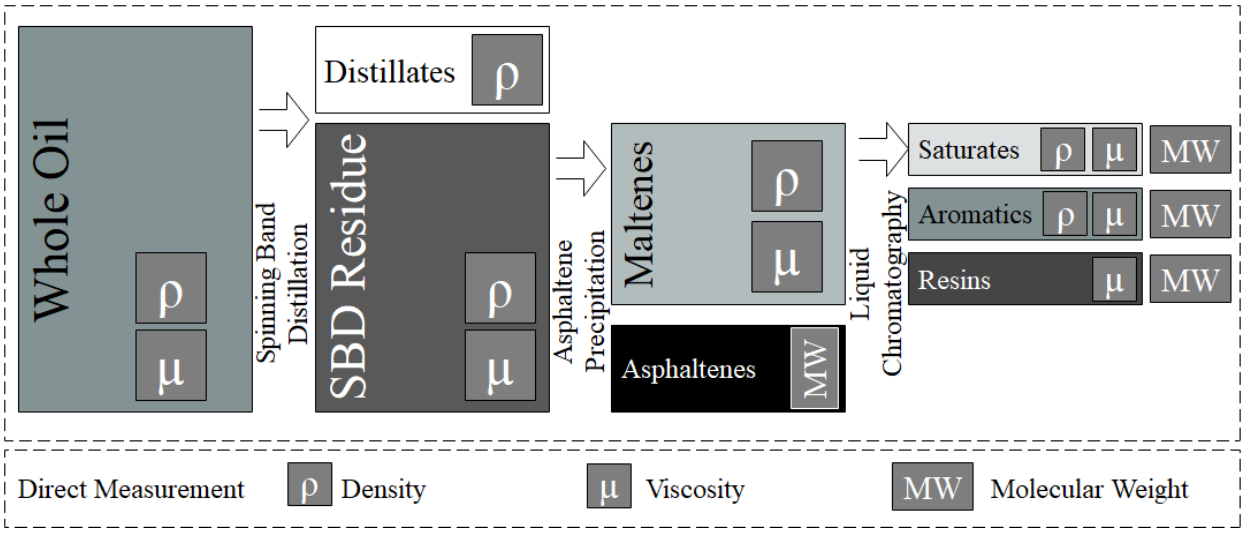

Figure 3-7. Property measurement flow for oil characterization.

3.5.1 Viscosity

The viscosities of fractions were measured in an Anton Paar MCR 52 Cone and Plate Rheometer. The apparatus is limited to measurements at atmospheric pressure and within a temperature range of -10°C to 140°C. The rheometer was calibrated with Canon Instrument Standards S020, S600, S300000, and N450000. The uncertainty of the viscosities based on the standards and a 90% confidence interval is ±6% (Marquez *et. al.*, 2020). The repeatability of the viscosity measurements in this thesis is provided in Appendix G.

To measure a viscosity, approximately 1 cm^3 of sample was added on top of the plate and the cone was placed at the measuring position. After reaching a constant temperature, the shear stress was measured at five different shear rates. The viscosity at the measuring temperature was determined from the shear stress slope versus the shear rate. The response was linear (Newtonian) for all of the data reported in this thesis.

3.5.2 Density

The densities of the samples were measured in an Anton Paar DMA 4500M vibrating tube density meter. The instrument was factory calibrated with air and distilled water. Calibration checks were performed with air, toluene, and reverse osmosis water. The precision and repeatability of the

densities measured in this apparatus are 0.01 kg/m³ and 0.05 kg/m³, respectively. The repeatability of the density measurements in this thesis is provided in Appendix G.

3.5.3 Molecular Weight

Two Jupiter Model 833 Vapour Pressure Osmometers (VPO) were used to measure the molecular weights of the SARA fractions. Details of the apparatus and procedure are available elsewhere (Yarranton *et. al.,* 2018). The VPO was calibrated and standardized using sucrose octaacetate and octacosane, respectively. All SARA fraction measurements were performed in toluene at 50°C. The asphaltene sample was the C5-asphaltenes after removal of the toluene insolubles. The repeatability of the molecular weights is ±15%. The repeatability of the molecular weight measurements in this thesis is provided in Appendix G.

3.6 Solubility Measurements

Solubility parameters were determined by modeling solubility measurements with the MRS model, as will be in Chapter 4. The solubility measurements are asphaltene precipitation yields from solutions containing asphaltenes. Two sets of solubility measurements were performed: 1) asphaltenes and SAR fractions in solvents; 2) whole oils and residues in solvents. In the former case, the asphaltene fraction yield is defined as the mass of precipitated asphaltenes divided by the feed mass of asphaltenes. In the latter case, the asphaltene yield is defined as the mass of precipitated asphaltenes divided by the mass of whole oil or residue in the feed. All of the solubility measurements were performed at 21°C and atmospheric pressure. The repeatability of the asphaltenes yields is ±1 wt% except for the low volume measurements performed with saturates or aromatics where the repeatability is ±8 wt% (Yarranton *et. al.,* 2018). The repeatability of the solubility measurements in this thesis is provided in Appendix G.

3.6.1 Asphaltenes, Saturates, and Aromatics

Asphaltene Solubility: C5-asphaltenes (with TI removed) and toluene were added to a 30 mL glass vial to prepare a solution of 10 g/L of asphaltenes in toluene. The mixture was sonicated for at least 20 minutes to dissolve the asphaltenes completely. A specified amount of *n*-heptane was added to reach the desired mass ratio of *n*-heptane to the toluene-asphaltene mixture. The mixture was sonicated for 45 minutes and left to settle for 24 hours. The vial was then centrifuged at 3200

rpm for 5 minutes and the supernatant was removed with a pipette and discarded. Solvent washes were prepared at the initial precipitation ratio of *n*-heptane to toluene. The wash was added to the vial, sonicated to disperse the mixture, and the same steps of centrifuging and pipetting were repeated three times. The washed precipitates were dried in a fume hood for 24 h and then dried in a vacuum oven at 60°C and -21 kPa until a constant mass was reached.

Saturate Solubility: The saturate solubility test is similar to the asphaltene solubility test except that the precipitant is the saturate instead of *n*-heptane and the solvent wash was a mixture of 95 vol% *n*-heptane and 5 vol% toluene. Since it was very time-consuming to prepare sufficient volumes of saturates, the volume of solvent was scaled down to less than 2 mL to minimize the mass of saturates required for this procedure. Solutions of asphaltenes and toluene were prepared as described above. Then, a specified mass of saturate was added to the solution. The rest of the procedure, including centrifuging, washing, pipetting, and drying, is described above.

Aromatic Solubility: Toluene-insoluble-removed asphaltenes were added to the aromatics instead of toluene at 10 g/L. *n*-Heptane was added to achieve a specified mass ratio of *n*-heptane to aromatics. The volumes were scaled down as described for the saturates. The vial was agitated until the two phases dispersed and then sonicated for 60 minutes. The mixture was settled for 24 hours, centrifuged at 3200 rpm for 6 minutes, and the supernatant was removed by pipette and discarded. To wash the precipitate, *n*-heptane was added until the vial was approximately ¾ full. The vial was sonicated for 60 minutes, centrifuged, and the supernatant was again removed by pipette. The precipitate was dried in a fume hood for 24 hours and then in a vacuum oven at 60°C and -21 kPa until a constant mass was reached.

3.6.2 Whole Oil and Residue

Asphaltene yields were measured for whole oil and residues in two ways: 1) diluted with *n*-heptane; 2) mixed with toluene and then diluted with *n*-heptane. The latter procedure was developed for viscous fluids (Rodríguez *et al*., 2019).

Whole Oil or Residue in *n*-Heptane: A 30 mL weighed glass vial was filled up to ¾ of its capacity with a specified mass ratio of *n*-heptane to oil. The mixture was agitated by hand until a

homogeneous mixture was obtained. The mixture was then sonicated for 60 minutes and left to settle for 24 hours at ambient conditions. Then, the mixture was centrifuged at 4000 rpm for 6 minutes and the supernatant was removed with a pipette and discarded. The precipitate was washed at least three times by adding 15 mL of *n*-heptane to the vial and sonicating for 60 minutes each time. The vial was settled for 24 hours, centrifuged, and the supernatant removed once again. The precipitate in the vial was left in a fume hood for 24 h and then dried in a vacuum oven at 60°C and -21 kPa until a constant mass was reached.

Toluene-Diluted Whole Oil or Residue in *n*-Heptane: The bitumen was first diluted with toluene at a ratio of 0.5 g toluene to 1 g of bitumen. The mixture was sonicated for 100 min at a temperature up to 60°C to ensure complete dissolution. Then, *n*-heptane was added at the specified ratio. The rest of the procedure was as described above.

Chapter 4: Methodology

In this chapter, the methodology used to apply the Expanded Fluid viscosity model and Modified Regular Solution stability model for visbroken oils is outlined. The oil characterization methodology is discussed, and the Expanded Fluid and Modified Regular Solution models are presented. The methodology used to measure the properties required for the models is also outlined.

4.1 Oil Characterization

In order to use both EF model and MRS model for crude oils, the oil must be characterized, in other words, divided into pseudo-components that represent the distribution of properties in the oil. The characterization method for this study was chosen to be compatible with Symmetry Process™ software platform (Schlumberger, 2020). In this platform, the oil is divided into pseudo-components representing a series of boiling points, with each boiling cut subdivided into SARA fractions. A group of representative molecules that match both bulk and fraction physical properties are assigned to each pseudo-component. This method captures both the volatility and the chemical family of the cuts. The software applies a reaction model to obtain the representative molecules of the visbroken product. Each molecule in the product is then assigned to a boiling cut and SARA fraction to generate a new pseudo-components distribution.

There are too many pseudo-components in the Symmetry characterization to experimentally determine their properties in a reasonable time frame. Instead, a simplified and compatible methodology was developed (Rodriguez *et al.,* 2019; Marquez *et. al.,* 2020). In this case, the oil is characterized into a distillate fraction (components with boiling points less than 370°C) and a residue divided into saturates, aromatics, resins, and asphaltenes (SARA) fractions. To complete the characterization, the properties required for the EF and MRS models must be specified for each pseudo-component. In this case, the required properties are density, molecular weight, solubility parameter, and two viscosity model parameters (c_2 and ρ_s^o) that will be discussed later.

The modeling approach is shown in Figure 4-1. The feed oils and their products are characterized into pseudo-components based on their distillation and SARA assays. In Symmetry the reaction model would be used to predict the product compositions. However, in this study, all of these compositions are measured manually. The model parameters (molecular weight, density, viscosity, and solubility parameter for each pseudo-component) are also measured. Previously developed default values and correlations for these parameters will be tested and adapted as required. These correlations require the conversion as an input which is calculated from a SimDist assay using Eq. 2.1.

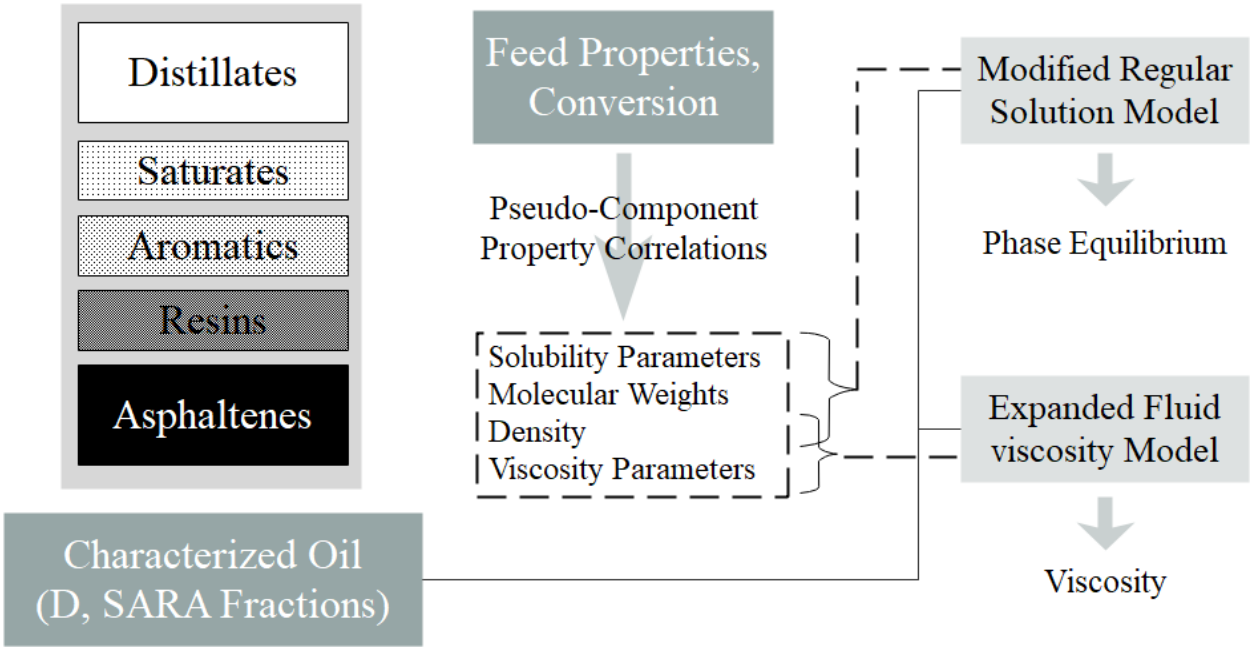

Figure 4-1. Modeling approach including oil characterization and property correlations.

4.2 Expanded Fluid Viscosity Model

4.2.1 Model Description

The Expanded Fluid (EF) model developed by Yarranton and Satyro (2009) correlates viscosity to density. The viscosity of a fluid is expressed as a departure from the dilute gas viscosity as follows:

$$\mu - \mu_G = 0.165(exp(c_2\beta) - 1) \tag{4.1}$$

where μ and μ_G are viscosity of the fluid and its diluted gas, respectively, c_2 is a fluid specific constant, and β captures the effect of the density on the viscosity and is given by:

$$\beta = \frac{1}{exp\left\{\left(\frac{\rho_s^*}{\rho}\right)^{0.65} - 1\right\} - 1} \tag{4.2}$$

where ρ is the density of the fluid and ρ_s^* is the compressed state density in a vacuum given by:

$$\rho_s^* = \frac{\rho_s^o}{exp(-c_3|P - P_0|)} \tag{4.3}$$

where P and P_0 are the pressure on the fluid and atmospheric pressure, respectively, and c_3 is a fluid specific constant. Therefore, the inputs to the model are the dilute gas viscosity, the fluid density, pressure, and the three fluid specific constants (c_2, c_3, and ρ_s^o).

A mixture is treated as a fluid with its fluid specific parameters, which are calculated from the component parameters as follows (Motahhari *et.al.*, 2011):

$$\rho_{s,mix}^0 = \left(\sum_{i=1}^{nc}\sum_{j=1}^{nc}\frac{w_i w_j}{2}\left(\frac{1}{\rho_{s,i}^0} + \frac{1}{\rho_{s,j}^0}\right)(1 - \alpha_{ij})\right)^{-1} \tag{4.4}$$

$$\frac{c_{2,mix}}{\rho_{s,mix}^0} = \sum_{i=1}^{nc}\sum_{j=1}^{nc}\frac{w_i w_j}{2}\left(\frac{c_{2,i}}{\rho_{s,i}^0} + \frac{c_{2,j}}{\rho_{s,j}^0}\right)(1 - \alpha_{ij}) \tag{4.5}$$

$$c_3 = \left(\sum_{i}^{nc}\frac{w_i}{c_{3,i}}\right)^{-1} \tag{4.6}$$

where w is the mass fraction of the component, nc is the number of components, and α_{ij} is the binary interaction parameter.

Ramos-Pallares *et al.* (2016) correlated the interaction parameter to the specific gravity (SG) and hydrogen to carbon ratio (H/C) as follows:

$$\alpha_{ij} = \alpha_{ij}^0 - \Delta\alpha_{ij} \tag{4.7}$$

$$\alpha_{ij}^0 = \begin{cases} 0.021 & \text{if} \quad \Delta SG_N \leq 0.165 \\ 0.038303 - 0.10487\Delta SG_N & \text{if} \quad \Delta SG_N > 0.165 \end{cases} \tag{4.8}$$

and

$$\Delta\alpha_{ij} = \begin{cases} 0.02756 - 0.1103\Delta\left({}^{H}/_{C}\right)_N & \text{if} \quad \Delta\left({}^{H}/_{C}\right)_N \leq 0.25 \\ 0 & \text{if} \quad \Delta\left({}^{H}/_{C}\right)_N > 0.25 \end{cases} \tag{4.9}$$

The parameters ΔSG_N and $\Delta\left({}^{H}/_{C}\right)_N$ are the normalized specific gravity and hydrogen-to-carbon ratio defined as follows:

$$\Delta SG_N = \frac{2\left|SG_i - SG_j\right|}{SG_i + SG_j} \tag{4.10}$$

$$\Delta\left({}^{H}/_{C}\right)_N = \frac{2\left|\left({}^{H}/_{C}\right)_i - \left({}^{H}/_{C}\right)_j\right|}{\left({}^{H}/_{C}\right)_i - \left({}^{H}/_{C}\right)_j} \tag{4.11}$$

To apply the EF model to pseudo-components, correlations are required for the fluid specific inputs: μ_G, c_2, c_3, and ρ_s^o. In this work, the viscosity of the liquid is much greater than the diluted gas viscosity, and therefore μ_G can be neglected. In addition, the viscosity measurements were at atmospheric conditions where the contribution of the c_3 term is negligible. Therefore, ρ_s^* is set equal to ρ_s^o and a value for c_3 is not required. The fluid density is determined from a volumetric mixing rule applied to the component densities. Consequently, the remaining required inputs are the pressure, density, c_2 and ρ_s^o for each component.

4.2.2 Density and Viscosity Parameters of Feed Oils

The properties of the feed components must be specified or set to default values. The densities of all the fractions are expressed as linear functions of temperature as follows:

$$\rho = \rho_{273} + b(T - 298) \tag{4.12}$$

where ρ is the density, b is a constant, T is the temperature in K, and the subscript *273* indicates the reference condition of 273 K. Therefore, the required inputs are temperature, ρ_{ref}, and b. Since this study involved measurements at atmospheric pressure, only the effect of temperature on the density and viscosity was considered. Marquez *et al.,* (2020) established default values for the density and viscosity parameters of the SARA fractions as provided in Table 4-1. The method to determine the distillate viscosity is discussed in Section 4.4.1.

Table 4-1. Recommended density and viscosity parameters for the SARA fractions of Western Canadian bitumen distillation residues (+370°C) from Marquez *et al.* (2020).

Fraction	$\boldsymbol{\rho_{273}}$ kg/m^3	**b** kg/m^{3}K	$\boldsymbol{c_2}$	$\boldsymbol{\rho_s^o}$ kg/m^3
Saturates	912.5	-0.6097	0.4054	962.8
Aromatics	1020.7	-0.6267	0.4489	1055.2
Resins	1065.7	-0.6134	0.6020	1082.2
Asphaltenes	1181.0	-0.6202	0.9879	1164.4

4.2.3 Density and Viscosity Parameters of Visbroken Oils

The properties of the visbroken components must be specified or determined from correlations. Marquez *et al.* (2020) developed a model to predict the density and viscosity of visbroken oils based on the feed oil properties and the conversion. The correlations for ρ_{REF} and b are provided in Table 4.2. The correlations for c_2 and ρ_s^o are provided in Table 4.3.

Table 4-2. Correlations for the density parameters of visbroken oil fractions (Marquez *et al.,* 2020)

Fraction	**Correlation**	
Distillates	$\rho_{REF}/\rho_{REF,0} = 1 + 0.01313[1 - exp(-0.1005X)]$	(4.13)
	$b/b_0 = 1 + 0.05676[1 - exp(-0.03981X)]$	(4.14)
Saturates	$\rho_{REF}/\rho_{REF,0} = 1 - 0.01914[1 - exp(-0.02418X)]$	(4.15)
	$b/b_0 = 1$	(4.16)
Aromatics and Resins	$\rho_{REF}/\rho_{REF,0} = 1 + 0.00064\,X$	(4.17)
	$b/b_0 = 1 + 0.00105\,X$	(4.18)
Asphaltenes	$\rho_{REF}/\rho_{REF,0} = 1 + 0.00061\,X$	(4.19)
	$b/b_0 = 1 + 0.08768[1 - \exp(-0.1842X)]$	(4.20)

Table 4-3. Correlations for the viscosity parameters of visbroken oil fractions (Marquez *et al.*, 2020)

Fraction	Correlation	
Saturates	$c_2/c_{2,0} = \begin{cases} 1 & X \leq 18.3\% \\ 1.05968 - 0.00298\,X & X > 18.3\% \end{cases}$	(4.21)
	$\rho_s^o/\rho_{s,0}^o = 1 - 0.00915[1 - \exp(-0.03556\,X)]$	(4.22)
Aromatics and Resins	$c_2/c_{2,0} = 1 - 0.00246\,X$	(4.23)
	$\rho_s^o/\rho_{s,0}^o = 1 + 0.00056\,X$	(4.24)
Asphaltenes	$c_2/c_{2,0} = 1 - 0.219[1 - exp(-0.073\,X)]$	(4.25)
	$\rho_s^o/\rho_{s,0}^o = 1 + 0.00024$	(4.26)

4.3 Modified Regular Solution Model

The Modified Regular Solution model (MRS) is an activity coefficient-based phase equilibrium model that includes contributions from the internal energy and entropy of mixing. The model applies to regular solutions where there is no excess volume and enthalpy of mixing. Hirschberg *et al.* (1984) were the first to apply this approach to asphaltenes. They based the enthalpy of mixing on the Scatchard-Hildebrand theory (Scatchard, 1949; Hildebrand, 1949). The entropy of mixing was based on the lattice theory for mixtures of polymers and solvents (Flory, 1941; Huggins, 1941). Yarranton and Masliyah (1996) adapted the MRS model to treat asphaltenes as a mixture of pseudo-components rather than a single pseudo-component. They successfully fitted and predicted asphaltene fractional yields in asphaltene-solvent systems. The model has been extended to predict asphaltene precipitation for blends, live oils, crude oils, and reacted fluids (Alboudwarej *et al.*, 2003; Akbarzadeh *et al.*, 2004, 2005; Tharanivasan *et al.*, 2011; Powers *et al.*, 2016; Yarranton *et al.*, 2018). Recently, Rodriguez *et al.*, (2019) adopted the MRS model and developed correlations to predict the stability of visbroken oils, knowing the conversion of the reaction and the feed properties.

The model assumes that asphaltene precipitation is a liquid-liquid equilibrium between a light liquid phase and a heavy liquid phase. The light phase is rich in solvents and includes all the

components. The heavy liquid phase is rich in asphaltene and includes only asphaltenes and resins. The ratio of the mole fractions of the *i* component in each phase is expressed as:

$$K_i = \frac{x_i^H}{x_i^L} = \frac{\gamma_i^L}{\gamma_i^H} \tag{4.27}$$

where *K* is the partition coefficient, *x* is the mole fraction, γ is the activity coefficient, subscript *i* indicates a component, and superscripts *L* and *H* indicate the light phase and heavy phase, respectively. The activity coefficient in a liquid phase is defined as (Prausnitz *et. al.,* 1999):

$$\ln(\gamma_i^\alpha) = \ln\left(\frac{v_i}{v_{mix}}\right) + 1 - \frac{v_i}{v_{mix}} + \frac{v_i}{RT}\sum_j^n\sum_k^n \phi_j^\alpha \phi_k^\alpha (D_{ij} - 0.5D_{jk}) \tag{4.28}$$

where α indicates the phase, *R* is the universal gas constant, *T* is the absolute temperature, v is the molar volume, ϕ is the volume fraction, and subscript *mix* indicates the mixture. The term D_{jk} is defined as follows:

$$D_{jk} = (\delta_j - \delta_k)^2 + 2l_{jk}\delta_j\delta_k \tag{4.29}$$

where δ is the solubility parameter and l_{jk} is the interaction parameter between the two components j and k.

The binary interaction parameter captures the deviation of the average internal energy of the mixture from a geometric mean. They are usually only required for mixtures of dissimilar molecules. For mixture that can be treated as a solution without a strong interaction between the compounds, the binary interaction parameters are zero and Eq. 4.28 reduces to:

$$ln(\gamma_i^\alpha) = ln\left(\frac{v_i^\alpha}{v_m^\alpha}\right) + 1 - \frac{v_i^\alpha}{v_m^\alpha} + \frac{v_i^\alpha}{RT}(\delta_i - \delta_m)^2 \tag{4.30}$$

where the solubility parameter and the molar volume of the mixtures are defined as follows:

$$\delta_m = \sum_i^m \Phi_i \delta_i \tag{4.31}$$

$$v_m^\alpha = \sum x_i^\alpha v_i \tag{4.32}$$

Substituting Eq. 4.30 for each phase into Eq. 4.27 gives the following expression for the equilibrium ratio:

$$K_i = exp\left(ln\left(\frac{v_i^H}{v_m^H}\right) - ln\left(\frac{v_i^L}{v_m^L}\right) - \frac{v_i^H}{v_m^H} + \frac{v_i^L}{v_m^L} + \frac{v_i^H}{RT}(\delta_i^H - \delta_m^H)^2 - \frac{v_i^L}{RT}(\delta_i^L - \delta_m^L)^2\right) \quad (4.33)$$

In this model, only resins and asphaltenes can partition to both phases. The equilibrium phase amounts and compositions are calculated from a liquid-liquid flash algorithm. The asphaltene yields are calculated from the heavy phase mass and composition and the known mass of bitumen in the feed. The inputs to the model are the feed composition, molar volume (in practice the density and molecular weight) and solubility parameter of each component. In this thesis, the binary interaction parameters were set to zero in all cases except for mixtures of bitumen, toluene, and an *n*-alkane. These mixtures have previously been shown to require a binary interaction parameter between toluene and asphaltenes (Rivero, 2021).

4.3.1 Properties of Solvents and Feed Oils

Solvents

The solubility measurements are performed in mixtures that include pure component solvents, and therefore the solvent properties are required to model the data. The solvents used in this project are toluene and *n*-heptane and their density, molecular weight, and solubility parameters at the standard conditions are provided in Table 4-4.

Table 4-4. Properties of toluene and *n*-heptane at standard conditions (Tharanivasan *et.al.*, 2011)

Solvent	**Density** kg/m^3	**Molecular Weight** g/mol	**Solubility Parameter** MPa$^{0.5}$
n-Heptane	681	100	15.2
Toluene	866	92	18.3

Distillates, Saturates, Aromatics, and Resins

Each of the distillates, saturates, aromatics, and resins are treated as a uniform fraction represented by its average properties. The density and molecular weight of the distillates are determined from the distillation assay as will be explained in Section 4.4. The solubility parameter of the distillates and all the properties of the saturates, aromatics, and resins must be specified or taken from default values. Rodriguez *et. al.*, (2019) established these default values and they are provided in Table 4-5. The solubility of the resins is set equal to the minimum asphaltene solubility parameter.

Table 4-5 Recommended values of molecular weights and solubility parameters for the SARA fractions of Western Canadian bitumen from Rodriguez *et. al.*, (2019). Asphaltene parameters are for asphaltenes dissolved in bitumen.

Fraction	**Molecular Weight** g/mol	**Solubility Parameter** $MPa^{0.5}$
Distillates	217	18.7
Saturates	606	16.5
Aromatics	637	21.0
Resins	1204	19.9
Asphaltene (average)	3000	-
Asphaltenes (minimum)	-	19.9
Asphaltenes (maximum)	-	20.6

Asphaltenes

The asphaltenes are assumed to consist of a distribution of nano-aggregates. To represent this distribution, the asphaltenes are subdivided into 30 pseudo-components of uniform intervals of increasing molecular weight. The mole fraction of each pseudo-component is obtained from the Gamma probability function for the molecular weight, expressed as follows:

$$f(MW) = \frac{(MW - MW_{mono})^{\alpha-1}}{\beta^{\alpha}\Gamma(\alpha)} exp\left(\frac{MW_{mono} - MW}{\beta}\right) \tag{4.34}$$

$$\beta = \frac{\left(MW_{avg} - MW_{mono}\right)}{\alpha} \tag{4.35}$$

where MW and α are the molecular weight and the Gamma shape factor, respectively. The subscript $mono$ and avg represent monomer and average molecular weights, respectively. For unreacted oils, the monomer, average, and maximum molecular weights are set to 800, 3000, and 30,000 g/mol, respectively, and the shape factor is set to unity (Yarranton *et al.*, 2018; Powers *et al.*, 2016).

The densities of the asphaltene pseudo-components are obtained from the following equation (Powers *et al.*, 2016):

$$\rho_A = \rho_{min} + (\rho_{max} - \rho_{min})\big(1 - exp(-w_A\tau)\big) \quad (4.36)$$

where ρ, w, and τ are the density, cumulative mass fraction, and the shape factor of the density distribution. The subscript *A* denotes an asphaltene pseudo-component and subscripts *min* and *max* refer to the minimum and maximum densities (at $w_A = 0$ and $w_A = 1$), respectively. The ρ_{min} parameter is set to 1050 kg/m³ and ρ_{max} is adjusted such that the calculated average density equals the experimentally determined value discussed in Section 4.4.

The solubility parameters of the asphaltene pseudo-components are obtained from the following equation (Powers *et al.*, 2016):

$$\delta = \delta_{min} + (\delta_{min} - \delta_{max})(w_A)^n \quad (4.37)$$

where δ, w_A, and n are the solubility of each asphaltene pseudo-component, cumulative mass fraction, and the shape factor exponent. The minimum and maximum solubility parameters, δ_{min} and δ_{max}, are determined by fitting the MRS model to the experimental solubility data, typically asphaltene yields from mixtures of the oil and *n*-heptane or *n*-pentane at ambient conditions.

4.3.2 Properties of Visbroken Oils

Rodriguez *et al.* (2019) developed a series of correlations that correlates the fraction properties to the conversion of the visbreaking reaction. The correlations for molecular weight, density, and solubility parameter are given in Tables 4-6 to 4-8, respectively. The correlations for c_2 and ρ_s^o are provided in Table 4-3. Some of their correlations are used in modeling in this project while for the rest updated correlations have been proposed based on the results discussed in Chapter 6 and 7.

Table 4-6 Molecular weight correlations to visbreaking conversion (Rodriguez *et al.*, 2019)

Fraction	**Correlation**	
Distillates	$MW = MW_f\big[1 - 0.139\big(1 - exp(-0.116X)\big)\big]$	(4.38)
Saturates	$MW = MW_f\big[1 - 0.122\big(1 - exp(-0.512X)\big)\big]$	(4.39)
Aromatics and Resins	$MW = MW_f\big[1 - 0.306\big(1 - exp(-0.095X)\big)\big]$	(4.40)
Asphaltenes	$MW = MW_f\big[1 - 0.338\big(1 - exp(-0.1X)\big)\big]$	(4.41)

Table 4-7 Density correlations to visbreaking conversion (Rodriguez *et al.*, 2019)

Fraction	**Correlation**	
Distillates	$\rho = \rho_f\left[1 - 0.174\left(1 - exp(-0.0823X)\right)\right]$	(4.42)
Saturates	$\rho = \rho_f[1 - 0.00020X]$	(4.43)
Aromatics and Resins	$\rho = \rho_f[1 - 0.00050X]$	(4.44)
Asphaltenes	$\rho = \rho_f[1 - 0.00196X]$	(4.45)

Table 4-8 Solubility correlation to visbreaking conversion (Rodriguez *et al.*, 2019)

Fraction	**Correlation**	
Distillates	$\delta = \delta_f\left[1 - 0.118\left(1 - exp(-0.069X)\right)\right]$	(4.46)
Saturates	$\delta = \delta_f\left[1 - 0.074\left(1 - exp(-0.084X)\right)\right]$	(4.47)
Aromatics	$\delta = \delta_f[1 - 0.000925X]$	(4.48)
Resins	$\delta = \ \delta_{min}\ of\ bitumen\ Asph.$	(4.49)
C5 Asphaltenes minimum	$\delta = 20.2\left[1 + 0.455\left(1 - exp(-0.00033X)\right)\right]$	(4.50)
C5 Asphaltenes maximum	$\delta = 21.3\left[1 + 0.090\left(1 - exp(-0.075X)\right)\right]$	(4.51)
Bitumen Asph. minimum	$\delta = 20.2\left[1 + 0.056\left(1 - exp(-0.0226X)\right)\right]$	(4.52)
Bitumen Asph. maximum	$\delta = \delta_f + \Delta\delta\left(1 - exp(-0.00930\Delta\delta X)\right)$ $\Delta\delta = 23.22 - \delta_f$	(4.53)

4.3.3 Model Output

The Modified Regular Solution model was implemented using an in-house program coded in Visual Basic. The pressure (0.1 MPa in this case), temperature (293 K), and solvent type and mass fraction are specified. The model then calculates the moles of each component in each phase from which the asphaltene yield is calculated. The yields are plotted versus the solvent mass content in the feed. If asphaltenes were precipitated from oil by adding *n*-heptane, the yield is the ratio of precipitated asphaltene to the initial oil amount. If asphaltenes were precipitated from solvent

solutions, saturates, aromatics, and asphaltenes, the yield is the ratio of precipitated asphaltene to the initial added amount of asphaltenes.

4.4 Methodology for Property Determination

The following properties were measured for the feed oils.

- SimDist, SBD assay, SARA assay.
- density of distillates.
- molecular weight, density, and viscosity of saturates, and aromatics.
- molecular weight and viscosity of resins.
- solubility parameter of saturates and aromatics.
- density and viscosity of whole oil, maltenes, and residue.
- asphaltene yields from whole oil, whole oil with 0.5 g/g toluene, and residue with 0.5 g/g toluene.

Not all of the fraction properties could be measured directly. The molecular weight and viscosity of the distillates were determined from correlations. The density and viscosity of the whole oil, maltenes, and residue were used to determine the resin density parameters and the asphaltene density and viscosity parameters. The asphaltene yields were used to determine the distillate and asphaltene solubility parameters.

The following properties were measured for the visbroken oils.

- SimDist, SBD assay, SARA assay.
- density of distillates.
- density and viscosity of saturates and aromatics.
- viscosity of resins.
- density and viscosity of whole oil, maltenes, and residue.
- asphaltene yields from whole oil, whole oil with 0.5 g/g toluene, and residue with 0.5 g/g toluene.

Molecular weights of reacted fractions were not measured because the measurements are time consuming and molecular weights were not required for the viscosity model and had negligible

impact on the MRS model. They were determined from previously developed correlations instead. The solubility parameters of the saturates and aromatics for the reacted fractions were not measured for the same reason. The density of the resins, density and viscosity of the asphaltenes, and the solubility parameters of the distillates and asphaltenes were determined as described for the feed oils. The indirect methods to determine properties are discussed below.

4.4.1 Distillate Properties

The density of the distillate components was measured directly. The boiling point curve with AET was obtained from the SBD run. The molecular weight and viscosity of the distillates were calculated from the boiling curve. First, the boiling curve was divided into boiling cuts, each representing 2 mL of distilled volume. Then the specific gravity and molecular weight were calculated for each boiling fraction with the following iterative method:

1. Guess an initial molecular weight for each boiling cut (every 2 mL).
2. Calculate the specific gravity of each cut as a function of boiling point and molecular weight with the correlation from Sánchez-Lemus *et al.* (2016).
3. Calculate the boiling points based on the specific gravity and molecular weight with the modified Soreide correlation (Sánchez-Lemus *et al.*, 2016).
4. Adjust the molecular weights to minimize the least square error between the calculated and measured boiling points.
5. Calculate the specific gravity of the whole distillates with the specific gravity of each fraction, assuming an ideal mixture.
6. If the calculated specific gravity matches the measured specific gravity, exit. Otherwise, multiply the specific gravity of each boiling point with the ratio of the measured to calculated specific gravity of whole distillates and return to Step 1.

After the specific gravity of each boiling point is obtained, the cumulative mass fraction is calculated from the distilled volume and calculated density of each cut. The average molecular weight of the distillates is from the masses and molecular weights of the cuts. The distillates viscosity parameters are determined from correlations developed by Ramos-Pallares *et al.* (2016). The c_2 parameter of each cut is determined as a departure from a reference value as follows:

$$c_2 = {c_2}^0 - \Delta c_2 \tag{4.54}$$

where ${c_2}^0$ is the parameter value for the reference component and Δc_2 is the deviation from the reference component with the same normal boiling point. The reference value is given by:

$${c_2}^0 = 1.882 \times 10^{-3} exp(0.0058855\, T_b) + 0.3674 {T_b}^{-0.1177} \tag{4.55}$$

where T_b is the normal boiling point (K). The departure value is given by:

$$\Delta c_2 = -2.01417 \Delta SG^2 - 0.1324 \Delta SG \tag{4.56}$$

where ΔSG is given by:

$$\Delta SG = SG^\circ - SG \tag{4.57}$$

where SG is the specific gravity of the pseudo-component and SG° is the reference specific gravity given by:

$$SG^\circ = 1.098[1 - exp(-0.00148 T_b^{1.1128})] \tag{4.58}$$

The parameter ρ_s^0 is calculated as follows:

$$\rho_s^0 = \rho_T \left[1 + ln\left(1 + \frac{c_2}{ln\left(1 + \frac{\mu_T - \mu_0}{0.165}\right)} \right) \right]^{1/0.65} \tag{4.59}$$

where ρ_T and μ_T are the density and the viscosity, respectively, at a reference temperature chosen to be 37.7°C (Ramos-Pallares *et al.*, 2016). The reference function is given by:

$$ln\left(\mu_{37.7} + \frac{250}{T_b}\right) = ln\left(\mu_{37.7}^\circ + \frac{250}{T_b}\right)\left(\frac{1+2f}{1-2f}\right)^2 \tag{4.60}$$

$$f = -|x| \Delta SG + 53.2315 \frac{\Delta SG^2}{{T_b}^{0.5}} \tag{4.61}$$

$$x = 3.7012 - \frac{73.02779}{T_b^{0.5}} \tag{4.62}$$

$$\log\left(\log\left(\mu_{37.7}^\circ + 1\right)\right) = (0.0036 T_b - 2.0942) 0.95^{T_b/200} \tag{4.63}$$

4.4.2 Resin and Asphaltene Density

The resin density was calculated from the maltene density as follows:

$$\frac{w_{Resins}}{\rho_{Resins}} = \frac{1}{\rho_{Maltenes}} - \frac{w_{Saturates}}{\rho_{Saturates}} - \frac{w_{Aromatics}}{\rho_{Aromatics}} \tag{4.64}$$

where *w* with the component subscript is the weight fraction of that component in the maltenes. The maltene, saturate, and aromatic densities were measured directly. It was assumed that there was no excess volume of mixing. Similarly, the asphaltene density was calculated from the SBD residue density as follows:

$$\frac{w_{Asphaltenes}}{\rho_{Asphaltenes}} = \frac{1}{\rho_{Residue}} - \frac{w_{Maltenes}}{\rho_{Maltenes}} \tag{4.65}$$

where *w* with the component subscript is the weight fraction of the component in the residue. The residue density was measured directly. The resin and asphaltene densities were determined over the temperature range of the other property measurements and the calculated densities were fitted with Eq. 4.64 and 4.65 to obtain the density parameters (ρ_{Ref} and *b*) for both fractions.

4.4.3 Viscosity Model Parameters for SARA Fractions

The viscosity parameters (c_2 and ρ_s^o) of the saturates, aromatics, and resins were obtained by fitting the measured viscosities with the EF Model. The following optimization function (OF) was used to fit the data:

$$OF = \sum \left[\ln \left(\frac{\mu_{pr}}{\mu_{Me}} \right)^2 \right] \tag{4.66}$$

where μ_{pr} and μ_{Me} are the predicted and measured viscosities, respectively.

The asphaltene viscosity parameters c_2 and ρ_s^o were obtained indirectly from the viscosity of the SBD residue. The residue viscosity was calculated using the EF model as recombination of the SARA components. The mass fractions and the viscosity parameters of saturates, aromatics, and resins were previously determined and the asphaltene parameters were adjusted to fit the residue viscosity.

4.4.4 Solubility Parameters for Distillates and SARA Fractions

Extracted Asphaltenes Solubility Parameters

The solubility parameters of the extracted asphaltenes were required to model the saturate and aromatic solubility measurements. The extracted asphaltenes were mixed with toluene and precipitated with *n*-heptane. The MRS model was fitted to the measured yields to obtain the minimum and maximum solubility parameter of the extracted asphaltenes. The solvent properties

are known and the molecular weight and density of the extracted asphaltenes were measured independently. Therefore, the only unknowns in the model were the asphaltene solubility parameters adjusted to fit the measured yields.

Saturates and Aromatics Solubility Parameters

The solubility parameter of the saturates were determined from measured asphaltene yields from solutions of saturates, toluene, and asphaltenes. The properties of toluene are known and the properties of the extracted asphaltenes were obtained as described previously. The solubility parameter of the aromatics was determined similarly from measured asphaltene yields from solutions of aromatics, *n*-heptane, and asphaltenes.

Distillate Solubility Parameter and Asphaltene Solubility Parameters in Oil

The solubility parameters of the distillates and of the asphaltenes dissolved in oil were determined from the asphaltene yields from the whole oil, whole oil with 0.5 g/g toluene, and residue with 0.5 g/g toluene each mixed with *n*-heptane. The properties of *n*-heptane are known. The molecular weight and density of the asphaltenes were set as described in Section 4.3. The molecular weight and density of the distillates were determined as described in Section 4.4.1. Therefore, the only unknowns are the solubility parameters of the distillates and the asphaltenes.

The distillates are not present in the residue, and therefore, the yields from the residue+toluene mixture were modeled to obtain the asphaltene solubility parameters (δ_{min} and δ_{max}). Then the whole oil+toluene mixture was modeled to obtain the distillate parameters. Finally, the whole was modeled to obtain another set of asphaltene parameters. The two sets of asphaltene parameters were consistent with each other and were averaged to obtain the final set of parameters.

Chapter 5: Visbreaking Dataset

The dataset for this thesis consists of composition, density viscosity and solubility data for the following feeds (all from Western Canada) and their visbroken products: two bitumens (WC-B-A3 and WC-B-A4), a vacuum residue (WC-VB-A1), and a partially deasphalted oil (WC-DAO-A1). The vacuum residue and deasphalted oil were obtained from oil sand process streams derived from feeds similar to the WC-B-A4 bitumen. The data for the WC-B-A3 bitumen were measured previously (Marquez *et. al.*, 2020; Rodriguez *et. al.*, 2019). The rest of the data were measured in this thesis. The reaction conditions for visbreaking the four oils are provided in Table 5-1 The composition and property data for all of the oils are presented and discussed below.

Table 5-1. List of the feed and product oils and their reaction conditions. The data for WC-B-A3 and its products were obtained elsewhere (Marquez *et. al.*, 2020; Rodriguez *et. al.*, 2019).

Sample	Reaction Conditions	Conversion (%)
WC-B-A3	Feed	-
WC-B-A3-VIS5a	6.55 MPa, 420ºC, 10 min	5.1
WC-B-A3-VIS5b	6.55 MPa, 430ºC, 10 min	4.9
WC-B-A3-VIS8	6.55 MPa, 440ºC, 10 min	8.1
WC-B-A3-VIS19	6.55 MPa, 430ºC, 20 min	19.3
WC-B-A3-VIS38	6.55 MPa, 440ºC, 20 min	38.1
WC-B-A4	Feed	
WC-B-A4-VIS24	1.72 MPa, 450ºC, 8 min	24.3
WC-B-A4-VIS32	1.72 MPa, 450ºC, 12 min	32.2
WC-DAO-A1	Feed	-
WC-DAO-A1-VIS15	6.55 MPa, 450ºC, 8 min	15.2
WC-DAO-A1-VIS29	6.55 MPa, 450ºC, 12 min	28.7
WC-VB-A1	Feed	-
WC-VB-A1-VIS15	1.72 MPa, 430ºC, 15 min	15.0
WC-VB-A1-VIS9	1.72 MPa, 430ºC, 10 min	8.9

5.1 Conversion and Oil Composition

The SimDist boiling curve for each feed and product is shown in Figure 5-1. The conversion of the products was calculated using Eq. 2.1 and the mass fraction of the +524°C cut from the SimDist. The conversions are provided in Table 5-1. Figure 5-1 shows that SimDist assays shift to the right in all cases because the light fraction content increased with increasing conversion. The spinning band distillation (SBD) assays were consistent with the SimDist assays for all of the samples to within the error of the measurements, as shown in the examples provided in Figure 5-2.

The composition of the feeds and their visbroken products are provided in Table 5-2. The mass fractions of the saturates, aromatics, and resins were similar in all four feeds and the main differences in their composition were the mass fractions of the distillates and asphaltenes. The WC-VB-A1 feed oil had no distillates and a high asphaltene content relative to the other oils. As expected, the partially deasphalted oil had a lower asphaltene content than the other oils.

Figure 5-3 shows the changes in oil composition with the conversion. The most notable change in the composition of the oils was the increase in the distillate content with the conversion, which was observed for every oil, as shown in Figure 5-3a. The increase in the distillate content is consistent with the removal of side chains from the molecules in the heavier fractions (Rodriguez *et. al.*, 2019; Speight 2019; Gray 2019, 2015).

Figure 5-3b shows that there was relatively little change in the saturate, aromatic, and resin content of the residue with conversion in all cases. It appears that these fractions were little affected by the visbreaking reactions. Figure 5-3c shows that the asphaltene content for the WC-B-A3, WC-DAO-A1, and WC-VB-A1 oils initially decreased with increasing conversion and then increased above approximately 10% conversion. The minimum varied by a few percent for the different feeds. It appears that, at low conversion, dealkylation and splitting reactions are dominant but, at higher conversions, condensation reactions cause the asphaltene content to increase (Rodriguez *et. al.*, 2019; Gray 2019; Speight 2019; Carbognani *et. al.*, 2007).

Table 5-2 shows that the toluene insoluble (TI) content of the A3 bitumen increased at a conversion of 38%, indicating that some former asphaltenes were now insoluble in toluene and that coke formation may have been initiated. Microcarbon residue data were consistent with the TI contents and are provided in Appendix D. The TI content in the WC-B-A4, WC-DAO-A1, and WC-VB-A1 oils did not change with the conversion. Hence, the asphaltenes remained soluble and no coke formation occurred up to approximately 30% conversion.

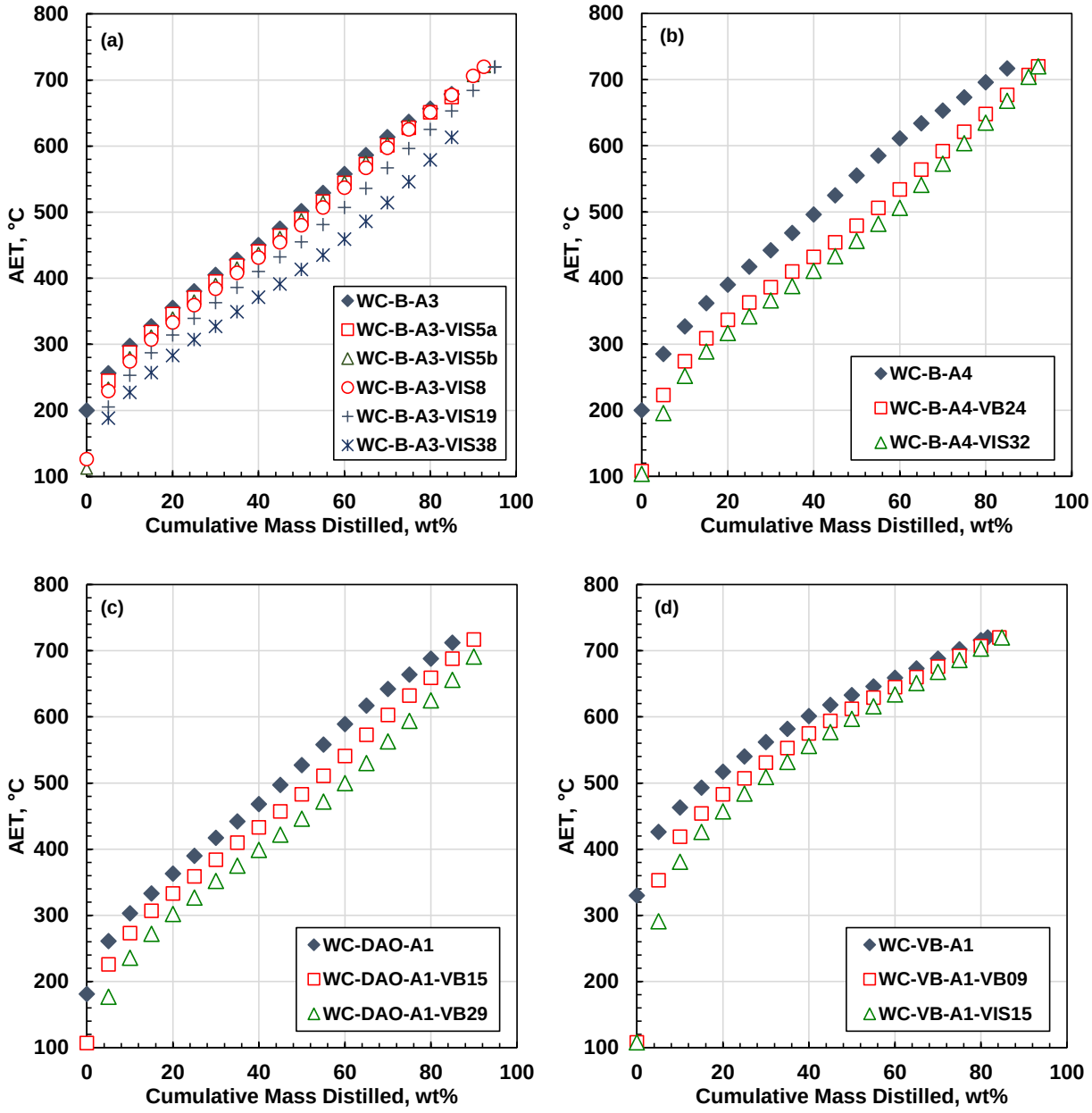

Figure 5-1. SimDist assays for the four feeds (closed symbols) in the dataset and their products (open symbols): a) WC-B-A3; b) WC-B-A4; c) WC-DAO-A1; d) WC-VB-A1.

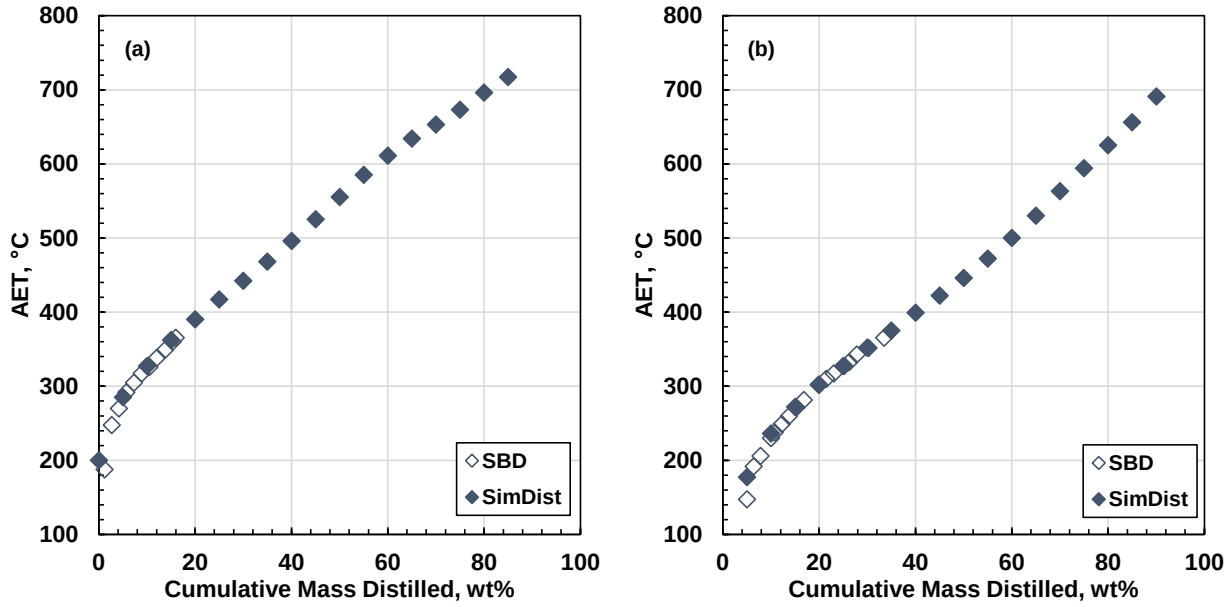

Figure 5-2. Comparison of SBD and SimDist assays for: a) WC-B-A4 bitumen; b) WC-DAO-A1-VIS29 visbroken product.

Table 5-2. Composition of the feed oils and their visbroken products. The repeatability was within ± 0.2, 0.2, 0.7, 0.6, and 0.2 wt% for the distillates, saturates, aromatics, resins, asphaltenes, and toluene insolubles (TI) components, respectively.

Sample	Distillates wt%	Saturates wt%	Aromatics wt%	Resins wt%	Asphaltenes wt%	TI wt%
WC-B-A3	22.1	9.1	32.5	16.4	19.6	0.3
WC-B-A3- VIS5a	22.8	9.5	33.1	16.2	18.1	0.3
WC-B-A3- VIS5b	26.7	8.2	31.5	15.7	17.7	0.2
WC-B-A3- VIS8	28.6	8.1	29.8	14.9	18.4	0.2
WC-B-A3- VIS19	33.3	8.4	27.8	12.7	17.4	0.4
WC-B-A3- VIS38	37.6	6.9	25.1	10.0	19.1	1.3
WC-B-A4	16.0	11.3	33.3	20.9	18.1	0.1
WC-B-A4-VIS24	27.2	10.2	30.3	15.0	17.3	0.0
WC-B-A4-VIS32	30.8	9.7	28.9	12.8	17.7	0.0
WC-DAO-A1	22.4	11.3	32.9	17.4	15.9	0.0
WC-DAO-A1-VIS13	26.5	11.3	31.7	18	12.5	0.0
WC-DAO-A1-VIS29	33.6	10.3	29.6	14.9	11.5	0.0
WC-VB-A1	0.0	9.7	35.5	22.2	31.8	0.8
WC-VB-A1-VIS15	3.8	10.3	38.6	20.0	27.3	0.6
WC-VB-A1-VIS9	7.3	10.1	36.1	18.9	27.5	0.7

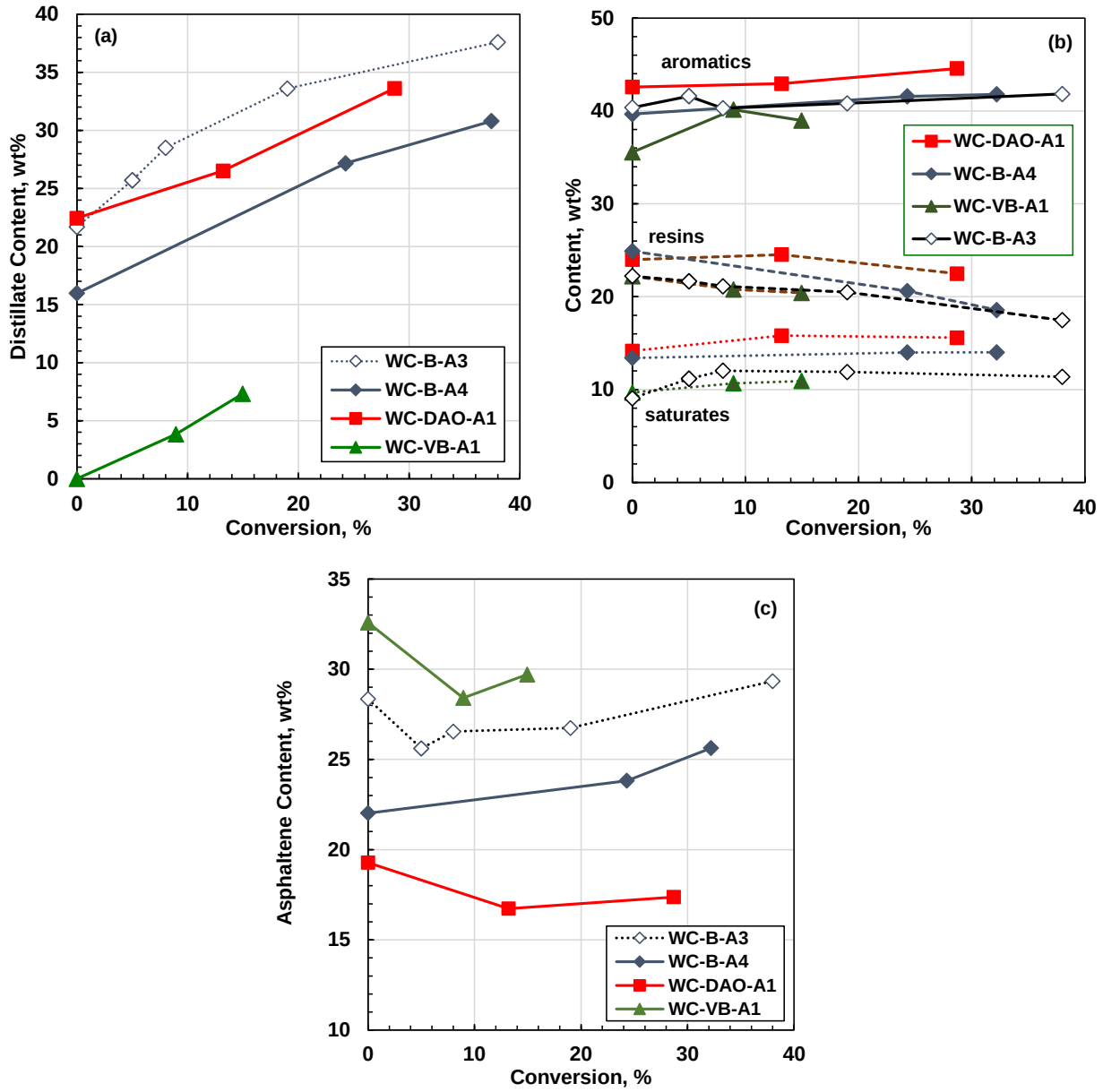

Figure 5-3. Effect of conversion on oil composition: a) distillates content in the whole oil; b) saturate, aromatic, and resin contents in the SBD residue; c) asphaltene content in the SBD residue. The repeatability of the distillate, saturate, aromatics, resin, and asphaltene contents were 0.4, 0.05, 1.05, 0.62, 0.71 wt%, respectively.

5.2 Density and Viscosity

5.2.1 Whole Oil

The measured densities and viscosities of the whole oils as a function of temperature are provided in Appendix A and B. Figures 5-4a and 5-5a show the effect of visbreaking on the density and

viscosity, respectively of the four oils in this study. All of the measurements shown here are reported at 20°C, except for the viscosity of the WC-VB-A1 oil which is reported at 80°C. The viscosity of WC-VB-A1 was much higher than the other oils and the higher temperature was used to put the viscosities on the same scale. To facilitate the comparison of the properties versus conversion trends, the normalized density and viscosities of the oils are also plotted in Figure 5-4b and 5-5b, respectively. The normalized property is defined as the property of the visbroken product divided by the same property of the feedstock.

The repeatability of the measurements is provided in the figure captions. Since the visbreaking experiment and subsequent property measurements require two months per run, the reproducibility of the experiments was not assessed directly. However, there were two indirect indications of the reproducibility of the data. First, two runs were performed on the WC-B-A3 oil at a conversion of approximately 5 wt%. The runs were performed on two different samples from the same source oil and at two different temperatures (420 and 430°C). Despite these differences, the properties of the two samples differed by less than 1% (3.13 kg/m^3) in density and 13% in viscosity. The deviation of the whole oil viscosity was higher, 51%, but was considered to be an outlier based on the maltene and vacuum bottom viscosities. Second, the reproducibility can be inferred from the consistency of the trends in the properties with conversion. The property trends are expected to be smooth and monotonic. The WC-B-A3 oil had sufficient data to establish such a trend and the deviations from this trend suggest a reproducibility of ±1.1 kg/m³ in density and ±30.4% in viscosity.

The density of all of the oils decreased with the increased conversion, consistent with increased distillate yield giving a more paraffinic and lighter oil. The one exception is the density of the WC-B-A3 oil at 38% conversion, which is higher than the density at lower conversions. It is possible that the condensation reactions at high conversions increased the aromaticity and consequently increased the density of the oil (Rodriguez *et. al.,* 2019). It is also possible that the difference is a result of experimental error. The data point was obtained from a previous study and could not be repeated. Similarly, visbreaking reduced the viscosity of oils exponentially by almost two orders of magnitude at conversions above approximately 30%.

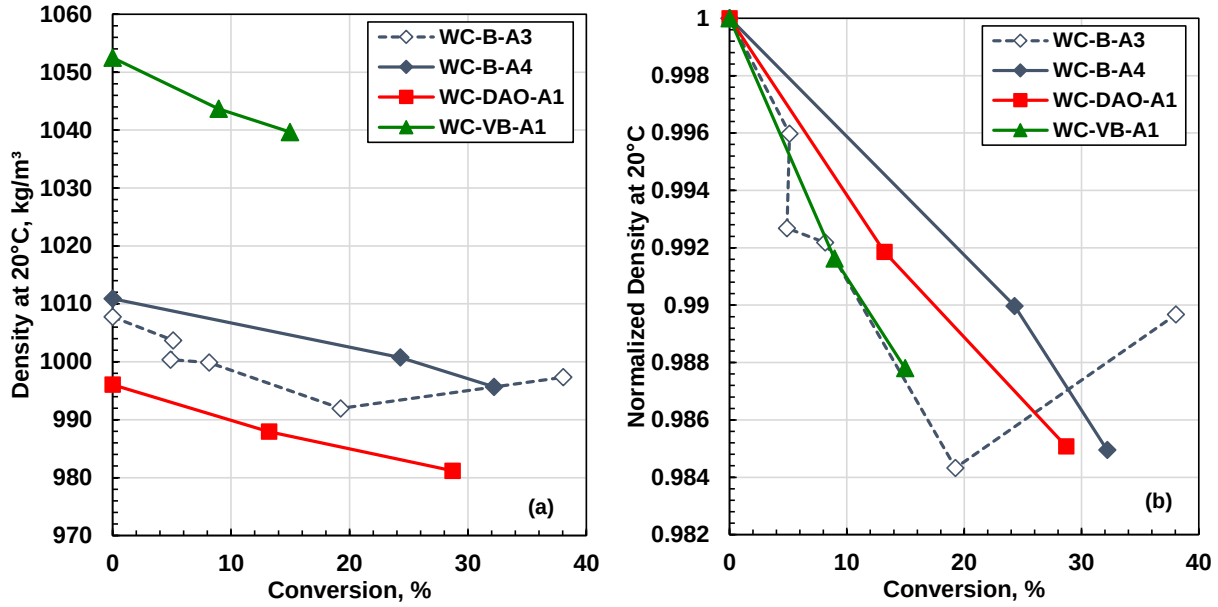

Figure 5-4. Effect of visbreaking on the whole oil density at 20°C and atmospheric pressure: a) absolute density; b) relative density. The repeatability of the density measurements was ±0.15 kg/m³ (±0.0001 for relative density).

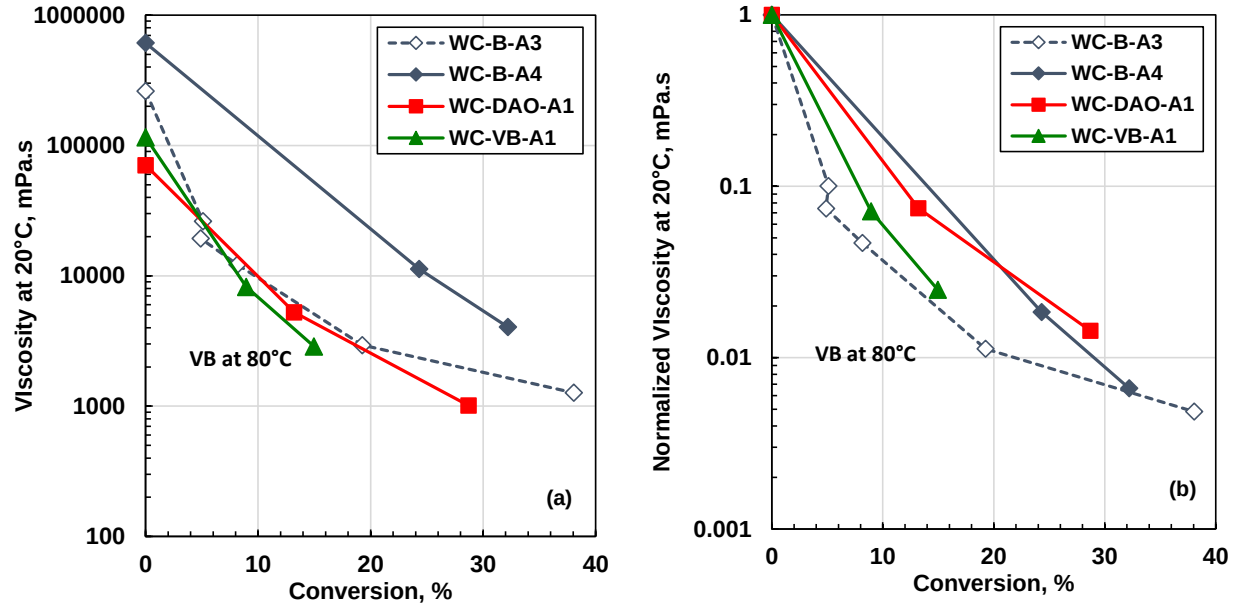

Figure 5-5. Effect of visbreaking on the whole oil viscosity at atmospheric pressure: a) absolute viscosity; b) relative viscosity. Data at 20°C except for WC-VB-A1 at 80°C.

5.2.2 Maltenes

The measured densities and viscosities of the maltenes as a function of temperature are provided in Appendix A and B. Figures 5-6 and 5-7 show the effect of visbreaking on the density and viscosity, respectively, of the four maltenes in this study at 50°C. The maltene densities of the WC-B-A3, WC-B-A4, and WC-DAO-A1 oils followed the same linear increase with increasing conversion, consistent with a loss of side chains, leaving a more aromatic and therefore denser residual fraction. The maltene viscosities decreased with increasing conversion, consistent with a reduction in molecular weight and less entanglement after the loss of side chains. The WC-VB-A1 maltene densities and viscosities were higher than the maltenes from the other oils because light ends were removed when the original oil was distilled to produce the vacuum bottoms. The WC-VB-A1 maltene density did not follow a consistent trend with conversion, and it is not clear if the inconsistency arose from experimental error or a real difference in behavior. Its viscosity decreased with increasing conversion like the other oils.

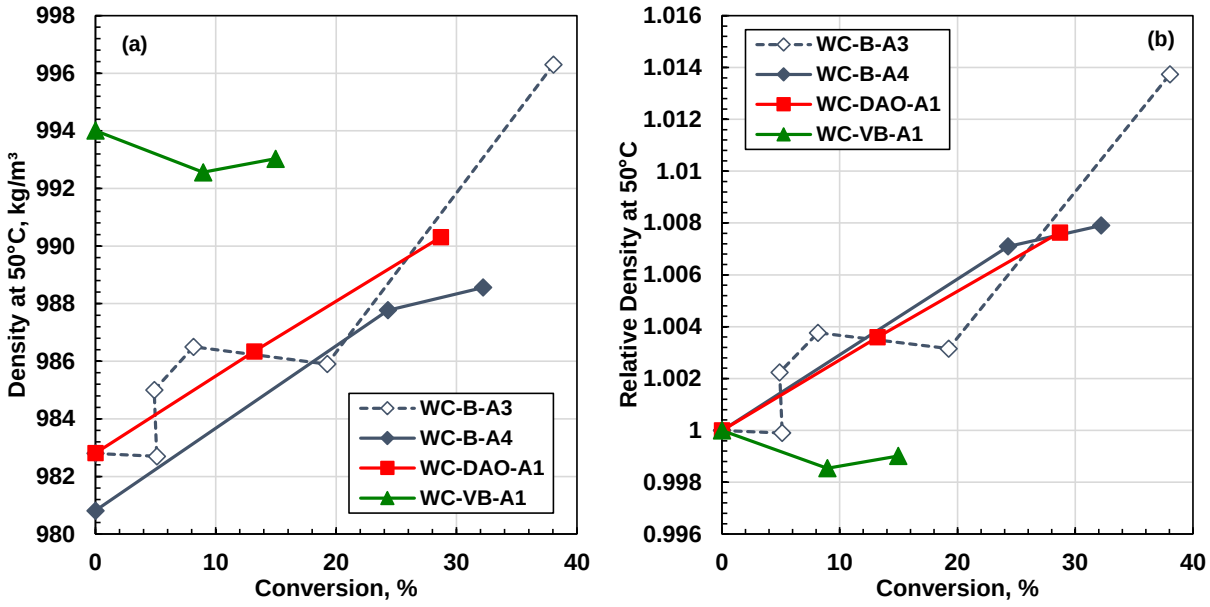

Figure 5-6 Effect of visbreaking on the maltenes density at atmospheric pressure and 50°C: a) absolute density; b) relative density.

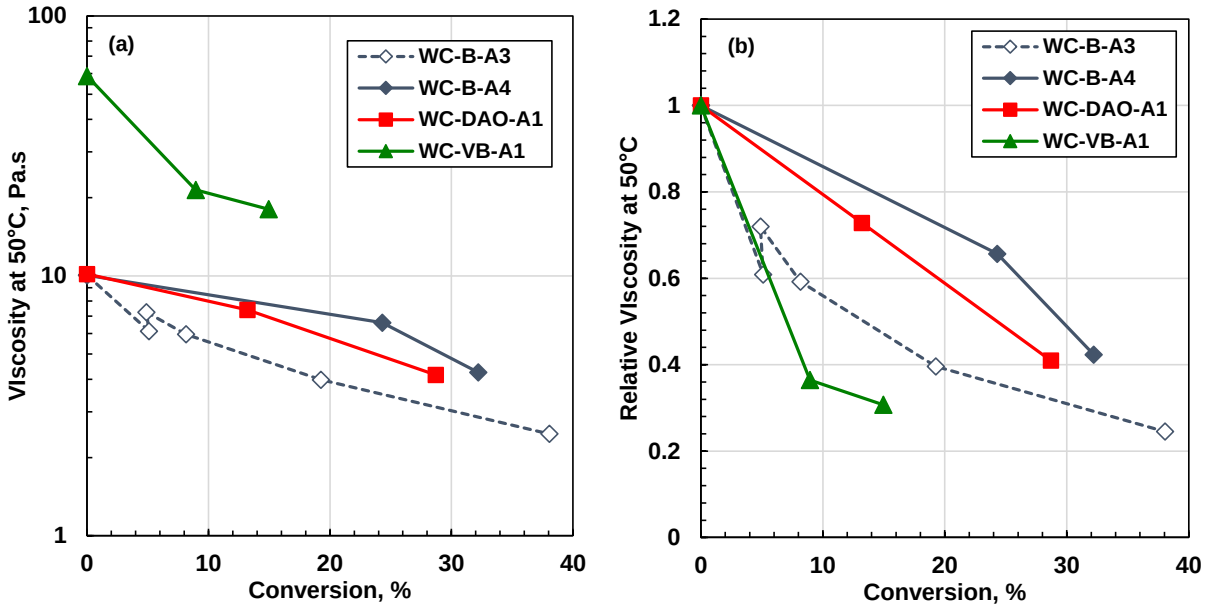

Figure 5-7. Effect of visbreaking on the maltenes viscosity at atmospheric pressure and 50°C: a) absolute viscosity; b) relative viscosity.

5.2.3 Residue

The measured densities and viscosities of the maltenes and residues as a function of temperature are provided in Appendix A and B. Figures 5-8a and 5-9a show the effect of visbreaking on the density and viscosity, respectively of the four residues in this study. The trends in the residue densities and viscosities were similar to those of the maltenes. In general, their density increased with increasing conversion and their viscosities decreased. The WC-VB-A1 oil residues had a higher density and viscosity than the other residues because the WC-VB-A1 feed had its light ends removed. As with the maltenes, the WC-VB-A1 residue density did not follow a consistent trend with conversion and it is not clear if the inconsistency arose from experimental error or a real difference in behavior. Its viscosity decreased with increasing conversion like the other oils. One difference from the maltenes is that the WC-DAO-A1 residues had lower density and viscosity than the other residues because the original feed oil had been partially deasphalted.

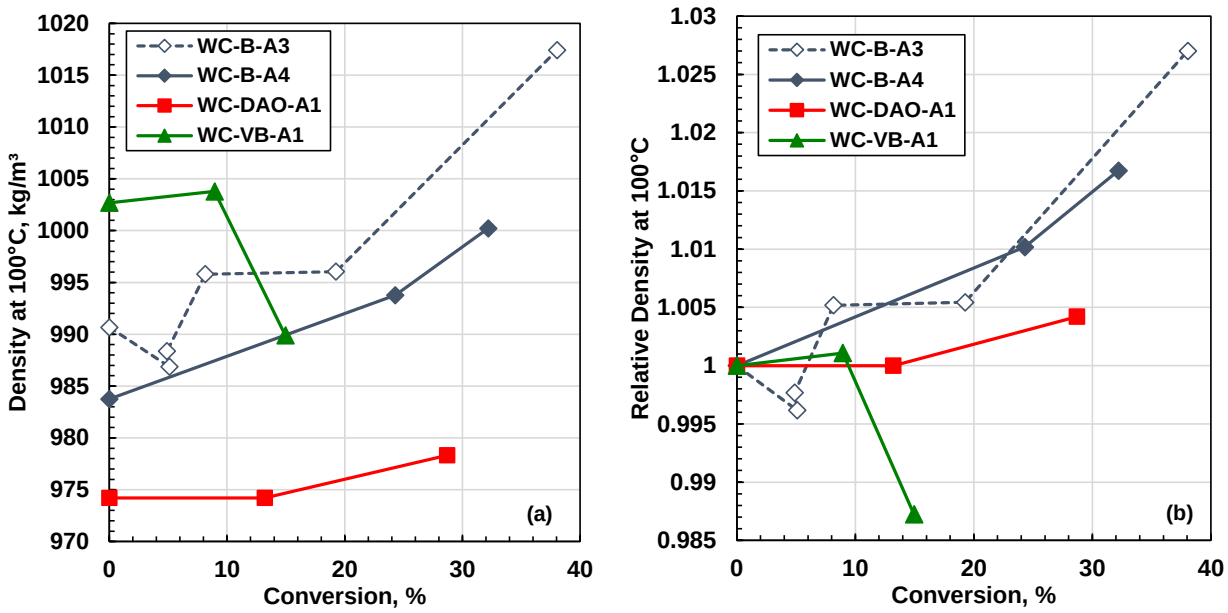

Figure 5-8. Effect of visbreaking on the SBD residue density at atmospheric pressure and 100°C: a) absolute density; b) relative density.

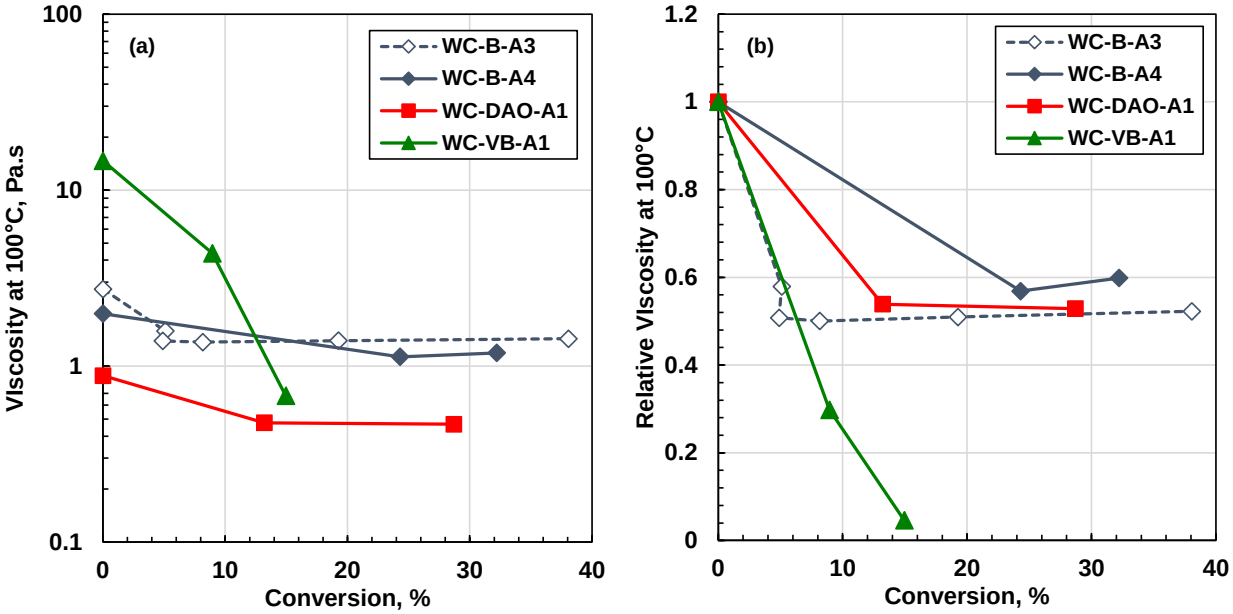

Figure 5-9. Effect of visbreaking on the SBD residue viscosity at atmospheric pressure and 100°C: a) absolute viscosity; b) relative viscosity.

5.2.4 Distillates

Recall that the viscosity of the distillates was calculated from the SBD assay using correlations (Eqs. 4-54 to 4-63). The viscosities of the distillates from WC-DAO-A1 feed and its visbroken products were measured to test the correlations. The viscosity predicted by the correlation matched the measurements to within the measurement error of ±10%, as shown in Table 5-3. The small increase in density for the WC-DAO-A1-VIS15 sample is attributed to experimental error because it is challenging to control the loss of volatiles from the distillates and because the addition of side change fragments is expected to reduce the viscosity as noted below. Therefore, the correlations were used to determine the distillate viscosities in all cases. The distillate densities were measured. The measured densities and calculated viscosities of the distillates from each of the four oils and their visbroken products are provided in Appendices A and B, respectively.

Table 5-3. Comparison of measured and correlated distillate fraction viscosities at 10°C.

Oil	**Measurement mPa·s**	**Correlation mPa·s**	**Deviation %**
WC-DAO-A1	17.8	18.7	5.1
WC-DAO-A1-VIS15	18.8	18.5	1.6
WC-DAO-A1-VIS29	10.9	10.5	4.1

Figure 5-10 shows that the distillate densities decreased with the conversion except for the WC-VB-A1 oil. There were no distillates in the WC-VB-A1 feed oil and therefore the distillates from its reacted products were exclusively material generated by the reactions. Figure 5-10 shows that the distillate reaction products have a density of approximately 875 kg/m³. The distillates in the products from the other oils were a mixture of the reaction products and the original distillates from the feed. Their density likely decreased because relatively low-density reaction products were added to the original distillates. Figure 5-11 shows that while, there is some scatter, the distillate viscosity tended to decrease with increasing conversion in all cases.

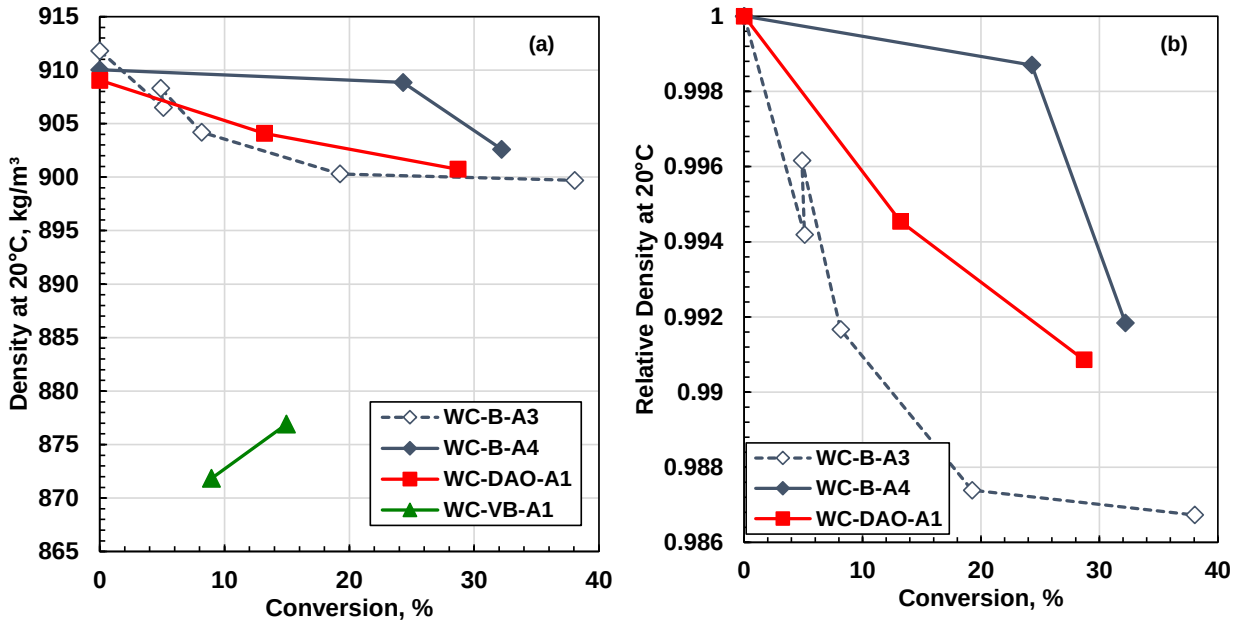

Figure 5-10. Effect of visbreaking on the distillate density at 20°C and atmospheric pressure: a) absolute density; b) relative density. The WC-VB-A1 feed had no distillates and therefore its relative density could not be calculated.

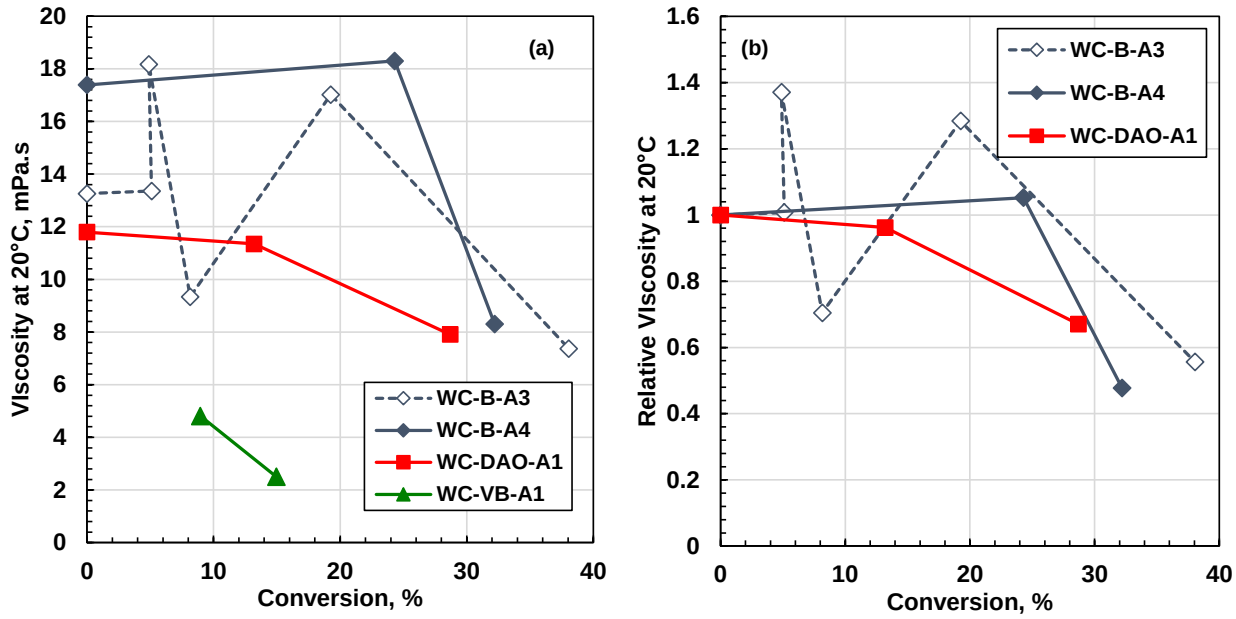

Figure 5-11. Effect of visbreaking on the distillate viscosity at 20°C and atmospheric pressure: a) absolute viscosity; b) relative viscosity. The WC-VB-A1 feed had no distillates and therefore its relative viscosity could not be calculated.

5.2.5 SARA Fractions

The densities and viscosities of the SARA fractions from each of the four oils and their visbroken products are provided in Appendix A and B. The density and viscosity of the saturates and aromatics and the density of the resins were measured. The viscosity of the resins and the density and viscosity of the asphaltenes were determined by fitting the property model to the maltene and residue density and viscosity data.

Figure 5-12 shows that, in general, the saturate density changed little with increasing conversion with a slight decrease in some cases. It appears that there was little alteration of the saturate densities or any alternations were compensated by the addition of fragments generated by the reactions. Figures 5-13 and 5-14 show that the aromatic and resins densities both increased approximately linearly with increasing conversion, consistent with a loss of side chains. Figure 5-15 shows that there are no consistent trends in the asphaltene density with the conversion. Recall that the asphaltene densities were calculated indirectly from the residue densities. Therefore, the calculated values reflect several factors, including real changes, the accumulation of experimental errors, and deviations from the volumetric mixing rule used in the density calculation. Any real trends in the data may be obscured by the measurement errors and model deviations.

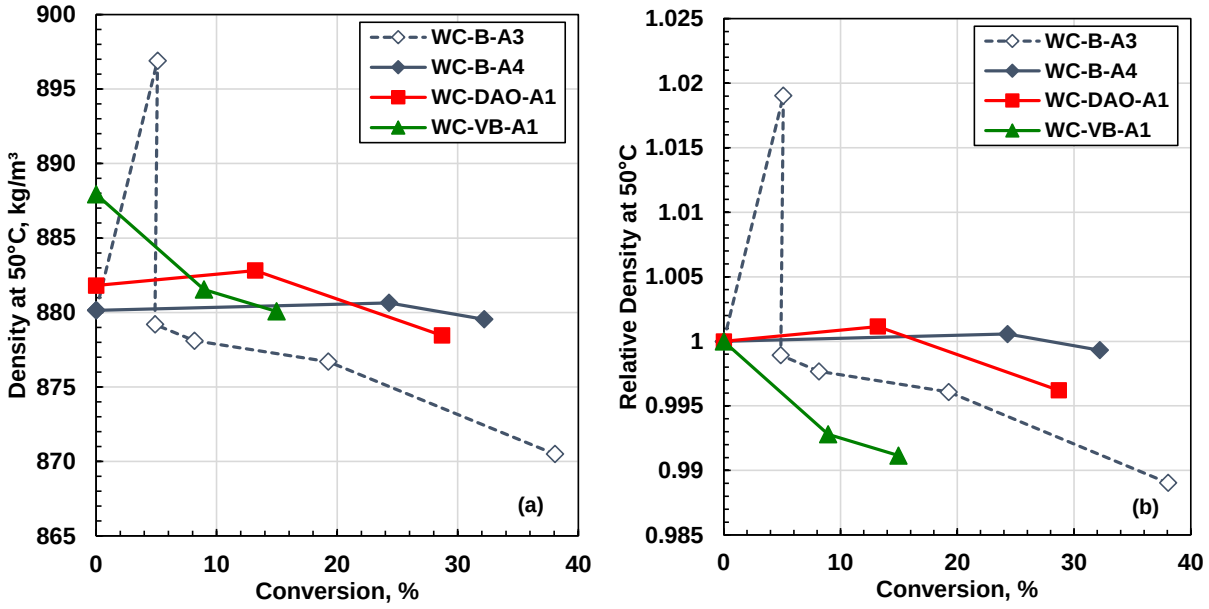

Figure 5-12. Effect of visbreaking on the saturate densities at 50°C and atmospheric pressure: a) absolute density; b) relative density.

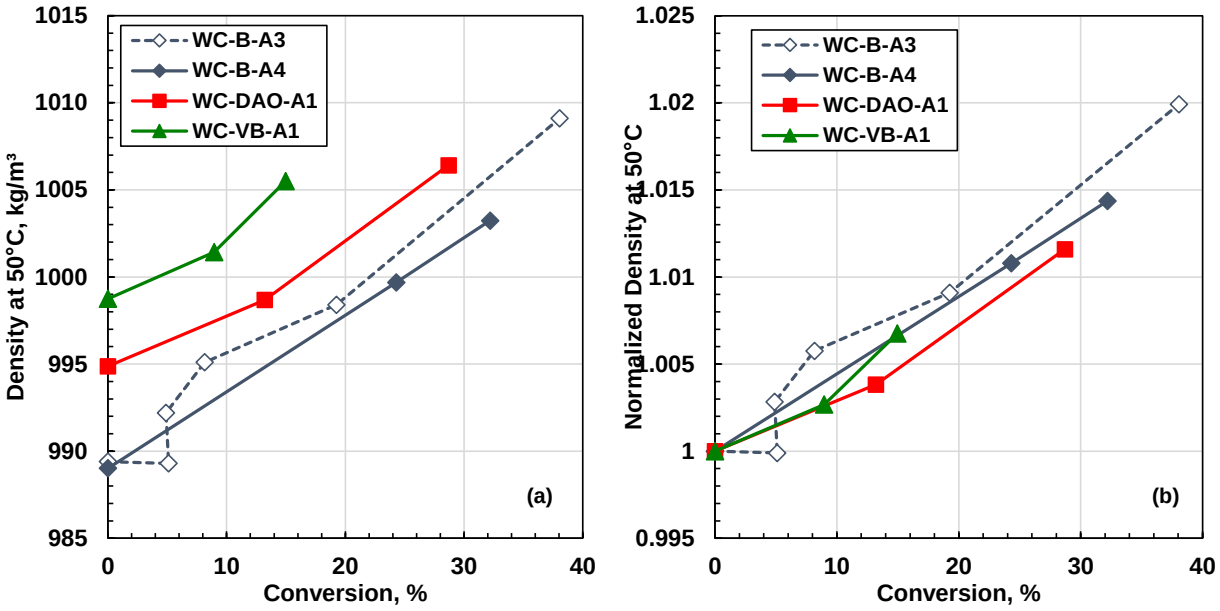

Figure 5-13. Effect of visbreaking on the aromatic densities at 50°C and atmospheric pressure: a) absolute density; b) relative density.

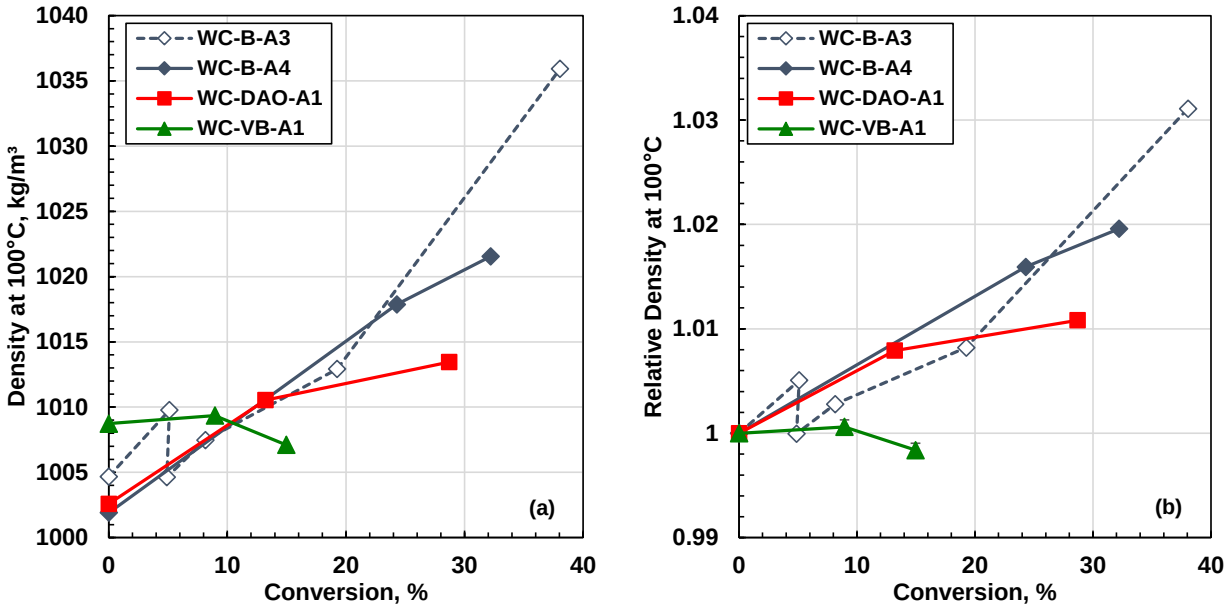

Figure 5-14. Effect of visbreaking on the resin densities at 100°C and atmospheric pressure: a) absolute density; b) relative density.

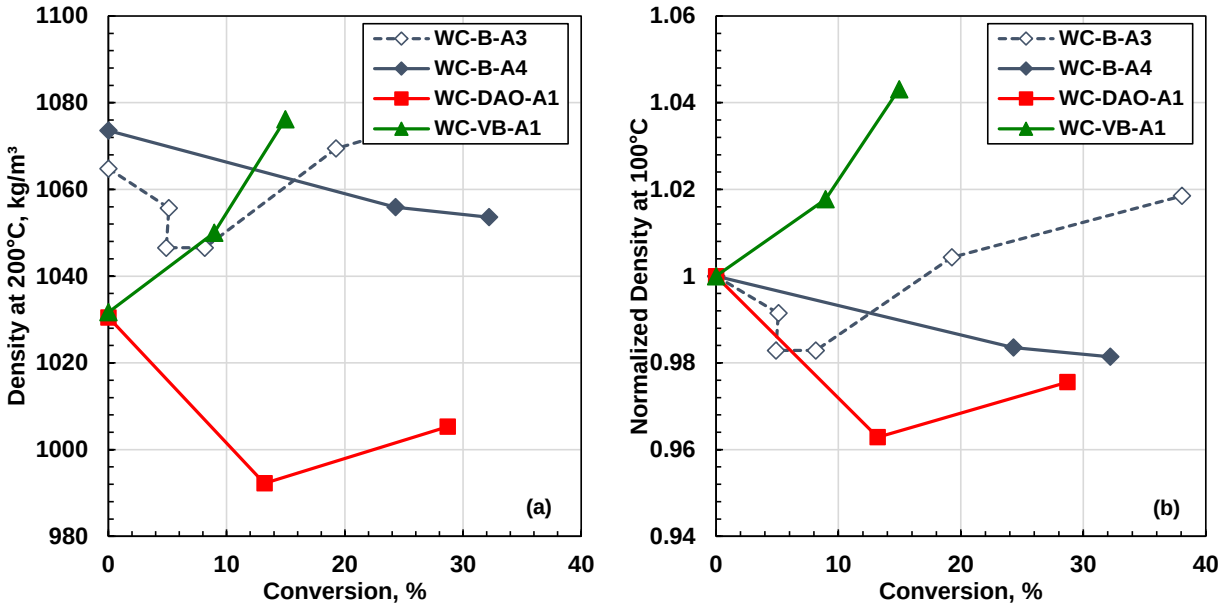

Figure 5-15. Effect of visbreaking on the asphaltene densities at 200°C and atmospheric pressure: a) absolute density; b) relative density. The densities were calculated from the residue densities.

Figure 5-16 shows that, in general, the saturate viscosity decreased with increasing conversion consistent with the addition of low-density side chain fragments from the reactions. The changes in viscosity (and density) were most prominent for the WC-VB-A1 oil. This saturates from this oil were depleted of their lightest fraction and therefore had a higher density and viscosity than the saturates from the other oils. Therefore, the low density and viscosity reaction fragments had a greater relative impact on the density and viscosity of the saturates in the visbroken product for this oil.

Figure 5-17 shows that the aromatic viscosities decreased with increasing conversion. The most significant changes were observed in the WC-VB-A1 oil, likely for the same reason discussed for its saturate fraction. Figure 5-18 shows that there are no consistent trends in the resin density with conversion. As with the asphaltene densities, these were calculated values and any real trends in the data may be obscured by the measurement errors and model deviations. Figure 5-19 shows that the asphaltene viscosities decrease dramatically with increasing conversion, consistent with previous results (Marquez *et. al.,* 2020). The exception is the viscosity of the WC-VB-A1-VIS15 product. It is likely that experimental error caused this deviation since no other unusual trends were observed for this sample.

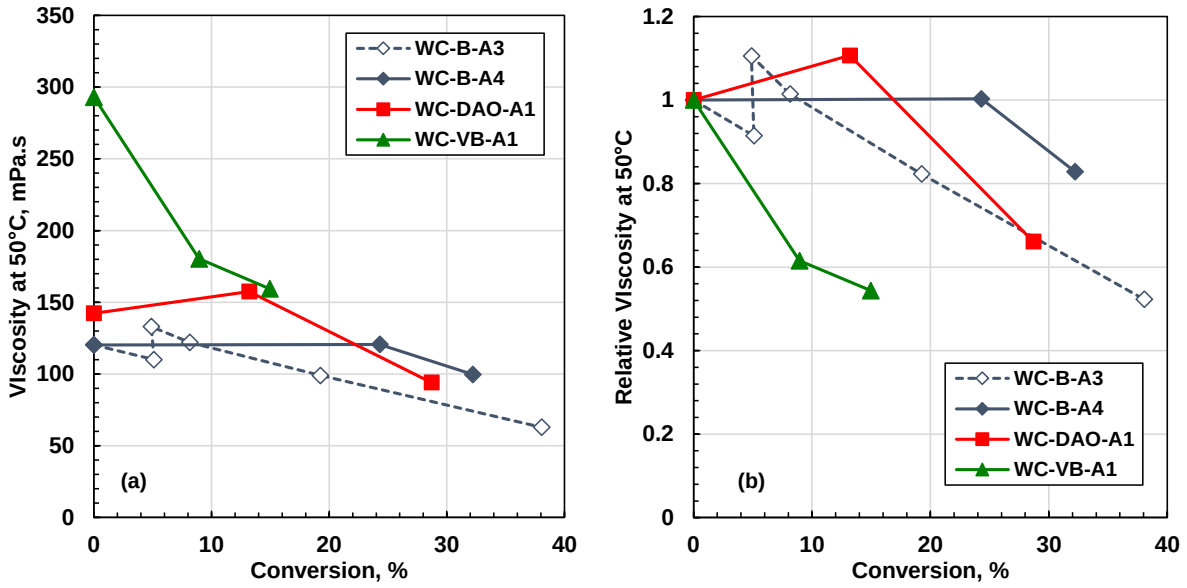

Figure 5-16. Effect of visbreaking on the saturate viscosities at 50°C and atmospheric pressure: a) absolute density; b) relative viscosity.

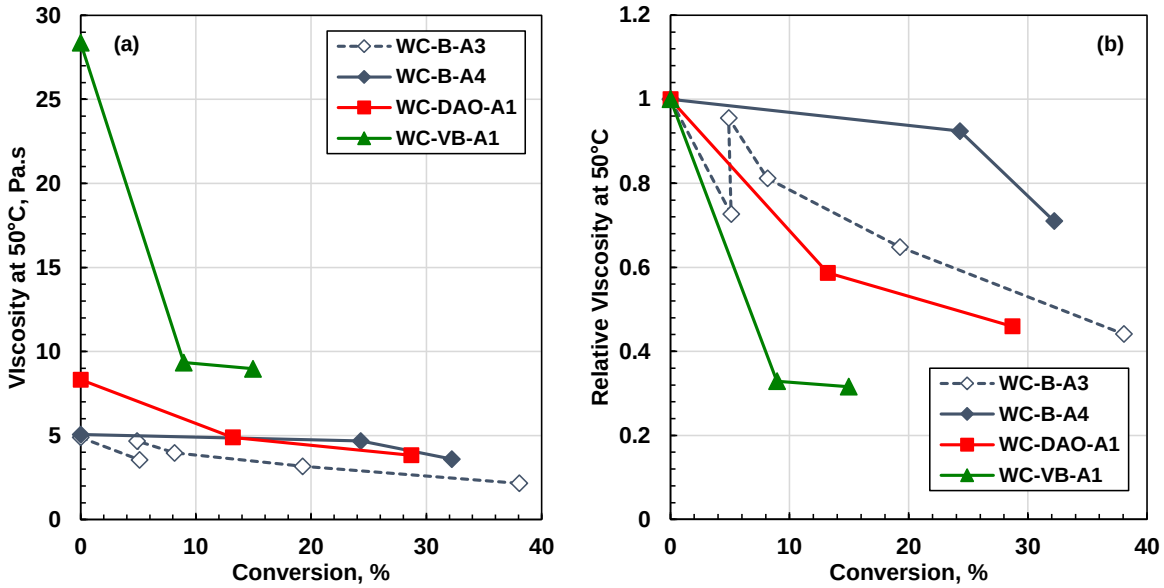

Figure 5-17. Effect of visbreaking on the aromatic viscosities at 50°C and atmospheric pressure: a) absolute density; b) relative viscosity.

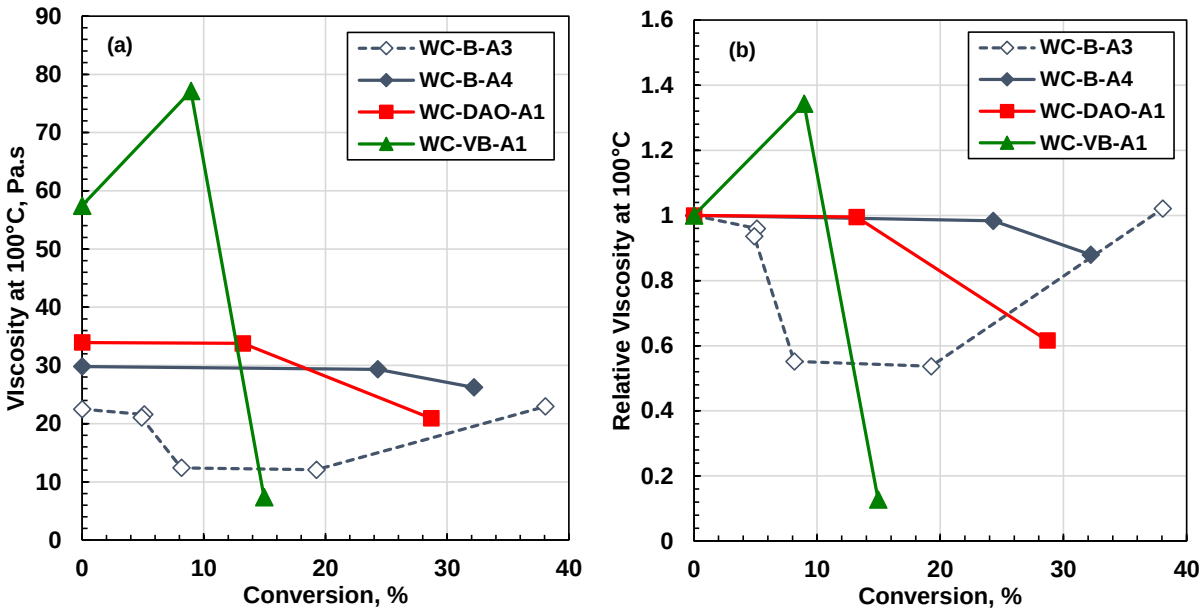

Figure 5-18. Effect of visbreaking on the resin viscosities at 100°C and atmospheric pressure: a) absolute viscosity; b) relative viscosity.

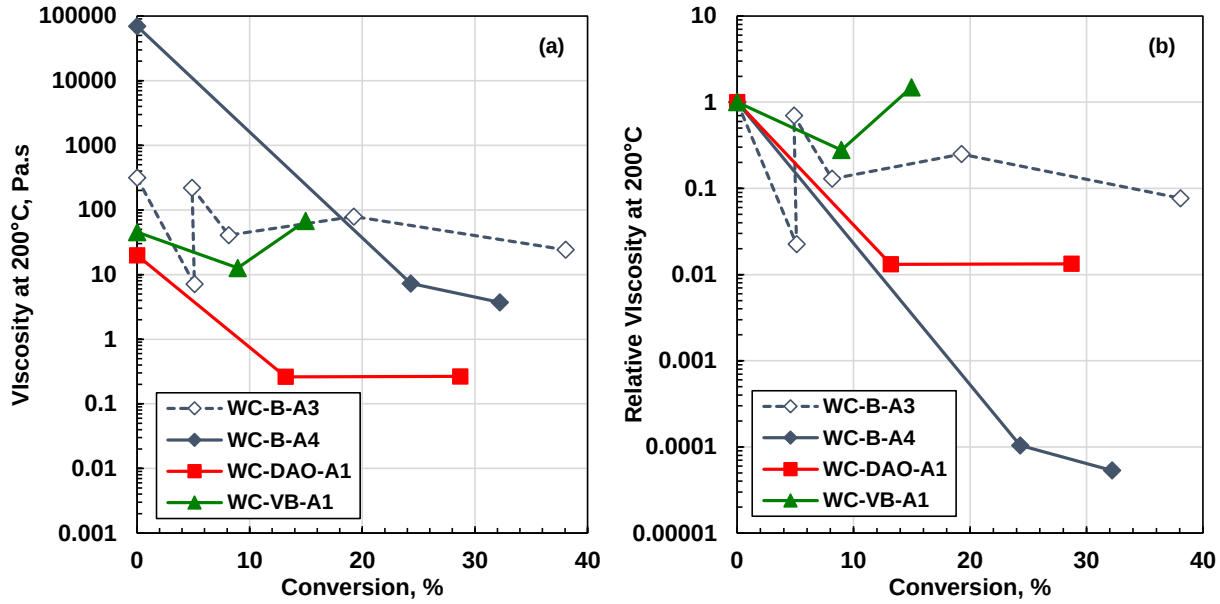

Figure 5-19. Effect of visbreaking on the asphaltene viscosities at 200°C and atmospheric pressure: a) absolute viscosity; b) relative viscosity. The asphaltene viscosities were calculated form modeling the residue viscosities.

5.2.6 Fitted Model Parameters

The density model requires two parameters ($\rho_{REF,}$ b) determined from fitting density data versus temperature. The viscosity model also requires two parameters (ρ_s^o and c_2) determined from fitting viscosity data versus temperature. The density and viscosity data for each component are provided in Appendix A and B. The fitted parameters are listed in Tables 5-4 to 5-8 for the distillates, saturates, aromatics, resins, and asphaltenes, respectively.

Table 5-4. Fitted density and viscosity model parameters for the distillates of the four oils in this study.

Sample	A kg/m³	B kg/m³K	c_2	ρ_s^o kg/m³
WC-B-A3	925.47	-0.685	0.232	984.89
WC-B-A3- VIS5a	920.26	-0.689	0.231	978.59
WC-B-A3- VIS5b	922.22	-0.695	0.232	976.44
WC-B-A3- VIS8	918.21	-0.700	0.231	982.56
WC-B-A3- VIS19	914.37	-0.702	0.229	980.63
WC-B-A3- VIS38	914.02	-0.717	0.229	981.56
WC-B-A4	923.67	-0.680	0.231	978.47
WC-B-A4-VIS24	922.65	-0.690	0.232	976.89
WC-B-A4-VIS32	916.55	-0.696	0.234	983.97
WC-DAO-A1	922.71	-0.683	0.239	986.05
WC-DAO-A1-VIS13	917.94	-0.692	0.228	977.84
WC-DAO-A1-VIS29	914.75	-0.700	0.232	982.32
WC-VB-A1	-	-	-	-
WC-VB-A1-VIS15	886.79	-0.748	0.216	955.69
WC-VB-A1-VIS9	891.71	-0.739	0.222	982.58

Table 5-5. Fitted density and viscosity model parameters for the saturates of the four oils in this study.

Sample	A kg/m³	B kg/m³K	c_2	ρ_s^o kg/m³
WC-B-A3	912.45	-0.610	0.404	962.48
WC-B-A3- VIS5a	909.11	-0.610	0.396	959.72
WC-B-A3- VIS5b	909.63	-0.608	0.408	960.44
WC-B-A3- VIS8	908.61	-0.610	0.406	959.92
WC-B-A3- VIS19	907.36	-0.613	0.401	960.06
WC-B-A3- VIS38	900.91	-0.610	0.384	955.70
WC-B-A4	910.46	-0.606	0.396	960.17
WC-B-A4-VIS24	911.03	-0.608	0.392	960.25
WC-B-A4-VIS32	910.01	-0.609	0.394	961.25
WC-DAO-A1	912.53	-0.614	0.444	969.58
WC-DAO-A1-VIS13	913.38	-0.611	0.448	970.17
WC-DAO-A1-VIS29	909.28	-0.616	0.419	966.27
WC-VB-A1	918.09	-0.603	0.458	970.14
WC-VB-A1-VIS15	911.77	-0.605	0.436	964.75
WC-VB-A1-VIS9	910.36	-0.606	0.433	963.98

Table 5-6. Fitted density and viscosity model parameters for the aromatics of the four oils in this study.

Sample	A kg/m³	B kg/m³K	c_2	ρ_s^o kg/m³
WC-B-A3	1020.76	-0.628	0.443	1054.37
WC-B-A3- VIS5a	1020.83	-0.629	0.440	1056.03
WC-B-A3- VIS5b	1023.71	-0.630	0.461	1060.21
WC-B-A3- VIS8	1026.70	-0.631	0.439	1061.19
WC-B-A3- VIS19	1030.19	-0.635	0.428	1064.53
WC-B-A3- VIS38	1041.31	-0.642	0.403	1074.88
WC-B-A4	1021.63	-0.652	0.456	1055.67
WC-B-A4-VIS24	1031.11	-0.628	0.446	1066.12
WC-B-A4-VIS32	1034.87	-0.633	0.414	1066.65
WC-DAO-A1	1026.20	-0.626	0.444	1057.01
WC-DAO-A1-VIS13	1030.11	-0.629	0.432	1062.73
WC-DAO-A1-VIS29	1038.30	-0.638	0.419	1070.42
WC-VB-A1	1029.76	-0.620	0.482	1059.70
WC-VB-A1-VIS15	1032.65	-0.625	0.457	1065.24
WC-VB-A1-VIS9	1036.91	-0.628	0.447	1068.23

Table 5-7. Fitted density and viscosity model parameters for the resins of the four oils in this study.

Sample	A kg/m³	B kg/m³K	c_2	ρ_s^o kg/m³
WC-B-A3	1065.39	-0.607	0.595	1081.59
WC-B-A3- VIS5a	1071.21	-0.614	0.601	1088.16
WC-B-A3- VIS5b	1066.12	-0.615	0.594	1081.96
WC-B-A3- VIS8	1066.12	-0.615	0.594	1081.96
WC-B-A3- VIS19	1074.48	-0.616	0.555	1089.26
WC-B-A3- VIS38	1100.33	-0.644	0.537	1109.76
WC-B-A4	1060.07	-0.582	0.602	1077.71
WC-B-A4-VIS24	1080.96	-0.631	0.623	1097.73
WC-B-A4-VIS32	1082.26	-0.617	0.560	1093.28
WC-DAO-A1	1066.43	-0.620	0.622	1081.83
WC-DAO-A1-VIS13	1072.43	-0.619	0.602	1085.93
WC-DAO-A1-VIS29	1074.15	-0.618	0.557	1086.59
WC-VB-A1	1069.29	-0.606	0.624	1083.69
WC-VB-A1-VIS15	1070.38	-0.610	0.647	1085.34
WC-VB-A1-VIS9	1068.53	-0.614	0.631	1083.84

Table 5-8. Fitted density and viscosity model parameters for the asphaltenes of the four oils in this study.

Sample	A kg/m³	B kg/m³K	c_2	ρ_s^o kg/m³
WC-B-A3	1177.12	-0.562	0.980	1169.93
WC-B-A3- VIS5a	1179.76	-0.620	0.969	1173.55
WC-B-A3- VIS5b	1177.41	-0.654	0.970	1187.47
WC-B-A3- VIS8	1177.41	-0.654	0.963	1188.76
WC-B-A3- VIS19	1186.08	-0.583	0.940	1176.65
WC-B-A3- VIS38	1203.65	-0.596	0.901	1183.88
WC-B-A4	1179.90	-0.532	0.980	1169.28
WC-B-A4-VIS24	1172.55	-0.583	0.930	1166.51
WC-B-A4-VIS32	1178.46	-0.624	0.913	1162.45
WC-DAO-A1	1133.79	-0.516	0.980	1170.64
WC-DAO-A1-VIS13	1129.46	-0.686	0.953	1192.44
WC-DAO-A1-VIS29	1134.71	-0.647	0.921	1206.51
WC-VB-A1	1159.08	-0.637	0.980	1170.64
WC-VB-A1-VIS15	1172.67	-0.613	0.961	1188.74
WC-VB-A1-VIS9	1184.91	-0.544	0.949	1188.74

5.3 Molecular Weight

The molecular weights of the SARA fractions of the feed oils were measured using VPO while the molecular weight of the distillates was determined from the SBD assay, as explained in Chapter 4. The molecular weights of the reacted fraction were not measured. The numbers are shown in Table 5-9. The WC-VB-A1 oil had no distillates and so no molecular weight is reported. In general, the molecular weight of each fraction does not vary from oil to oil beyond the experimental error of ±15%.

The asphaltene molecular weights are apparent molecular weights for extracted asphaltene nanoaggregates dissolved in toluene. Since asphaltenes self associate differently in crude oil than in a pure solvent, these measurements do not represent the average apparent molecular weight of the asphaltenes in the bitumen. They were used only for modeling the solubility measurements of saturates and aromatics in mixtures of asphaltenes and a pure solvent.

Table 5-9. The molecular weight of distillates, saturates, aromatics, resins, and extracted asphaltenes from the four feed oils. NM indicates that no measurement was performed.

Sample	Distillates g/mol	Saturates g/mol	Aromatics g/mol	Resins g/mol	Asphaltenes g/mol
WC-B-A3	220	610	640	1200	4100
WC-B-A4	210	570	600	1150	5160
WC-DAO-A1	210	480	650	1010	4560
WC-VB-A1	-	580	600	1350	NM

5.4 Solubility

To use the MRS model, the solubility parameters of the distillates, saturates, aromatics, and resins are required as well as the minimum and maximum solubility parameter of the asphaltenes in the oil. As explained in Chapter 4, an attempt was made to determine the solubility parameters of the saturates and aromatics in the feeds by modeling asphaltene yields from solutions of asphaltenes (extracted from the WC-B-A4 bitumen), the oil fraction, and either toluene or *n*-heptane. These measurements are time-consuming and were not performed for the products. The distillate and asphaltene solubility parameters for all feeds and their products were determined by modeling

asphaltene yields from whole oils and residues diluted with toluene and mixed with *n*-heptane. The resin solubility parameter was set to the minimum asphaltene solubility parameter of the same oil. The determination of the solubility parameters is discussed in more detail below.

5.4.1 Extracted Asphaltenes, Saturates, and Aromatics in Pure Solvents

The solubility parameters of the WC-B-A4 extracted asphaltenes in toluene must be determined before modeling solubility data from solutions with the saturates or aromatics. Figure 5-20 shows the fraction of asphaltenes precipitated from mixtures of the WC-B-A4 asphaltenes, toluene, and *n*-heptane. These data were fitted with the MRS model to obtain the minimum and maximum solubility parameters of 20.0 and 21.7 $MPa^{0.5}$, respectively. These values are similar to the previously reported minimum and maximum asphaltene solubility parameter of asphaltenes extracted from the WC-B-A3 bitumen, 19.9 and 21.25 $MPa^{0.5}$, respectively (Rodriguez *et. al.*, 2019).

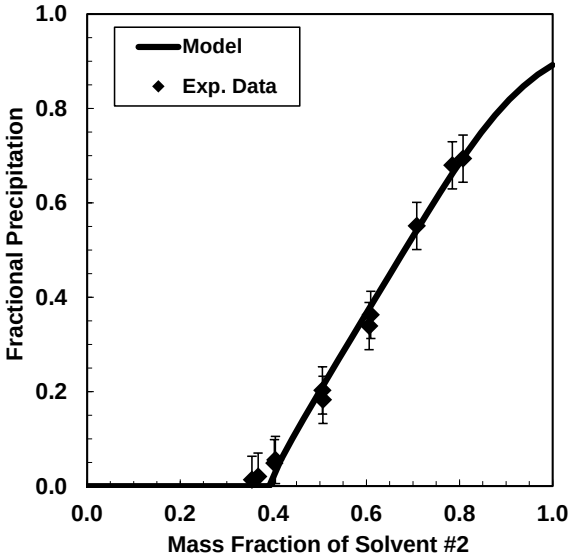

Figure 5-20. Yield plot of A4 extracted asphaltenes and the fitted curve using the Modified Regular Solution model to obtain solubility parameter.

Figure 5-21a shows the measured and modeled fractional asphaltene precipitation from solutions of asphaltenes, *n*-heptane, and WC-B-A4 aromatics. Figure 5-21b shows the same type of data from solutions of asphaltenes, toluene, and WC-B-A4 saturates. Similar results were obtained for

the aromatics and saturates from the other oils, as shown in Appendix E. The fitted solubility parameters are summarized in Table 5-10. The fitted aromatic solubility parameters for the aromatics were consistent with each other and with previous values from Rodriguez *et. al.*, (2019). An average value of 20.8 MPa0.5 is recommended for aromatics. The fitted saturate solubility parameters were too low to be physically plausible (15.8 $MPa^{0.5}$ compared with 15.3 for *n*-heptane, a much smaller and more paraffinic molecule). Therefore, the previously determined value of 16.5 $MPa^{0.5}$ from Rodriquez *et. al.*, (2019) is recommended. The effect of visbreaking on the solubility parameters was not examined; instead, previously established correlations will be used in the MRS model.

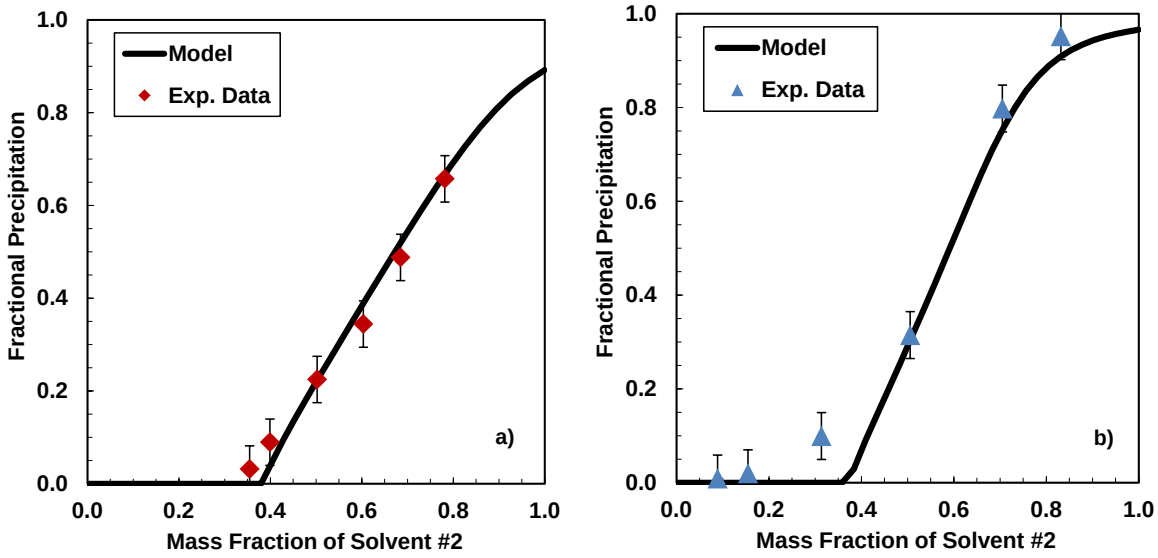

Figure 5-21. Yield plot of solutions of asphaltenes, *n*-heptane, and a) WC-B-A4 aromatics and b) WC-B-A4 saturates. The curves were fitted using the Modified Regular Solution model to obtain the solubility parameter.

Table 5-10. Composition of solubility parameters of fractions of feed oils. The 90% confidence intervals for the measured solubility parameters are ± 0.5 and 0.2 $MPa^{0.5}$ for the saturates and aromatics, respectively.

Oil	Saturates $MPa^{0.5}$	Aromatics $MPa^{0.5}$
WC-B-A3	16.5	21.0
WC-B-A4	15.8	20.7
WC-DAO-A1	16.2	20.7
WC-VB-A1	16.1	20.7
Recommended Value	16.5	20.8

5.4.2 Asphaltenes in Oils

Distillate and Asphaltene Solubility Parameters

Figure 5-22 show the measured and fitted asphaltene yields from the whole oil+toluene mixtures. The onset shift to lower *n*-heptane contents and the yields increase with increasing conversion indicating that the asphaltenes became less soluble in the oil. The decrease in solubility is expected because the reacted oils contain more distillates which are poor solvents for asphaltenes. As will be shown later, the asphaltene solubility parameters also increase, indicating that the asphaltenes themselves become less soluble in the oil. Both these effects were discussed by Rodriguez *et. al.*, (2019).

The repeatability of the measurements is provided in the figure captions. The reproducibility was assessed in terms of the onset of precipitation because the yield curves follow from the onset and have a consistent profile versus solvent content above the onset. As discussed in Section 2.1, there were two indirect indications of the reproducibility of the data. First, two runs were performed on the WC-B-A3 oil at a conversion of approximately 5 wt%. The runs were performed on two different samples from the same source oil and at two different temperatures (420 and 430°C). Despite these differences, the onset of precipitation from these two samples differed by less than 7% wt%. Second, the reproducibility can be inferred from the consistency of the trends in the properties with conversion. The property trends are expected to be smooth and monotonic. The

onset of precipitation is plotted versus conversion in Figure 5.23 for the WC-B-A3 oil (the oil with the most conversion data points). A reproducibility of ±2.0 wt% was determined from the deviations of the onset deviations from fitted trend based on a 90% confidence interval.

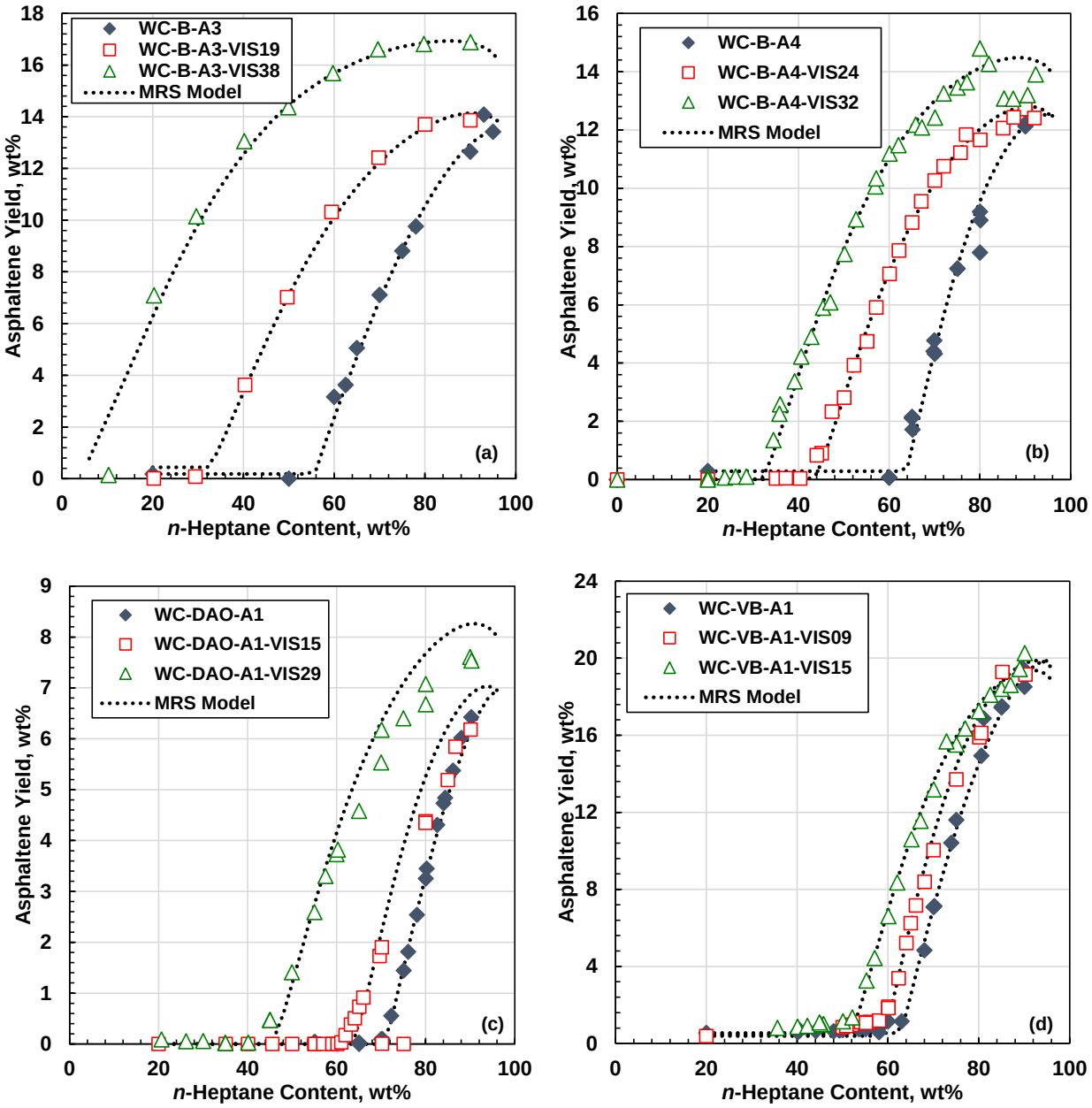

Figure 5-22. Measured and modeled asphaltene yields from whole oil diluted with 0.5 g toluene per g oil and mixed with *n*-heptane at 20°C and atmospheric pressure: a) WC-B-A3; b) WC-B-A4; c) WC-DAO-A1; d) WC-VB-A1.

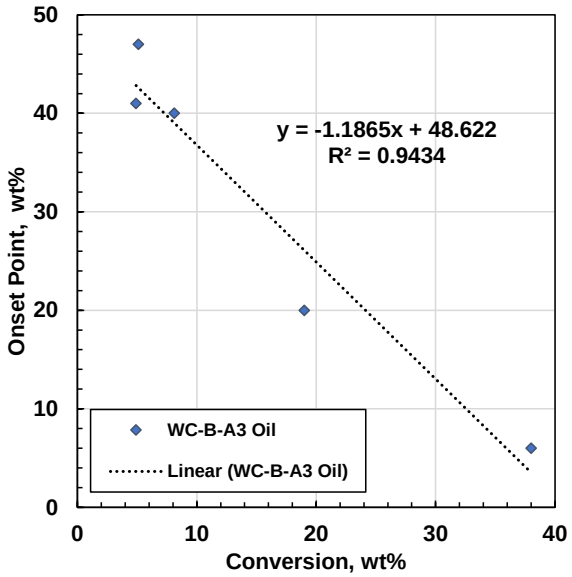

Figure 5-23. The effect of conversion on the onset of precipitation for the WC-B-A3 oil.

The distillate and minimum and maximum asphaltene solubility parameter were determined by modeling asphaltene yields from the whole oils mixed with *n*-heptane and from whole oil and residues each diluted with 0.5 g toluene per g oil and then mixed with *n*-heptane. The measured composition, density, molecular weight were used as the model inputs. The binary interaction parameter between toluene and asphaltenes was set to 0.1 as discussed later in this section. The saturate and aromatic solubility parameters were set to the recommended values. The only difference between the whole oil and the residue was the distillates, and therefore, the distillate parameters were used to match this difference. Then, the asphaltene parameters were optimized to match to all of the yield data. Figure 5-24 shows the measured and modeled asphaltene yields from the WC-B-A4 whole oil, whole+toluene, and residue+toluene each diluted with *n*-heptane. The fitted model matches the data to within the experimental error. Similar results were obtained for the other oils and products, as shown in Appendix F. The fitted solubility parameters are summarized in Table 5-11.

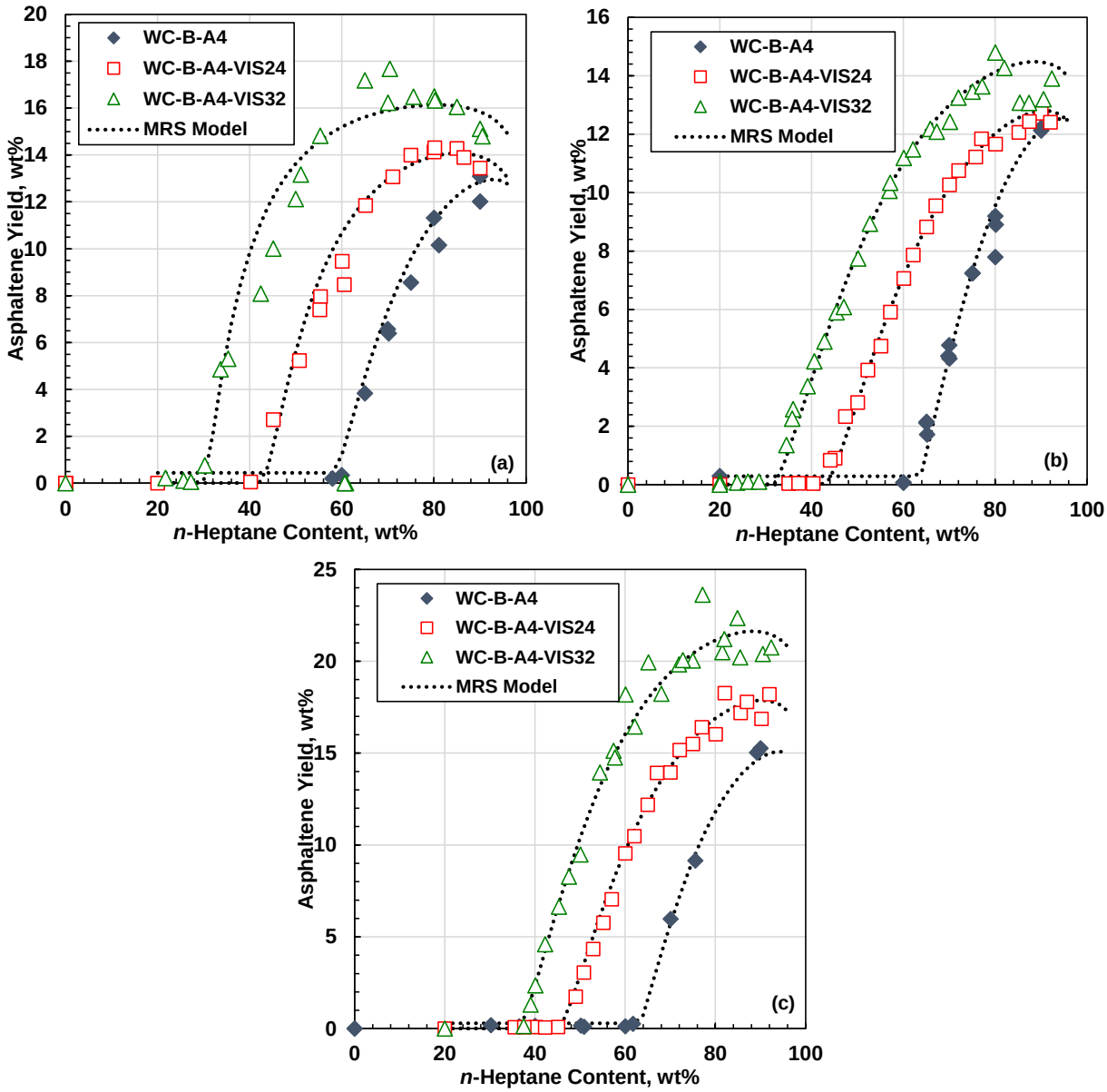

Figure 5-24. Measured and modeled asphaltene yields from a) WC-B-A4 whole oil, b) whole oil with 0.5 g/g toluene, c) SBD residue with 0.5 g/g toluene, each mixed with *n*-heptane at 20°C and atmospheric pressure.

Table 5-11. Fitted distillate and minimum and maximum asphaltenes solubility parameters.

Sample	δ_{dist} $MPa^{0.5}$	δ_{min} $MPa^{0.5}$	δ_{max} $MPa^{0.5}$
WC-B-A3	18.7	19.73	20.57
WC-B-A3- VIS5a	18.4	20.09	20.69
WC-B-A3- VIS5b	18.2	20.21	20.83
WC-B-A3- VIS8	17.9	20.15	20.90
WC-B-A3- VIS19	17.4	20.45	21.09
WC-B-A3- VIS38	16.7	20.81	21.58
WC-B-A4	18.7	19.88	20.35
WC-B-A4-VIS24	17.2	20.20	20.80
WC-B-A4-VIS32	16.9	20.43	21.03
WC-DAO-A1	18.7	19.53	20.14
WC-DAO-A1-VIS13	17.8	19.93	20.34
WC-DAO-A1-VIS29	17.1	20.14	20.73
WC-VB-A1	-	19.55	20.40
WC-VB-A1-VIS15	17.0	19.95	20.55
WC-VB-A1-VIS9	17.0	20.00	20.75

Toluene-Asphaltene Binary Interaction Parameter

Asphaltene yields were measured for whole oils mixed with *n*-heptane and whole oils diluted with toluene and then mixed with *n*-heptane. Rodriguez *et. al.*, (2019) found that the MRS model could not exactly match the two types of measurements with a single set of asphaltene solubility parameters, as shown in Figure 5-25. Recently, Rivero (2021) demonstrated that a binary interaction parameter between asphaltenes and toluene is required to match yield data for mixtures of bitumen, toluene, and *n*-heptane. A binary interaction parameter of 0.01 was found to provide consistent model predictions for both types of yield data with the same asphaltene solubility parameters, as shown for one example in Figure 5-24. Similar results were obtained for all of the oils. Therefore, the binary interaction parameter between asphaltenes and toluene was set to 0.01 for all of the modeling in this thesis.

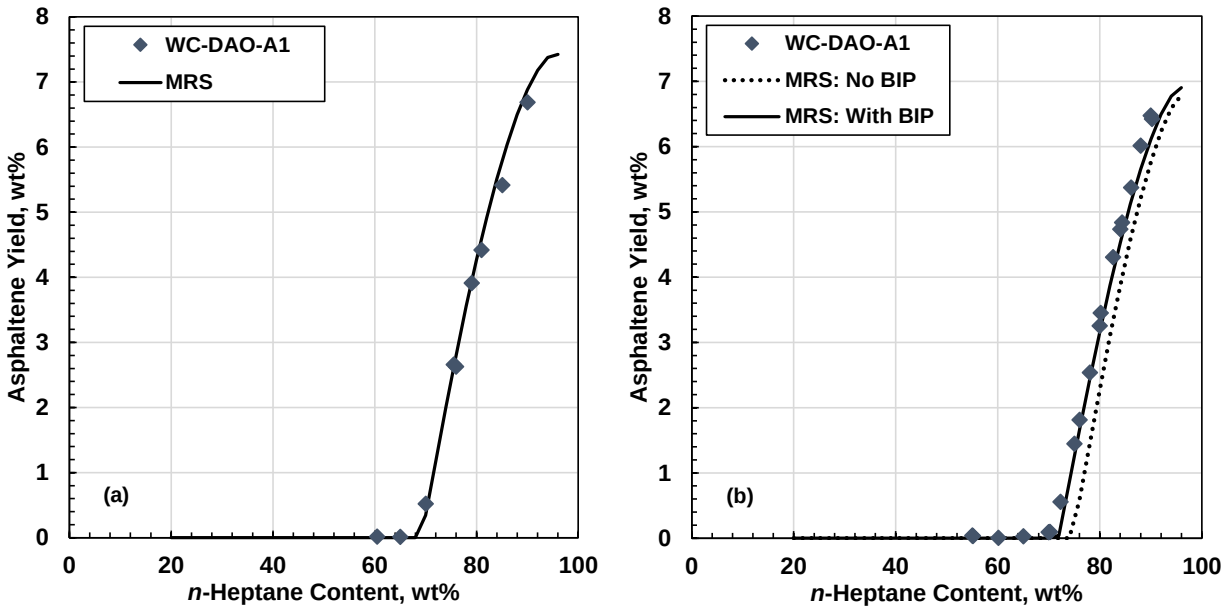

Figure 5-25. The effect of a toluene-asphaltene binary interaction parameter of 0.01 on fitting the yield data from the WC-DAO-A1 oil: a) whole oil (results with and without the BIP are the same because there is no toluene); b) whole oil with 0.5 g toluene per g oil.

Chapter 6: Density and Viscosity Model Performance

This chapter presents the modeling of the density and viscosity of the visbroken oils from the thesis dataset. First, the performance of the density and viscosity models with the previous set of density and viscosity parameter correlations is discussed. Then, updated parameter correlations and recommended default properties are proposed. The performance of the models with the updated correlations is discussed and a tuning method is presented.

6.1 Previous Correlations

Marquez *et. al.* (2020) developed model parameter correlations to predict the density and viscosity of oils that undergo visbreaking reactions. The density and viscosity models and the parameter correlations were presented in Chapter 4. Figures 6-1 to 6-3 show the performance of the viscosity and density models with these correlations for the WC-B-A3, WC-B-A4, and WC-DAO-A1. One weakness of the previous correlations is that the viscosity of the product distillates cannot be predicted unless their boiling curve and densities are measured in order to apply the correlations given in Chapter 4. The density parameters for the feed distillates are required to correlate the density of the reacted distillates. However, the WC-VB-A1 feed oil did not contain any distillates and therefore the correlations could not be used to predict the density or viscosity of the distillates for the products from this oil. Therefore, the density and viscosity of the SBD residues are shown for this oil in Figure 6-4 instead of the whole oils, some of which contain distillates.

The correlations match the measured densities and viscosities for the WC-B-A4 visbroken products as well or even better than for the WC-B-A3 products on which the correlation was developed. However, the correlations consistently over-predicted the density and viscosity of the visbroken products from WC-DAO-A1 oil. The performance of the correlations on density and viscosity of WC-VB-A1 SBD residues was inconsistent. It is possible that different oils react differently, and their properties change differently with the conversion. It is also possible that the correlations were overfitted to bitumen data and could be better generalized to other oil fractions.

In addition, the correlations must be modified to predict densities and viscosities for products from feeds without distillates.

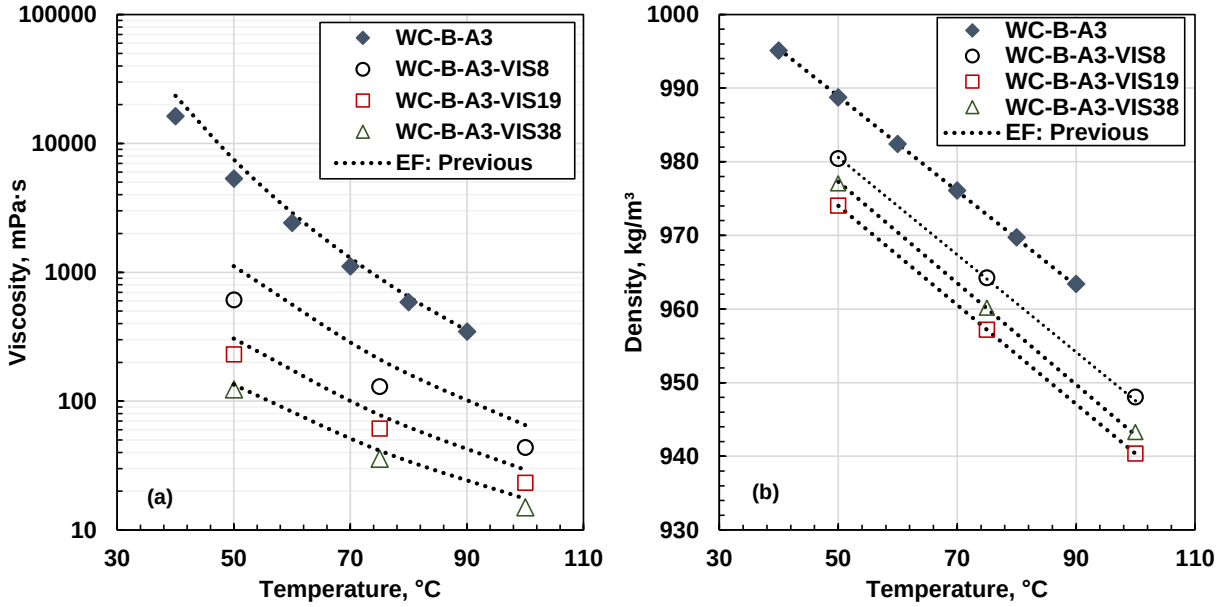

Figure 6-1. Measured and modeled values of WC-B-A3 feed and products a) viscosity and b) density.

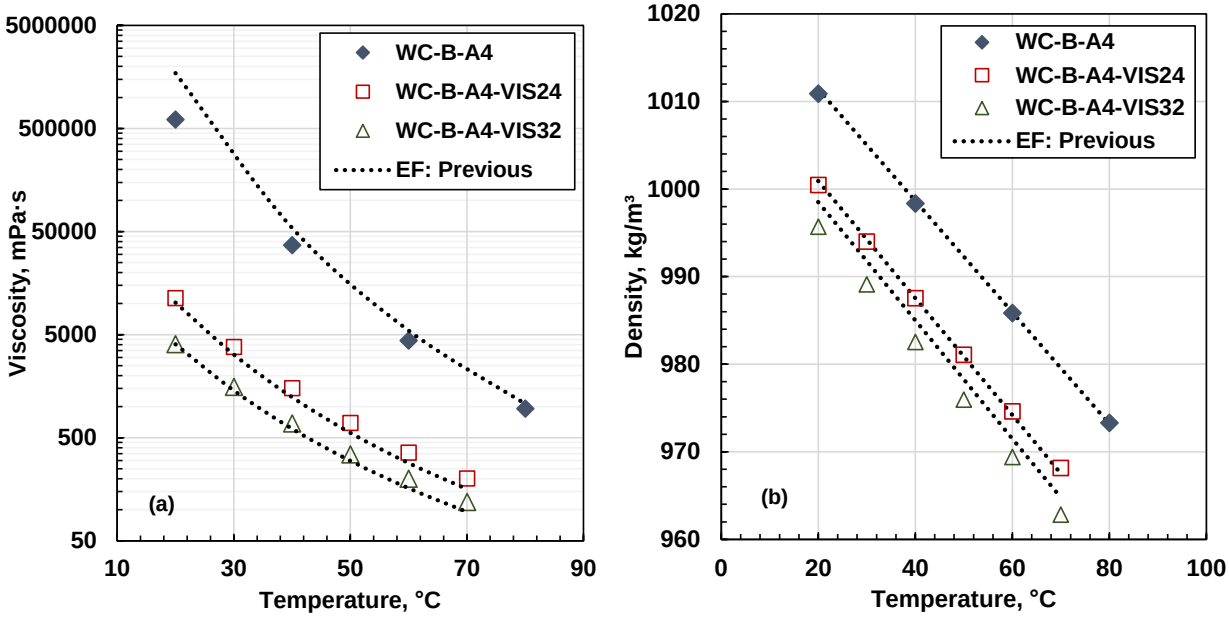

Figure 6-2. Measured and modeled values of WC-B-A4 feed and products a) viscosity and b) density.

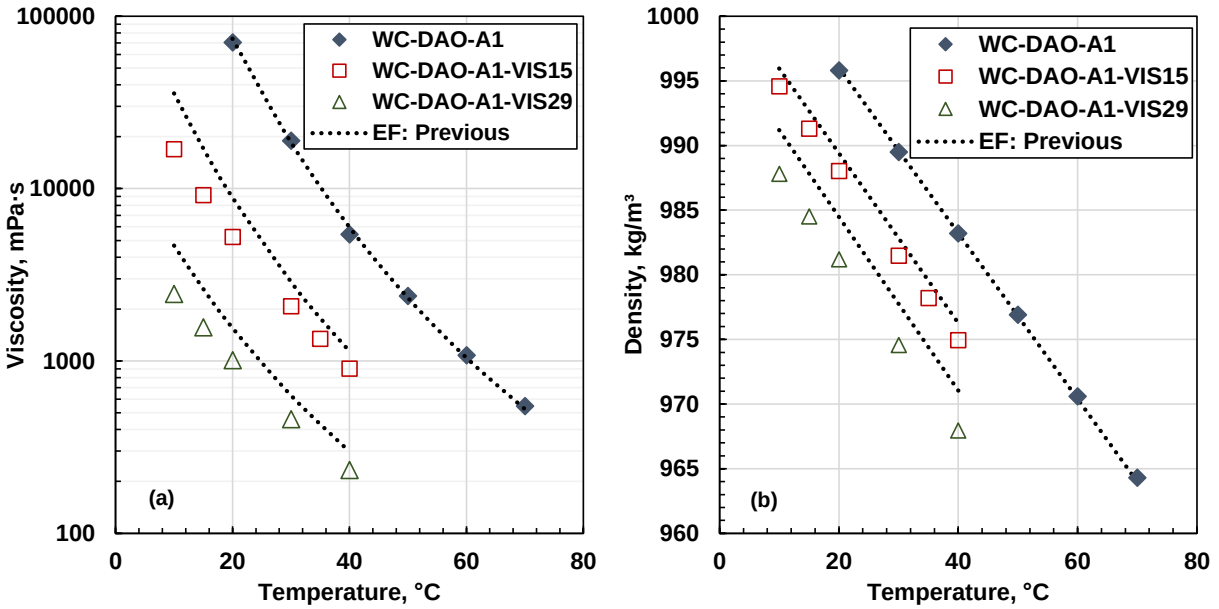

Figure 6-3 Measured and modeled values of WC-DAO-A1 feed and products a) viscosity and b) density.

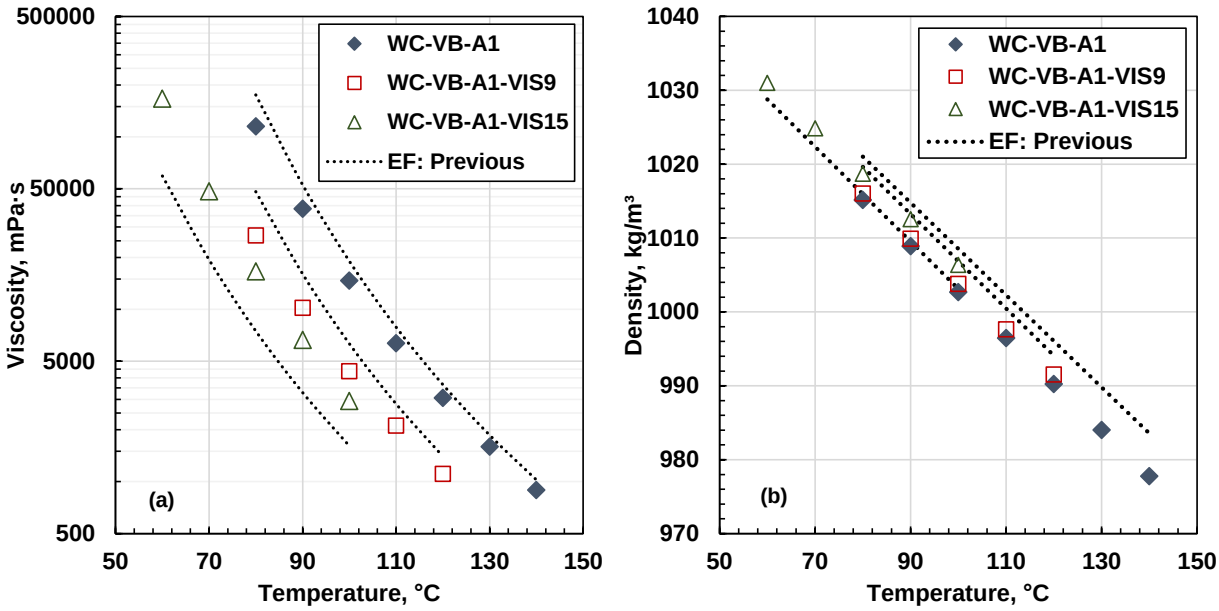

Figure 6-4 Measured and modeled values of WC-VB-A1 feed and products a) viscosity and b) density.

6.2 Updated Correlations

Recommended values or correlations are required for the density and viscosity model parameters of the distillates and SARA fractions of the feed oils and their products. The model parameters are the slope and intercept of density versus temperature (ρ_{Ref} and b) and the EF model fluid specific inputs (c_2 and ρ_s^o). The updated correlations are presented below.

6.2.1 Density

Distillates

Figures 6-5a and 6-5b show the density intercept and slope, respectively, for the distillates from the oils in the thesis dataset. The visbroken distillates from feeds that contained distillates to begin with all follow a similar trend. However, the density of the distillates generated from the WC-VB-A1 vacuum bottoms are much lower. Since there were no distillates in this feed oil, it appears that the distillates generated by visbreaking have a lower density than the distillates naturally found in the bitumen. Therefore, the density of the distillates in the products from each of the oils were determined as the average density of the original distillates and the generated distillates, as follows:

$$\rho_{REF,D} = \left[\frac{1 - w_{new}}{\rho^o_{REF,D}(1 + 0.000387X)} + \frac{w_{new}}{888}\right]^{-1} \tag{6.1}$$

$$b_D = \left[\frac{1 - w_{new}}{b^o_D} + \frac{w_{new}}{-0.740}\right]^{-1} \tag{6.2}$$

where subscript D denotes the distillates and w_{new} is the relative generated distillate fraction and is defined as:

$$w_{new} = \frac{w_{dist} - w^o_{dist}}{w_{dist}} \tag{6.3}$$

where w^o_{dist} and w_{dist} are the weight fractions of distillates in the feed oil and the reacted oil, respectively. When a feed contains distillates, the feed density intercept and slope are obtained from measurements as before. If measurements are not available, the recommended values are 924 kg/m^3 and -0.682 kg/m^{3}K. When the feed does not contain distillates, w_{new} equals unity and the feed terms in Eqs. 6.1 and 6.2 become zero.

The correlated densities matched the measured distillate densities with an AAD of 2.8 kg/m^3 (0.31%) and a MAD of 7.0 kg/m^3 (0.77%). The R^2 correlation coefficients for the density intercept

and slope are 0.91 and 0.89, respectively. Figure 6-5 also shows that the updated correlation is similar to the previous correlation except for the WC-VB-A1 oil. The updated correlation can be applied for feeds with no distillates such as the vacuum bottoms, an improvement from the previous correlation.

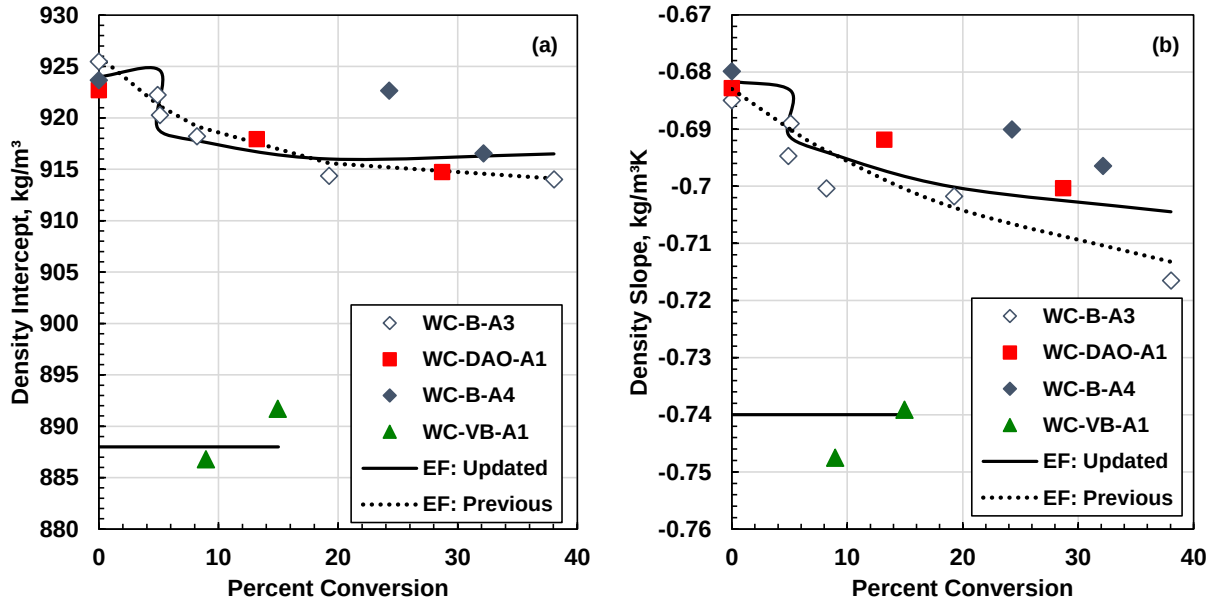

Figure 6-5. Measured and correlated density parameters for the distillates from the thesis dataset as a function of conversion: a) intercept (ρ_{Ref}); b) slope (b). The updated correlated values depend on composition and are different for each oil; the upper and lower solid lines on the plot are for the WC-B-A3 and WC-VB-A1 oils, respectively. The previous correlation (dashed line) from Marquez *et. al.* (2020) is independent of composition.

Saturates

Figures 6-6a and 6-6b show the density intercept and slope, respectively, for the saturates from the oils in the thesis dataset. The previous slope from Marquez *et. al.* (2020) of -0.610 kg/m³K was consistent with all of the data and was retained as is. The correlations for the intercept was updated for the WC-B-A3, WC-B-A4, and WC-DAO-A1 oils as follows:

$$\rho_{REF,S} = 912(1 - 0.00017X) \tag{6.4}$$

where subscript S denotes the saturates. The saturates from the WC-VB-A1 oil were different from the other saturates because this oil was a vacuum residue and the light ends of the saturates stripped off during the distillation. The intercept in Eq. 6.4 was adjusted for this oil to the measured value

of 918.1 kg/m³ to account for the light end losses. The correlated densities after this adjustment matched the measured saturate densities with an AAD of 2.4 kg/m³ (0.27%) and a MAD of 5.2 kg/m³ (0.59%). The R^2 correlation coefficient for the density intercept is 0.36; the R^2 for the slope is undefined because it was a constant. The WC-VB-A1 oil was not included in the error calculations because its saturates were altered by the distillation. There are currently insufficient data to develop a predictive method for this intercept value for vacuum bottom oils. Hence, Eq. 6.4 only applies to non-distilled oils.

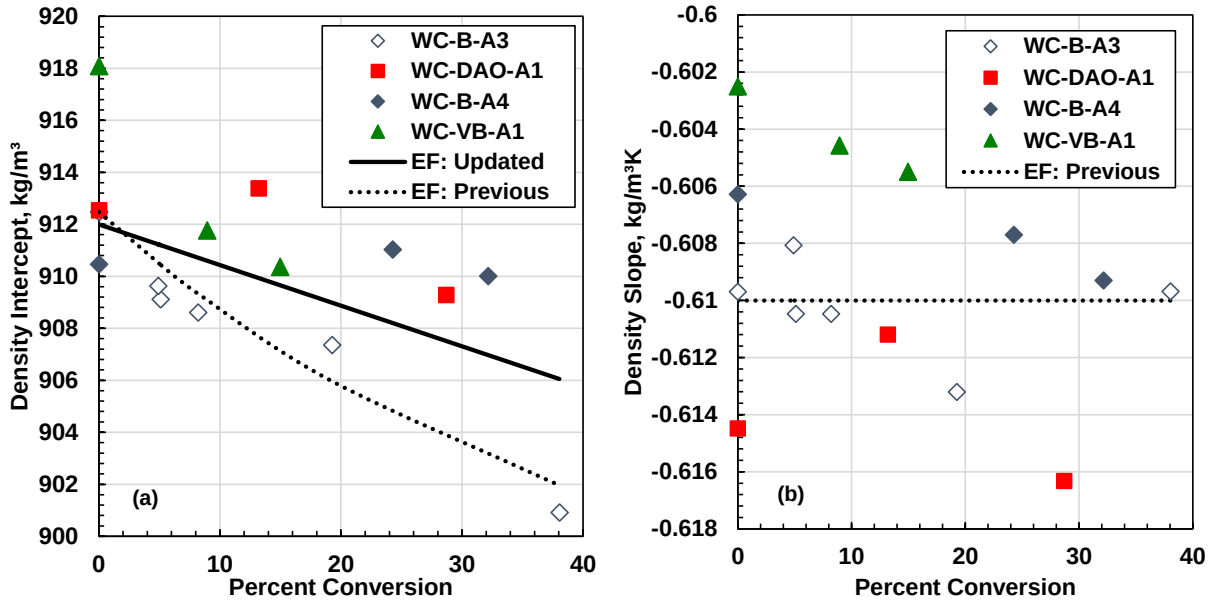

Figure 6-6. Measured and correlated density parameters for the saturates from the thesis dataset as a function of conversion: a) intercept (ρ_{Ref}); b) slope (b).

Aromatics

Figures 6-7a and 6-7b show the density intercept and slope, respectively, for the aromatics from the oils in the thesis dataset. Yarranton *et. al.* (2018) observed that the density of resins and aromatics followed the same proportional change with the conversion. The trends of the previous correlations with conversion were simultaneously tuned to the aromatic and resin data for the WC-B-A3 oils. The same approach was followed for the updated correlations using the data from the WC-B-A3, WC-B-A4, and WC-DAO-A1 oils and their products. The updated correlations for the aromatic density parameters changed only slightly from the previous correlations and are given by:

$$\rho_{REF,A} = 1021.9(1 + 0.00047X) \quad (6.5)$$

$$b_A = -0.625(1 - 0.00056X) \quad (6.6)$$

where subscript *A* denotes the aromatics. As described for the saturates, the intercept in Eq. 6.5 was adjusted for WC-VB-A1 oil to the measured value of 1029.8 kg/m³ to account for the light end losses. The correlated densities after this adjustment matched the measured aromatic densities with an AAD of 1.6 kg/m³ (0.16%) and a MAD of 3.7 kg/m³ (0.37%). The R^2 correlation coefficients for the density intercept and slope are 0.89 and 0.09, respectively. The WC-VB-A1 oil was not included in the error calculations because its aromatics were altered by the distillation. Eq. 6.5 only applies to non-distilled oils.

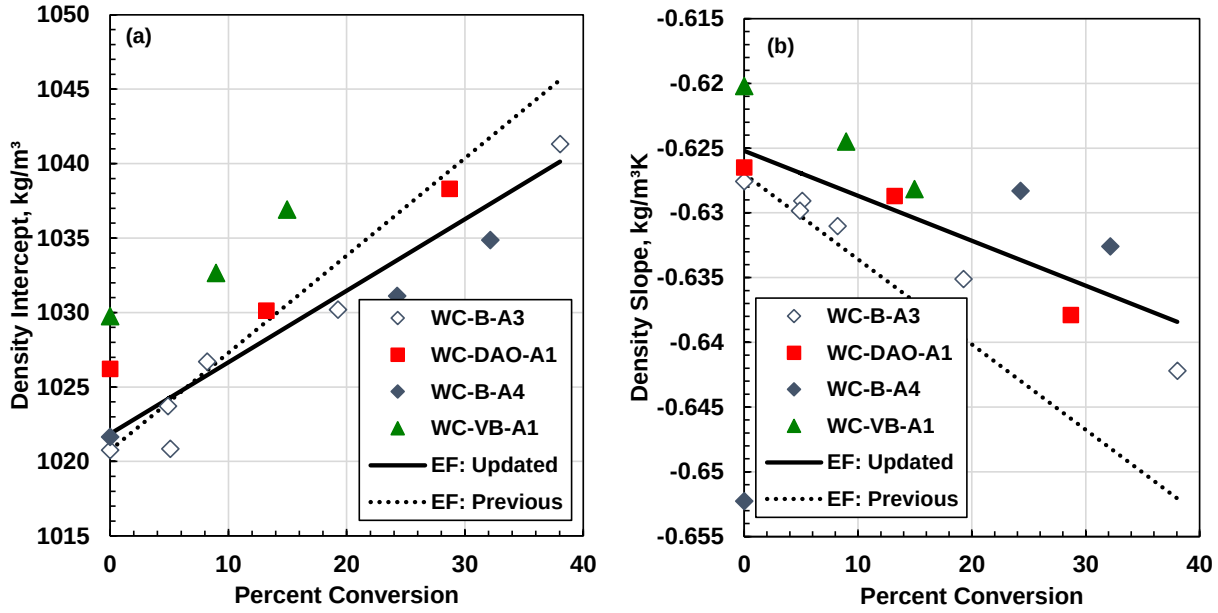

Figure 6-7. Measured and correlated density parameters for the aromatics from the thesis dataset as a function of conversion: a) intercept (ρ_{Ref}); b) slope (b).

Resins

Figures 6-8a and 6-8b show the density intercept and slope, respectively, for the resins from the oils in the thesis dataset. The density of the resins was obtained indirectly from the density of maltenes, saturates, and aromatics. Hence, the density of the resins accumulates errors from separation losses, non-ideal mixing, and measurement errors in the saturate, aromatic, and maltene fractions. As a result, two outliers are shown in Figure 6-8, but omitted from the correlation

development. The updated correlations for the resin density parameters changed only slightly from the previous correlations and are given by:

$$\rho_{REF,R} = 1064.7(1 + 0.00047X) \quad (6.7)$$

$$b_R = -0.611(1 - 0.00056X) \quad (6.8)$$

where subscript *R* denotes the resins. The intercept in Eq. 6.7 was again adjusted for WC-VB-A1 oil to the measured value of 1069.3 kg/m³ to account for the light end losses. The correlated densities after this adjustment matched the calculated resin densities with an AAD of 3.3 kg/m³ (0.32%) and a MAD of 8.3 kg/m³ (0.82%). The R^2 correlation coefficients for the density intercept and slope are 0.75 and 0.51, respectively.

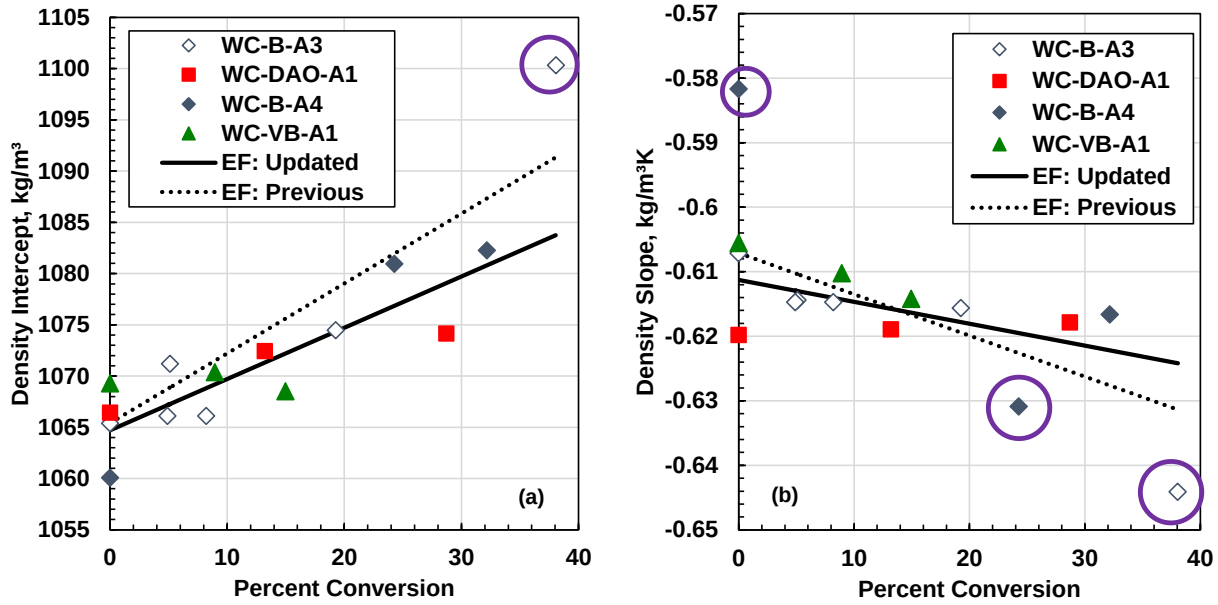

Figure 6-8. Calculated and correlated density parameters for the resins from the thesis dataset as a function of conversion: a) intercept (ρ_{Ref}); b) slope (b). Outliers not used in the data fitting are indicated by circles.

Asphaltenes

Figures 6-9a and 6-9b show the density intercept and slope, respectively, for the asphaltenes from the oils in the thesis dataset. The densities of asphaltenes were calculated indirectly from maltenes and SBD residues. Therefore, as with the resins, the calculated asphaltene density parameters compensate for errors such as the ideal mixing assumption, density measurement errors in the other fractions, and separation losses during the asphaltene and distillate separations. In this case, there

were no obvious outliers. However, the intercepts for the WC-DAO-A1 oil and its products are lower than the other oils because this oil was partially deasphalted.

The density intercept and slope were updated to constant values of 1078.6 kg/m³ and -0.609 kg/m³K, respectively. The density intercept does not apply to the deasphalted oil and there is currently no method to predict the density intercept for other partially deasphalted oils. Hence, the asphaltene density intercept for these oils must be determined independently. For the WC-DAO-A1 oil and its products, the intercept was set to 1144.1 kg/m³. The densities correlated with the relevant density intercept matched the calculated asphaltene densities with an AAD of 7.6 kg/m³ (0.69%) and a MAD of 26 kg/m³ (2.4%). The relatively high error likely reflects the uncertainties in the calculated asphaltene densities.

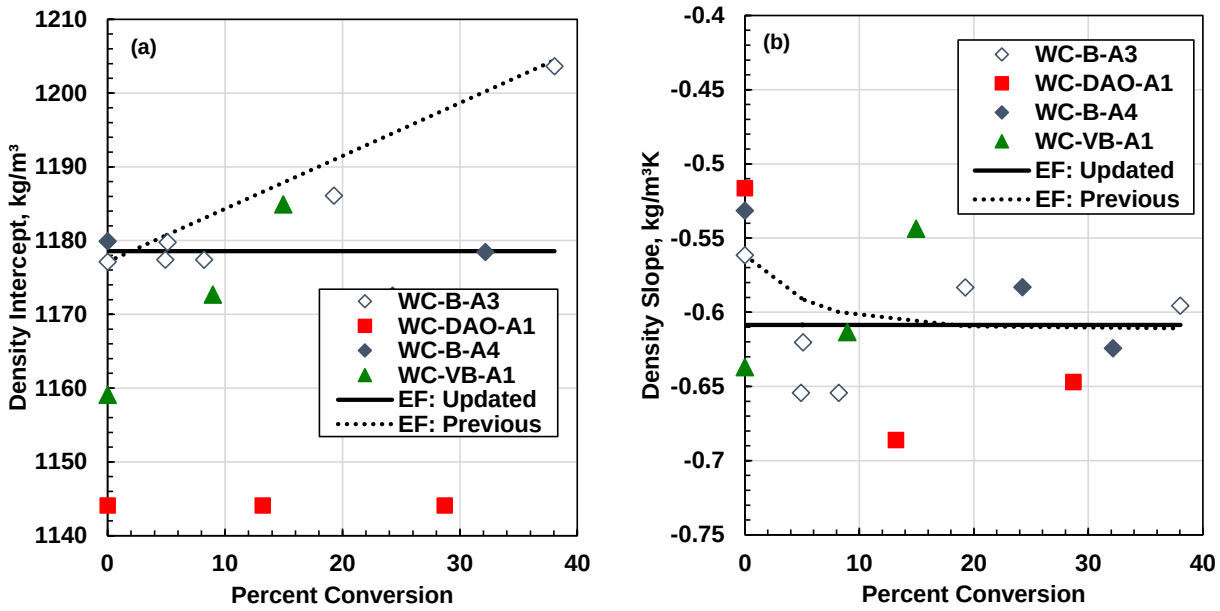

Figure 6-9. Calculated and correlated density parameters for the asphaltenes from the thesis dataset as a function of conversion: a) intercept (ρ_{Ref}); b) slope (b). The asphaltene density intercept values for WC-DAO-A1 oils were obtained from fitings to the new default values.

6.2.2 Viscosity

Distillates

Figures 6-10a and 6-10b show the parameters c_2 and $\rho°_s$, respectively, for the distillates from the oils in the thesis dataset. The parameters were set to constant values of 0.232 and 981 kg/m³ for c_2

and ρ_s^o, respectively. The distillates from the WC-VB-A1 oil and its products were generated by reaction and likely differ from the mixtures of reacted and unreacted distillates in the other oils. However, the viscosity parameters for the WC-VB-A1 oil and products were too scattered to justify a different correlation. The EF model with the correlated parameters and densities matched the calculated distillate viscosities with an AARD of 22% and a MARD of 55%. With these recommended values, it is no longer necessary to calculate the feed parameters from a distillation assay.

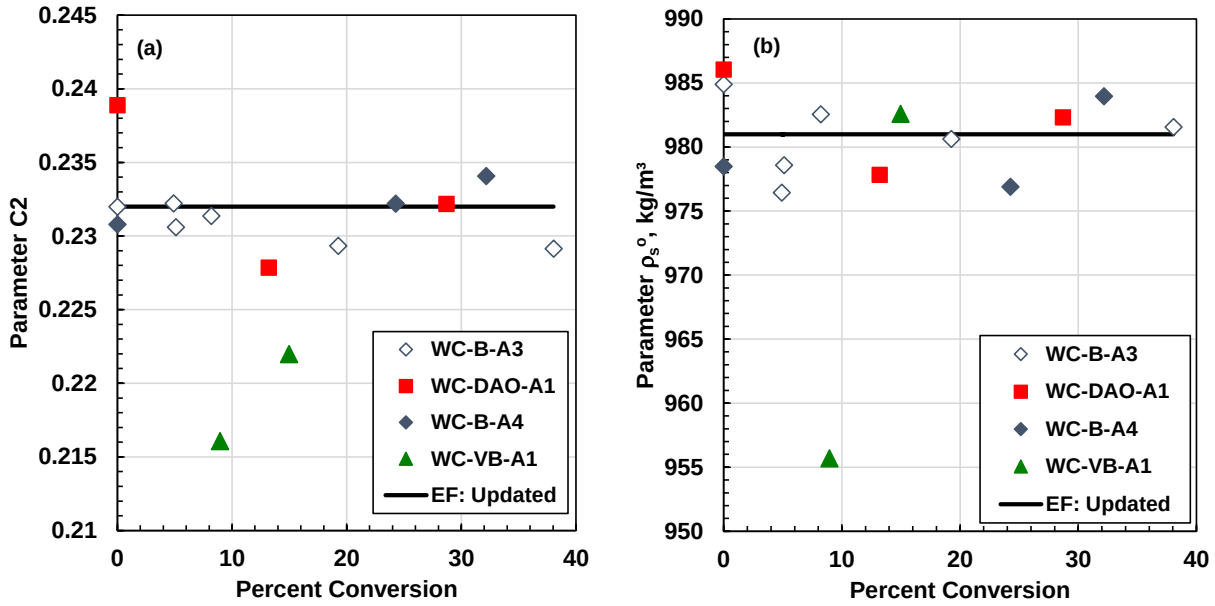

Figure 6-10. Calculated and correlated viscosity parameters for the distillates from the thesis dataset as a function of conversion: a) c_2; b) ρ_s^o.

Saturates

Figures 6-11a and 6-11b show the parameters c_2 and $\rho°_s$, respectively, for the saturates from the oils in the thesis dataset. The parameters from the WC-DAO-A1 and WC-VB-A1 differed from the bitumen values, although they gave similar viscosities when input into the EF model. These oils both underwent distillation in the oil sand process and their saturates may have been altered. Note that although the WC-DAO-A1 saturate densities did not appear to be affected, their viscosity was. Therefore, the parameter correlations were updated based on the data from the WC-B-A3 and WC-B-A4 oils and their products only as follows:

$$c_{2,S} = 0.404(1 - 0.000382X) \quad (6.9)$$

$$\rho^o_{s,S} = 961.1(1 - 0.000075X) \quad (6.10)$$

The updated correlations differ only slightly from the previous correlations. For the sake of simplicity, the above correlations were also applied to the WC-DAO-A1 and WC-VB-A1 oils and their products. The EF model with the correlated parameters and densities matched the measured saturate viscosities with an AARD of 19% and a MARD of 56%. The R^2 correlation coefficients for the c_2 and $\rho°_s$, viscosity parameters are 0.13 and 0.08, respectively. The WC-VB-A1 and WC-DAO-A1 oils were not included in the error calculations because their aromatics were altered as discussed above. The R^2 are very low because the parameters are nearly constant. Nonetheless, accounting for the small change does improve the viscosity prediction shown later. The correlation could be improved if more data were available to determine the effect of distillation on the saturate properties.

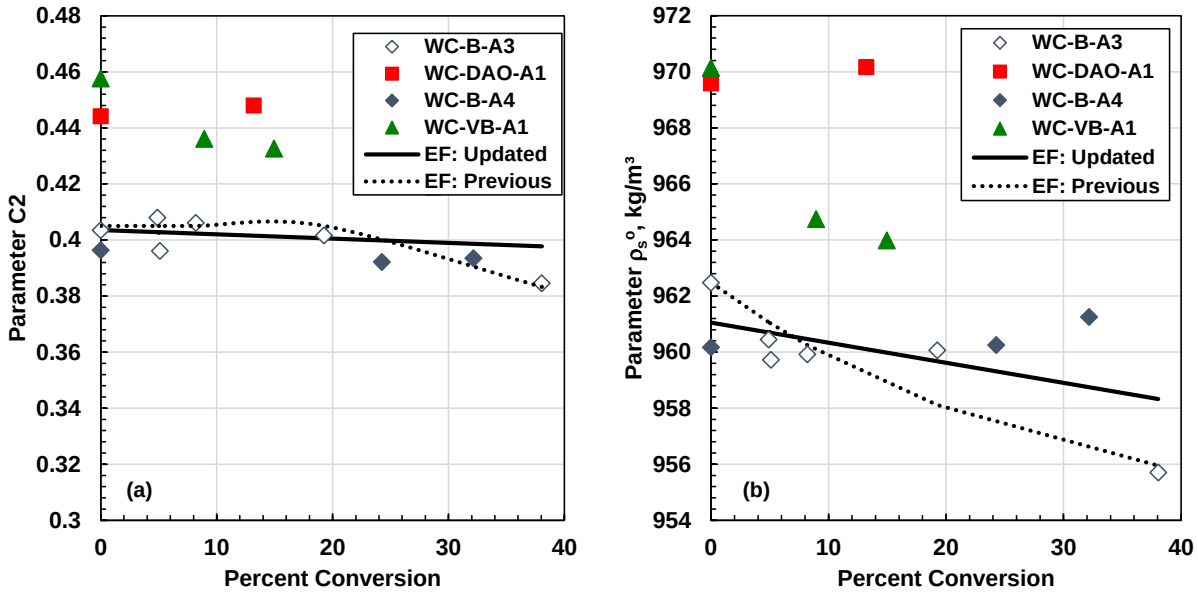

Figure 6-11. Measured and correlated viscosity parameters for the saturates from the thesis dataset as a function of conversion: a) c_2; b) ρ_s^o.

Aromatics

Figures 6-12a and 6-12b show the parameters c_2 and $\rho°_s$, respectively, for the aromatics from the oils in the thesis dataset. The parameters from the WC-VB-A1 differed from those of the other oils suggesting that the aromatics from this oil may have been altered by its distillation. Therefore, the

parameter correlations were updated based on the data from the other three oils and their products only. The correlations for c_2 and ρ°_s were updated slightly and are provided below:

$$c_{2,A} = 0.449(1 - 0.00246X) \quad (6.11)$$

$$\rho^o_{s,A} = 1056.0(1 + 0.000423X) \quad (6.12)$$

For simplicity, the above correlations were also applied to the WC-VB-A1 oils and their products. The EF model with the correlated parameters and densities matched the measured aromatic viscosities with an AARD of 22% and a MARD of 82%. The R^2 correlation coefficients for the c_2 and ρ°_s, viscosity parameters are 0.70 and 0.91, respectively. The WC-VB-A1 was not included in the error calculations because its aromatics were altered by the distillation. The correlation could be improved if more data were available to determine the distillation effect on the aromatic properties.

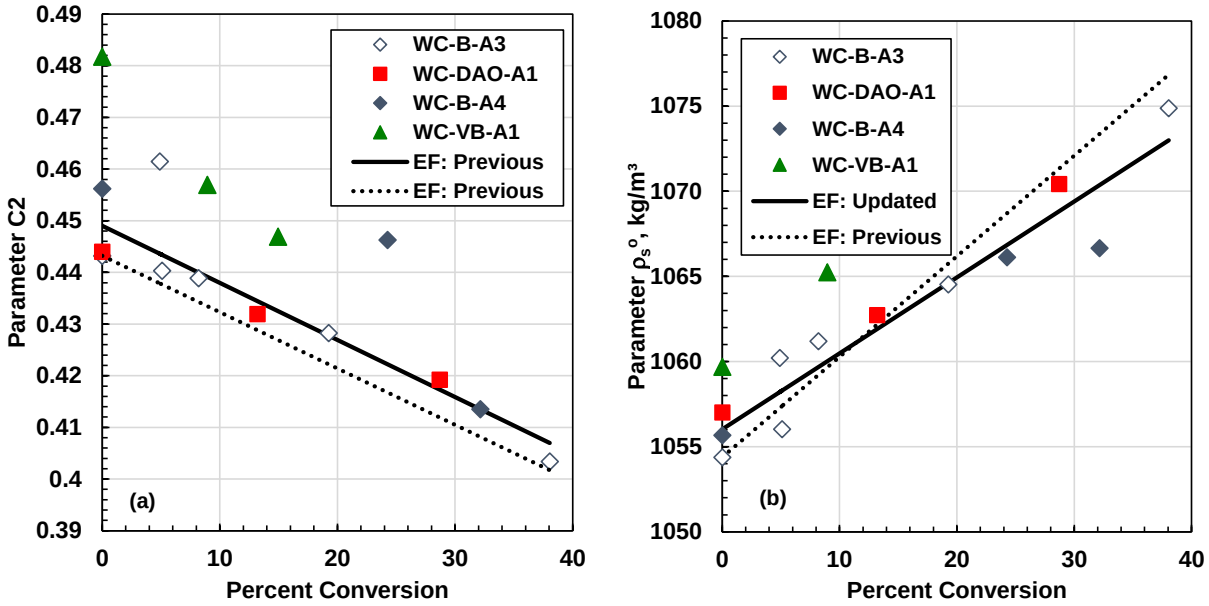

Figure 6-12. Measured and correlated viscosity parameters for the aromatics from the thesis dataset as a function of conversion: a) c_2; b) ρ_s^o.

Resins

Figures 6-13a and 6-13b show the parameters c_2 and ρ°_s, respectively, for the resins from the oils in the thesis dataset. The parameters from the WC-VB-A1 again differed from those of the other oils and were not used to update the correlations. The updated correlations are given by:

$$c_{2,R} = 0.603(1 - 0.00208X) \quad (6.13)$$

$$\rho^{o}_{s,R} = 1081.2(1 + 0.000352X) \quad (6.14)$$

For the sake of simplicity, the above correlations were also applied to the WC-VB-A1 oils and their products. The EF model with the correlated parameters and densities matched the measured aromatic viscosities with an AARD of 22% and a MARD of 98%. The R^2 correlation coefficients for c_2 and $\rho°_s$, viscosity parameters were 0.42 and 0.68, respectively. Again, the correlation could be improved if more data were available to determine the distillation effect on the resin properties.

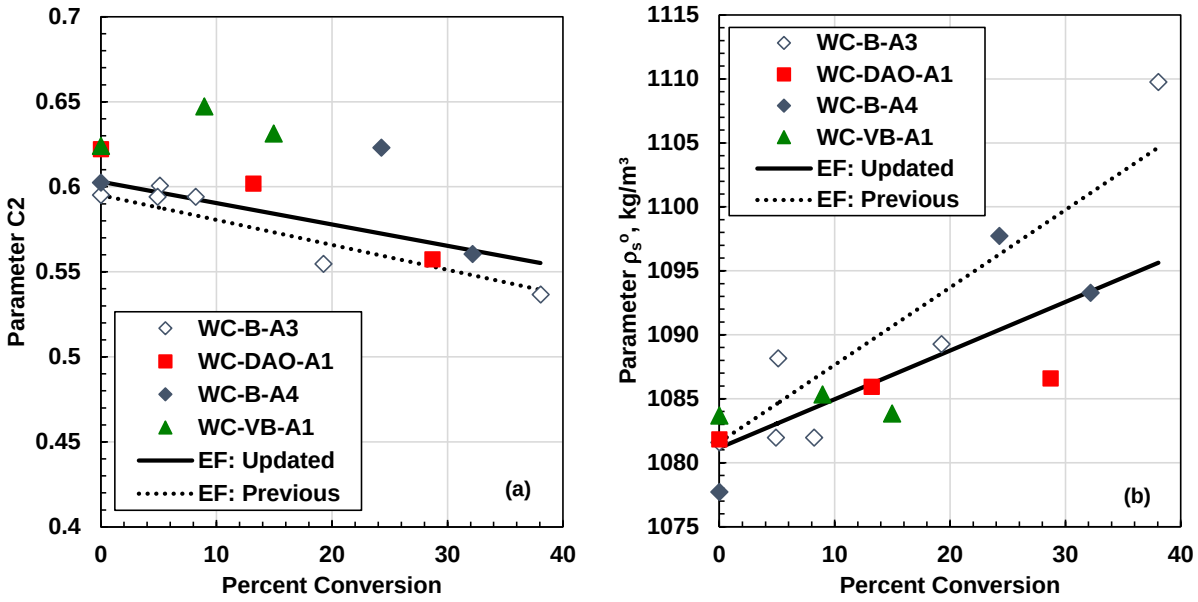

Figure 6-13. Calculated and correlated viscosity parameters for the resins from the thesis dataset as a function of conversion: a) c_2; b) ρ_s^o.

Asphaltenes

Figures 6-14a and 6-14b show the parameters c_2 and $\rho°_s$, respectively, for the asphaltenes from the oils in the thesis dataset. The EF parameters for asphaltenes were obtained indirectly from the viscosity of the whole oil as explained in Chapter 4. The calculated values were affected by all the experimental errors for the other fractions and any deficiencies in the model assumptions. As a result, there was too much scatter in the calculated values to simultaneous fit both c_2 and ρ_s^o. Instead, the c_2 parameter was constrained to a negative linear relation to conversion and only ρ_s^o was fitted. The slope of the c_2 correlation was set based on the resin correlation (Eq. 6.13) but was

adjusted to obtain a positive slope in ρ_s^o correlation also to be consistent with the resin correlation (Eq. 6.14). The updated correlations for the asphaltenes are as follows:

$$c_{2,As} = 0.98(1 - 0.00211X) \quad (6.15)$$

$$\rho^o_{s,As} = 1169.95(1 - 0.000397X) \quad (6.16)$$

where subscript *As* denotes the asphaltenes. Although the asphaltenes from the deasphalted oil had different densities than the asphaltenes from the other oils, their viscosity parameters were similar and included in the above correlation. The asphaltene viscosities could not be measured, and therefore, the asphaltene correlations could not be directly tested. Instead, the deviations in the whole oil and residue fractions will be assessed later. The R^2 correlation coefficient for the $\rho°_s$ correlation was only 0.04, likely reflecting the accumulation of errors discussed above. Although the correlation is poor, accounting for the small change with conversion does improve the viscosity predictions shown later for most of the oils.

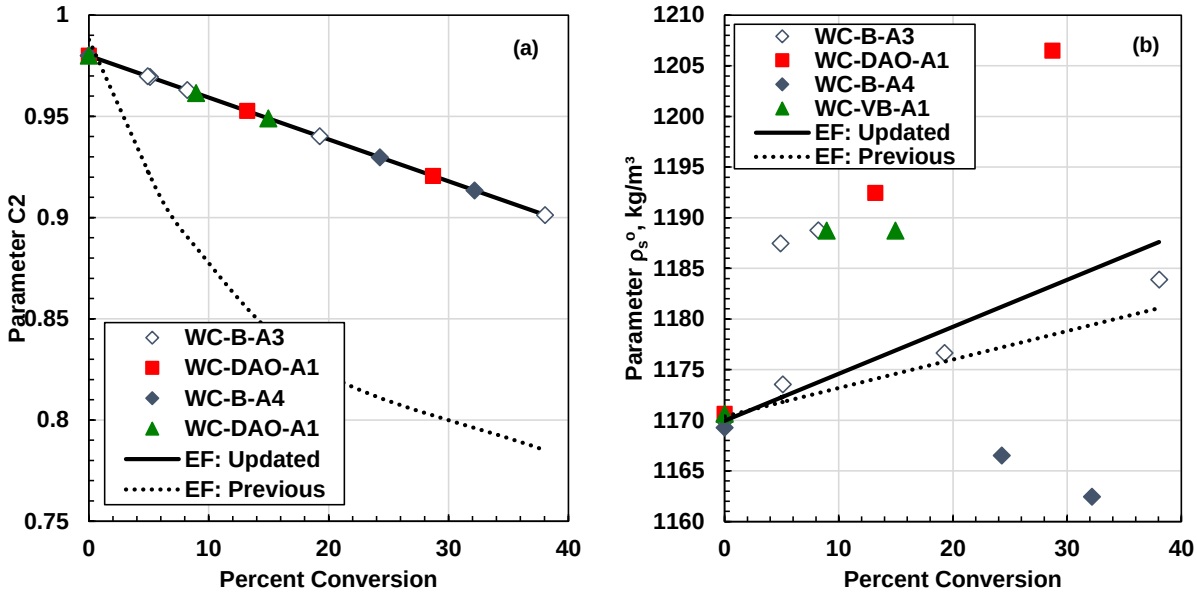

Figure 6-14. Calculated and correlated viscosity parameters for the asphaltenes from the thesis dataset as a function of conversion: a) c_2; b) ρ_s^o.

Viscosity Binary Interaction Parameter between Distillates and Asphaltenes

Visbreaking changes the chemistry of the oil, and consequently, the interaction between the oil components also changes. Marquez *et. al.*, (2020) found that for visbreaking it was sufficient to adjust the binary interaction parameter between the two most dissimilar fractions, the distillates

and the asphaltenes. They proposed a correction factor to be added to the binary interaction parameter from the original EF model formulation.

Experimentally derived corrections to the distillate/asphaltene binary interaction parameter were obtained by fitted to EF model to both residue viscosities (no distillates) and whole oil viscosities (with distillates). Then, the correlation for the binary interaction parameter increment was updated as follows:

$$\Delta\alpha_{Dist-Asph} = 0.10[1 - \exp(-X)] \tag{6.17}$$

where $\Delta\alpha_{Dist-Asph}$ is the increment to the binary interaction parameter. Figure 6.15 compares the previous and updated correlations to the experimentally derived values. The performance of the correlation is best evaluated by considering the EF model's ability to match viscosity data from both whole oils and residues, shown later. The R^2 correlation coefficient for this correlation is 0.62.

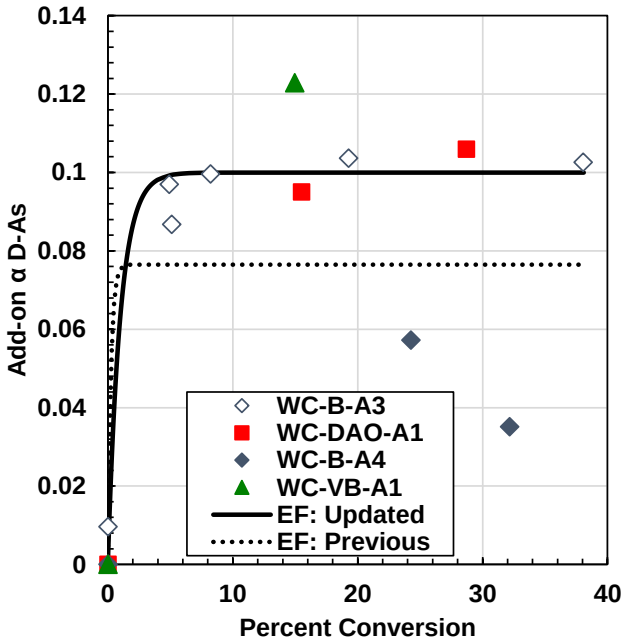

Figure 6-15. Fitted and correlated distillates-asphaltenes binary interaction parameter increment.

6.3 Model Evaluation

The viscosity and density of maltenes, SBD residue, and the whole oils were measured directly and provide a test of the density and viscosity models with the proposed correlations. The deviations in the predicted properties from the previous and updated correlations are presented below for each of the above oil fractions.

Maltenes

The maltenes are mixtures of saturates, aromatics, and resins. Hence, testing the correlations on maltene properties provides a test of both the model parameter correlations and the mixing rules used in the property models. Figures 6-16 to 6-19 show the measured and modeled viscosities of the WC-B-A3, WC-B-A4, WC-DAO-A1, and WC-VB-A1 maltenes, respectively. Table 6-1 lists the deviations of calculated maltene densities and viscosities from the measured data for the property models with the previous (Marquez *et. al.*, 2020) and updated correlations. Both correlations gave overall deviations of less than 2 kg/m³ in density and 20% in viscosity compared with the experimental error of 0.05 kg/m³ and 6%. While higher than experimental error, the deviations are typical for modeling the density and viscosity of petroleum fluids (Motahhari *et. al.*, 2013; Ramos-Pallares *et. al.*, 2016), confirming the validity of the mixing rules. The results for both correlations are similar because the properties of these fractions did not vary significantly between the different oils, or in the case of the vacuum bottoms, the differences were accounted for independently.

Table 6-1. Deviations in the predicted maltene density and viscosity from the previous (Marquez *et. al.*, 2020) and updated correlations.

Oil	Density			Viscosity		
	AAD kg/m³	MAD kg/m³	Bias kg/m³	AARD %	MARD %	Bias %
Previous Correlation						
WC-B-A3	1.1	2.3	1.1	14	17	8.2
WC-B-A4	1.9	2.6	1.9	24	34	-24.0
WC-DAO-A1	2.0	2.8	-0.8	19.1	25	-19.1
WC-VB-A1	2.8	4.9	2.5	34	55	21.0
AVERAGE	**1.6**	-	**1.2**	**19**	-	**-3.5**
Updated Correlation						
WC-B-A3	1.2	2.7	0.3	27	40	0.3
WC-B-A4	0.8	2.0	0.6	14	20	-11.1
WC-DAO-A1	1.7	2.5	-1.7	16	19	-5.8
WC-VB-A1	2.1	3.5	2.0	43	74	35.2
AVERAGE	**1.3**	-	**0.3**	**19**	-	**21.5**

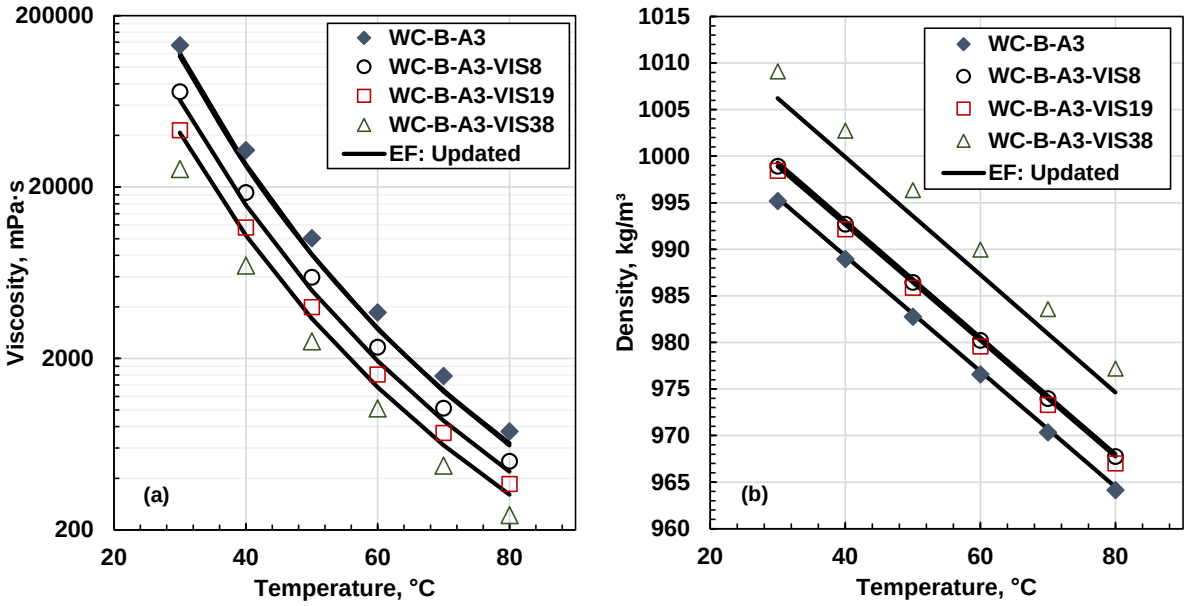

Figure 6-16. Measured and modeled properties of the WC-B-A3 feed and product maltenes: a) viscosity; b) density.

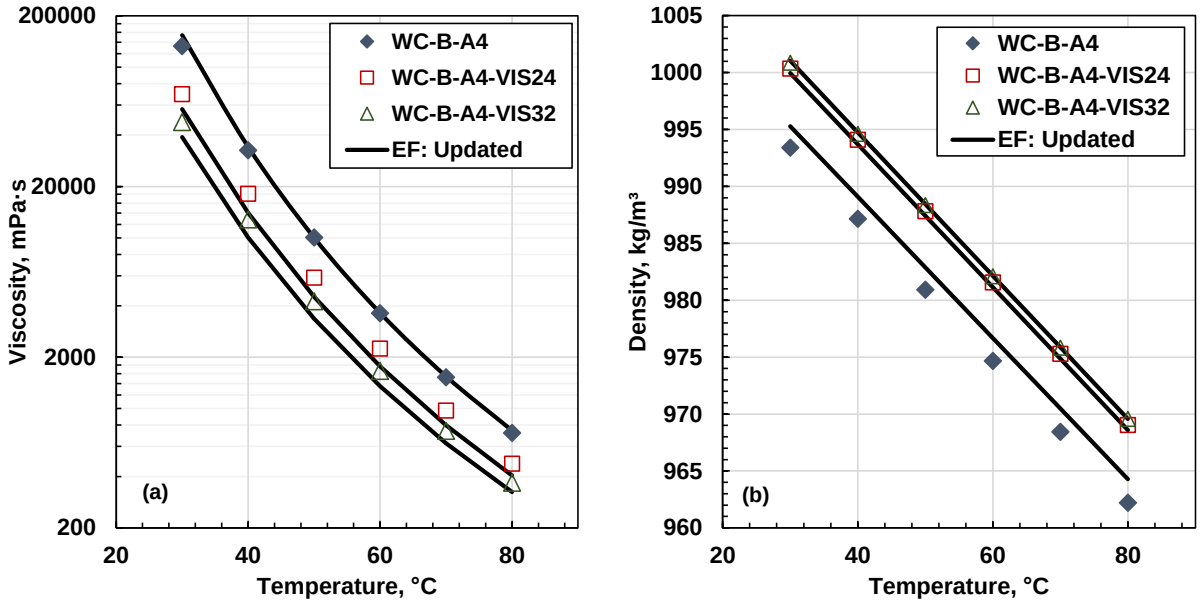

Figure 6-17. Measured and modeled values of WC-B-A4 feed and product maltenes a) viscosity; b) density.

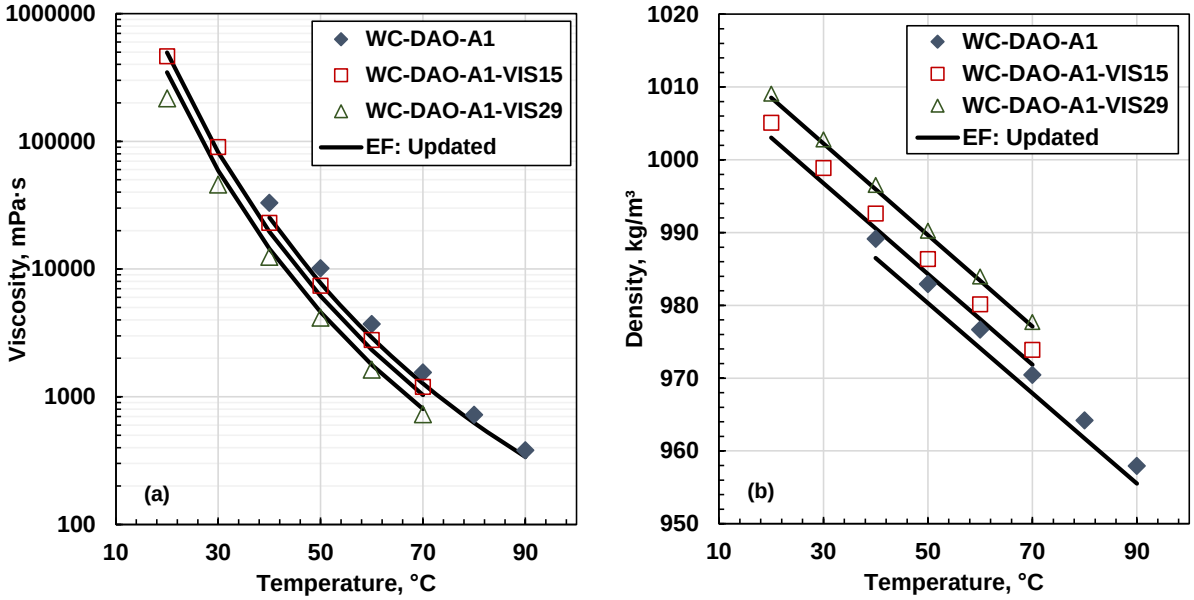

Figure 6-18. Measured and modeled properties of WC-DAO-A1 feed and product maltenes: a) viscosity; b) density.

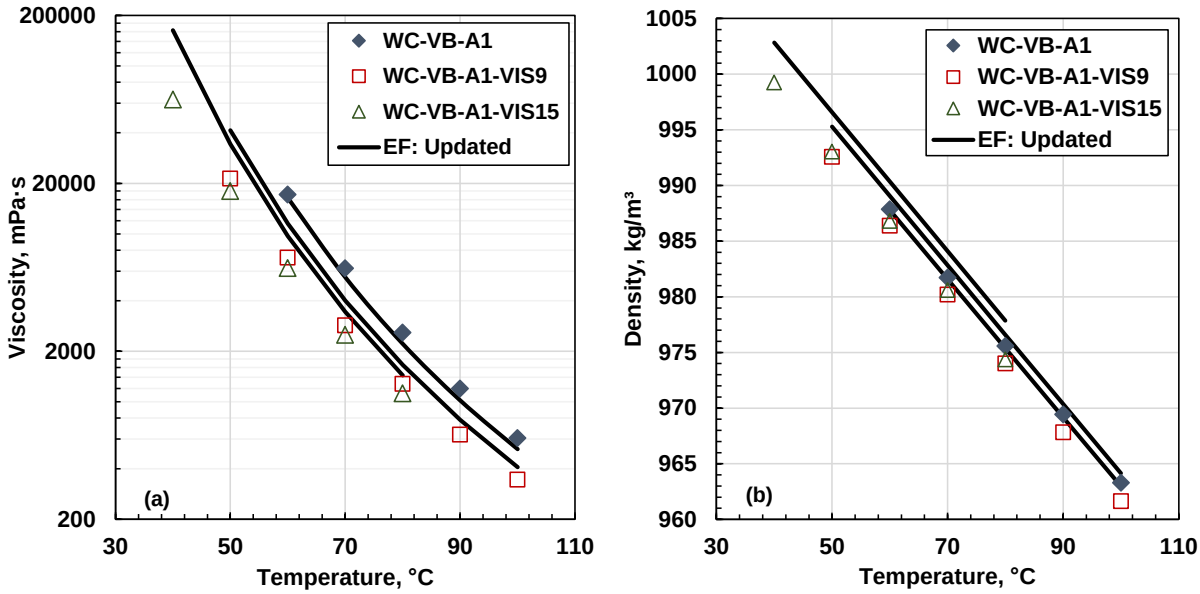

Figure 6-19. Measured and modeled properties of WC-VB-A1 feed and product maltenes: a) viscosity; b) density.

SBD Residue

The residues are mixtures of maltenes (saturates, aromatics, and resins) and asphaltenes. Hence, testing the correlations on residue properties provides a test of both the asphaltene model parameter correlations and the mixing rules used in the property models. Figures 6-20 to 6-23 show the measured and modeled viscosities of the WC-B-A3, WC-B-A4, WC-DAO-A1, and WC-VB-A1 residues, respectively. Table 6-2 lists the deviations of calculated residue densities and viscosities from the measured data for the property models with the previous and updated correlations. Both correlations gave overall deviations of less than 3 kg/m³ in density and 30% in viscosity. The errors are higher than observed for the maltenes. All of the errors in the measurements and model assumptions accumulated in the calculated asphaltene properties. The higher error for the predicted residue properties reflects this accumulation of error. The previous correlation errors were lower than the updated correlation because the asphaltene properties in the previous correlation were obtained from the residue data. In contrast, the properties in the updated correlations were obtained from both residue and whole oil data.

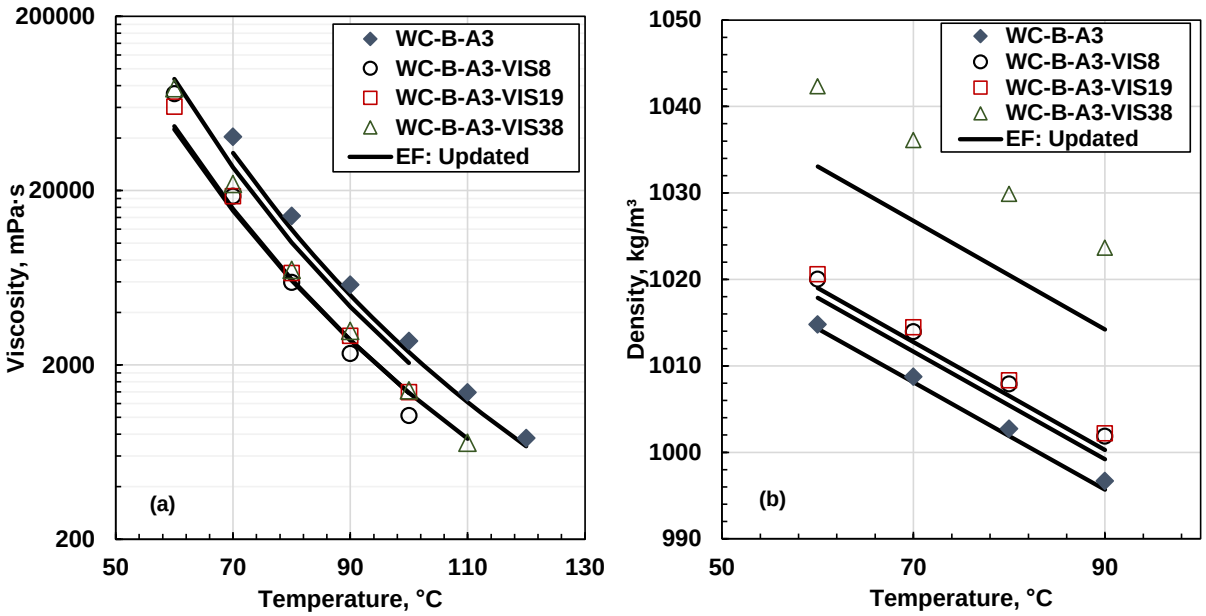

Figure 6-20. Measured and modeled properties of WC-B-A3 feed and product SBD residues: a) viscosity; b) density.

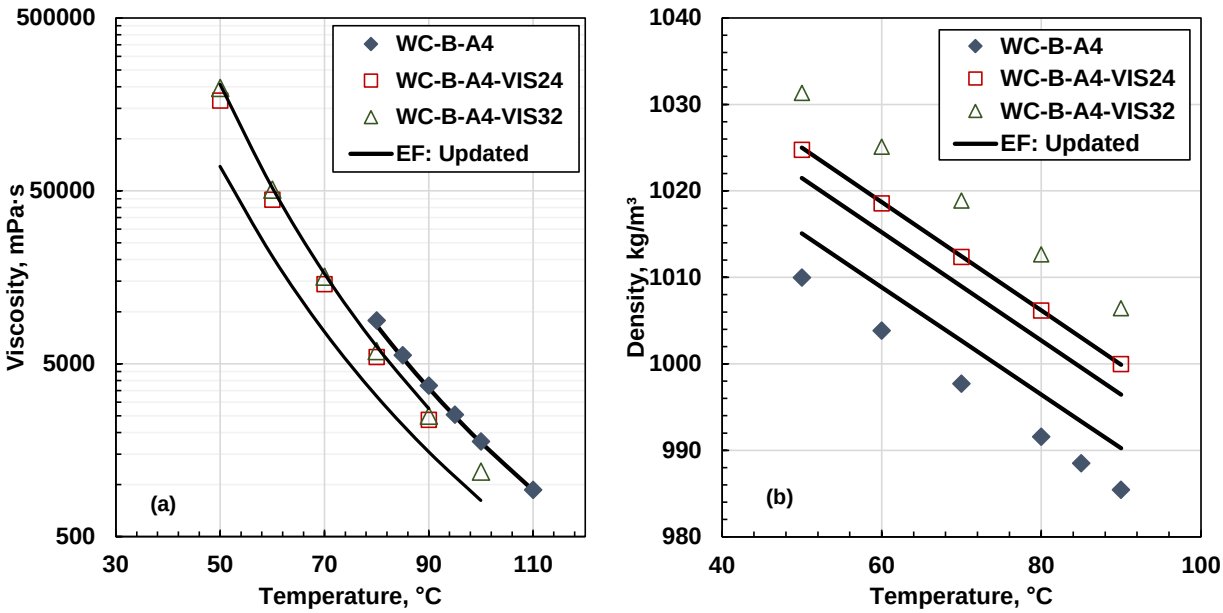

Figure 6-21. Measured and modeled properties of WC-B-A4 feed and product SBD residues: a) viscosity; b) density.

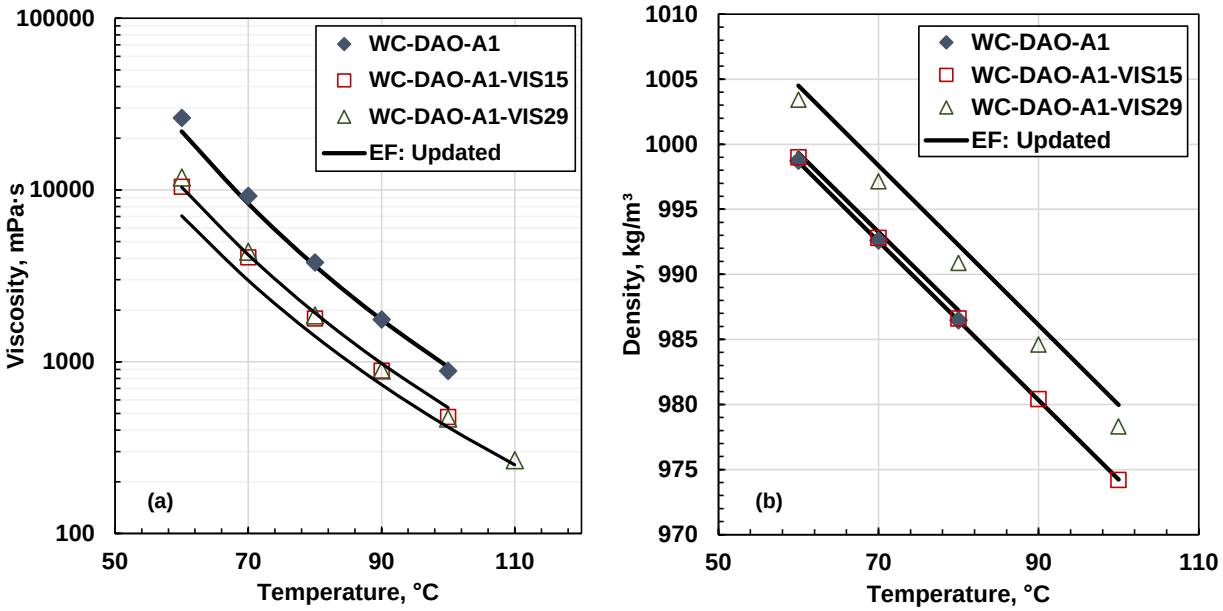

Figure 6-22. Measured and modeled properties of WC-DAO-A1 feed and product SBD residues: a) viscosity; b) density.

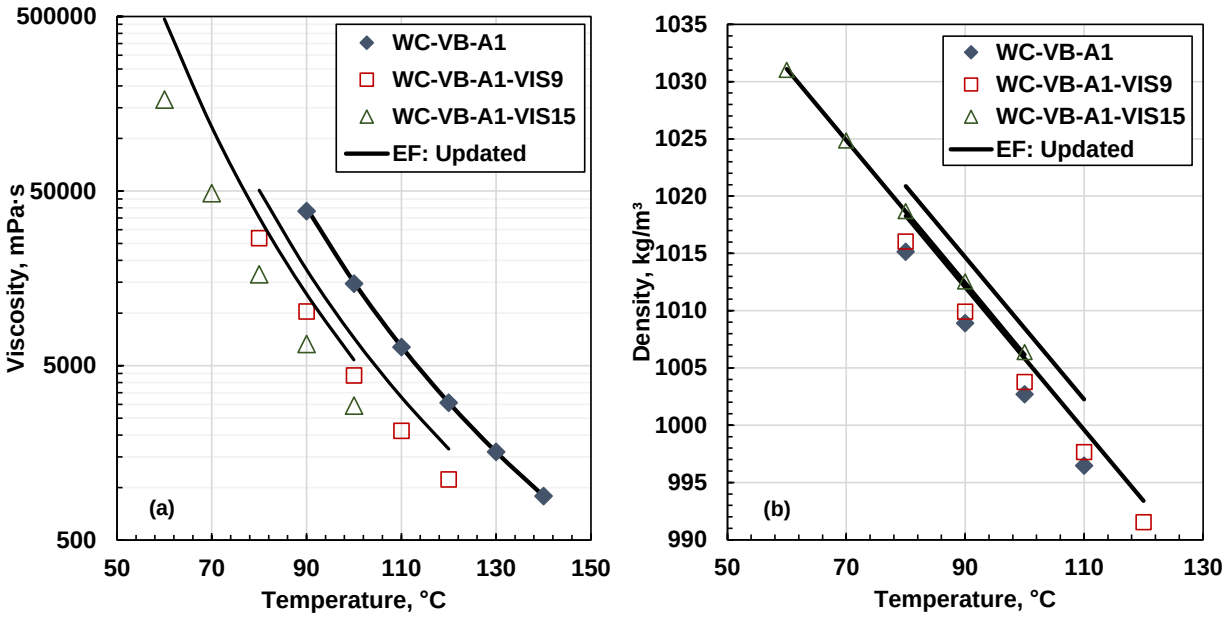

Figure 6-23. Measured and modeled WC-VB-A1 feed and product SBD residues properties: a) viscosity; b) density.

Table 6-2. Deviations in the predicted SBD residue density and viscosity from the previous (Marquez *et. al.*, 2020) and updated correlations.

Oil	Density			Viscosity		
	AAD kg/m³	MAD kg/m³	Bias kg/m³	AARD %	MARD %	Bias %
Previous Correlation						
WC-B-A3	1.4	2.0	0.2	24	51.8	18.7
WC-B-A4	2.0	4.8	1.7	25	35.2	-19.3
WC-DAO-A1	2.3	5.4	2.3	12	26.3	-9.3
WC-VB-A1	3.9	5.8	2.1	45	55.1	21.0
AVERAGE	**1.9**	**-**	**1.6**	**21**	**-**	**-0.8**
Updated Correlation						
WC-B-A3	2.9	9.4	-2.0	24	54.2	8.2
WC-B-A4	4.9	6.5	-1.7	48	48.3	-9.3
WC-DAO-A1	0.8	1.4	0.7	12	21.7	-7.3
WC-VB-A1	2.6	5.8	2.6	64	123.9	64.3
AVERAGE	**2.8**	-	**0.4**	**28**	-	**14.0**

Whole Oil

The whole oils are mixtures of residues (saturates, aromatics, resins, and asphaltenes) and distillates. Hence, testing the correlations on whole oil properties provides a test of both the distillate model parameter correlations and the mixing rules used in the property models. Figures 6-24 to 6-27 show the measured and modeled viscosities of the WC-B-A3, WC-B-A4, WC-DAO-A1, and WC-VB-A1 whole oils, respectively. Table 6-3 lists the deviations of calculated whole oil densities and viscosities from the measured data for the property models with the previous and updated correlations. Both correlations gave overall deviations of less than 2 kg/m³ in density. However, the updated correlations significantly reduced the viscosity prediction error (18.7% versus 48%). The improvement is attributed partly to tuning the asphaltene parameters to both whole oils and residues. However, the main reason for the improvement is that the updated correlations were based on the whole dataset while the previous correlation was based on data from the WC-B-A3 oil only.

The errors in the updated correlations for the whole oils are almost the same as those observed for the residues. Hence, the distillate correlations, correlation for the binary interaction parameter

adjustment, and the mixing rules did not add significantly to the overall error of the models. Finally, the updated correlations provide predictions for the WC-VB-A1 products where the previous correlations could not.

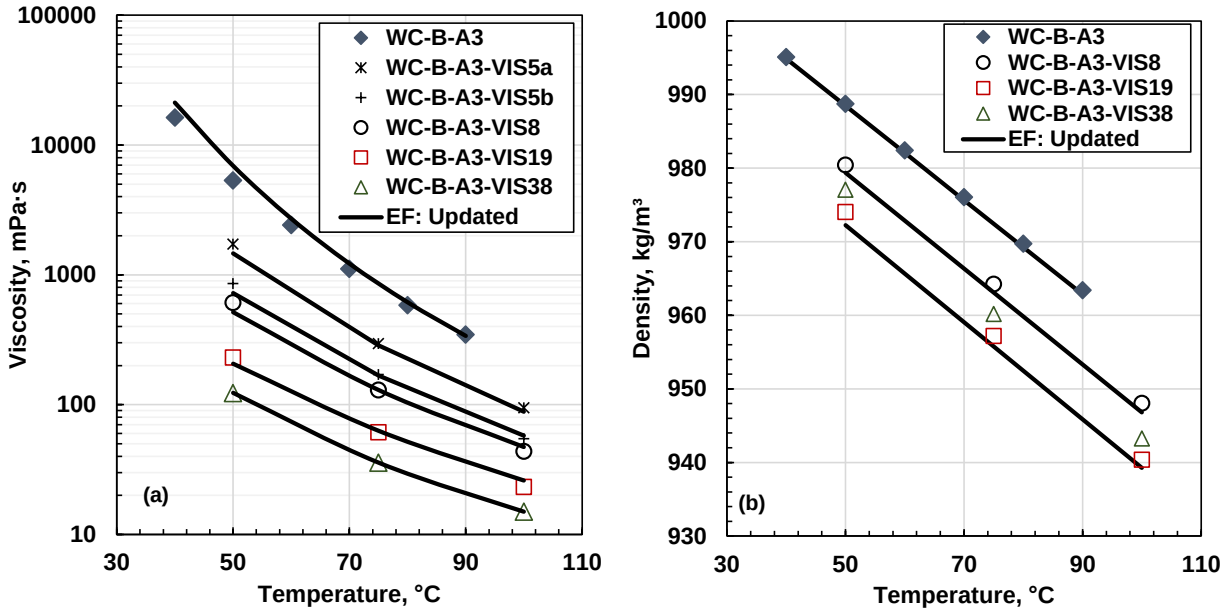

Figure 6-24. Measured and modeled properties of WC-B-A3 feed and product whole oils: a) viscosity; b) density.

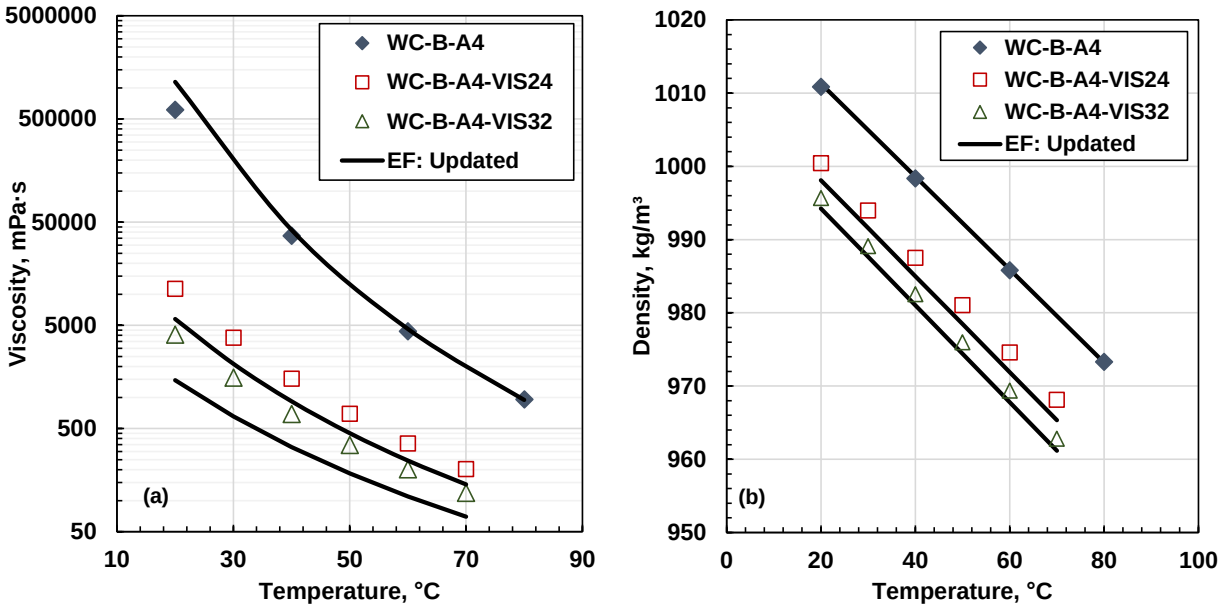

Figure 6-25. Measured and modeled properties of WC-B-A4 feed and product whole oils: a) viscosity; b) density.

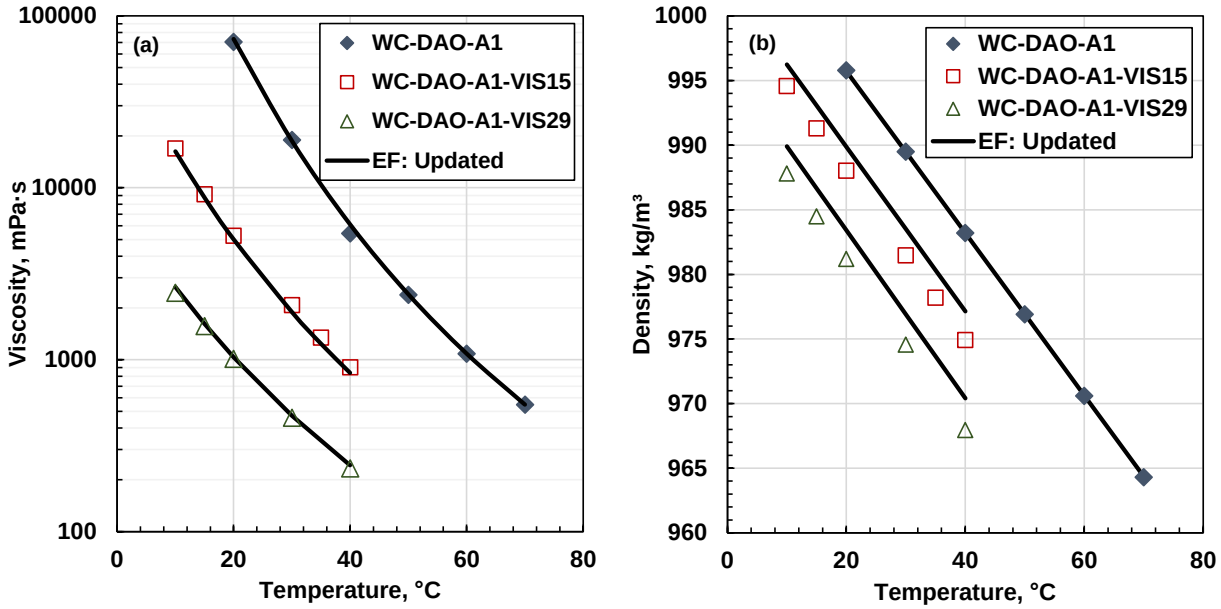

Figure 6-26 Measured and modeled values of WC-DAO-A1 feed and product oils a) viscosity and b) density.

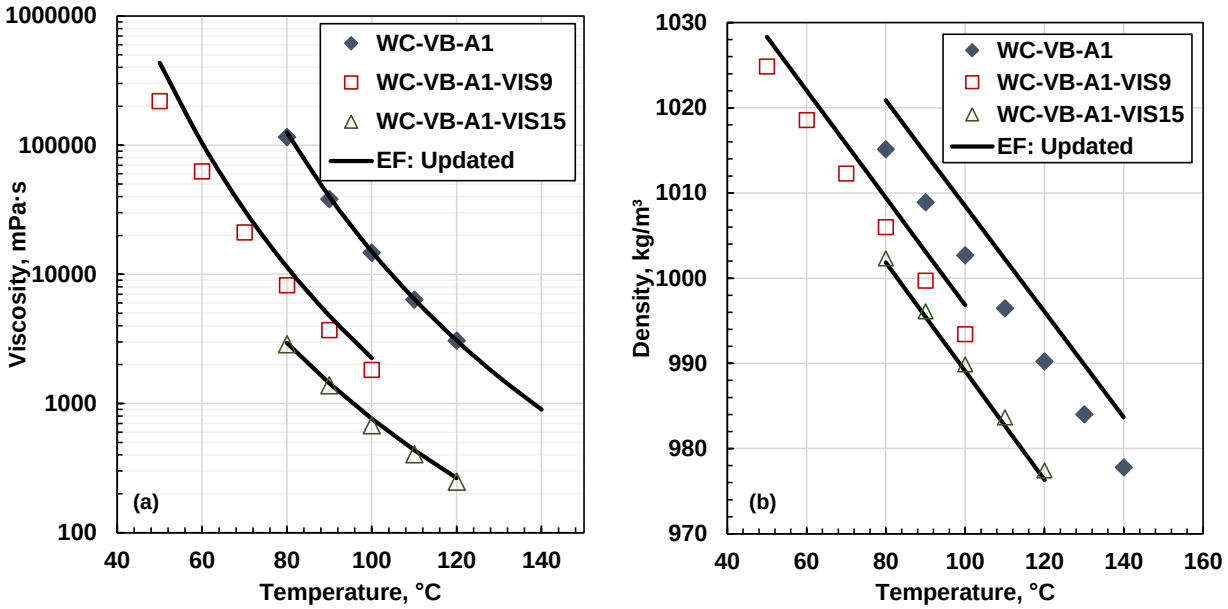

Figure 6-27 Measured and modeled values of WC-VB-A1 feed and product oils a) viscosity and b) density.

Table 6-3. Deviations in the predicted whole oil density and viscosity from the previous (Marquez *et. al.*, 2020) and updated correlations.

Oil	Density			Viscosity		
	AAD kg/m³	MAD kg/m³	Bias kg/m³	AARD %	MARD %	Bias %
Previous Correlation						
WC-B-A3	0.7	1.4	0.6	41	73	41
WC-B-A4	1.0	2.4	1.0	19	29	-0.3
WC-DAO-A1	2.4	2.4	3.5	84	89	-5
WC-VB-A1	NA	NA	NA	NA	NA	NA
AVERAGE	**1.4**	-	**1.7**	**48**	-	**11.7**
Updated Correlation						
WC-B-A3	1.2	3.2	-0.4	10	14.8	3.5
WC-B-A4	1.4	2.6	-1.3	32	51.1	-28
WC-DAO-A1	1.8	2.0	1.8	12	5.5	-7.3
WC-VB-A1	2.1	5.8	1.3	28.5	50.3	28.5
AVERAGE	**1.5**	-	**0.4**	**18.7**	-	**2.4**

Chapter 7: Stability Correlations Model Performance

This chapter presents the modeling of the stability of the visbroken oils from the thesis dataset. First, the performance of the MRS model with the previous set of property correlations is discussed. Then, updated correlations and recommended default properties are proposed. The performance of the model with the updated set of correlations is discussed and a tuning method is proposed.

7.1 Performance of MRS Model with Previous Correlations

Rodriguez *et. al.* (2019) developed a series of correlations to predict the stability of oils that undergo visbreaking reactions and they were presented in Chapter 4. Figure 7-1 shows the performance of these correlations for the whole oils with 0.5 g/g toluene from the dataset used in this thesis. One weakness of the previous correlations is that the properties of the feed distillates are required. However, the WC-VB-A1 feed oil did not contain any distillates, and therefore, the correlations could not be used to predict the yields for products of this oil. Instead, the yield curve of the residue with 0.5 g/g is shown for this oil in Figure 7-1d.

Figure 7-1a shows that, as expected, the correlations match the yield data for the WC-B-A3 bitumen better than for the other oils because the correlations were developed using data from that oil. The correlations consistently and significantly over-predict the yields from all of the visbroken products from the other oils. The highest errors are for the WC-DAO-A1 products. Different oils may react differently and their properties change differently with the conversion. It is also possible that the correlations were overfitted to the data from a single oil and could be better generalized. In addition, the correlations must be modified to predict yields for products from feeds without distillates.

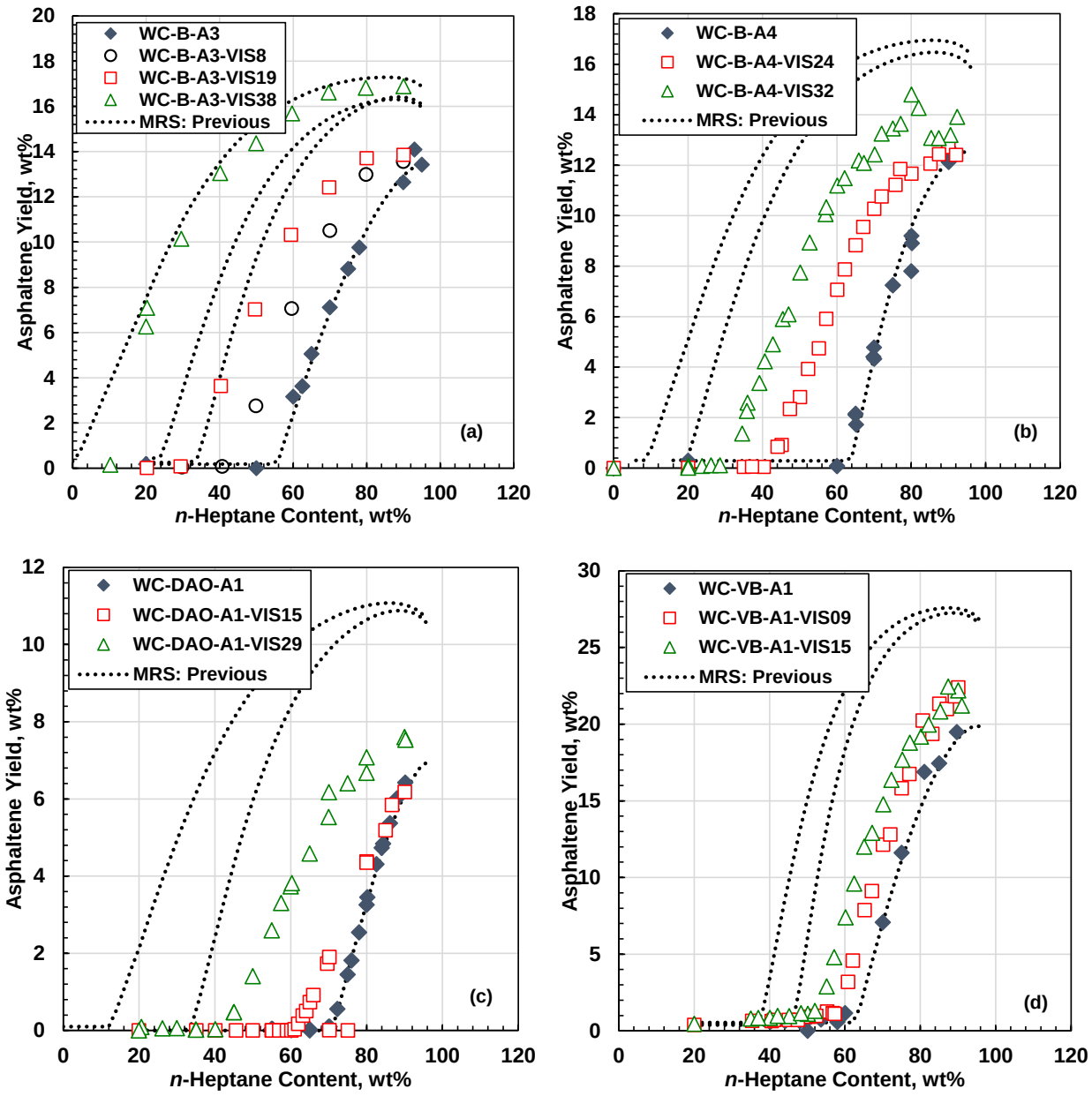

Figure 7-1. Measured and modeled (MRS model with correlations from Rodriguez *et. al.*, (2019) yields for mixtures of oil with 0.5 g/g toluene diluted with *n*-heptane: a) WC-B-A3 whole oil; b) WC-B-A4 whole oil; c) WC-DAO-A1 whole oil; d) WC-VB-A1 residue. The repeatability of the yield measurements was ±0.2 wt%.

7.2 Updated Correlations

Recommended values or correlations are required for the molecular weight, density, and solubility parameter of the distillates and SARA fractions of the feed oils and their products. The updated correlations for density were presented in Chapter 6. The updated correlations for molecular weight and solubility parameter are presented below.

7.2.1 Molecular Weight

Distillates

Figure 7-2 show the molecular weight of the distillate fractions determined from the SBD assay as discussed in Chapter 4. The visbroken distillates from feeds that contained distillates to begin with all follow a similar trend. However, the molecular weight of the distillates generated from the WC-VB-A1 vacuum bottoms are much lower. Since there were no distillates in this feed oil, it appears that the distillates generated by visbreaking have a lower molecular weight than the distillates naturally found in the bitumen. Therefore, the molecular weight of the distillates in the products from each of the oils were determined as the average molecular weight of the original distillates and the generated distillates, as follows:

$$MW_D = \left[\frac{1 - w_{new}}{212} + \frac{w_{new}}{160}\right]^{-1} \tag{7.1}$$

The molecular weight of the original distillates and generated distillates that best fit the data in Figure 7-2 were 160 and 212 g/mol, respectively. The updated correlation fit the molecular weights of the distillate fractions with an AAD of 5.7 g/mol (AARD of 3%) and an R^2 correlation coefficient of 0.82. Figure 7-2 also shows that the updated correlation is similar to the previous correlation except for the WC-VB-A1 oil. The updated correlation can be applied for feeds with no distillates such as the vacuum bottoms, a notable improvement from the previous correlation.

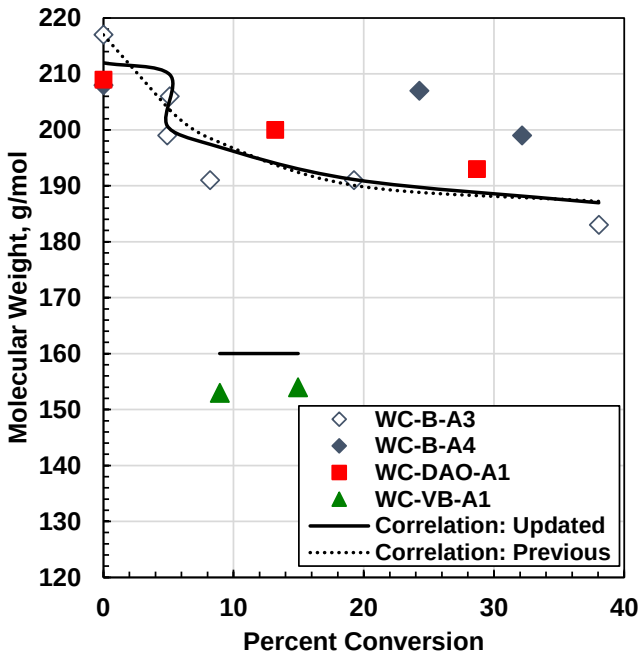

Figure 7-2. Measured and correlated molecular weights of the distillates from the thesis dataset as a conversion function. The updated correlated values depend on the composition and are different for each oil; the upper and lower solid lines on the plot are for the WC-B-A3 and WC-VB-A1 oils, respectively. The previous correlation (dashed line) is independent of composition.

SARA Fractions

The MRS model is not sensitive to the molecular weights of the saturate, aromatic, and resins fractions and therefore, they were only measured for the feed oils. The measured molecular weights for a given fraction varied by less than 10% which is smaller than the ±15% error of the measurement. Therefore, the average value was determined for each fraction and is the recommended value for any oil. The recommended values only changed slightly from the previous values and are provided in Table 7-1. The asphaltene molecular weight in oil cannot be measured and was left at the previous default value of 3000 g/mol. The original correlations from Rodriguez *et. al.*, (2019), Eqs. 4-38 and 4-41, are used to determine the molecular weights of the reacted SARA fractions with the conversion and the recommended values in Table 7-1 as inputs.

Table 7-1. Previous and updated recommended molecular weights for the feed saturates, aromatics, and resins.

Fraction	Previous Molecular Weight g/mol	Updated Molecular Weight g/mol
Saturates	600	580
Aromatics	640	620
Resins	1200	1200
Asphaltenes	3000	3000

7.2.2 Solubility Parameters

Distillates

Figure 7-3 shows the solubility parameter of the distillate fractions. Interestingly, the solubility parameter of the visbroken distillates from the WC-VB-A1 oil follows the same trend as the other oils. In other words, purely generated distillates and mixed original and generated distillates behaved similarly. It appears that the contribution of the generated distillates is similar enough to the changes in the original distillates that the effects cannot be distinguished. Therefore, the solubility parameter of the distillates was fitted solely as a function of conversion as follows:

$$\delta_D = 18.7\left[1 - 0.0996\left(1 - exp(-0.06009X)\right)\right] \quad (7.2)$$

The correlation captures distillates solubility parameter with an AAD of 0.4 $MPa^{0.5}$ (AARD of 2.0%) and an R^2 correlation coefficient of 0.76. The coefficient of 18.7 $MPa^{0.5}$ is the average feed value found for the distillates, as discussed in Chapter 5. Figure 7-3 shows that the updated correlation gives slightly lower distillates solubility parameters than the previous correlation.

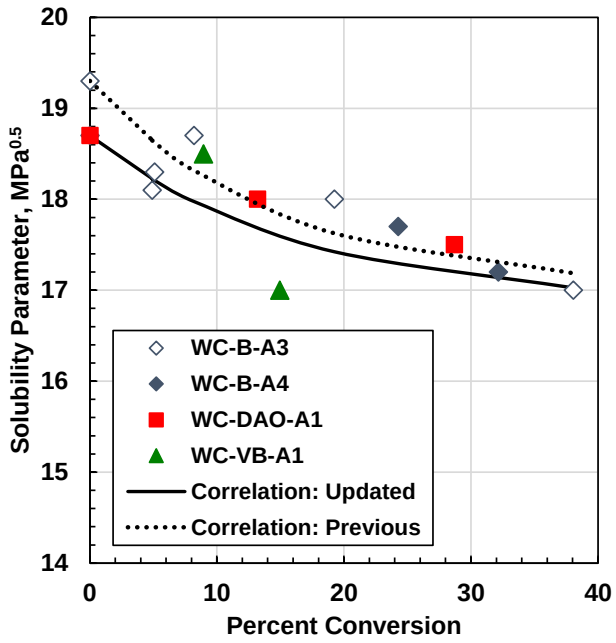

Figure 7-3. Experimentally derived and correlated solubility parameters of the distillates from the thesis dataset as a function of conversion.

Saturates and Aromatics

The MRS model is not sensitive to the relatively small differences in the saturate and aromatic solubility parameters from different feeds. Therefore, only the feed parameters were measured. The updated recommended feed values from Chapter 5 are provided in Table 7-2. There was little change from the previous values. The original Rodriguez *et. al.*, (2019) correlations (Eqs. 4.47 and 4.48) are retained to determine the solubility parameters of visbroken saturates and aromatics using the recommended feed values and conversion as inputs.

Table 7-2. Previous and updated recommended solubility parameters for the feed saturates and aromatics.

Fraction	**Previous Solubility Parameter MPa$^{0.5}$**	**Updated Solubility Parameter MPa$^{0.5}$**
Saturates	16.5	16.5
Aromatics	21.0	20.8

Asphaltenes

Figures 7-4a and 7-5a show the minimum and maximum asphaltene solubility parameters, respectively. Recall that the minimum and maximum solubility parameters of the feed asphaltenes are determined by fitting yield data, usually for the whole oil diluted with *n*-heptane. Therefore, it is only necessary to correlate how these parameters change with the conversion. Therefore, the experimentally derived minimum and maximum solubility parameters were normalized to the feed value to determine the trend with conversion, as shown in Figures 7-4b and 7-5b, respectively. The following correlations were fitted to the relative solubility of asphaltenes:

$$\delta_{min} = \delta_{min,Feed}[1 + 0.001169X] \quad (7.3)$$

$$\delta_{max} = \delta_{max,Feed}[1 + 0.000826X] \quad (7.4)$$

where the subscript min and max indicate the minimum and maximum asphaltene solubility parameter and the subscript $Feed$ specifies the value for the feed oil. The updated correlations fit the minimum and maximum asphaltenes solubility parameters with an AAD of 0.15 $MPa^{0.5}$ (0.75%) and 0.06 $MPa^{0.5}$ (0.34%), respectively. The R^2 correlation coefficients were 0.78 and 0.87, respectively.

The updated minimum solubility parameter correlation is similar to the previous correlation but remains linear and gives higher solubility parameters at conversions above 10%. The updated maximum solubility parameter correlation gives significantly lower solubility parameters than the previous correlation. The net effect is to give a narrower range of asphaltene solubility parameters with greater solubility in the oil on average. Note that the asphaltene solubility parameters shown on the plot were determined from modeling yield data with the updated model correlations for all other parameters and therefore are not the same as the values used to determine the previous correlation.

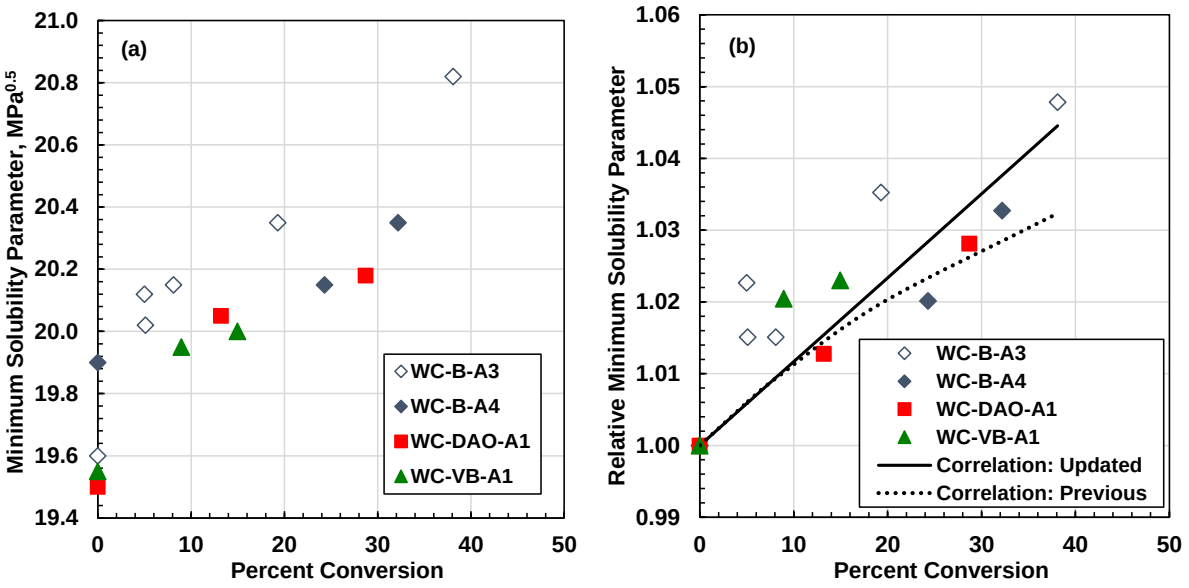

Figure 7-4. Experimentally derived and correlated minimum asphaltene solubility parameters from the thesis dataset as a function of conversion: a) absolute solubility parameter; b) relative solubility parameter.

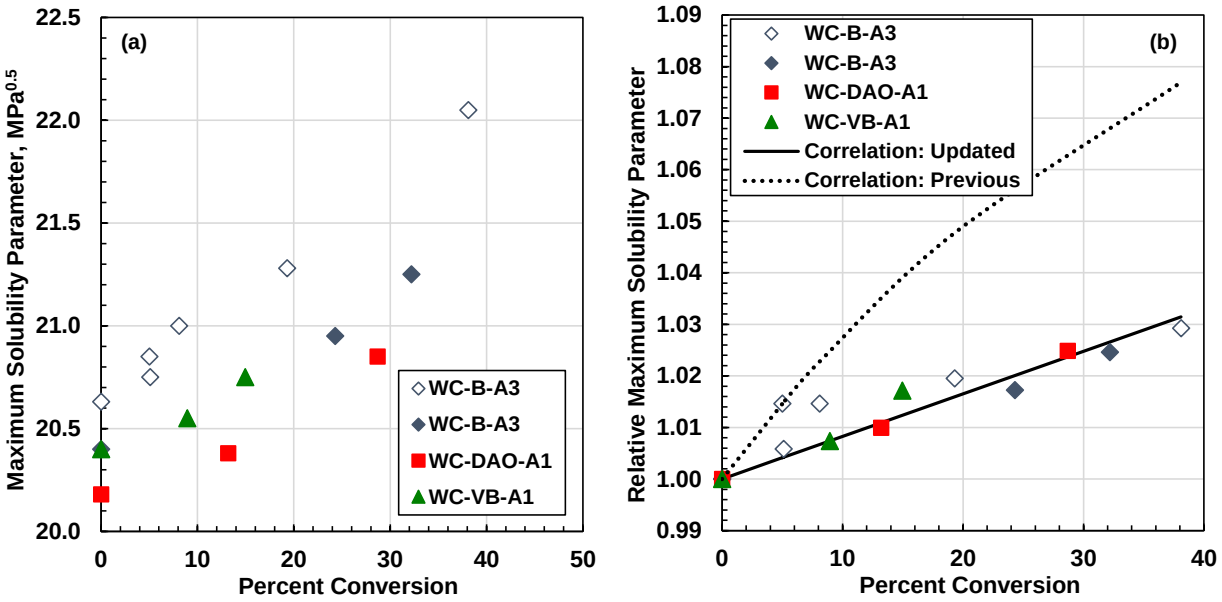

Figure 7-5. Experimentally derived and correlated maximum asphaltene solubility parameters from the thesis dataset as a function of conversion: a) absolute solubility parameter; b) relative solubility parameter.

7.3 Model Evaluation

The predicted yields from the MRS model with the updated correlations are compared with the measured data in Figures 7-6 to 7-9 for the WC-B-A3, WC-B-A4, WC-DAO-A1, and WC-SB-A1 oils, respectively. The deviations in the predicted onsets and yields are summarized in Tables 7-3 and 7-4, respectively. The overall deviations in the predicted onsets and yields from the updated model were 5.6 wt% *n*-heptane and 2.3 wt%, respectively, compared with 25 wt% *n*-heptane and 2.8 wt% for the previous model.

The updated model tended to underestimate the asphaltene solubility (under-predict the yields, over-predict the onsets) in the WC-B-A3 oil and overestimate the asphaltene solubility in the WC-B-A4 bitumen. The average error from the updated model in the predicted onsets for the respective oil were 10.9 and 4.3 wt% *n*-heptane compared with 12.2 and 31.3 wt% for the previous model. The average error in the predicted yields from the updated model were 3.0 and 1.3 wt% compared with 2.8 and 3.0 wt% for the previous model. It is likely that the oils react slightly differently and the updated correlations represent an average reactivity which provides a lower overall error.

The correlated WC-DAO-A1 and WC-VB-A1 onsets and yields were both generally deviated by less than 5 wt% from the data, almost within the experimental error of ±3 wt% *n*-heptane for the onset and ±3 wt% for the yields. However, the model tended to under-predict yields at high dilution. The model was also able to predict the yields from the WC-VB-A1 vacuum bottoms where the previous model could not. As noted In Section 7.1, the deviations for these oils were much higher for the previous model.

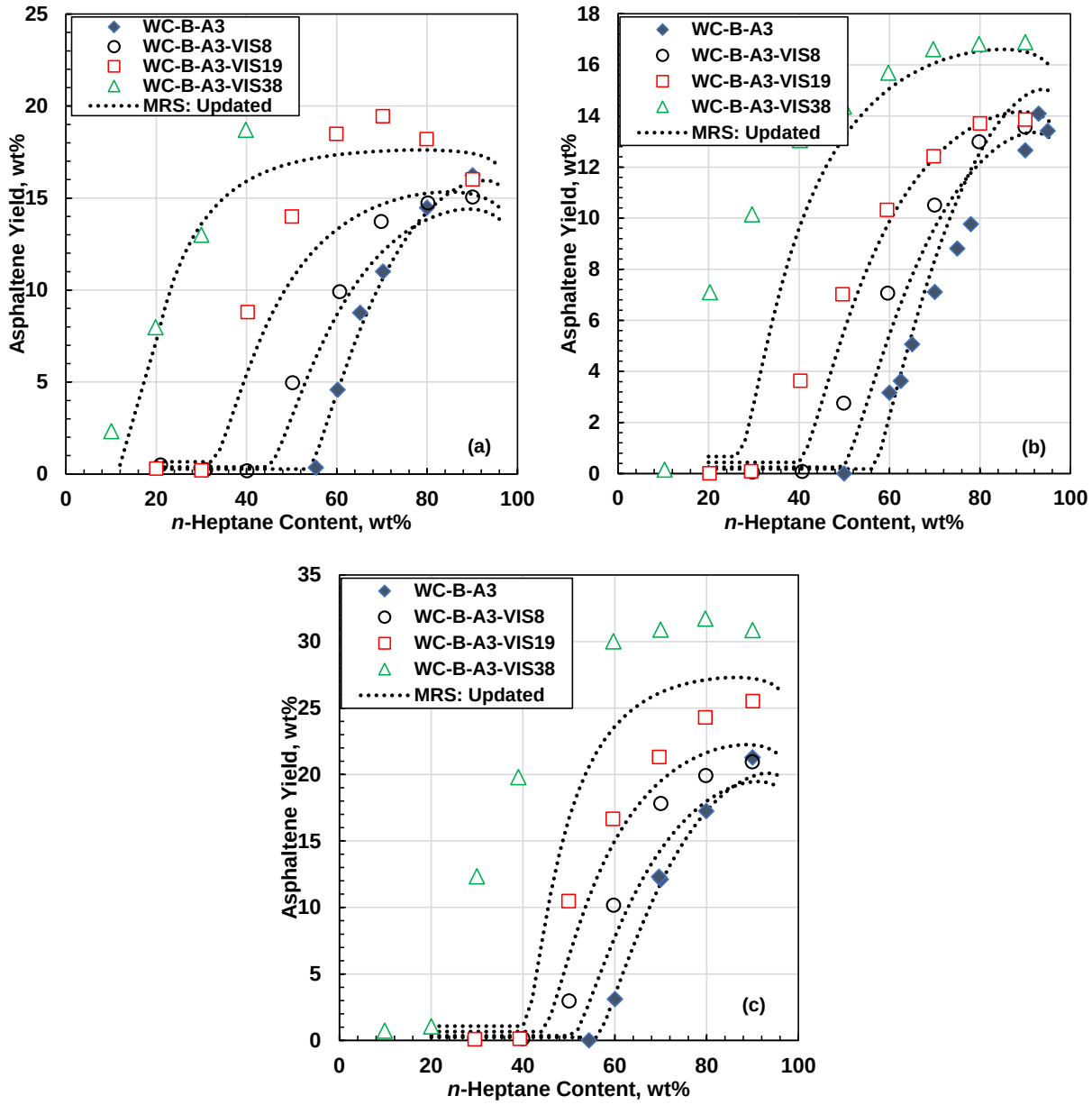

Figure 7-6. Measured and modeled WC-B-A3 asphaltene yields from: a) whole oil; b) whole oil diluted with 0.5 g toluene per g oil; c) SBD residue oil diluted with 0.5 g toluene per g oil.

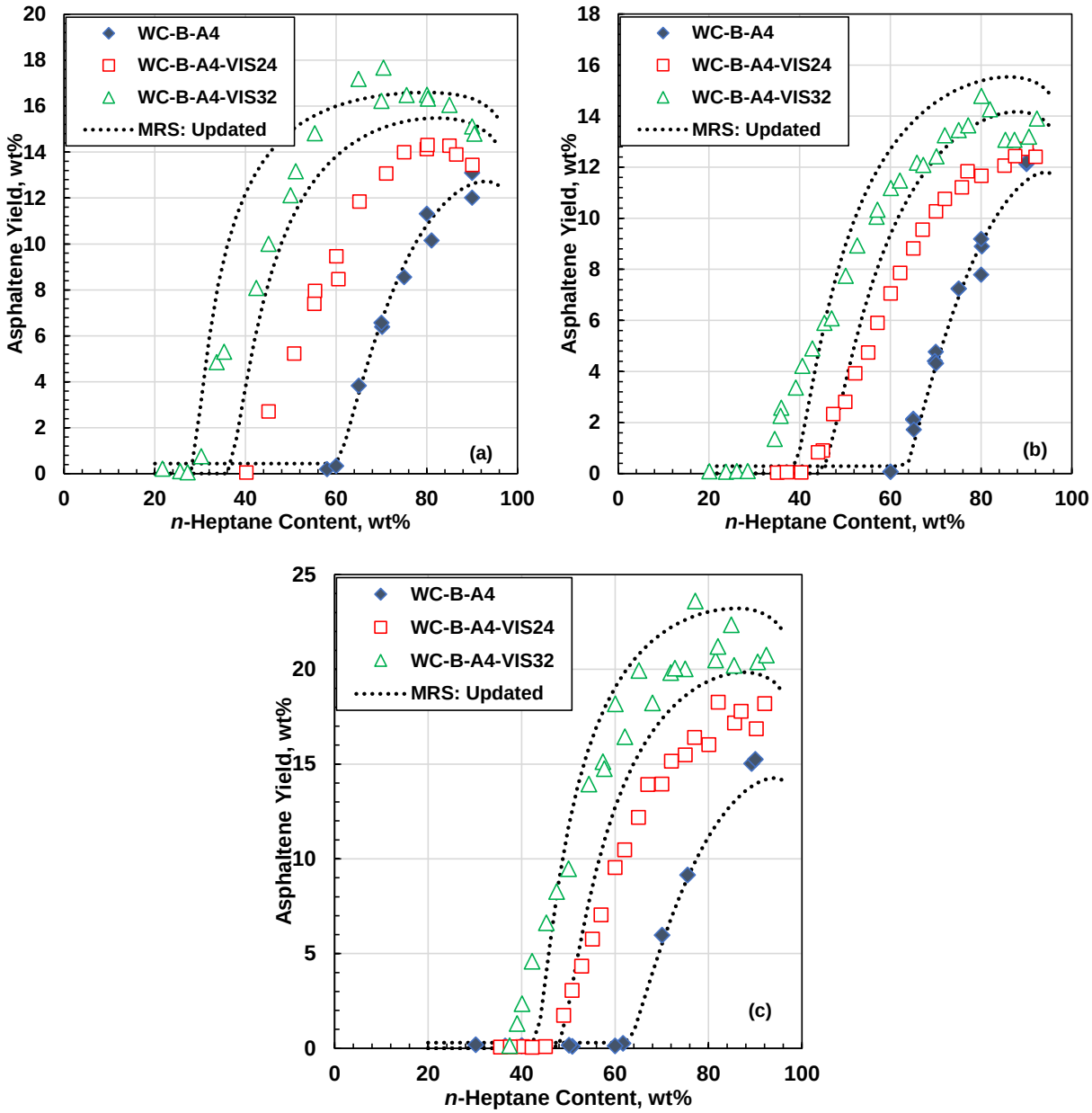

Figure 7-7. Measured and modeled WC-B-A4 asphaltene yields from: a) whole oil, b) whole oil diluted with 0.5 g toluene per g oil and c) SBD residue oil diluted with 0.5 g toluene per g oil.

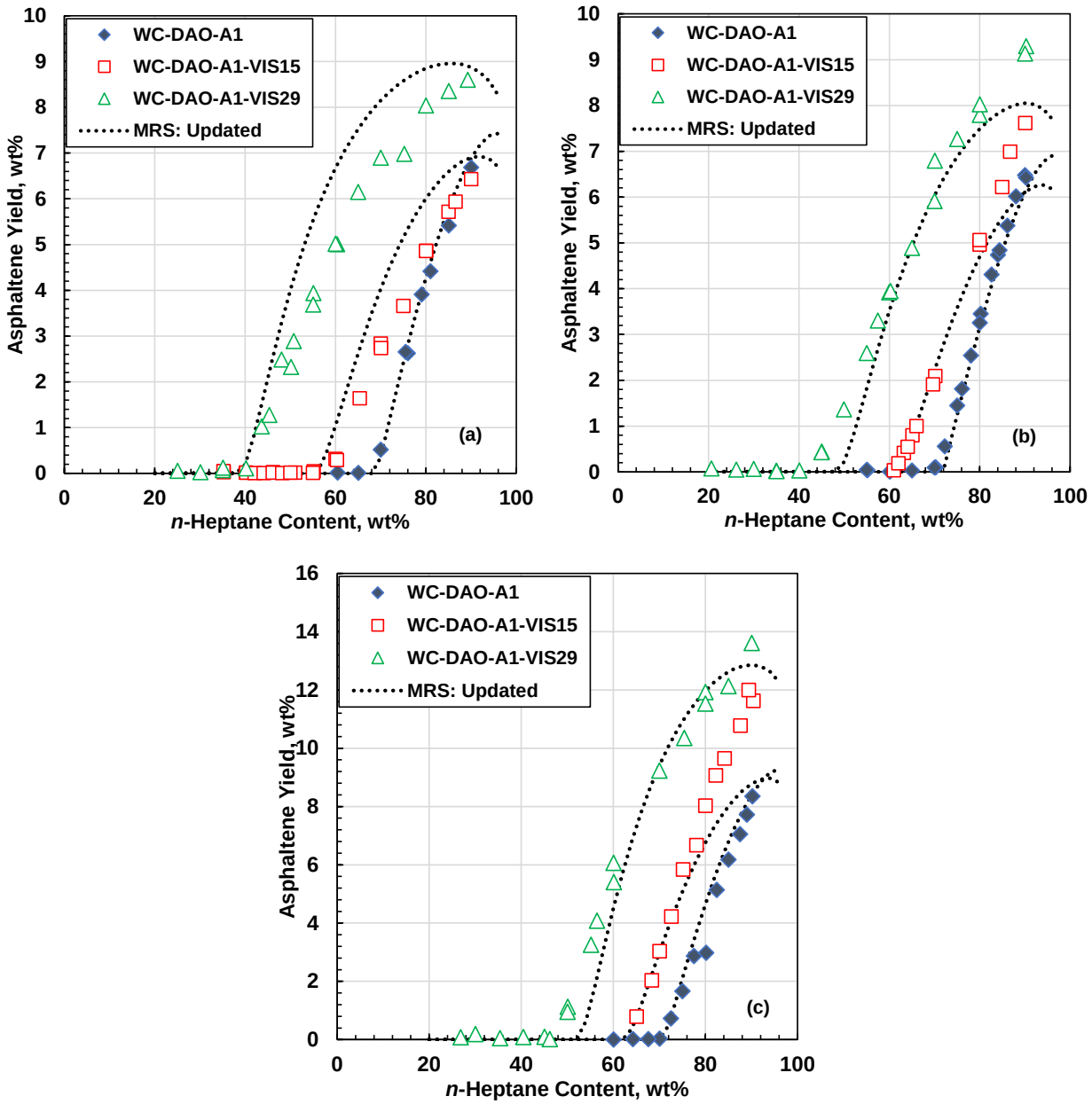

Figure 7-8. Measured and modeled WC-DAO-A1 asphaltene yields from: a) whole oil, b) whole oil diluted with 0.5 g toluene per g oil and c) SBD residue oil diluted with 0.5 g toluene per g oil.

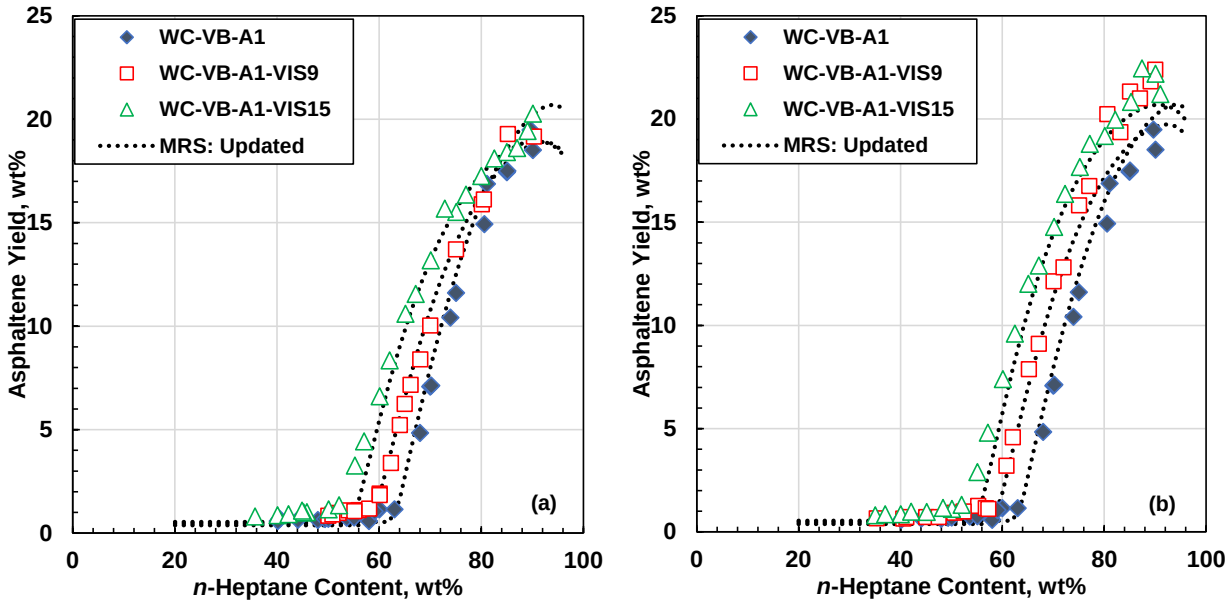

Figure 7-9. Measured and modeled WC-VB-A1 asphaltene yields from: a) whole oil diluted with 0.5 g toluene per g oil and b) SBD residue oil diluted with 0.5 g toluene per g oil.

Table 7-3. Absolute deviation of the predicted onsets (wt% *n*-heptane) from the previous and updated MRS model. +T indicates that oil was mixed with 5 g/g toluene.

Oil	Whole Oil wt%	Whole Oil+T wt%	SBD Residue+T wt%	Overall wt%
Previous Model				
WC-B-A3	13.2	6.8	4.6	8.2
WC-B-A4	51.0	23.5	19.5	31.3
WC-DAO-A1	42.5	28.5	26.5	32.5
WC-VB-A1	NM	2.0	2.5	2.3
All	35.6	19.1	15.9	**23.5**
Updated Model				
WC-B-A3	5.8	7.8	6.6	6.7
WC-B-A4	5.0	5.0	3.0	4.3
WC-DAO-A1	1.5	5.5	4.0	3.7
WC-VB-A1	NM	2.0	2.5	2.3
All	4.1	5.1	4.0	**4.4**
Tuned Model				
WC-B-A3	8.8	3.0	4.2	**5.3**

Table 7-4. Absolute deviation of the predicted yields from the previous and updated MRS model. +T indicates that oil was mixed with 5 g/g toluene.

Oil	Whole Oil wt%	Whole Oil+T wt%	Residue+T wt%	Overall wt%
Previous Model				
WC-B-A3	3.0	1.6	2.0	2.2
WC-B-A4	1.5	3.0	4.5	3.0
WC-DAO-A1	0.8	1.0	2.0	1.3
WC-VB-A1	NM	6.0	4.5	5.3
All	1.8	2.9	3.3	**2.6**
Updated Model				
WC-B-A3	4.0	0.6	3.6	2.7
WC-B-A4	0.5	1.5	2.0	1.3
WC-DAO-A1	0.5	0.8	2.5	1.3
WC-VB-A1	NM	1.0	1.5	1.0
All	1.7	1.2	2.8	**1.6**
Tuned Model				
WC-B-A3	2.8	0.8	2.2	**1.9**

7.4 Tuning the Model

If yield data are available for a reacted product, the model can be tuned to potentially improve the predicted yields at other conversions. The proposed tuning method is to modify the conversion as follows:

$$X_{adj} = \xi X \tag{7.5}$$

where X_{adj} is the adjusted conversion and ξ is a tuning constant. The WC-B-A3 oil was selected to test the tuning method because this oil had data at several conversions. The model was tuned to match the yield curve for the WC-B-A3-VIS8 run and the tuned value of ξ was 1.5. The model was then used to predict the yield curves at other conversions. Figure 7-10 shows the tuned and predicted yield curves and Tables 7-3 and 7-4 show the deviations of the tuned model onset and yield predictions, respectively. The model deviations for the onsets and yields decreased from 6.7 wt% *n*-heptane (untuned) to 5.3 wt% *n*-heptane (tuned) and from 2.7 wt% (untuned) to 1.9 wt% (tuned), respectively. The model matches the yield curves to within experimental error at all conversions except for the 38% conversion. The yields at 38% conversion are significantly underestimated. It is possible that the reaction pathways changed at such a high conversion and

the model correlations no longer apply. Hence, the proposed correlations may only apply to approximately 32% conversion, the highest conversion examined where the model matched the data (WC-B-A4-VIS32).

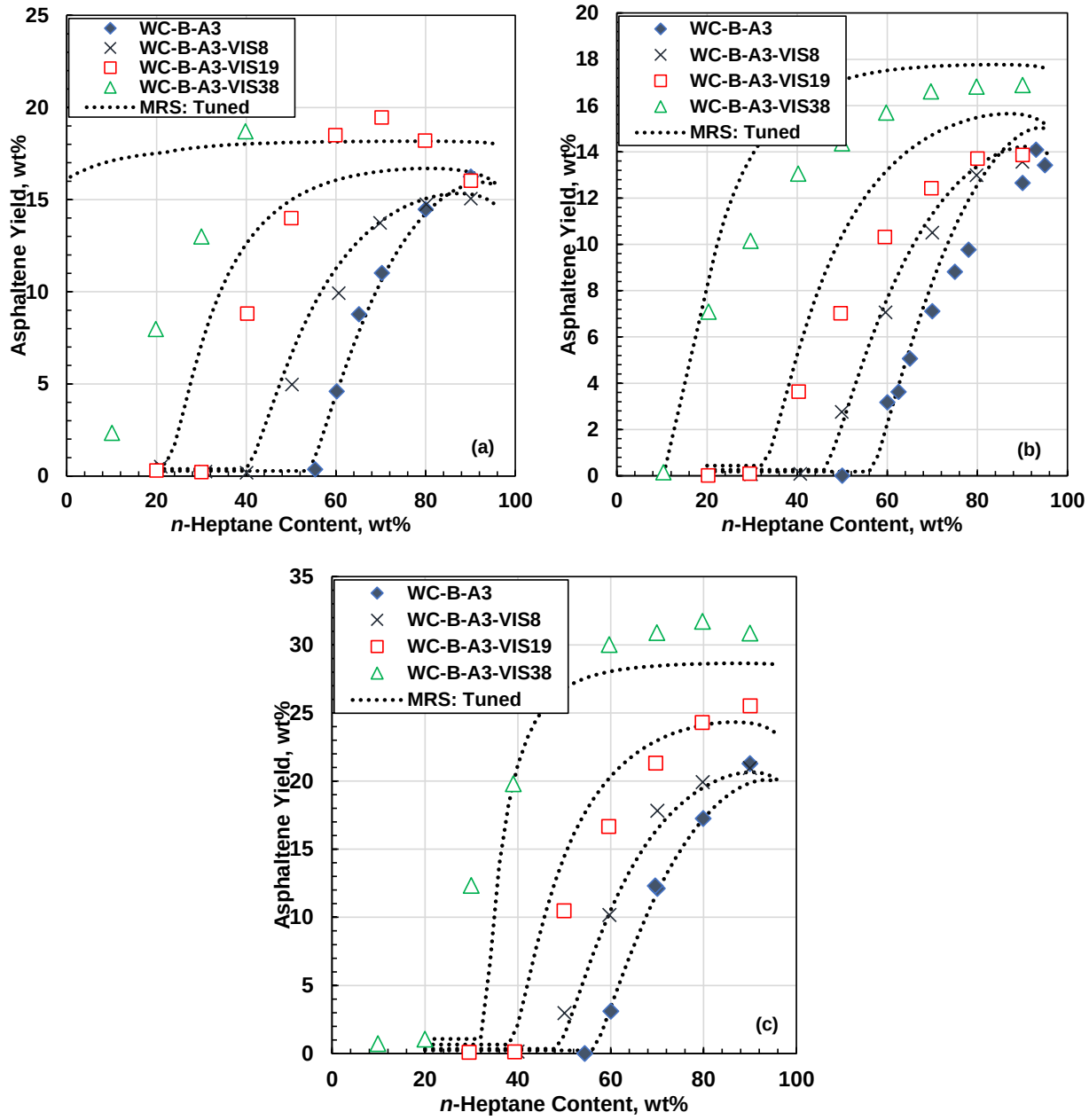

Figure 7-10. Measured and tuned ($\xi = 1.5$) model WC-B-A3 asphaltene yields from: a) whole oil; b) whole oil diluted with 0.5 g toluene per g oil; c) SBD residue oil diluted with 0.5 g toluene per g oil.

Chapter 8: Conclusions and Recommendations

The main contribution of this thesis is to update the Expanded Fluid viscosity and Modified Regular Solution stability models for heavy oil applications involving fractionated oils. The methodology was adapted from the previous studies and is compatible with Symmetry™ process simulator. In this approach, the oils are characterized into distillates and SARA (saturates, aromatics, resins, and asphaltenes) fractions. The required properties for each fraction are determined from recommended feed values and correlations to conversion. These properties are then inputted into the models to predict the density, viscosity, and stability of the visbroken products.

The first part of the contribution was to provide a dataset of oil compositions and properties for the oil and its fractions. The dataset included four different feed oils from Western Canada and eleven reacted products from these oils. The data for the one oil (WC-B-A3 bitumen and its products) were obtained from elsewhere (Rodriguez *et. al.*, 2019; Marquez *et. al.,* 2019). The data for three of the oils (WC-B-A4, WC-DAO-A1, and WC-VB-A1) were collected in this study. The molecular weight, density, viscosity, and solubility parameters for each fraction were either measured or determined indirectly from other measurements. Distillations and compositions in terms of distillates and SARA fractions were measured for all of the feeds and products. This dataset illustrates the changes in the oils after visbreaking and can be used not only to develop property correlations but also to test reaction models.

The second part of the contribution was to update the recommended feed values and the previously developed correlations for the density and viscosity parameters for each visbroken fraction as a function of the feed properties and conversion. It was demonstrated that the Expanded Fluid viscosity model with the updated correlations matched the measured viscosities of whole oils, maltenes, and residues with an absolute relative deviation of 28%. A volumetric mixing rule with the correlated densities matched the densities of the same oils with an absolute deviation of 1.5

kg/m³. The method required no adjustment of the WC-B-A3, WC-B-A4, and WC-DAO-A1 oils and can be used as a predictive method. However, the recommended parameters for the vacuum bottom oil saturates and aromatics were adjusted to the measured values to account for the light end losses. The saturates and aromatics from the WC-VB-A1 oil were different from the other saturates because this oil was a vacuum residue and the light ends of the saturates stripped off during the distillation. There was not enough data to develop a completely predictive method for vacuum bottom oils.

Similarly, the recommended feed values and correlations to conversion were updated for the molecular weight and solubility parameters for each fraction. The Modified Regular Solution model with the updated correlations matched the asphaltene precipitation data from the same oils with absolute deviations of 4.4 wt% *n*-heptane for the onset and 2.3 wt% for the yield.

The required inputs for the models are a SimDist assay used to determine the conversion and a distillation assay and residue SARA assay used to determine the oil composition. If the models are used independently, these assays must be obtained for the feed and products. In addition, one set of precipitation data for the feed oil (usually from mixtures of the oil and *n*-heptane) is required to obtain the asphaltene solubility parameters of the feed. For vacuum bottom oils, it is also necessary to determine the effect of the original vacuum distillation on the density and viscosity of the saturates, aromatics, and resins of the feed. The post-distillation properties must either be measured or determined from an independent method. The remaining properties for all oils can be obtained from recommended feed values and the updated property correlations. The models can be coupled with a reaction model to predict the required fluid compositions. In this case, the product assays are not required. The models apply to visbroken Western Canadian bitumens and bitumen fractions, but caution is advised for oils from other sources, which may react differently than the Western Canadian oils. Other conclusions and recommendations are presented below.

8.1 Conclusions

It was confirmed that the property changes in visbroken bitumen are consistent with side-chain removal, mainly from the resins and asphaltenes and an accumulation of fragments in the

distillates. As observed previously (Rodriguez *et. al.,* 2019; Marquez *et. al.,* 2019), the most significant changes in the chemistry of the visbroken products were the increase in the distillates content and the asphaltene solubility parameters. Visbreaking decreased the overall stability of the oil both by decreasing the solubility of asphaltenes and by decreasing the ability of the surrounding environment to keep the asphaltenes soluble. It was demonstrated that visbreaking has a similar effect on both the vacuum bottom and deasphalted oil feeds.

Visbreaking has a similar effect on the properties of each oil. It reduced the density of each oil linearly with a 15 kg/m^3 reduction at 20°C and a 30% conversion. The viscosity of each oil decreased exponentially with a two order of magnitude reduction at 30% conversion. The stability of the reacted oils decreased with increasing conversion with the onset of asphaltene precipitation in mixtures of oil and *n*-heptane decreasing by approximately 30 wt% *n*-heptane.

The partially deasphalted oil had lower density and viscosity than bitumen and had a higher capacity for visbreaking before becoming unstable. For example, the onset point of WC-B-A4 oil decreased from an initial value of 60% to a value of 30% *n*-heptane at approximately 30% conversion. The WC-DAO-A1 oil was more stable with an initial onset of near 70 wt% *n*-heptane that decreased to 40% after a conversion of near 30%. The relative change in the properties of both oils was similar.

The vacuum bottom feed contained no distillates, and therefore, the distillates in its products originated only from the visbreaking reactions. These distillates were much lighter and less viscous than the non-reacted distillates from the other oils. This observation was used to modify the distillates property correlations such that the distillates of a reacted oil are a combination of the original distillates and the lighter reaction product distillates. The new distillates correlations applied to all of the feed oils, whereas the previous correlations only applied to feeds that already contained distillates.

The density and viscosity of the saturate, aromatic, and resin fractions of the vacuum bottom oil were higher than observed in the other oils. The light ends likely been removed from these fractions

when during the original vacuum distillation. Nonetheless, the properties of these fractions changed with conversion on a similar trend as the fractions from the other oils.

8.2 Recommendations

It is recommended to investigate the effect of different extents of deasphalting prior to visbreaking. In particular, deasphalt a feed oil to different ultimate asphaltene contents and measure the density, viscosity, and stability of the deasphalted oil after visbreaking. Then, test the models and correlations. In addition, investigate how much additional conversion can be obtained at different extents of deasphalting.

It is also recommended to investigate the effect of deasphalting after visbreaking. The visbreaking process could be pushed to conversions near the point that destabilizes the oil and the product could be restabilized by partial deasphalting. It is not obvious *a priori* if deasphalting before visbreaking or visbreaking before deasphalting is the most efficient method to reduce diluent requirements.

The density of the resins and density and viscosity of the asphaltenes were determined indirectly. It is recommended to use a direct method to measure these properties and use the data to test the mixing rules in the models. One option is to measure these properties for melted asphaltenes. However, new equipment will be needed because the temperatures required to melt the asphaltenes exceed the temperature limits of the apparatus currently available for this project.

The effect of visbreaking reaction on density, viscosity, and stability of the oils is currently being modeled with one parameter, the conversion. However, the conversion is a function of temperature and the residence time. It is possible that the effects of visbreaking can be better represented by correlating to both temperature and residence time. It is recommended to investigate different temperature and residence time combinations to determine if the conversion is a sufficient correlating parameter. If not, the property correlations could be updated to be functions of both temperature and residence time. Similarly, an analysis of the gas product may identify different reaction pathways at different conditions that can be used to improve the property correlations. For

example, the impact of olefin formation, resin partitioning to asphaltenes and asphaltene partitioning to resins could be included in the correlations. To do so, the correlations would have to be more directly tied to a reaction model and a large amount of data would be required.

The saturates and aromatics fractions of the vacuum bottom oil (WC-VB-A1) were denser and more viscous than the same fractions from the other oils. It is recommended to investigate a wider range of vacuum bottoms in order to develop a recommended property values for their saturate and aromatic fractions.

It is recommended to use a reaction model, such as the reaction model in Symmetry™ software, to predict the composition of the visbroken products from the lab visbreaker unit. The correlation developed in this thesis could be applied to the predicted product composition to assess the cumulative of error from the reactor and property models. The error assessment could be used to identify the most critical areas to tune or improve the reaction model.

Chapter 9: References

Aasberg-Petersen, Kim, Kim Knudsen, and Aage Fredenslund. **1991**. "Prediction of Viscosities of Hydrocarbon Mixtures." *Fluid Phase Equilibria*, 70 (2-3), 293-308.

Abivin, Patrice, Shawn D. Taylor, and Denise Freed. **2012**. "Thermal Behavior and Viscoelasticity of Heavy Oils." in Energy and Fuels, *Fuel, 67*(12), 1714-1715.

Abolala, Mostafa, Kiana Peyvandi, and Farshad Varaminian. **2015**. "Modeling the Viscosity of Pure Imidazolium-Based Ionic Liquids Using SAFT-VR-Mie EoS." *Fluid Phase Equilibria*, 394, 61-70.

Adlard, E. R. **1995**. "Chromatography in the Petroleum Industry." *Analysis*, Elsevier Science.

Afra, S., H. G. Alrashidi, and H. A. Nasr-El-din. **2017**. "Interrelationship Between Asphaltene Precipitation Methods and Asphaltene Characteristics and Self-Association Behavior." in *SPE Latin American and Caribbean Petroleum Engineering Conference Proceedings*, 185542.

Agrawal, P., F. F. Schoeggl, M. A. Satyro, S. D. Taylor, and H. W. Yarranton. **2012**. "Measurement and Modeling of the Phase Behavior of Solvent Diluted Bitumens." *Fluid Phase Equilibria*, 334, 51-64.

Akbarzadeh, Kamran, Hussein Alboudwarej, William Y. Svrcek, and Harvey W. Yarranton. **2005**. "A Generalized Regular Solution Model for Asphaltene Precipitation from N-Alkane Diluted Heavy Oils and Bitumens." *Fluid Phase Equilibria*, 232, 159-170.

Akbarzadeh, Kamran, Amandeep Dhillon, William Y. Svrcek, and Harvey W. Yarranton. **2004**. "Methodology for the Characterization and Modeling of Asphaltene Precipitation from Heavy Oils Diluted with N-Alkanes." *Energy and Fuels*, 18, 1434-1441.

Al-Soufi, H. H., Z. F. Savaya, H. K. Mohammed, and I. A. Al-Azawi. **1988**. "Thermal Conversion (Visbreaking) of Heavy Iraqi Residue." *Fuel*, 1714-1712.

Alboudwarej, H., J. Beck, W. Y. Svrcek, H. W. Yarranton, and K. Akbarzadeh. **2002**. "Sensitivity of Asphaltene Properties to Separation Techniques." *Energy and Fuels, 16*(2), 462-469.

Alboudwarej, Hussein, Kamran Akbarzadeh, James Beck, William Y. Svrcek, and Harvey W. Yarranton. **2003**. "Regular Solution Model for Asphaltene Precipitation from Bitumens and Solvents." *AIChE Journal*, 49 (11), 2948-2956.

Ali, Latif H. and Khalid A. Al-Ghannam. **1981**. "Investigations into Asphaltenes in Heavy Crude Oils. I. Effect of Temperature on Precipitation by Alkane Solvents." *Fuel*, 11, 1043-1046.

Alimohammadi, Sepideh, Sohrab Zendehboudi, and Lesley James. **2019**. "A Comprehensive Review of Asphaltene Deposition in Petroleum Reservoirs: Theory, Challenges, and Tips." *Fuel*, 252 (1), 753-791.

Allal, A., C. Boned, and A. Baylaucq. **2001**. "Free-Volume Viscosity Model for Fluids in the Dense and Gaseous States." *Physical Review E - Statistical Physics, Plasmas, Fluids, and Related Interdisciplinary Topics*, 64 (1).

Allal, A., M. Moha-Ouchane, and C. Boned. **2001**. "A New Free Volume Model for Dynamic Viscosity and Density of Dense Fluids versus Pressure and Temperature." *Physics and Chemistry of Liquids*, 39 (1), 1-30.

Altgelt, Klaus H. and Mieczyslaw M. Boduszynski. **1994**. Composition and Analysis of Heavy Petroleum Fractions.

Andersen, Simon I. and Kulbir S. Birdl. **1990**. "Influence of Temperature and Solvent on the Precipitation of Asphaltenes." *Fuel Science and Technology International*, 8:6, 593-615.

Ardrey, R. A. **2004**. Liquid Chromatography-Mass Spectrometry: An Introduction. Robert E. Ardrey.

Arya, Alay, Xiaodong Liang, Nicolas Von Solms, and Georgios M. Kontogeorgis. **2016**. "Modeling of Asphaltene Onset Precipitation Conditions with Cubic Plus Association (CPA) and Perturbed Chain Statistical Associating Fluid Theory (PC-SAFT) Equations of State." *Energy and Fuels*, 30 (8), 6835-6852.

Arya, Alay, Xiaodong Liang, Nicolas Von Solms, and Georgios M. Kontogeorgis. **2017**. "Modeling of Asphaltene Precipitation from Crude Oil with the Cubic Plus Association Equation of State." *Energy and Fuels*, 31 (2) 2063-2075.

ASTM. **2008**. "D2887 - 08, Standard Test Method for Boiling Range Distribution of Petroleum Fractions by Gas Chromatography ASTM." in *Annual Book of ASTM Standards*.

ASTM. **2015**. "Standard Test Method for Distillation of Petroleum Products and Liquid Fuels at Atmospheric Pressure." *Book of Standards*.

ASTM Standard D2892. **2009**. "Test Method for Distillation of Crude Petroleum (15-Theoretical Plate Column)." *Fuel Processing Technology*.

Baled, Hseen O., Isaac K. Gamwo, Robert M. Enick, and Mark A. McHugh. **2018**. "Viscosity Models for Pure Hydrocarbons at Extreme Conditions: A Review and Comparative Study." *Fuel*, 218, 89-111.

Baltatu, Monica E. **1982**. "Prediction of the Liquid Viscosity for Petroleum Fractions." *Industrial and Engineering Chemistry Process Design and Development*, 21 (1), 192-195.

Barré, L., J. Jestin, A. Morisset, T. Palermo, and S. Simon. **2009**. "Relation between Nanoscale Structure of Asphaltene Aggregates and Their Macroscopic Solution Properties." *Oil & Gas Science and Technology* - Revue de l'IFP, 64 (5), 617-628.

Baylaucq, A., C. K. Zéberg-Mikkelsen, P. Daugé, and C. Boned. **2002**. "Dynamic Viscosity and Density of Heptylbenzene and Heptylcyclohexane up to 100 MPa." *Journal of Chemical and Engineering Data*, 47 (4), 997-1002.

Blas, Felipe J. and Lourdes F. Vega. **1997**. "Thermodynamic Behaviour of Homonuclear and Heteronuclear Lennard-Jones Chains with Association Sites from Simulation and Theory." *Molecular Physics*, 92, 135-150.

Boned, C., A. Allal, A. Baylaucq, C. K. Zéberg-Mikkelsen, D. Bessieres, and S. E. Quiñones-Cisneros. **2004**. "Simultaneous Free-Volume Modeling of the Self-Diffusion Coefficient and Dynamic Viscosity at High Pressure." *Physical Review E - Statistical, Nonlinear, and Soft Matter Physics*, 64(1 Pt 1), 011203 .

Brons, Glen and Jimmy M. Yu. **1995**. "Solvent Deasphalting Effects on Whole Cold Lake Bitumen." *Energy and Fuels*, 9 (4), 641–647.

Burgess, Ward A., Deepak Tapriyal, Isaac K. Gamwo, Bryan D. Morreale, Mark A. McHugh, and Robert M. Enick. **2012**. "Viscosity Models Based on the Free Volume and Frictional Theories for Systems at Pressures to 276 MPa and Temperatures to 533 K." *Industrial and Engineering Chemistry Research*, 51, 51, 16721–16733.

Burgess, Ward A., Deepak Tapriyal, Bryan D. Morreale, Yee Soong, Hseen O. Baled, Robert M. Enick, Yue Wu, Babatunde A. Bamgbade, and Mark A. McHugh. **2013**. "Volume-Translated Cubic EoS and PC-SAFT Density Models and a Free Volume-Based Viscosity Model for Hydrocarbons at Extreme Temperature and Pressure Conditions." *Fluid Phase Equilibria*, 9, 2, 275–279.

Carbognani, Lante, Manuel F. Gonzalez, and Pedro Pereira-Almao. **2007**. "Characterization of Athabasca Vacuum Residue and Its Visbroken Products. Stability and Fast Hydrocarbon Group-Type Distributions." Energy and Fuels, 21 (3), 1631-1639.

Di Carlo, S. and B. Janis. **1992**. "Composition and Visbreakability of Petroleum Residues." Chemical Engineering Science, 47 (9-11), 2695-2700.

Carrillo, Jesús Alirio and Laura Milena Corredor. **2013**. "Upgrading of Heavy Crude Oils: Castilla." Fuel Processing Technology, 28, 3, 1811–1819.

Casalini, Anna, Achille Mascherpa, and Carmen Vecchi. **1990**. "Modifications Induced by Visbreaking on Composition and Structure of Atmospheric Residues." *Fuel Science and Technology International*, 8,427-445.

Castañeda, L. C., J. A. D. Muñoz, and J. Ancheyta. **2012**. "Combined Process Schemes for Upgrading of Heavy Petroleum." in Fuel, 100, 110-127.

Castillo, Javier and Arno De Klerk. **2019**. "Visbreaking of Deasphalted Oil from Bitumen at 280-400 °c." Energy and Fuels, 33, 1, 159–175.

Chacón-PatinÌo, Martha L., Steven M. Rowland, and Ryan P. Rodgers. **2018**. "Advances in Asphaltene Petroleomics. Part 3. Dominance of Island or Archipelago Structural Motif Is Sample Dependent." Energy and Fuels, 32, 9, 9106–9120.

Chacón-Patiño, Martha L., Steven M. Rowland, and Ryan P. Rodgers. **2017**. "Advances in Asphaltene Petroleomics. Part 1: Asphaltenes Are Composed of Abundant Island and Archipelago Structural Motifs." Energy and Fuels, 31, 12, 13509–13518.

Chen, Sheng Li, Sheng Sheng Jia, Yun Hua Luo, and Suo Qi Zhao. **1994**. "Mild Cracking Solvent Deasphalting: A New Method for Upgrading Petroleum Residue." Fuel.73, (3), 439-442.

Christensen, P. L. and A. A. Fredenslund. **1980**. “A Corresponding States Model for the Thermal Conductivity of Gases and Liquids.” Chemical Engineering Science, 35, 4, 871-875.

Cohen, Moreel H. and David Turnbull. **1959**. “Molecular Transport in Liquids and Glasses.” The Journal of Chemical Physics, 31 (5), 1164-1169.

Collett, Charles T. and Christopher D. Robson. **2010**. Handbook of Computational Chemistry Research, Nova Science Publishers.

Dawson, W. H., E. Chornet, P. Tiwari, and M. Heitz. **1989**. “Hydrogenation of Individual Components Isolated from Athabasca Bitumen Vacuum Resid.” in *American Chemical Society*, Division of Petroleum Chemistry, Preprints, 34(2), 384-394.

Dente, M., G. Bozzano, and G. Bussani. **1997**. “A Comprehensive Program for Visbreaking Simulation: Product Amounts and Their Properties Prediction.” Computers and Chemical Engineering, 21 (10), 1125-1134.

Díaz, O. Castellanos, J. Modaresghazani, M. A. Satyro, and H. W. Yarranton. **2011**. “Modeling the Phase Behavior of Heavy Oil and Solvent Mixtures.” Fluid Phase Equilibria, 304, (1-2), 74-85.

Doolittle, Arthur K. **1951**. “Studies in Newtonian Flow. II. the Dependence of the Viscosity of Liquids on Free-Space.” Journal of Applied Physics, 22 (12), 1471-1475.

Drews, AW. **2008**. “Standard Test Method for Distillation of Heavy Hydrocarbon Mixtures (Vacuum Potstill Method).” Manual on Hydrocarbon Analysis, 6th Edition 826-826–16.

El-Gendy, Nour Shafik and James G. Speight. **2015**. Handbook of Refinery Desulfurization, CRC Press.

Ely, James F and H. J. Hanley. **1981**. "NBS TECHNICAL NOTE 1039 / National Bureau of Standards for the Prediction Viscosity and Thermal Conductivity.", 20 (4), 323-332.

Ely, James F. and H. J. M. Hanley. **1981**. "Prediction of Transport Properties. 1. Viscosity of Fluids and Mixtures." Industrial and Engineering Chemistry Fundamentals, 20 (4), 323-332.

Eyring, Henry. **1936**. "Viscosity, Plasticity, and Diffusion as Examples of Absolute Reaction Rates." The Journal of Chemical Physics, 4, 283.

Fahim, Mohamed A., Taher A. Alsahhaf, and Amal Elkilani. **2010a**. Fundamentals of Petroleum Refining. *Elsevier*, Chapter 7.

Fahim, Mohamed A., Taher A. Alsahhaf, and Amal Elkilani. **2010b**. "Refinery Feedstocks and Products." in Fundamentals of Petroleum Refining, Elsevier B.V.

Flory, Paul J. **1941**. "Thermodynamics of High Polymer Solutions." *The Journal of Chemical Physics*, 660-661.

Fossen, Martin, Johan Sjøblom, Harald Kallevik, and Joakim Jakobsson. **2007**. "A New Procedure for Direct Precipitation and Fractionation of Asphaltenes from Crude Oil." Journal of Dispersion Science and Technology, 28(1), 193-197.

Gonzalez, Doris L., P. David Ting, George J. Hirasaki, and Walter G. Chapman. **2005**. "Prediction of Asphaltene Instability under Gas Injection with the PC-SAFT Equation of State." Energy and Fuels, 19, 4, 1230–1234.

Government of Alberta. **2020**. Annual Report Energy 2019-2020.

Gray, Murray R. **2015**. Upgrading Oilsands Bitumen and Heavy Oil. The University of Alberta Press.

Gray, Murray R. **2019**. “Fundamentals of Partial Upgrading of Bitumen.” Energy and Fuels, 33, 8, 6843–6856.

Gray, Murray R., Rik R. Tykwinski, Jeffrey M. Stryker, and Xiaoli Tan. **2011**. “Supramolecular Assembly Model for Aggregation of Petroleum Asphaltenes.” in Energy and Fuels, 25, 7, 3125–3134.

Gray, R. Murray. **1994**. Upgrading Petroleum Residues and Heavy Oils. Marcel Dekker, Inc.

Henderson, J. H. and L. Weber. **1965**. “Physical Upgrading of Heavy Crude Oils by the Application of Heat.” Journal of Canadian Petroleum Technology, 4 (04), 206-212.

Hildebrand, Joel H. **1949**. “A Critique of the Theory of Solubility of Non-Electrolytes.” Chemical Reviews, 44 (1), 37-45.

Hirschberg, A., L. N. J. deJong, B. A. Schipper, and J. G. Meijer. **1984**. “INFLUENCE OF TEMPERATURE AND PRESSURE ON ASPHALTENE FLOCCULATION.” *Society of Petroleum Engineers Journal*, 24 (3), 283-293.

Hu, Yu Feng and Tian Min Guo. **2001**. “Effect of Temperature and Molecular Weight of N-Alkane Precipitants on Asphaltene Precipitation.” *Fluid Phase Equilibria*, 192 (1-2), 13-25.

Huggins, Maurice L. **1941**. “Solutions of Long Chain Compounds.” *The Journal of Chemical Physics*, 9, 440.

Hughey, C. A., C. L. Hendrickson, R. P. Rodgers, A. G. Marshall, and K. Qian. **2001**. “Kendrick Mass Defect Spectrum: A Compact Visual Analysis for Ultrahigh-Resolution Broadband Mass Spectra.” Analytical Chemistry, 73(19), 4676-4681.

Hwang, Jongsic. **1993**. “Application of Dynamic Supercritical Fluid Extraction.” The University of Utah.

Jewell, D. M., J. H. Weber, J. W. Bunger, Henry Plancher, and D. R. Latham. **1972**. "Ion-Exchange, Coordination, and Adsorption Chromatographic Separation of Heavy-End Petroleum Distillates." *Analytical Chemistry*, 44, 8, 1391–1395.

Johnston, K. A., F. F. Schoeggl, M. A. Satyro, S. D. Taylor, and H. W. Yarranton. **2017**. "Phase Behavior of Bitumen and N-Pentane." *Fluid Phase Equilibria*, 442, 1-19.

Joshi, Jyeshtharaj B., Aniruddha B. Pandit, Kamal L. Kataria, Rohit P. Kulkarni, Ashish N. Sawarkar, Deepak Tandon, Yad Ram, and Man Mohan Kumar. **2008**. "Petroleum Residue Upgradation via Visbreaking: A Review." *Industrial and Engineering Chemistry Research*, 47, 8960-8988.

Juyal, P., D. Merino-Garcia, and S. I. Andersen. **2005**. "Effect on Molecular Interactions of Chemical Alteration of Petroleum Asphaltenes. I." *Energy and Fuels*, 19, 4, 1272–1281.

Kharrat, Abdel M., Jose Zacharia, V. John Cherian, and Allwell Anyatonwu. **2007**. "Issues with Comparing SARA Methodologies." *Energy and Fuels*, 21 (6), 3618-3621.

Krishna, R., Y. K. Kuchhal, G. S. Sarna, and I. D. Singh. **1988**. "Visbreaking Studies on Aghajari Long Residue." *Fuel*, 67 930, 379-383.

Kumar, Ashutosh, Amr Henni, and Ezeddin Shirif. **2011**. "Heavy Oil Viscosity Modeling with Friction Theory." in *Energy and Fuels*, 25 (2), 493-498.

De La Porte, J. J. and C. A. Kossack. **2014**. "A Liquid Phase Viscosity-Temperature Model for Long-Chain n-Alkanes up to C64H130 Based on the Free Volume Theory." *Fuel*, 136, 156-164.

De La Porte, J. J., R. W. Zimmerman, and C. A. Kossack. **2014**. "Modelling Heavy Oil Viscosity during Thermal Stimulation Using the Free Volume Theory." in *Proceedings - SPE Annual Technical Conference and Exhibition*, 170817.

Lababidi, Haitham M. S., Hawraa M. Sabti, and Faisal S. Alhumaidan. **2014**. "Changes in Asphaltenes during Thermal Cracking of Residual Oils." *Fuel*, 117, 59-67.

Lee, Jung Moo, Sangcheol Shin, Seonju Ahn, Jeong Hwan Chun, Ki Bong Lee, Sungyong Mun, Sang Goo Jeon, Jeong Geol Na, and Nam Sun Nho. **2014**. "Separation of Solvent and Deasphalted Oil for Solvent Deasphalting Process." *Fuel Processing Technology*, 119 (7), 204-210.

Li, Zhidong and Abbas Firoozabadi. **2010a**. "Cubic-plus-Association Equation of State for Asphaltene Precipitation in Live Oils." *Energy and Fuels*, 24 (2), 1106-1113.

Li, Zhidong and Abbas Firoozabadi. **2010b**. "Modeling Asphaltene Precipitation by N-Alkanes from Heavy Oils and Bitumens Using Cubic-plus-Association Equation of State." *Energy and Fuels*, 24, 2, 1106–1113.

Lindeloff, Niels, Karen Schou Pedersen, Hans Petter Rønningsen, and Jess Milter. **2004**. "The Corresponding States Viscosity Model Applied to Heavy Oil Systems." *Journal of Canadian Petroleum Technology*, 42 (2–4) 195– 207.

Llovell, F., R. M. Marcos, and L. F. Vega. **2013**. "Free-Volume Theory Coupled with Soft-SAFT for Viscosity Calculations: Comparison with Molecular Simulation and Experimental Data." *Journal of Physical Chemistry* B, 117, 27, 8159–8171.

Llovell, Fèlix, Josep C. Pàmies, and Lourdes F. Vega. **2004**. "Thermodynamic Properties of Lennard-Jones Chain Molecules: Renormalization-Group Corrections to a Modified Statistical Associating Fluid Theory." *Journal of Chemical Physics*, 121(21), 10715-24.

Llovell, Fèlix and Lourdes F. Vega. **2006**. "Global Fluid Phase Equilibria and Critical Phenomena of Selected Mixtures Using the Crossover Soft-SAFT Equation." *Journal of Physical Chemistry* B, 49 (4) , 1883-1899.

Luhning, R. W., A. Anand, T. Blackmore, and D. S. Lawson. **2002**. "Pipeline Transportation of Emerging Partially Upgraded Bitumen." in *Canadian International Petroleum Conference* 2002, CIPC 2002, 205.

Luo, Peng, Xiaoqi Wang, and Yongan Gu. **2010**. "Characterization of Asphaltenes Precipitated with Three Light Alkanes under Different Experimental Conditions." *Fluid Phase Equilibria*, 291(2), 103-110.

Mancilla-Polanco, A., F. F. Schoeggl, K. Johnston, W. D. L. Richardson, H. W. Yarranton, and S. D. Taylor. 2017. "The Phase Behavior of Heavy Oil and Propane Mixtures." in *Society of Petroleum Engineers* - SPE Canada Heavy Oil Technical Conference **2017**, 1-26.

Mannistu, K. D., H. W. Yarranton, and J. H. Masliyah. **1997**. "Solubility Modeling of Asphaltenes in Organic Solvents." *Energy and Fuels,* 11, 3, 615–622.

Maples, Roobert E. **2000**. Petroleum Refinery Process Economics, *Pennwell*.

Marquez, A., F. F. Schoeggl, S. D. Taylor, G. Hay, and H. W. Yarranton. **2020**. "Viscosity of Characterized Visbroken Heavy Oils." *Fuel*, 271, 117606.

Marquez, Andres. **2019**. "Viscosity of Characterized Visbroken Heavy Oils." University of Calgary.

Marshall, Alan G. and Ryan P. Rodgers. **2004**. "Petroleomics: The Next Grand Challenge for Chemical Analysis." *Accounts of Chemical Research*, 37, 1, 53–59.

Marshall, Alan G. and Ryan P. Rodgers. **2008**. "Petroleomics: Chemistry of the Underworld." *Proceedings of the National Academy of Sciences of the United States of America*, 105 (47) 18090-18095.

Meng, Xianyang and Jiangtao Wu. **2013**. "Viscosity Modeling of Some Oxygenated Fuels." *Fuel*, 107, 309-314.

Mohammed, Isah, Mohamed Mahmoud, Dhafer Al Shehri, Ammar El-Husseiny, and Olalekan Alade. **2021**. "Asphaltene Precipitation and Deposition: A Critical Review." *Journal of Petroleum Science and Engineering*, 23, 11, 5611–5625.

Moharam, Hassan M. and Mohamed A. Fahim. **1995**. "Prediction of Viscosity of Heavy Petroleum Fractions and Crude Oils Using a Corresponding States Method." *Industrial and Engineering Chemistry Research*, 34, 11, 4140–4144.

Motahhari, H., M. A. Satyro, S. D. Taylor, and H. W. Yarranton. **2013**. "Extension of the Expanded Fluid Viscosity Model to Characterized Oils." in *Energy and Fuels*, 27 (4), 1881-1898.

Motahhari, H., M. A. Satyro, and H. W. Yarranton. **2011**. "Predicting the Viscosity of Asymmetric Hydrocarbon Mixtures with the Expanded Fluid Viscosity Correlation." *Industrial and Engineering Chemistry Research*, 50 (22), 12831-12843.

Mullins, Oliver C., Hassan Sabbah, Joëlle Eyssautier, Andrew E. Pomerantz, Loïc Barré, A. Ballard Andrews, Yosadara Ruiz-Morales, Farshid Mostowfi, Richard McFarlane, Lamia Goual, Richard Lepkowicz, Thomas Cooper, Jhony Orbulescu, Roger M. Leblanc, John Edwards, and Richard N. Zare. **2012**. "Advances in Asphaltene Science and the Yen-Mullins Model." in *Energy and Fuels*, 26, 3986-4003.

Murgich, Juan. **2003**. "Molecular Simulation and the Aggregation of the Heavy Fractions in Crude Oils." *Molecular Simulation*, 29 (6-7), 451-61.

Okhotnikova, E. S., Yu M. Ganeeva, T. N. Yusupova, V. I. Morozov, I. N. Frolov, and G. V. Romanov. **2011**. "High-Molecular-Mass Asphaltene Fraction and Its Effect on the Structure and Stability of Oxidized Bitumens." *Petroleum Chemistry*, 51, pages187–191.

Oliveira, Mariana B., Samuel V.D. Freitas, Felix Llovell, Lourdes F. Vega, and João A. P. Coutinho. **2014**. "Development of Simple and Transferable Molecular Models for Biodiesel Production with the Soft-SAFT Equation of State." *Chemical Engineering Research and Design*, 108, 4, 1450–1457.

Pedersen, Karen Schou and Aage Fredenslund. **1987**. "An Improved Corresponding States Model for the Prediction of Oil and Gas Viscosities and Thermal Conductivities." *Chemical Engineering* Science, 42 (1), 182-186.

Pedersen, Karen Schou, Aage Fredenslund, Peter L. Christensen, and Per Thomassen. **1984**. "Viscosity of Crude Oils." *Chemical Engineering Science*, 39 (6), 1011-1016.

Peng, Ding Yu and Donald B. Robinson. **1976**. "A New Two-Constant Equation of State." *Industrial and Engineering Chemistry Fundamentals*, 60 (3) , 1463-1472.

Perez Claro, Y. A., F. F. Schoeggl, S. D. Taylor, and H. W. Yarranton. **2019**. "Phase Behavior of Mixtures of Bitumen and N-Butane." *Energy and Fuels*, 33, 9, 8530–8543.

Polishuk, Ilya and Abraham Yitzhak. **2014**. "Modeling Viscosities of Pure Compounds and Their Binary Mixtures Using the Modified Yarranton-Satyro Correlation and Free Volume Theory Coupled with SAFT+Cubic EoS." *Industrial and Engineering Chemistry Research*, 53, 2, 959–971.

Powers, D. P., H. Sadeghi, H. W. Yarranton, and F. G. A. Van Den Berg. **2016**. "Regular Solution Based Approach to Modeling Asphaltene Precipitation from Native and Reacted Oils: Part 1, Molecular Weight, Density, and Solubility Parameter Distributions of Asphaltenes." *Fuel*, 178, 218-233.

Prausnitz, John M., Rüdiger N. Lichtenthaler, and Edmundo Gomes de Azevedo. **1999**. Molecular Thermodynamics of Fluid-Phase Equilibria (3rd Ed.). Upper Saddle River, N.J.: Prentice Hall PTR.

Quiñones-Cisneros, Sergio E., Claus K. Zéberg-Mikkelsen, and Erling H. Stenby. **2000**. "The Friction Theory (f-Theory) for Viscosity Modeling." *Fluid Phase Equilibria*, 178 (1-2), 1-16.

Quiñones-Cisneros, Sergio E., Claus K. Zéberg-Mikkelsen, and Erling H. Stenby. **2001a**. "One Parameter Friction Theory Models for Viscosity." *Fluid Phase Equilibria*, 56 (24), 7007-7015.

Quiñones-Cisneros, Sergio E., Claus K. Zéberg-Mikkelsen, and Erling H. Stenby. **2001b**. "The Friction Theory for Viscosity Modeling: Extension to Crude Oil Systems." *Chemical Engineering Science*, 56 (24), 7007-7015.

Quiñones-Cisneros, Sergio E., Claus K. Zéberg-Mikkelsen, and Erling H. Stenby. **2003**. "Friction Theory Prediction of Crude Oil Viscosity at Reservoir Conditions Based on Dead Oil Properties." *Fluid Phase Equilibria*, 212 (1-2), 233-243.

Ramos-Pallares, F., F. F. Schoeggl, S. D. Taylor, M. A. Satyro, and H. W. Yarranton. **2016**. "Predicting the Viscosity of Hydrocarbon Mixtures and Diluted Heavy Oils Using the Expanded Fluid Model." in *Energy and Fuels*, 30 (5), 3575-3595.

Ramos-Pallares, F., S. D. Taylor, M. A. Satyro, R. A. Marriott, and H. W. Yarranton. **2016**. "Prediction of Viscosity for Characterized Oils and Their Fractions Using the Expanded Fluid Model." *Energy and Fuels*, 30 (9), 7134-7157.

Rastegari, Khashayar, William Y. Svrcek, and Harvey W. Yarranton. **2004**. "Kinetics of Asphaltene Flocculation." *Industrial and Engineering Chemistry Research*, 43, 21, 6629-6637.

Riazi, M. **2005**. Characterization and Properties of Petroleum Fractions, First Edition.

Rivero, Javier. **2021**. "Asphaltene Precipitation from Bitumen/Multicomponent Solvent Mixtures." University of Calgary.

Robert A. Meyers, Ph. D. **2016**. "UOP VISBREAKING PROCESS." in Handbook of Petroleum Refining Processes. New York: *McGraw-Hill Education*.

Rodriguez, S., E. N. Baydak, F. F. Schoeggl, S. D. Taylor, G. Hay, and H. W. Yarranton. **2019**. "Regular Solution Based Approach to Modeling Asphaltene Precipitation from Native and Reacted Oils: Part 3, Visbroken Oils." *Fuel*, 257.

Rodríguez, Sandra. **2018**. "The Stability of Visbroken Heavy Oil Against Asphaltene Precipitation." University of Calgary.

Rogel, E. **1997**. "Theoretical Estimation of the Solubility Parameter Distributions of Asphaltenes, Resins, and Oils from Crude Oils and Related Materials." *Energy and Fuels*, 11, 4, 920–925.

Rogel, Estrella, Michael Moir, and Matthias Witt. **2015**. "Atmospheric Pressure Photoionization and Laser Desorption Ionization Coupled to Fourier Transform Ion Cyclotron Resonance Mass Spectrometry to Characterize Asphaltene Solubility Fractions: Studying the Link between Molecular Composition and Physical Behav." *Energy and Fuels*, 29, 7, 4201–4209.

Rogel, Estrella, Cesar Ovalles, and Michael Moir. **2010**. "Asphaltene Stability in Crude Oils and Petroleum Materials by Solubility Profile Analysis." *Energy and Fuels*, 24, 8, 4369–4374.

Rueda-Velásquez, Rosa I. and Murray R. Gray. **2017**. "A Viscosity-Conversion Model for Thermal Cracking of Heavy Oils." *Fuel*, 197, 82-90.

Sánchez-Lemus, M. C., F. Schoeggl, S. D. Taylor, and H. W. Yarranton. **2016**. "Physical Properties of Heavy Oil Distillation Cuts." *Fuel*, 180, 457-472.

Sawarkar, Ashish N., Aniruddha B. Pandit, Shriniwas D. Samant, and Jyeshtharaj B. Joshi. **2007**. "Petroleum Residue Upgrading via Delayed Coking: A Review." *Canadian Journal of Chemical Engineering*, 85 (1), 1-24.

Scatchard, George. **1949**. “Equilibrium in Non-Electrolyte Mixtures.” *Chemical Reviews*, 44 (1), 7-35.

Schlumberger Software. **2020**. “Symmetry Process Software Platform, User Manual.”

Shadbahr, Khosravani, Khorasheh, **2011** “Development of a continuous kinetic model for visbreaking reactions.” *Scientia Iranica*, 18(3), 465-469.

Shen, Gulou, Christoph Held, Jyri Pekka Mikkola, Xiaohua Lu, and Xiaoyan Ji. **2014**. “Modeling the Viscosity of Ionic Liquids with the Electrolyte Perturbed-Chain Statistical Association Fluid Theory.” *Industrial and Engineering Chemistry Research*, 53, 52, 20258–20268.

Shen, Z., Z. Cao, X. Zhu, and X. Li. **2008**. “Visbreaking of Chinese Oil Sand Bitumen.” *Petroleum Science and Technology*, 26(14), 1676-1683.

Shu, W. R. and V. N. Venkatesan. **1983**. “KINETICS OF THERMAL VISBREAKING OF A COLD LAKE BITUMEN.” in Preprints - *Annual Technical Meeting of the Petroleum Society of CIM*, 23 (2), 60-64.

Shukla, Ashutosh K. **2018**. Analytical Characterization Methods for Crude Oiland Related Products.

Sivaramakrishnan, Kaushik, Arno Klerk, and Vinay Prasad. **2019**. “Viscosity of Canadian Oilsands Bitumen and Its Modification by Thermal Conversion.” , 115–199.

Soave, Giorgio. **1972**. “Equilibrium Constants from a Modified Redlich-Kwong Equation of State.” *Chemical Engineering Science*, 27, 1197-1203.

Soto-Castruita, Enrique, Patsy V. Ramírez-González, Ulises Martínez-Cortés, and Sergio E. Quiñones-Cisneros. **2015**. “Effect of the Temperature on the Non-Newtonian Behavior of Heavy Oils.” *Energy and Fuels*, 29 (5), 2883-2889.

Speight, James G. **1998**. "The Chemistry and Physics of Coking." *Korean Journal of Chemical Engineering*, 15, 1-8.

Speight, James G. **2006**. The Chemistry and Technology of Petroleum. Boca Raton: *CRC Press/Taylor & Francis*, Chapter 14, 17, 20.

Speight, James G. **2011**. The Refinery of the Future. William Andrew, *Elsevier Inc*.

Speight, James G. **2014**. The Chemistry and Technology of Petroleum. Boca Raton: *CRC Press/Taylor & Francis*.

Speight, James G. **2017**. "Industrial Organic Chemistry." in Environmental Organic Chemistry for Engineers, *Elsevier Inc*.

Speight, James G. **2019**. "Heavy Oil Recovery and Upgrading." Pp. i–ii in Heavy Oil Recovery and Upgrading. *Elsevier*.

Stenby, E. H. and W. Yan. **2005**. "Composition and Physical Properties of Hydrocarbons." *Encyclopaedia of Hydrocarbons* I:31–64.

Stryjek, R. and J. H. Vera. **1986**. "PRSV: An Improved Peng—Robinson Equation of State for Pure Compounds and Mixtures." *The Canadian Journal of Chemical Engineering*, 64(2), 323-333.

Tan, Sugata P., Hertanto Adidharma, Brian F. Towler, and Maciej Radosz. **2005**. "Friction Theory and Free-Volume Theory Coupled with Statistical Associating Fluid Theory for Estimating the Viscosity of Pure n-Alkanes." *Industrial and Engineering Chemistry Research*, 44 (22), 8409-8418.

Tannous, Joy H. and Arno de Klerk. **2019**. "Asphaltenes Formation during Thermal Conversion of Deasphalted Oil." *Fuel*, 255, 115786.

Tavakkoli, Mohammad, Marty R. Grimes, Xiaoyu Liu, Caitlin K. Garcia, Sarah C. Correa, Quinton J. Cox, and Francisco M. Vargas. **2015**. "Indirect Method: A Novel Technique for Experimental Determination of Asphaltene Precipitation." *Energy and Fuels*, 272 , 117708.

Teja, A. S. and P. Rice. **1981**. "Generalized Corresponding States Method for the Viscosities of Liquid Mixtures." *Industrial and Engineering Chemistry Fundamentals*, 473 , 1-16.

Tham, M. J. and K. E. Gubbins. **1970**. "Correspondence Principle for Transport Properties of Dense Fluids. Nonpolar Polyatomic Fluids." *Industrial and Engineering Chemistry Fundamentals*, 9 (1), 63-70.

Tharanivasan, Asok Kumar, Harvey W. Yarranton, and Shawn D. Taylor. **2011**. "Application of a Regular Solution-Based Model to Asphaltene Precipitation from Live Oils." in *Energy and Fuels*, 25 (2), 528-538.

Ting, P. David, George J. Hirasaki, and Walter G. Chapman. **2003**. "Modeling of Asphaltene Phase Behavior with the SAFT Equation of State." in *Petroleum Science and Technology*, 21 (3-40), 647-661.

Tojima, M., S. Suhara, M. Imamura, and A. Furuta. **1998**. "Effect of Heavy Asphaltene on Stability of Residual Oil." *Catalysis Today*, 43, 347– 351.

Trejo, F., G. Centeno, and J. Ancheyta. **2004**. "Precipitation, Fractionation and Characterization of Asphaltenes from Heavy and Light Crude Oils." *Fuel*, 83 (16), 2169-2175.

Trejo, Fernando and Jorge Ancheyta. **2007**. "Characterization of Asphaltene Fractions from Hydrotreated Maya Crude Oil." *Industrial and Engineering Chemistry Research*, 46, 23, 7571–7579.

Trejoa Fernando, Mohan S. Ranab, Jorge Ancheyta. **2010**. “Thermogravimetric determination of coke from asphaltenes, resins and sedimentsand coking kinetics of heavy crude asphaltenes.” *Catalysis Today*, 150, 3–4, 272-278.

Wiehe, Irwin A. **1992**. “A Solvent-Resid Phase Diagram For Tracking Resid Conversion.” *Industrial and Engineering Chemistry Research*, 31, 530-536.

Wiehe, Irwin A. **1993**. “A Phase-Separation Kinetic Model for Coke Formation.” *Industrial and Engineering Chemistry Research*, 32, 2447-2454.

Wiehe, Irwin A., Harvey W. Yarranton, Kamran Akbarzadeh, Parviz M. Rahimi, and Alem Teclemariam. **2005**. “The Paradox of Asphaltene Precipitation with Normal Paraffins.” *Energy and Fuels*, 19 (4), 1261-1267.

Xu, Yingnian, Yoshikata Koga, and Otto P. Strausz. **1995**. “Characterization of Athabasca Asphaltenes by Small-Angle X-Ray Scattering.” *Fuel*, 74 (7), 960-964.

Yarranton, H. W., D. P. Ortiz, D. M. Barrera, E. N. Baydak, L. Barré, D. Frot, J. Eyssautier, H. Zeng, Z. Xu, G. Dechaine, M. Becerra, J. M. Shaw, A. M. McKenna, M. M. Mapolelo, C. Bohne, Z. Yang, and J. Oake. **2013**. “On the Size Distribution of Self-Associated Asphaltenes.” *Energy and Fuels*, 27 (9), 5083-5106.

Yarranton, H. W., D. P. Powers, J. C. Okafor, and F. G. A. van den Berg. **2018**. “Regular Solution Based Approach to Modeling Asphaltene Precipitation from Native and Reacted Oils: Part 2, Molecular Weight, Density, and Solubility Parameter of Saturates, Aromatics, and Resins.” *Fuel*, 215, 766-777.

Yarranton, H. W. and M. A. Satyro. **2009**. “Expanded Fluid-Based Viscosity Correlation for Hydrocarbons.” *Industrial and Engineering Chemistry Research*, 48 (7), 3640-3648.

Yarranton, Harvey W. **2005**. “Asphaltene Self-Association.” *Journal of Dispersion Science and Technology*, 26, 5-8.

Yarranton, Harvey W., Hussein Alboudwarej, and Rajesh Jakher. **2000**. “Investigation of Asphaltene Association with Vapor Pressure Osmometry and Interfacial Tension Measurements.” *Industrial and Engineering Chemistry Research*, 39 (8), 2916-2924.

Yarranton, Harvey W., William A. Fox, and William Y. Svrcek. **2007**. “Effect of Resins on Asphaltene Self-Association and Solubility.” *Canadian Journal of Chemical Engineering*, 21 (1), 274-285.

Yarranton, Harvey W. and Jacob H. Masliyah. **1996**. “Molar Mass Distribution and Solubility Modeling of Asphaltenes.” *AIChE Journal*, 42 (12), 3533−3543.

Yoshimura, Masatoshi, Christian Boned, Guillaume Galliéro, Jean Patrick Bazile, Antoine Baylaucq, and Hideharu Ushiki. 2010. “Influence of the Chain Length on the Dynamic Viscosity at High Pressure of Some 2-Alkylamines: Measurements and Comparative Study of Some Models.” *Chemical Physics*, 369 (2-3), 126-137.

Zachariah, Ashley and Arno De Klerk. **2017**. “Partial Upgrading of Bitumen: Impact of Solvent Deasphalting and Visbreaking Sequence.” *Energy and Fuels*, 31, 9, 9374–9380.

Zheng, Fang, Quan Shi, Germain Salvato Vallverdu, Pierre Giusti, and Brice Bouyssiere. **2020**. “Fractionation and Characterization of Petroleum Asphaltene: Focus on Metalopetroleomics.” *Processes*, 8(11), 1504.

Zou, X., X. Zhang, and J. M. Shaw. **2005**. “The Phase Behavior of Athabasca Vacuum Bottoms + N-Alkane Mixtures.” in *SPE/PS-CIM/CHOA International Thermal Operations and Heavy Oil Symposium Proceedings*, 22 (02): 265–272.

Appendix A: Density Data Measured in this Thesis

Table A-1. Density of whole oils at atmospheric pressure.

Temp. °C	WC-B-A4 kg/m³			WC-DAO-A1 kg/m³			WC-VB-A1 kg/m³		
	Feed	VIS24	VIS32	Feed	VIS15	VIS29	Feed	VIS9	VIS15
15	1014.0	-	-	999.3	-	-	-	-	-
15.6	1013.7	-	-	998.9	991.3	893.4	-	-	-
20	1010.9	1000.8	-	996.1	990.9	980.4	-	-	-
30	1004.6	-	-	989.7	988.0	-	1042.8	-	-
40	998.3	987.6	-	983.3	981.5	967.1	1038.4	1031.1	-
50	992.1	981.1	976.0	977.0	975.0	960.4	1033.3	1024.8	-
60	985.8	974.6	969.4	970.6	968.4	953.8	1027.5	1018.5	1014.8
70	979.6	968.2	962.8	964.3	962.0	-	1021.4	1012.3	1008.6
80	973.3	961.7	956.3	958.0	955.5	-	1015.3	1006.0	1002.3
90	967.0	955.2	949.7	951.7	948.5	-	1008.8	999.7	996.1

Table A-2. Density of SBD residue at atmospheric pressure.

Temp. °C	WC-B-A4 kg/m³			WC-DAO-A1 kg/m³			WC-VB-A1 kg/m³		
	Feed	VIS24	VIS32	Feed	VIS15	VIS29	Feed	VIS9	VIS15
15	1028.0	-	-	-	-	-	-	-	-
15.6	1027.9	-	-	-	-	-	-	-	-
20	1026.9	-	-	-	-	-	-	-	-
30	1022.2	-	-	-	-	-	-	-	-
40	1016.1	1031.0	1037.6	-	-	1021.0	-	1040.5	1043.3
50	1010.0	1024.7	1031.3	1004.9	1005.2	1014.7	-	1034.4	1037.2
60	1003.8	1018.5	1025.1	998.7	999.0	1008.4	-	1028.3	1031.1
70	997.7	1012.3	1018.9	992.6	992.8	1002.2	-	1022.2	1024.8
80	991.6	1006.2	1012.7	986.5	986.6	995.9	-	1016.0	1018.7
90	985.5	1000.0	1006.4	980.4	980.4	989.6	-	1009.9	1012.5

Table A-3. Density of maltenes at atmospheric pressure.

Temp. °C	WC-B-A4 kg/m³			WC-DAO-A1 kg/m³			WC-VB-A1 kg/m³		
	Feed	VIS24	VIS32	Feed	VIS15	VIS29	Feed	VIS9	VIS15
15	1002.8	-	-	-	-	-	-	-	-
15.6	1002.4	-	-	-	-	-	-	-	-
20	999.6	-	-	-	-	-	-	-	-
30	993.3	-	-	-	998.9	1009.8	-	-	-
40	987.1	-	-	-	992.6	996.6	-	-	-
50	980.8	-	-	982.8	986.3	990.3	-	-	-
60	974.7	980.6	982.1	976.6	980.1	984.0	987.9	986.4	986.8
70	968.4	974.3	975.8	970.4	973.9	977.7	981.7	980.2	980.6
80	962.2	968.0	969.6	964.2	967.6	971.4	975.6	974.0	974.4
90	956.0	961.9	963.3	957.9	961.4	965.2	969.4	967.8	968.2

Table A-4. Density of distillates at atmospheric pressure.

Temp. °C	WC-B-A4 kg/m³			WC-DAO-A1 kg/m³			WC-VB-A1 kg/m³		
	Feed	VIS24	VIS32	Feed	VIS15	VIS29	Feed	VIS9	VIS15
15	913.5	910.5	906.1	912.5	907.6	904.2	-	875.6	880.6
15.6	913.1	910.1	905.7	912.1	907.2	903.8	-	875.1	880.2
20	910.0	907.1	902.6	909.1	904.1	900.7	-	871.8	876.9
30	903.3	900.1	895.7	902.2	897.2	893.7	-	864.4	869.5
40	896.5	893.2	888.7	895.4	890.3	886.7	-	856.9	862.1

Table A-5. Density of saturates at atmospheric pressure.

Temp. °C	WC-B-A4 kg/m³			WC-DAO-A1 kg/m³			WC-VB-A1 kg/m³		
	Feed	VIS24	VIS32	Feed	VIS15	VIS29	Feed	VIS9	VIS15
15	-	-	-	903.3	-	900.1	-	-	-
15.6	901.1	-	-	903.0	-	899.7	-	-	-
20	899.4	-	-	900.3	-	896.9	906.1	899.8	898.4
30	892.3	-	-	894.1	-	890.8	900.0	893.7	892.2
40	886.2	-	-	888.0	-	884.6	893.9	887.6	886.1
50	880.2	-	-	-	-	878.5	887.9	881.5	880.1
60	874.1	874.6	873.5	-	876.7	872.3	881.9	875.5	874.0
70	868.0	868.5	867.4	-	870.6	866.2	875.9	869.4	868.0
80	862.0	862.4	861.3	-	864.5	860.0	869.9	863.4	861.9
90	855.9	856.3	855.2	-	858.4	853.8	-	857.4	855.9

Table A-6. Density of aromatics at atmospheric pressure.

Temp. °C	WC-B-A4 kg/m³			WC-DAO-A1 kg/m³			WC-VB-A1 kg/m³		
	Feed	VIS24	VIS32	Feed	VIS15	VIS29	Feed	VIS9	VIS15
15.6	1011.4								
20	1008.7								
30	1002.1								
40	995.5			1001.2					1011.8
50				994.9					1005.5
60		993.4	997.0	988.6	992.4	1000.1	992.5	995.2	999.2
70		987.1	990.5		986.1	993.6	986.4	988.9	992.9
80		980.8	984.2	976.1	979.8	987.3	980.2	982.7	986.6
90		974.6	978.0	969.9	973.6	980.9	973.9	976.5	980.4

Table A-7. Estimated density of resins at atmospheric pressure.

Temp. °C	WC-B-A4 kg/m³			WC-DAO-A1 kg/m³			WC-VB-A1 kg/m³		
	Feed	VIS24	VIS32	Feed	VIS15	VIS29	Feed	VIS9	VIS15
40	1036.8	1068.3	1057.6	1041.6	1047.7	1049.9	1045.1	1046.0	1044.0
50	1031.0	1049.4	1051.4	1035.4	1041.5	1043.8	1039.0	1039.9	1037.8
60	1025.2	1043.1	1045.3	1029.2	1035.3	1037.7	1033.0	1033.8	1031.7
70	1019.4	1036.8	1039.1	1023.0	1029.1	1031.7	1026.9	1027.7	1025.5
80	1013.5	1030.5	1032.9	1016.8	1022.9	1025.6	1020.8	1021.6	1019.4
90	1007.7	1024.2	1026.8	1010.6	1016.7	1019.5	1014.8	1015.5	1013.3

Table A-8. Estimated density of asphaltenes at atmospheric pressure.

Temp. °C	WC-B-A4 kg/m³			WC-DAO-A1 kg/m³			WC-VB-A1 kg/m³		
	Feed	VIS24	VIS32	Feed	VIS15	VIS29	Feed	VIS9	VIS15
40	1133.9	1160.9	1153.5	1113.1	1102.0	1108.8	1133.6	1148.1	1163.2
50	1128.4	1143.4	1147.3	1108.0	1095.2	1102.4	1127.2	1142.0	1157.7
60	1122.9	1137.6	1141.0	1102.8	1088.3	1095.9	1120.9	1135.9	1152.3
70	1117.3	1131.7	1134.8	1097.6	1081.4	1089.4	1114.5	1129.7	1146.9
80	1111.8	1125.9	1128.5	1092.5	1074.6	1082.9	1108.1	1123.6	1141.4
90	1106.3	1120.1	1122.3	1087.3	1067.7	1076.5	1101.8	1117.5	1136.0

Appendix B: Viscosity Data Measured in this Thesis

Table B-1. Viscosity of oils at atmospheric pressure.

Temp. °C	WC-B-A4 mPa·s			WC-DAO-A1 mPa·s			WC-VB-A1 mPa·s		
	Feed	VIS24	VIS32	Feed	VIS15	VIS29	Feed	VIS9	VIS15
0	-	-	-	-	64000	7600	-	-	-
10	-	-	-	-	17000	2500	-	-	-
20	611000	11000	4000	70500	5200	1000	-	-	-
30	-	3900	1600	19000	2100	460	-	-	-
40	36900	1500	690	5400	900	230	-	-	-
50	-	710	340	2400	-	-	-	220000	-
60	4400	370	200	1080	-	-	-	63000	-
70	-	210	120	550	-	-	-	21000	-
80	960	-	-	-	-	-	115000	8200	2900
90	-	-	-	-	-	-	38000	3700	1400
100	-	-	-	-	-	-	14700	1800	680
110	-	-	-	-	-	-	6400	-	400
120	-	-	-	-	-	-	3100	-	250
130	-	-	-	-	-	-	1600	-	-
140	-	-	-	-	-	-	900	-	-

Table B-2. Viscosity of SBD residue at atmospheric pressure.

Temp. °C	WC-B-A4 mPa·s			WC-DAO-A1 mPa·s			WC-VB-A1 mPa·s		
	Feed	VIS24	VIS32	Feed	VIS24	VIS32	Feed	VIS24	VIS32
50	-	166000	197000	-	-	-	-	-	-
60	88200	44400	50700	26200	10400	11800	-	-	167000
70	28000	14400	15900	9230	4000	4400	-	-	48400
80	10000	5500	5900	3770	1800	1900	-	26800	16600
90	4200	2400	2500	1760	890	890	-	10200	6600
100	2000	1100	1190	884	480	470	-	4380	2900
110	1000	-	-	-	-	270	-	2100	-
120	-	-	-	-	-	-	-	1100	-

Table B-3. Viscosity of maltenes at atmospheric pressure.

Temp. °C	WC-B-A4 mPa·s			WC-DAO-A1 mPa·s			WC-VB-A1 mPa·s		
	Feed	VIS24	VIS32	Feed	Feed	VIS24	VIS32	VIS24	Feed
20	-	-	-	-	463000	217000	-	-	-
30	133000	69600	47800	-	90400	45900	-	-	280000
40	32600	18100	12800	33100	23000	12500	-	-	63100
50	10100	5850	4260	10200	7400	4200	-	21400	18000
60	3620	2250	1660	3700	2800	1600	17000	7200	6300
70	1500	970	740	1600	1200	730	6200	2900	2500
80	720	480	368	720	-	-	2600	1300	1100
90	-	-	-	380	-	-	1200	640	-
100	-	-	-	-	-	-	610	350	-

Table B-4. Estimated viscosity of distillates at atmospheric pressure.

Temp. °C	WC-B-A4 mPa·s			WC-DAO-A1 mPa·s			WC-VB-A1 mPa·s		
	Feed	VIS24	VIS32	Feed	VIS15	VIS29	Feed	VIS9	VIS15
30	11.0	11.3	5.9	8.0	7.6	7.9	-	3.5	2.0
40	7.4	7.6	4.3	5.7	5.4	5.6	-	2.6	1.6
50	5.3	5.4	3.3	4.3	4.0	4.1	-	2.1	1.4
60	4.0	4.0	2.6	3.3	3.1	3.2	-	1.7	1.2
70	3.1	3.1	2.1	2.7	2.4	2.5	-	1.4	1.0
80	2.5	2.5	1.8	2.2	2.0	2.1	-	1.2	0.9

Table B-5. Viscosity of saturates at atmospheric pressure.

Temp. °C	WC-B-A4 mPa·s			WC-DAO-A1 mPa·s			WC-VB-A1 mPa·s		
	Feed	VIS24	VIS32	Feed	VIS15	VIS29	Feed	VIS9	VIS15
0	-	-	-	-	9850	4240	-	-	11000
10	-	-	1970	2700	3190	1500	9100	-	3500
20	1720	-	-	1700	-	-	-	-	-
30	1080	1020	790	1000	1210	630	-	1630	1330
40	462	448	360	490	520	290	1300	710	590
50	220	220	180	250	-	-	580	340	290
60	120	120	100	-	-	-	290	180	160
70	-	-	-	-	-	-	-	100	-

Table B-6. Viscosity of aromatics at atmospheric pressure.

Temp. °C	WC-B-A4 mPa·s			WC-DAO-A1 mPa·s			WC-VB-A1 mPa·s		
	Feed	VIS24	VIS32	Feed	VIS15	VIS29	Feed	VIS9	VIS15
20	-	345000	-	795000	-	-	-	-	-
30	68000	62000	-	-	63400	49000	-	-	-
40	16500	15100	11300	-	15700	12200	115000	32200	-
50	5060	4700	3600	8300	4900	3800	28400	9300	9000
60	1860	1800	1400	2900	1900	1400	8800	3300	3200
70	800	750	590	1200	770	630	3200	1300	1300
80	390	-	290	560	380	310	1400	630	600
90	-	-	-	160	-	100	650	320	310
100	-	-	-	-	-	-	340	-	170

Table B-7. Viscosity of resins at atmospheric pressure.

Temp. °C	WC-B-A4 mPa·s			WC-DAO-A1 mPa·s			WC-VB-A1 mPa·s		
	Feed	VIS24	VIS32	Feed	VIS15	VIS29	Feed	VIS9	VIS15
70	1540000	-	-	-	-	-	-	-	-
80	338000	-	-	-	-	-	-	-	-
90	92700	87600	83100	-	-	-	-	277000	161000
100	29800	29000	26000	34000	34000	21000	57400	77000	49000
110	11700	11000	9600	13000	13000	7900	21000	27000	18000
120	5100	4800	4100	5700	5400	3400	8500	11000	7400
130	2400	2300	1900	2700	2500	1600	3900	5000	3400
140	-	1200	950	1400	1200	800	1900	2500	1700

Table B-8. Estimated viscosity of asphaltenes at atmospheric pressure.

Temp. °C	WC-B-A4 mPa·s			WC-DAO-A1 mPa·s			WC-VB-A1 mPa·s		
	Feed	VIS24	VIS32	Feed	VIS15	VIS29	Feed	VIS9	VIS15
30	8.E+49	2.E+15	4.E+17	2.E+16	4.E+08	7.E+08	4.E+53	9.E+22	2.E+26
40	7.E+35	2.E+13	9.E+14	3.E+14	5.E+07	1.E+08	1.E+36	8.E+18	5.E+21
50	7.E+27	6.E+11	8.E+12	7.E+12	1.E+07	2.E+07	1.E+27	1.E+16	3.E+18
60	4.E+22	4.E+10	2.E+11	4.E+11	2.E+06	4.E+06	3.E+21	7.E+13	8.E+15
70	1.E+19	3.E+09	1.E+10	3.E+10	7.E+05	1.E+06	6.E+17	1.E+12	1.E+14
80	2.E+16	4.E+08	1.E+09	4.E+09	2.E+05	4.E+05	1.E+15	6.E+10	3.E+12

Appendix C: Measured Distillation Curves

Table C-1. SBD assays for WC-B-A4 feed and its reacted products.

WC-B-A4		WC-B-A4-VIS24		WC-B-A4-VIS32	
Cumulative Fraction	**Boiling Temperature**	**Cumulative Fraction**	**Boiling Temperature**	**Cumulative Fraction**	**Boiling Temperature**
wt%	°C	wt%	°C	wt%	°C
1.18	187.5	2.87	151.1	3.95	150.8
2.65	247.3	4.69	211.8	4.93	184.7
4.18	269.8	5.33	226.3	7.03	215.2
5.73	291.6	6.61	241.2	8.64	233.4
7.30	304.6	8.56	261.3	9.74	244.9
8.88	317.2	9.22	269.9	10.56	253.7
10.48	325.8	11.21	285.8	11.39	260.7
12.08	338.3	12.02	294.0	13.07	274.7
13.70	348.7	20.09	341.2	13.64	280.2
15.32	359.8	20.09	341.2	15.91	292.8
15.98	365.3	27.09	374.2	17.05	301.1
-	-	-	-	18.21	307.3
-	-	-	-	19.36	314.9
-	-	-	-	20.52	320.6
-	-	-	-	22.27	330.0
-	-	-	-	22.86	332.5
-	-	-	-	24.62	340.2
-	-	-	-	25.21	345.4
-	-	-	-	26.40	348.2
-	-	-	-	29.97	368.1

Table C-2. SBD assay for WC-DAO-A1 feed and its reacted products.

WC-DAO-A1		WC-DAO-A1-VIS15		WC-DAO-A1-VIS29	
Cumulative Fraction wt%	**Boiling Temperature** °C	**Cumulative Fraction** wt%	**Boiling Temperature** °C	**Cumulative Fraction** wt%	**Boiling Temperature** °C
1.12	173.7	2.52	152.7	5.02	147.1
2.56	214.7	3.63	192.5	6.40	191.5
4.06	248.6	4.79	214.7	7.82	205.7
5.59	260.5	5.97	234.6	10.01	230.0
7.13	277.1	7.17	249.1	10.75	237.5
8.70	290.1	8.38	261.1	12.24	248.9
10.28	304.7	10.22	274.2	13.75	259.5
11.87	316.2	10.96	282.2	15.27	271.2
13.48	327.0	12.08	290.0	16.80	281.1
15.26	336.4	13.96	300.8	19.90	301.7
16.72	343.6	14.59	308.1	21.47	309.8
18.36	355.0	15.86	314.3	23.05	317.1
20.00	361.4	17.13	322.2	25.19	327.5
21.65	369.7	18.41	328.2	26.22	332.2
-	-	23.59	354.8	27.82	342.6
-	-	24.89	353.7	30.24	351.6
-	-	-	-	33.48	365.1

Table C-3. SBD assay for WC-VB-A1 reacted products.

WC-VB-A1-VIS9		WC-VB-A1-VIS15	
Cumulative Fraction wt%	**Boiling Temperature** °C	**Cumulative Fraction** wt%	**Boiling Temperature** °C
1.68	169.9	2.99	162.1
2.74	249.3	4.47	229.7
3.64	274.6	5.74	261.6
-	-	7.21	313.8

Table C-4. SimDist assays for all feeds and reacted products. Measured by Core Labs.

Cum. Fraction	WC-B-A4 °C			WC-DAO-A1 °C			WC-VB-A1 °C		
	Feed	VIS24	VIS32	Feed	VIS15	VIS29	Feed	VIS9	VIS15
0	200	108	104	181	107	81	330	108	108
5	285	223	196	261	226	177	426	353	291
10	327	274	252	303	273	236	463	419	381
15	362	309	289	333	307	272	493	454	426
20	390	337	317	363	333	302	517	483	457
25	417	363	342	390	359	327	540	507	484
30	442	386	366	417	384	352	562	531	509
35	468	410	388	442	410	375	582	553	532
40	496	432	411	468	433	399	601	575	556
45	525	454	433	497	457	422	618	594	577
50	555	479	456	527	483	446	633	612	597
55	585	506	482	558	511	472	646	629	616
60	611	534	506	589	541	500	659	645	634
65	634	564	541	617	573	530	673	660	651
70	653	592	573	642	603	563	688	676	668
75	673	621	604	664	632	594	702	692	686
80	696	648	635	688	659	625	716	707	703
85	717	677	668	712	688	656	-	-	720
90	-	707	704	-	717	691	-	-	-

Appendix D: MCR Data

Table D-1. MCR content of all of the feeds and reacted products. Measured by Core Labs.

Oil	**MCR Content** wt%
WC-B-A3	14.3
WC-B-A3-VIS5a	14.4
WC-B-A3-VIS5b	14.4
WC-B-A3-VIS8	14.7
WC-B-A3-VIS19	14.8
WC-B-A3-VIS38	16.8
WC-B-A4	13.8
WC-B-A4-VIS24	14.2
WC-B-A4-VIS32	14.8
WC-DAO-A1	11.0
WC-DAO-A1-VIS15	11.5
WC-DAO-A1-VIS29	11.6
WC-VB-A1	21.2
WC-VB-A1-VIS15	20.6
WC-VB-A1-VIS9	20.7

Appendix E: Asphaltene Yields of Saturates and Aromatics

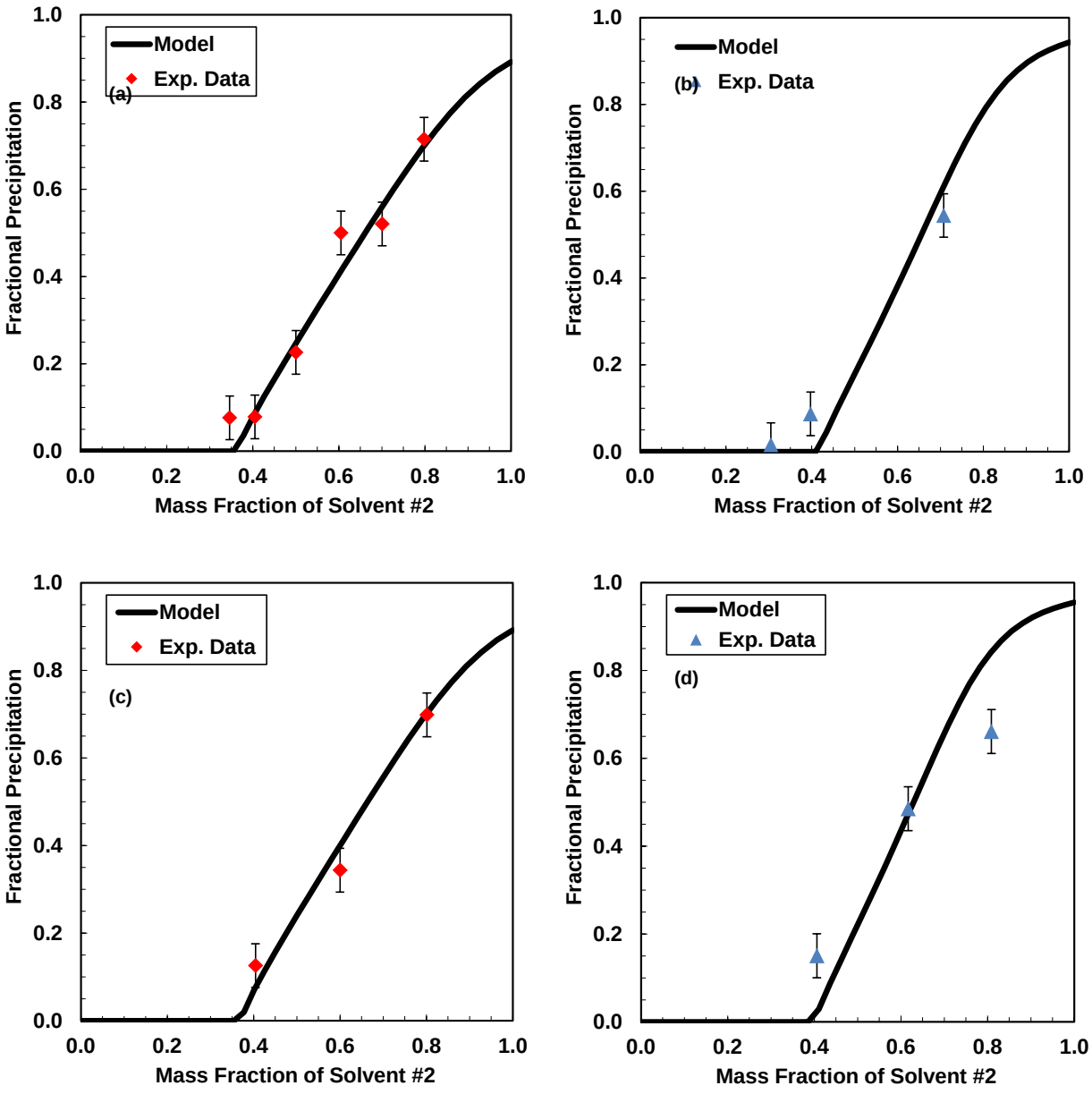

Figure E-9-1. Yield plot of solutions of asphaltenes, *n*-heptane, and a) WC-DAO-A1 aromatics, b) WC-DAO-A1 saturates, c) WC-VB-A1 aromatics, and d) WC-VB-A1 saturates. The curves were fitted using the Modified Regular Solution model to obtain solubility parameter.

Appendix F: Asphaltene Yields from Oils

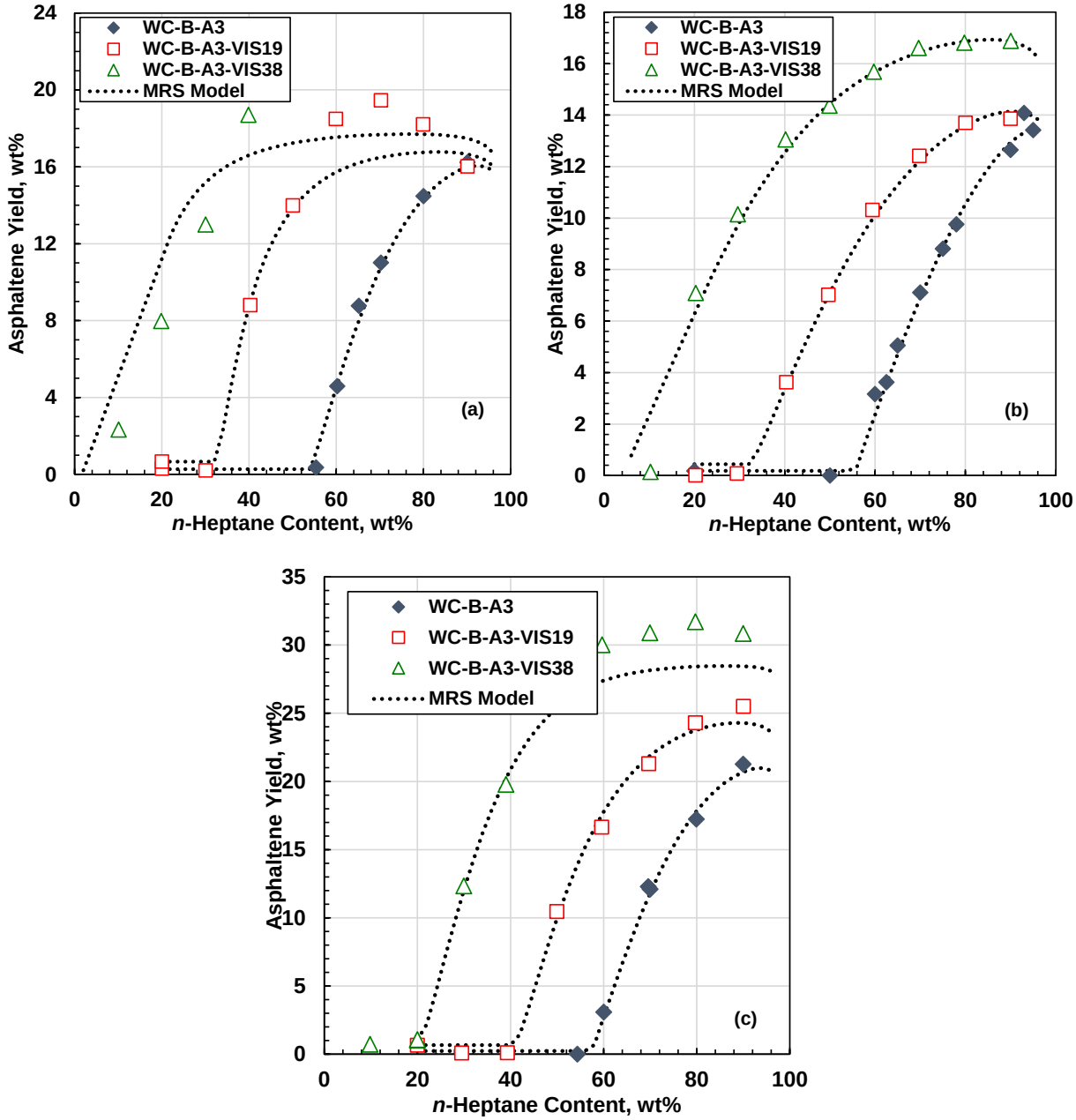

Figure F-9-2. Measured and modeled asphaltene yields from a) WC-B-A3 whole oil, b) whole oil with 0.5 g/g toluene, c) SBD residue with 0.5 g/g toluene, each mixed with *n*-heptane at 20°C and atmospheric pressure. Data from Rodriguez et al. (2019).

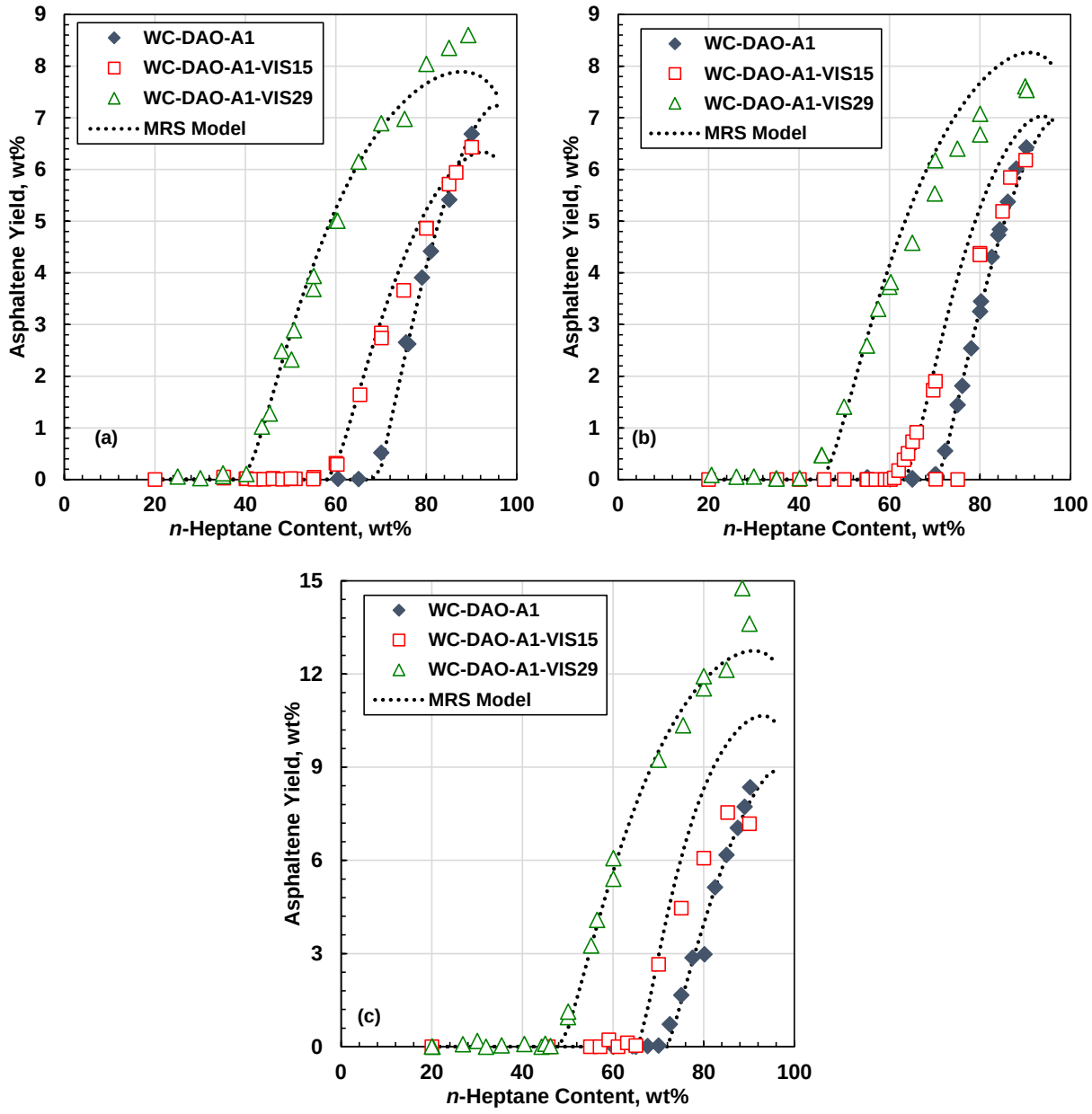

Figure F-9-3. Measured and modeled asphaltene yields from a) WC-DAO-A1 whole oil, b) whole oil with 0.5 g/g toluene, c) SBD residue with 0.5 g/g toluene, each mixed with *n*-heptane at 20°C and atmospheric pressure.

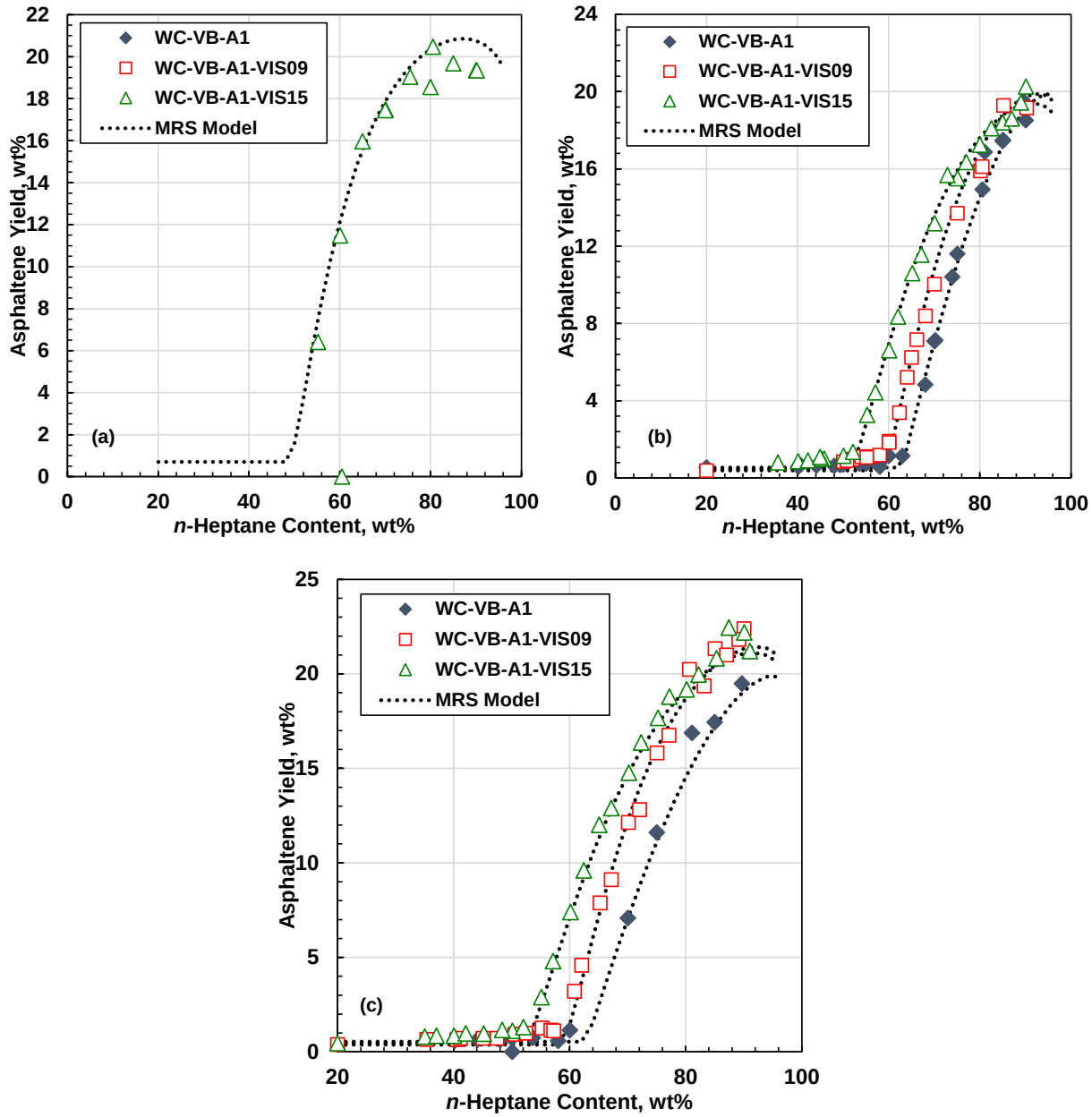

Figure F-9-4. Measured and modeled asphaltene yields from a) WC-VB-A1 whole oil, b) whole oil with 0.5 g/g toluene, c) SBD residue with 0.5 g/g toluene, each mixed with *n*-heptane at 20°C and atmospheric pressure.

Appendix G: Experimental Error

This appendix shows the experimental errors for each measurement type based on a 90% confidence interval (CI). One example of repeatability for each test is provided to demonstrate the errors. The errors for other experiments of the same tests were similar. In the tables below, M1, M2, etc. indicate the individual measurements.

Table G-1. Repeatability of density of WC-B-A4-VIS32 Maltenes. The deviations are within the previously reported repeatability of 0.5 kg/m³ (Marquez *et. al.,* 2020).

Temp. °C	M1 kg/m³	M2 kg/m³	CI kg/m³
60	982.33	982.12	0.15
70	976.00	975.78	0.15
80	969.75	969.55	0.14
90	963.54	963.33	0.15

Table G-2. Repeatability of viscosity of WC-B-A4-VIS32 oil. The deviations are within the previously reported repeatability of 6% (Marquez *et. al.,* 2020).

Temp. °C	M1 mPa·s	M2 mPa·s	CI mPa·s	CI %
20	4049	4135	59	1.45
30	1552	1581	20	1.26
40	688	700	8	1.12
50	345	351	4	1.12
60	201	195	4	1.98
70	119	118	0	0.21

Table G-3. Repeatability of distillate separation of WC-B-A4-VIS32 oil. The deviations are within the previously reported repeatability of 0.3 wt% (Rodriguez *et. al.,* 2019).

Fraction	M1 wt%	M2 wt%	M3 wt%	CI wt%
Distillates	31.1	30.6	30.2	0.4

Table G-4. Repeatability of SARA fractionation of residue from WC-VB-A1-VIS15 oil. The deviations are comparable with the previously reported repeatability of 0.7, 0.5, 0.4 and 1 wt% for saturates, aromatics, resins, and asphaltenes, respectively (Rodriguez *et. al.*, 2019).

Fraction	**M1**	**M2**	**M3**	**M4**	**CI**
	wt%	**wt%**	**wt%**	**wt%**	**wt%**
Saturates	10.9	10.9	10.9	10.8	0.05
Aromatics	39.0	36.2	38.1	38.6	1.05
Resins	20.4	22.1	21.3	21.8	0.62
Asphaltenes	29.7	30.8	29.7	28.8	0.71

Table G-5. Repeatability of SBD boiling points (WC-B-A4-VIS32 oil). The deviations are within the previously reported repeatability of 7 °C (Rodriguez *et. al.*, 2019).

Fraction	**M1**	**M2**	**M3**	**Std. Dev.**
wt%	**°C**	**°C**	**°C**	
0	151.1	151.1	150.8	0.1
5	185.8	187.0	184.2	1.1
10	247.7	255.1	254.6	3.4
15	292.1	295.0	295.1	3.4
20	318.0	324.8	324.0	3.0
25	343.5	342.9	340.3	5.7
30	367.7	373.4	369.0	11.8
			AVERAGE	**4.1**
			CI	**±3.0°C**

Table G-6. Repeatability of molecular weight measurements (WC-DAO-A1 oil). The deviations are within the previously reported repeatability of 15% (Rodriguez *et. al.*, 2019).

Fraction	**M1**	**M2**	**CI**	**CI**
	g/mol	**g/mol**	**g/mol**	**%**
Saturate	491	462	20	4.2
Resin	986	1038	36	3.6

Table G-7. Repeatability of SimDist boiling points (WC-DAO-A1-VIS15 oil). The deviations are within the previously reported repeatability of 1.5 °C (Rodriguez *et. al.,* 2019).

Fraction wt%	M1 °C	M2 °C	M3 °C	Std. Dev.
0	109	107	108	0.8
5	233	226	228	2.9
10	277	273	274	1.7
15	309	307	308	0.8
20	336	333	334	1.2
25	362	359	361	1.2
30	386	384	386	0.9
35	412	410	411	0.8
40	434	433	434	0.5
45	458	457	458	0.5
50	484	483	484	0.5
55	512	511	513	0.8
60	542	541	542	0.5
65	573	573	574	0.5
70	602	603	604	0.8
75	632	632	634	0.9
80	660	659	663	1.7
85	689	688	692	1.7
90	718	717	720	1.2
			AVERAGE	**1.1**
			CI	**±0.5°C**

Table G 8. Repeatability of asphaltene yield measurement (WC-B-A4-VIS32 oil). The deviations are within the previously reported repeatability of 0.5 wt% (Rodriguez *et. al.,* 2019).

Heptane Mass Fraction	M1 wt%	M2 wt%	Std. Dev.
0.26	0.1	0.1	0.0
0.34	4.9	5.3	0.2
0.50	12.7	13.2	0.3
0.70	16.2	17.7	0.8
0.80	16.3	16.5	0.1
0.90	15.1	14.8	0.1
		AVERAGE	**0.24**
		CI	**±0.20 wt%**